



# Characterising Functionally-Distinct Retinal Ganglion Cell Responses to High Frequency Electrical Stimulation

**Author:**

Muralidharan, Madhuvanthi

**Publication Date:**

2021

**DOI:**

<https://doi.org/10.26190/unsworks/23974>

**License:**

<https://creativecommons.org/licenses/by/4.0/>

Link to license to see what you are allowed to do with this resource.

Downloaded from <http://hdl.handle.net/1959.4/100267> in <https://unsworks.unsw.edu.au> on 2024-05-02



**UNSW**  
SYDNEY

# **Characterising Functionally-Distinct Retinal Ganglion Cell Responses to High Frequency Electrical Stimulation**

Madhuvanthi Muralidharan

A thesis in fulfilment of the requirements for the degree  
of Doctor of Philosophy

Graduate School of Biomedical Engineering

Faculty of Engineering

University of New South Wales

September 2021

#### ORIGINALITY STATEMENT

I hereby declare that this submission is my own work and to the best of my knowledge it contains no materials previously published or written by another person, or substantial proportions of material which have been accepted for the award of any other degree or diploma at UNSW or any other educational institution, except where due acknowledgement is made in the thesis. Any contribution made to the research by others, with whom I have worked at UNSW or elsewhere, is explicitly acknowledged in the thesis. I also declare that the intellectual content of this thesis is the product of my own work, except to the extent that assistance from others in the project's design and conception or in style, presentation and linguistic expression is acknowledged.

#### COPYRIGHT STATEMENT

I hereby grant the University of New South Wales or its agents a non-exclusive licence to archive and to make available (including to members of the public) my thesis or dissertation in whole or part in the University libraries in all forms of media, now or here after known. I acknowledge that I retain all intellectual property rights which subsist in my thesis or dissertation, such as copyright and patent rights, subject to applicable law. I also retain the right to use all or part of my thesis or dissertation in future works (such as articles or books).

For any substantial portions of copyright material used in this thesis, written permission for use has been obtained, or the copyright material is removed from the final public version of the thesis.

#### AUTHENTICITY STATEMENT

I certify that the Library deposit digital copy is a direct equivalent of the final officially approved version of my thesis.

UNSW is supportive of candidates publishing their research results during their candidature as detailed in the UNSW Thesis Examination Procedure.

Publications can be used in the candidate's thesis in lieu of a Chapter provided:

- The candidate contributed **greater than 50%** of the content in the publication and are the "primary author", i.e. they were responsible primarily for the planning, execution and preparation of the work for publication.
- The candidate has obtained approval to include the publication in their thesis in lieu of a Chapter from their Supervisor and Postgraduate Coordinator.
- The publication is not subject to any obligations or contractual agreements with a third party that would constrain its inclusion in the thesis.

The candidate has declared that **some of the work described in their thesis has been published and has been documented in the relevant Chapters with acknowledgement.**

A short statement on where this work appears in the thesis and how this work is acknowledged within chapter/s:

The work presented Chapter 5 is part of publication entitled "Neural activity of functionally different retinal ganglion cells can be robustly modulated by high-rate electrical pulse trains" published in the Journal of Neural Engineering in 2020 in which I am a joint first author. I contributed to three of the figures in the paper, and have used them (and the corresponding text) in this chapter. This work and the contributions of the second, joint first author has been described in a preamble to Chapter 5.

### Candidate's Declaration



**I declare that I have complied with the Thesis Examination Procedure.**

# Acknowledgements

I would like to take this opportunity to express my gratitude to several people who helped me in completing this PhD. First to my supervisors, Professor Nigel Lovell, Professor John Morley and Dr Tianruo Guo for their advice and guidance in my PhD journey. Thankyou Nigel, for leading such a collaborative team for me to thrive in, for your patience in replying to my relentless emailing, and for being the only willing participant in my discussions on American politics. The cohesive environment you have built, and the empathy and understanding you have shown towards me has made my PhD experience that much more enjoyable. Thankyou John, for always providing meaningful feedback and encouragement in my work and ensuring that the physical distance never impacted your supervision and guidance. Most importantly, thank you for giving me the opportunity to spend 3 hours every fortnight to sing the stresses of my PhD away alongside you and the Prosthetics. Last but not least, thankyou Tianruo. You have shown me a level of kindness and patience during my PhD that I did not think was possible. You have truly been my biggest cheerleader, oftentimes believing in me even when I didn't. Thank you for meticulously editing my numerous drafts of papers and abstracts, for buying me coffee and juice when I needed a break, and for checking to see if I had eaten during late-night experiments. These acts of compassion have meant a lot to me.

I would also like to extend my appreciation to other past and present members of GSBmE. Thank you to Dr Mohit Shivdasani and Dr David Tsai, for selflessly sacrificing many hours in teaching me various technical and practical aspects of my experimental work and bringing fresh perspectives and ideas when analysing and drawing conclusions from my data. Thank you to Dr John Yang, who taught me how to patch-clamp, and to Dr Aaron Gilmour and Dr Amr Al Abed for imparting their extensive wisdom on almost all aspects of the experiments and their patience in helping me debug the plethora of problems I encountered.

To my friends in LG, thank you for the memories over the last 4 years. I will cherish our lunch time discussions, the morning (and sometimes afternoon) coffee runs and the social gatherings. To my other friends in Sydney and interstate, thank you for maintaining my sanity, and for lending a much-needed ear when the going got tough. To Zehra, I wish you were here to share this moment with me but thank you for everything.

Finally, I would like to thank my family who have spent the last four years picking up the phone at all hours of the day only to tirelessly listen to my endless chatter about the experiment, the data, or in better moods, music, and gossip. To Anu, thank you for always understanding me, listening to me, and sticking by me. To Amma and Appa, thank you for giving me the confidence to start to this journey, and the support to continue it. I could not have done this without you.

# Abstract

Retinal implants aim to provide artificial vision to those profoundly blind by stimulating the residual network to elicit visual percepts. While human clinical trials have demonstrated encouraging results including the presence of visual percepts as well as partial visual restoration, the vision quality provided remains limited. One potential cause of this poor performance has been attributed to the indiscriminate activation of functionally-different retinal ganglion cell (RGC) types. To combat this problem, a promising strategy has been to design stimulation strategies that are capable of selectively, or preferentially, activating different cell types. One such approach to realise this goal has been through the use of high frequency stimulation (HFS) which was shown to be effective in preferentially activating two major retinal ganglion cell types– ON and OFF. While encouraging, the utility of the technique to target a broader range of cell types, and under different stimulation conditions and environments was still unclear.

The studies presented in this thesis were designed to improve the understanding of HFS-based preferential activation. Using in vitro whole-cell patch clamp of RGCs in mice (C57BL/6J and rd1), an investigation into whether HFS could be used to preferentially activate four major RGC types namely, ON-sustained (ONS), ON-transient (ONT), OFF-sustained (OFFS), and OFF-transient (OFFT), was undertaken. Results suggested that three of the four targeted cell types could be preferentially activated against the remaining population. A subsequent study documented the responses and the preferential activation capabilities of the aforementioned cell types when the high frequencies were modulated with short stimulation bursts, varying sequence orders and in a continuous waveform. It was shown that the ON (sustained and transient) RGCs typically exhibited more consistent responses and preferential activation regions irrespective of the frequency order, or when presented as a continuous waveform. A final study examined the responses of rd1 ON and OFF RGCs to HFS both with and without the presynaptic degenerate network. The network did appear to have an effect on the HFS-evoked responses, and particularly increased the variability of the responses which in turn affected the preferential activation of the cell types. Additionally, a comparison into the specific intrinsic properties between the rd1 and healthy RGCs found that these properties may differ between the cell groups. Overall, this thesis investigated the usefulness of HFS to preferentially activate different cell types and across various stimulation conditions and environments and found that HFS remains a viable stimulation technique to reduce indiscriminate activation of functionally-distinct cell types.

# Abbreviations

AC – amacrine cells

AIS – axon initial segment

ANOVA- analysis of variance

APT – action potential threshold

BC – bipolar cells

BS – brisk-sustained

BT - brisk-transient

CBC – cone bipolar cell

CBDC – charge balanced direct current

CR – classification ratio

DS – directionally-sensitive

e-STA - electrical spike-triggered average

GABA – Gamma aminobutyric acid

GCL – ganglion cell layer

HC – horizontal cells

HFS – high frequency stimulation

iGluR – ionotropic glutamate receptors

ILM – inner limiting membrane

INL – inner nuclear layer

IPL – inner plexiform layer

ISI - inter-spike interval

ITD - inter-trial delay

Kv – voltage-gated potassium channels

LVA – low-voltage activated

MEA - multielectrode arrays

mGluR6 – metabotropic glutamate receptor 6

MPDA - microphotodiode arrays  
Nav- voltage-gated sodium channels  
ONL – outer nuclear layer  
OFFS – OFF-sustained  
OFFT – OFF-transient  
ONS – ON-sustained  
ONT – ON-transient  
OPL – outer plexiform layer  
P - post-natal day  
PBS – phosphate buffer solution  
p-STA - photovoltaic STA  
Pt – Ir – platinum iridium  
RBC – rod bipolar cell  
RGC – retinal ganglion cells  
RMP – resting membrane potential  
RP – retinitis pigmentosa  
RPE – retinal pigment epithelium  
SEM – standard error of the mean  
SI - spike interval  
SNR – signal-to-noise ratio  
SOCB – sodium channel band  
STA – spike triggered average  
RCS – royal college of surgeons  
WT – wild-type

# Table of Contents

1	Introduction.....	15
1.1	Thesis Aims and Outline.....	16
1.1.1	Thesis Aims.....	16
1.1.2	Thesis Layout.....	17
2	Background.....	18
2.1	Visual System.....	18
2.1.1	Eye Anatomy.....	18
2.1.2	Retinal Physiology.....	18
2.2	Retinal Pigmentosa.....	24
2.2.1	Animal models.....	24
2.3	Retinal Implants.....	26
3	Survey of Stimulation Strategies to Differentially Activate Targeted RGC Types.....	29
3.1	Electrical Stimulation in Healthy Retina.....	33
3.1.1	Network-Mediated Stimulation.....	33
3.1.2	Direct Stimulation.....	38
3.1.3	Summary.....	44
3.2	Non-Electrical Stimulation.....	45
3.2.1	Optogenetic stimulation.....	45
3.2.2	Chemical Neurostimulation.....	45
3.2.3	Photothermal Stimulation.....	46
3.2.4	Micromagnetic Stimulation.....	46
3.3	Electrical Stimulation in Degenerate Retina.....	47
3.3.1	Retinal Remodelling.....	47
3.3.2	Electrical Stimulation.....	50
3.3.3	Summary.....	55
4	General Methods.....	56
4.1	Animal Preparation and Retinal Extraction.....	56
4.2	Patch Clamp Recordings.....	57
4.2.1	Patch Pipette Fabrication and Intracellular Solution.....	57
4.2.2	Whole-Cell Patch Clamp.....	57

4.2.3	Data Acquisition.....	58
4.2.4	Cell Classification .....	58
4.2.5	Synaptic Blockers .....	60
4.3	Extracellular Electrical Stimulation .....	61
4.3.1	Stimulating Electrode Fabrication.....	61
4.3.2	Stimulating Electrode Location.....	61
4.3.3	Threshold Stimulation .....	62
4.4	Data Analysis.....	63
4.4.1	Preferential Activation Maps .....	63
5	Preferential Activation of Four RGC types using HFS .....	67
5.1	Introduction.....	67
5.2	Methods.....	68
5.2.1	HFS Protocol .....	68
5.3	Results.....	69
5.3.1	Effect of Synaptic Blockers on Light Responses and Baseline Potential .....	69
5.3.2	HFS Responses of Four RGC Types .....	70
5.3.3	Preferential Activation of Four RGC Types .....	72
5.4	Discussion .....	73
5.4.1	Frequency and Amplitude-Dependent Responses .....	74
5.4.2	Preferential Activation of RGCs .....	75
5.4.3	Limitations .....	77
5.4.4	Future Work.....	78
5.5	Conclusions .....	79
6	RGC Responses to Temporally-Modulated HFS.....	80
6.1	Introduction.....	80
6.2	Methods.....	81
6.2.1	Extracellular Stimulation Protocols.....	81
6.2.2	Data Analysis.....	85
6.3	Results.....	88
6.3.1	RGCs Response to HFS in Static and Dynamic Conditions .....	88
6.3.2	Preferential Activation of RGCs with HFS under Static and Dynamic Conditions	92

6.3.3	RGCs Response to Different Frequency Orders .....	96
6.3.4	RGCs Response to Continuous HFS .....	101
6.3.5	RGCs Response to Optimised Dynamic HFS Waveform .....	110
6.3.6	Replication of a Pseudo-Randomised Spike Train .....	111
6.4	Discussion .....	113
6.4.1	Effects of High Frequency Modulation on the RGC Response and Preferential Activation Capabilities .....	113
6.4.2	Controlling RGC Activation with Optimised, Dynamic HFS Waveforms.....	117
6.4.3	Future Work .....	120
6.4.4	Conclusions .....	121
7	Response of rd1 RGCs to HFS .....	122
7.1	Introduction .....	122
7.2	Methods.....	123
7.2.1	Cell Classification .....	123
7.2.2	Synaptic Blockers .....	124
7.2.3	Extracellular Stimulation .....	125
7.2.4	Data Analysis.....	125
7.3	Results.....	127
7.3.1	Intrinsic Property Differences Between WT and rd1 RGCs .....	127
7.3.2	HFS in Degenerate Retina.....	129
7.3.3	Preferential Activation in Degenerate Retina.....	133
7.4	Discussion .....	134
7.4.1	Differences in Intrinsic Responses between WT and rd1 RGCs.....	134
7.4.2	HFS Responses in Degenerate Retina .....	137
7.4.3	Preferential Activation in Degenerate Retina.....	139
7.5	Future Work.....	140
7.6	Conclusions .....	140
8	Conclusions & Future Work.....	141
8.1	Conclusions .....	141
8.2	Future Work.....	146

# List of Figures

Figure 2.1 Schematic of the different retinal layers.....	19
Figure 2.2 Loss of photoreceptors in rd1 mouse retina.....	25
Figure 3.1 Family tree of different studies and corresponding stimulation methods to differentially activate retinal neurons. ....	30
Figure 4.1 Diagram showing classification of healthy RGCs based on their light response .	59
Figure 4.2 Representative OFF RGC classification in rd1 retina. ....	60
Figure 4.3 Location of the extracellular stimulating electrode. ....	62
Figure 4.4 Example individual and population response heat maps in response to HFS.....	65
Figure 5.1 Light response and baseline potential of four types of RGCs. ....	70
Figure 5.2 Population response maps of four RGC types to HFS.....	71
Figure 5.3 Preferential activation map of functionally-distinct RGC types. ....	73
Figure 6.1 Diagram illustrating the linearly increasing frequency modulation protocol for a given amplitude.....	82
Figure 6.2 Diagram of the 40-40-60 ms protocol for a given amplitude. ....	84
Figure 6.3 Diagram of pseudo-randomised spike train and the corresponding designed stimulus waveform .....	85
Figure 6.4 Diagram of spontaneous activity calculation.....	86
Figure 6.5 Population response maps of ON and OFF RGCs in response to HFS under static and dynamic conditions.....	89
Figure 6.6 Population response maps of four RGC types in response to HFS under static and dynamic HFS conditions. ....	91
Figure 6.7 Preferential activation maps for the ON and OFF RGCs in response to HFS under static and dynamic conditions. ....	93
Figure 6.8 Preferential activation maps of four types of RGCs in response to HFS under static and dynamic conditions.....	95
Figure 6.9 Population response maps of ON and OFF RGCs in response to HFS presented with different frequency orders. ....	97

Figure 6.10 Preferential activation maps of ON and OFF RHCs in response to HFS presented with different frequency orders. ....	98
Figure 6.11 Population response maps of four RGCs in response to HFS presented with different frequency orders .....	100
Figure 6.12 Preferential activation of four RGC types in response to HFS presented with different frequency orders .....	101
Figure 6.13 Population response maps of ON and OFF RGCs in response to continuous HFS. ....	103
Figure 6.14 Preferential activation maps of ON and OFF RGCs in response to continuous HFS. ....	104
Figure 6.15 Population response maps of four RGC types in response to continuous HFS. ....	105
Figure 6.16 Preferential activation maps for four RGC types in response to continuous HFS .....	106
Figure 6.17 Population response maps indicating the recovery properties of ON and OFF RGCs in response to continuous HFS.....	108
Figure 6.18 Population response maps indicating the recovery properties of four RGC types in response to continuous HFS. ....	109
Figure 6.19 Response of four RGC types to a dynamic, high frequency-modulated waveform. ....	111
Figure 6.20 ON and OFF RGC responses to a high-frequency modulated waveform designed to replicate the active and inactive regions of a pseudo-randomised spike train.....	112
Figure 6.21 Normalised spike counts of the ON and OFF RGC populations to 40-40-60 ms dynamic waveform. ....	118
Figure 7.1 Classification of rd1 ON and OFF RGCs based on their dendritic stratification, their rhythmic spontaneous activity, or both. ....	124
Figure 7.2 Representative rd1 ON and OFF RGCs before and after the application of synaptic blockers. ....	125
Figure 7.3 Baseline potentials of WT and rd1 ON and OFF RGCs before and after synaptic blockers. ....	128
Figure 7.4 Responses of WT and rd1 ON and OFF RGCs to depolarising somatic current injections.....	129

Figure 7.5 Population response maps of all rd1 RGCs in response to HFS before and after synaptic blockers. ....	131
Figure 7.6 Population response maps of rd1 ON and OFF RGCs in response to HFS before and after synaptic blockers.....	131
Figure 7.7 Population response maps of synaptically-isolated WT and rd1 ON and OFF RGCs in response to HFS. ....	132
Figure 7.8 Preferential activation maps of rd1 ON and OFF RGCs in response to HFS before and after synaptic blockers.....	134

# List of Tables

Table 3.1 Summary of electrical and photovoltaic-based studies (corresponding to the studies highlighted in black and red from Figure 3.1) investigating differential activation of retinal cell types .....	31
Table 3.2 Summary of degenerate studies on stimulation thresholds.....	52
Table 6.1 Summary of frequencies presented in each phase for the linearly increasing, linearly decreasing and randomised frequency modulation protocols. ....	83
Table 6.2 Summary of the spike numbers used in the design of the pseudo-randomised spike trains.....	84
Table 6.3 Preferential activation statistic values for RGC types under different stimulation conditions.....	94
Table 6.4 Summary of the preferential activation statistic values for the different RGC types during the linearly increasing, linearly decreasing and randomised modulation protocols. ..	99
Table 6.5 Summary of preferential activation statistics for four RGC types across the three phases of the linearly changing frequency modulation protocol.....	107
Table 6.6 Recovery statistic of cell types.....	109
Table 7.1 Summary of cell numbers identified with each criteria .....	124
Table 7.2 Difference statistic corresponding to HFS responses .....	130

# 1 Introduction

Out of the five primary senses, visual perception is arguably the most important sense humans possess. Given the reliance on vision to accomplish day-to-day activities, progressively blinding diseases such as retinitis pigmentosa (RP) [1] can have a profound and debilitating effect on a person's quality of life. Retinal implants aim to provide artificial vision to those with profound vision loss by electrically stimulating the remaining neurons in the diseased retina. Human trials have demonstrated the ability of these devices to elicit visual percepts, and achieve rudimentary tasks such as object detection, localisation, or navigation [2-6]. However, the level of artificially-elicited function is still limited and does not warrant the implantation of these devices in majority of the patients [7].

While there are many potential causes that can be attributed to this poor performance, one major reason may be the inability of implants to avoid indiscriminate activation of functionally-different retinal ganglion cells (RGCs) which uniquely encode different aspects of the visual scene [8]. For example, the four major cell types - ON-sustained (ONS), ON-transient (ONT), OFF-sustained (OFFS) and OFF-transient (OFFT) - that constitute the majority of the mammalian RGCs [9] all subserve different roles in vision. Specifically, ON and OFF RGCs respond to changes in luminance [10], while sustained cells detect the form, size and shape of the visual input, and the transient cells detect motion and changing scenes [11-13]. Given the specialisation and distinctive sensitivities of these functionally diverse cell types, the indiscriminate activation likely sends confusing retinal outputs to the brain potentially manifesting as poor artificial vision. A suggested approach to combat this problem has been to design stimulation strategies that are capable of selectively or preferentially activating functionally-different RGCs (e.g., ONS, ONT, OFFS and OFFT) in an attempt to replicate appropriate neural encoding. The ability to precisely control different retinal pathways in a retinal prosthesis is a key factor in eliciting improved visual percepts and in doing so, improve the quality-of-life for implant recipients.

High frequency stimulation (HFS) was previously shown to preferentially activate the ON and OFF RGCs across different high frequencies (1 – 8 kHz) and amplitude (10 – 240  $\mu$ A) combinations [14, 15]. However, the work to date has been limited to only preferentially activating the ON and OFF RGCs, with relatively idealistic stimulation conditions in healthy retina.

This thesis presents three studies which tests the performance of HFS to preferentially activate a broader range of RGC types (ONS, ONT, OFFS, and OFFT), under dynamic frequency

modulation and shorter stimulation durations and finally, in a more clinically-relevant degenerate mouse retina.

## 1.1 Thesis Aims and Outline

### 1.1.1 Thesis Aims

A promising strategy to potentially improve the vision provided by current retinal implants is to preferentially activate functionally-distinct RGC types. One approach to achieve this has been through HFS which has proven to be effective in preferentially targeted two major RGC types – ON and OFF cells – using specific high frequency and amplitude combinations [14, 15]. The work in this thesis aims to extend previous work by assessing the utility of HFS to activate a broader range of cell types, under varying stimulation conditions, and in a more clinically-relevant degenerate environment. To do this, the thesis aims to answer the following four questions:

**Aim 1: Can HFS be used to preferentially activate four functionally-distinct RGC types (ONS, ONT, OFFS, and OFFT) in healthy retina?**

Both Twyford et al. [14] and Guo et al. [15] showed that ON and OFF RGCs can be preferentially activated with respect to each other when stimulated with specific high frequencies and amplitudes. However, previous studies, for example Baden et al. [8] have indicated the large functional diversity of RGCs which are hypothesised to underlie some of the variability in the electrical responses [16]. Of these different cell types, sustained and transient (along with ON and OFF) RGCs constitute majority of the primate [9] and mice [8] population and subserve different roles in vision [12]. To assess the viability of HFS to preferentially activate a broader range of functionally-different RGCs, I further classified the ON and OFF RGCs as sustained and transient cells.

**Aim 2: How do different RGC types (ONS, ONT, OFFS, and OFFT) respond to a modulating frequency, and can these cell types be reliably controlled and preferentially activated with a dynamic waveform based on short, frequency bursts in healthy retina?**

Temporally-modulated amplitude waveforms have been so far used to extract distinct electrical filters from RGCs [17-19] or other spatiotemporal characteristics [20]. To the best of my knowledge, none of the studies (direct or indirect) have used temporal modulation of high frequencies as a means to preferential activate RGCs nor attempted to do so under practical stimulation conditions. For example, the stimulation parameters used in the HFS studies have so far been idealistic – the cells are stimulated at rest and the stimulation duration is also relatively long at 300 ms [15]. In this study, I was interested in studying how different RGC

types responded to continuous HFS with frequency modulated every 40 ms, under different frequency orders, and how this affected their ability to be preferentially activated.

**Aim 3: Do synaptically-isolated degenerate and healthy ON and OFF RGCs differ in their intrinsic characteristics and their HFS response?**

One of the over-arching assumptions made when designing stimulation strategies for retinal implants are that the RGCs remain stable during the course of degeneration. This stability implies that the intrinsic properties driven by the ionic composition of the cells are similar between healthy and degenerate retina. Different groups have studied the intrinsic property differences between healthy and degenerate retina but either did not classify the cell type [21], pharmacologically block the presynaptic network [22] or study the intrinsic properties in the presence and absence of the network [23]. Using characteristic intrinsic properties such as the baseline potential and response to somatic current injections, I explored the effects of the healthy and degenerate network on the intrinsic properties of the ON and OFF RGCs. Additionally, I compared the synaptically-isolated RGC HFS response to further identify if potential intrinsic differences between healthy and degenerate RGCs exist.

**Aim 4: How do degenerate ON and OFF RGCs respond to HFS and does their response change based on the presence or absence of the degenerate network and effect their ability to be preferentially activated?**

While numerous electrical stimulation studies have been conducted on degenerate rd1 mice [24-26], rd10 mice [16, 17, 27, 28], P23H rats [29], RCS rats [30, 31] and S334-ter line 3 rats [32, 33], none of the studies have attempted to preferentially activate functionally-distinct RGC types in the degenerate retina. In the final study I investigated the response of synaptically-intact and synaptically-isolated ON and OFF RGCs to HFS and their resulting preferential activation capabilities.

### 1.1.2 Thesis Layout

Chapter 2 provides an overview of the visual pathway, anatomy of the eye and the retina. Alongside this, a brief background into RP, degenerate animal models and visual prosthesis is also provided. Following this, in Chapter 3 a detailed review of studies attempting to selectively, or preferentially activate targeted cell types using electrical stimulation is discussed. Chapter 4 provides an overview of the general methods that were common across all the experiments in the thesis. Aims 1 – 4 are addressed in Chapter 5 – 7 respectively and each chapter contains additional chapter-specific methods, results and discussion based on the data from the study. Chapter 8 summarises the key findings from the thesis, the implications of the results and future directions of the work.

## 2 Background

### 2.1 Visual System

#### 2.1.1 Eye Anatomy

The eye consists of multiple structures which work together to convert visual images into electrical pulses which are then processed by the brain [34]. Light first enters the eye through the transparent cornea which encapsulates the pupil, iris and anterior chamber and is the primary light-focusing structure in the eye [34]. The cornea, alongside the lens, ensures that the light is focussed to the back of the eye. The iris is located above the ciliary body and regulates the amount of light entering the eyes by adjusting the pupil size. Under low light, it dilates the pupil to let more light in and under bright light, constricts the pupil to let less light in. The ciliary body is located between the iris and the choroid and secretes aqueous humor to oxygenate the cornea and the lens [34]. The choroid is located behind the retina and provides nutrients and oxygen. The sclera surrounds and protects the eye, and the vitreous body fills the eye between the lens and the back of the eye with a jelly-like substance. Lastly, the retina lies in the inner-most layer of the eye and is responsible for the conversion of the visual stimuli into electrical signals to be sent to the brain. As such, it is the most complex and pivotal structure in the eye.

#### 2.1.2 Retinal Physiology

The retina contains five main cell classes namely – the photoreceptors, bipolar cells (BCs), amacrine cells (ACs), horizontal cells (HCs) and RGCs. These cell classes are organised into different layers in the retina, with the photoreceptor cell bodies in the outer nuclear layer (ONL), the BCs, ACs and HCs in the inner nuclear layer (INL) and the RGCs in the ganglion cell layer (GCL). The synaptic connections between the photoreceptors, BCs and HCs takes place in the outer plexiform layer (OPL) and the synaptic connections between the BCs, ACs and GCs takes places in the inner plexiform layer (IPL) [35]. The retinal pigment epithelium (RPE) is located between the photoreceptors and the choroid. The RPE is heavily pigmented and therefore absorbs any stray light and prevents reflection back to the retina [35]. Figure 2.1 shows a diagrammatic representation of the layers of the retina and the cell types.

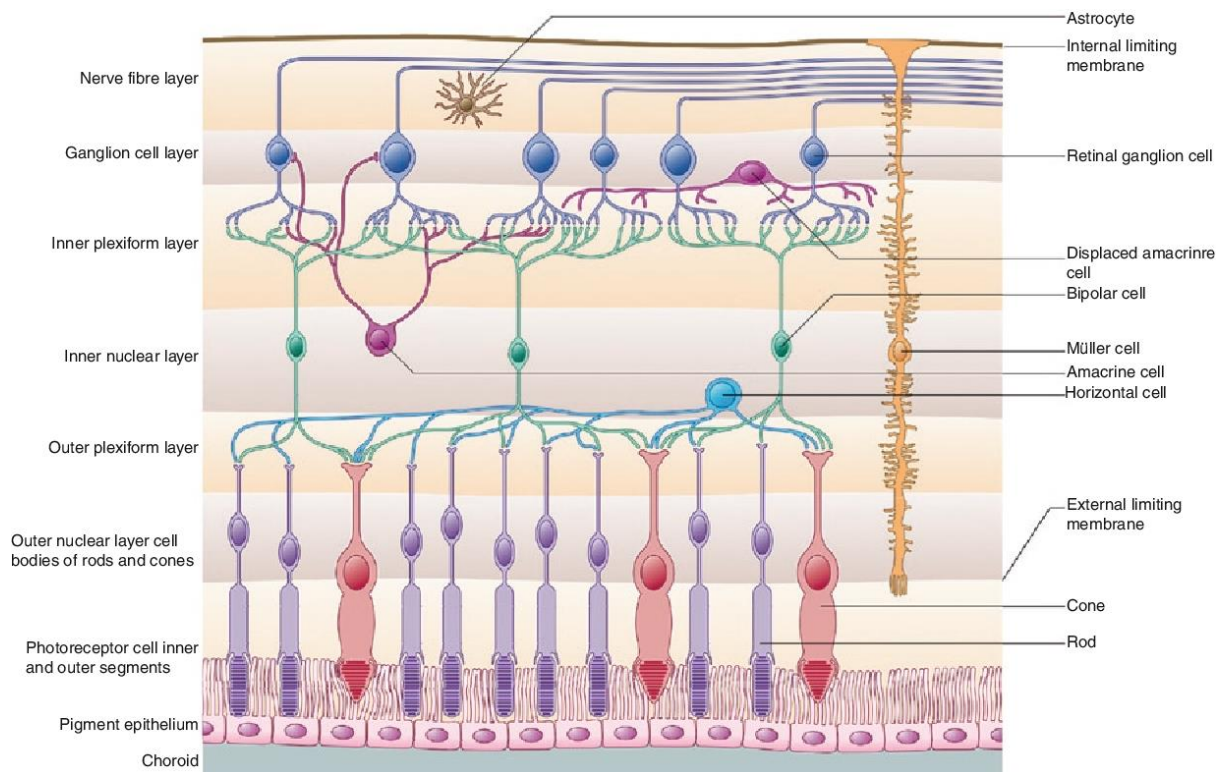


**Figure 2.1 Schematic of the different retinal layers.** The photosensitive cone and rod photoreceptors convert the light into electrical signals. The signal is then carried and appropriately modulated through the HCs, ACs and BCs and finally the RGCs which reside in the inner ganglion cell layer of the retina. The axons of the ganglion cells converge and carry the electrical signal to the brain for higher visual processing [36].

The structure of the retina is counter-intuitive, in which the photoreceptors responsible for the conversion of light into electrical signals (phototransduction) lie at the back of the retina. As such, light is required to pass through all the layers of the retina before being received by the photoreceptors. When the light hits the photoreceptors, the light-sensitive photopigments in the cells undergo conformational changes causing hyperpolarisation of the photoreceptors [35]. This triggers a cascading of events between the photoreceptors and the interneurons (BCs, ACs and HCs) and finally the RGCs whose axons form the optic nerve that sends information to the higher visual centres in the brain [37].

### 2.1.2.1 Photoreceptors

The retina contains two types of photoreceptors – rods and cones. Rods are sensitive to low-light and therefore mediate night vision, whereas cones are sensitive to bright-light and mediate day vision [35]. Structurally, photoreceptors have an outer segment, inner segment, cell body and a synaptic terminal. The outer segment is located in the distal part of the retina and contains visual pigments required for phototransduction [38, 39]. In rods, the photosensitive pigment is called rhodopsin while in cones, it is called photopsin. The inner

segment contains mitochondria and other organelles, the cell body contains the nucleus, and the synaptic terminal lies in the most proximal region of the retina, in which the BCs and HCs synapse [35, 39].

In the human retina, there are three types of cones which are sensitive to different wavelengths namely long-wavelength (L), medium-wavelength (M) and short-wavelength (S). They are also referred to as red, green, and blue cones [40]. The density of these cones is maximised at the fovea (located in the central retina) and is the region of highest visual acuity [35]. The density of the cones is lowest in the peripheral region. Conversely, rods (of which there is only one type) are located outside the fovea and dominant in the peripheral regions. Comparing rods and cones, cones are less-sensitive but faster-responding than rods to light. The convergence of rods and cones onto RGCs is higher in rods than cones i.e., many rods converge on a single RGC whereas fewer cones converge on an RGC. As such, the spatial resolution in the rod visual pathway is lower than in the cone pathway [41].

In the dark or 'inactive' state, photoreceptors are kept in a depolarised state by the presence of cyclic GMP-sodium channels which allows sodium ions to flow freely across the cell membrane [35]. When light hits the photoreceptors however, the photopigments in the outer segments undergo conformational changes ultimately leading to the closure of the cyclic GMP-sodium channels and the hyperpolarisation of the photoreceptor [42]. The primary neurotransmitter released by photoreceptors is glutamate, which is released in the dark due to the depolarised state of the photoreceptors but ceases in the light due to the hyperpolarisation [35]. BCs and HCs synapse with the photoreceptors in the OPL and the cessation of glutamate due to the light triggers the next level of signalling in the inner retina.

#### *2.1.2.2 Bipolar Cells*

The mammalian retina contains 12 different BC types, 11 of which synapse with cones and 1 with synapses with rods [43, 44]. Broadly, these cell types can be classified into three groups – the ON cone bipolar cells (ON CBC) and the OFF cone bipolar cells (OFF CBC) which synapse with the cones, and the ON rod bipolar cells (ON RBC) which synapse with the rods. The ON and OFF BCs also differ in their responses to light, mediated by their different glutamate receptors. ON BCs express sign-inverting metabotropic receptors (mGlu6) which keep the cell hyperpolarised when the photoreceptors release glutamate (i.e., in the dark), but depolarised in the absence of glutamate (i.e., in the light). On the other hand, OFF BCs express sign-conserving ionotropic receptors (iGlu6) therefore the cell membrane mimics the state of the photoreceptors (hyperpolarised in the light, depolarised in the dark) [35, 40, 41]. These different receptors are the first distinction between the parallel ON and OFF pathway which are responsible for detecting light images on a darker background, and dark images on

a lighter background, respectively [10]. The ON and OFF classes can be further subdivided into their sustained and transient components (ONS, ONT, OFFS, and OFFT) [41, 45, 46]. These differences are thought to arise from either (1) differences in the glutamate receptors, specifically ionotropic AMPA receptors related to sustained light responses and kainate receptors related to transient light responses observed in OFF CBCs [47] or (2) through an inhibitory feedback loop in which a subpopulation of displaced amacrine cells truncate the sustained excitatory response to the ganglion cells [48].

Morphologically, these four BC types have axon terminals that stratify in different regions of the IPL. The IPL has two distinct regions – the upper region closest to the INL is referred to as the OFF sublamina and the lower region closest to the GCL referred to as the ON sublamina [49]. The axons of the ON and OFF BCs terminate in their respective sublaminae, OFFS BCs axons terminate in the peripheral OFF sublamina, ONS BCs in the inner ON sublamina and ONT and OFFT BCs in the centre of the IPL [40, 50, 51].

#### *2.1.2.3 Horizontal Cells*

In the mammalian retina, there are two main types of HCs (HI and HII) which together work to modulate the visual signal. Anatomically, HI types have smaller dendritic trees and have synapses primarily with M and L photoreceptor cones, while their thick axons terminate in the rods. Conversely, HII types have more intricate dendritic trees and primary synapse with S photoreceptor cones while their shorter axons terminate in cones [38]. Broadly, the function of HCs is to provide inhibitory feedback to the photoreceptors to ensure they do not become saturated under bright light and essentially work within a physiological operating range. This is achieved by monitoring the average illumination on the retina and then subtracting a proportional amount from the local photoreceptor signal [40, 44]. HCs also contribute to “centre-surround” phenomenon due to the lateral inhibition of the surrounding photoreceptors. For example, when a centre cone is excited, the feedback signal of the HC is increased to both the centre and the neighbouring cones. Given that the signals from all the cones are carried to the BCs and the RGCs, this means the RGCs laying directly under a spatially-confined stimulus will be excited while the surrounding RGCs will be inhibited giving rise to the centre-surround organisation [44]. The exact mechanism in which the HCs feedback onto the photoreceptors is still under investigation [40].

#### *2.1.2.4 Amacrine Cells*

There are ~30 different types of ACs which modulate the RGCs by either synapsing on them directly, or indirectly through BCs or other ACs [41, 44, 52, 53]. Despite this diversity, ACs are typically grouped with respect to their dendritic field diameters specifically – narrow-field (30 – 150  $\mu\text{m}$ ), small-field (150 – 300  $\mu\text{m}$ ), medium-field (300 – 500  $\mu\text{m}$ ) and wide-field (>500  $\mu\text{m}$ )

[54]. In vertebrate retina, the majority of the ACs use inhibitory neurotransmitters gamma-aminobutyric (GABA) or glycine [35, 54]. Glycinergic ACs tend to be small-field and receive inputs from BCs and transmit to the RGCs as well as other ACs and BCs. The most common glycinergic ACs is the All AC which plays a pivotal role in distinguishing the ON and OFF pathways in the rod network by connecting with both the ON and OFF CBCs [35]. The importance of this All AC – ON CBC network will be further discussed in this thesis, particularly in network-mediated electrical stimulation studies. On the other hand, GABAergic ACs tend to be wide-field and interact with many more BCs and GCs [35].

#### 2.1.2.5 *Retinal Ganglion Cells*

The RGCs are the final output neurons of the retina and at the most basic level, can be physiologically classified based on their light response [10, 55, 56], and morphologically classified based on their dendritic structure [57-60].

In 1938, Hartline et al. [10] first established three types of RGCs based on their light responses. Namely, ON RGCs which respond with a high frequency burst at the onset of light followed by a sustained response for the duration of the light stimulus, OFF RGCs which only respond at the cessation of light and ON-OFF RGCs which respond both to the onset and cessation of the light. Following this, Kuffler et al. [55] found distinct receptive fields of the ON and OFF RGCs specifically, ON centre-OFF surround and OFF centre-ON surround. Later studies further classified the receptive fields of ON and OFF RGCs as those that have linear summation with a 'transient' response to light (Y or  $\alpha$ -RGCs) or non-linear summation with a 'sustained' response to light (X or  $\beta$ -RGCs) in cat retina [59-61] and occupied distinct regions in the IPL [53]. The sustained and transient cells were found to be analogous with midget and parasol cells in the primate retina, respectively [62]. In the mouse retina, Krieger et al. [63] showed the presence of four  $\alpha$ -RGCs – ON sustained, ON transient, OFF sustained, and OFF transient – all which had a unique light response and dendritic stratification. However, it is not clear what the equivalent homologs are in primate retina.

Apart from these major cell types, other studies have further classified the RGCs either based solely on their dendritic structures [57, 58, 64, 65], light response [56] or a combination of both light and morphological structure [8] with the latter study proposing ~32 functionally-different RGC types in the mouse retina. In addition to these RGC types, another important cell class are the intrinsically photosensitive RGCs (ipRGCs). These cells express melanopsin and can respond to light without photoreceptor input [66]. As such, ipRGCs are also thought of as a ganglion cell photoreceptor which work to mediate the circadian rhythm and other non-image forming functions [67]. Given the sparsity of ipRGCs (~0.2 – 4% in mammalian retina [68, 69]),

they were not identified as a separate RGC type but were included as part of the broader RGC population during the analysis.

In addition to morphological and visual response differences, RGCs also have distinct intrinsic electrophysiological differences. Two commonly used intrinsic electrophysiological properties are the resting membrane potential (RMP), or baseline potential, which reflects the individual ionic components intracellular and extracellular to the cell, and the permeability of the cell [70]. The second property is the RGCs response to depolarising and/or hyperpolarising current steps which are injected intracellularly into the cell soma. These properties have been shown to be unique to the different RGC types using *in vitro* [22, 57, 58] and *in silico* [71, 72] methods. With respect to the *in vitro* studies, the results were based on RGCs which were connected to the retinal network, i.e., received external synaptic input. To identify the role that the synaptic input played in shaping the response of these electrophysiological properties, specifically the baseline potential, Margolis et al. [73] compared the baseline potential of ON and OFF RGCs with and without pharmacological blockade of the synaptic network and found that the synaptic inputs did influence the baseline properties of the cell types. In the same study, they further found that in the absence of synaptic inputs, OFF RGCs exhibited regular spontaneous activity and strong post-inhibitory rebound firing compared to the ON RGCs.

The differences identified in the intrinsic electrophysiological properties are in part due to the ionic channel compositions of the RGCs. To this end, different studies have used *in vitro* [73, 74] and *in silico* [71, 72] methods to identify ionic channel differences between RGC types. For example, Margolis et al. [73] showed that the persistent sodium current  $I_{NaP}$  is active even at rest for the OFF RGCs and therefore, generates the maintained spontaneous firing of the OFF but not ON RGCs. With respect to the rebound firing properties of the OFF RGCs, studies have suggested different ionic channel contributions namely the combined sodium and potassium current  $I_h$  [71], and calcium currents -  $I_{CaT}$  [71] and low-voltage activated (LVA) channels [72, 74]. In addition to these differences, other studies have focussed on identifying the presence and relative density of specific ionic channel subtypes, particularly the sodium channel subtypes (Nav). Studies have indicated the presence of Nav 1.1 [75, 76], 1.2 [75-77], 1.6 [75-77], and 1.8 [78] channels in different regions of adult mice [78] and rat [75-77] RGCs. Of these subtypes, only Nav 1.6 channels were quantitatively compared between functionally-identified RGCs. Specifically, Raghuram et al. [79] compared the relative density of the Nav 1.6 channels in the axon initial segment (AIS) between  $\alpha$ -ON and OFF RGCs in the mouse, however, did not find any significant difference.

Previous studies have shown that Nav 1.6 channels aid in maintaining sustained firing potentially due to a resistance to slow activation [80], larger persistent currents [80, 81], and presence of a resurgent current which aids in a faster transition from the inactive to active

states [80, 81]. As such, it is likely that a cell's ability to follow high frequency pulse trains (as used in this thesis) rely at least in part, on the presence of Nav 1.6. Furthermore, the differential response of the different types of RGCs may be able to be attributed to the relative density of this sodium channel subtype and across different morphological compartments. The role of Nav 1.6 channels in the differential response of ON and OFF RGCs is further discussed in Chapter 3, Section 3.1.2.2.3 and Chapter 6, Section 6.4.1.3.

## **2.2 Retinal Pigmentosa**

RP is an inherited and progressive disease that has a prevalence of approximately 1 in 4000 people [1] and can be inherited as an autosomal-dominant (30-40%), autosomal recessive (50-60%) or X-linked (5-15%) trait [1]. Around 45 different genes were found to cause RP, however three genes – rhodopsin (25% of autosomal-dominant RP), USH2A (20% of autosomal-recessive) and RPGR (70% of X-linked) – were found to account for ~30% of all RP cases [1].

The disease itself is characterised by the loss of photoreceptors and retinal pigment deposits which are largely concentrated in the peripheral retina but spares the central retina [82]. Typically, the rods degenerate first followed by secondary degeneration of the cones. Clinically, this implies that the patient loses their night vision before losing their day vision [82]. The disease progression typically occurs over three stages – early stage, middle stage, and late stage [82]. In the early stage, the primary symptom is night blindness due to the degeneration of rods. The onset of the early stage may present in the younger or adolescent years [1, 82]. In the middle stage, there is progressive loss in peripheral vision during both day and night. By the end stage, the patients become increasingly debilitated due to the complete loss of peripheral vision leading to tunnel vision [82]. While RP is largely associated with the loss of photoreceptors, studies have shown that the degeneration of photoreceptors triggers a long process of retinal remodelling of the inner retinal network [83-85]. An overview of these changes, and the challenges they pose with respect to electrical stimulation are discussed further in Chapter 3, Section 3.3.

### **2.2.1 Animal models**

Different animal models have been used to study retinal degeneration and aid in designing restorative therapies. While higher-order mammals including dogs and cats, and recently, monkeys, have been shown to have naturally-occurring hereditary retinal degenerations similar to human RP [86-88], they are limited in their availability. Additionally, these animal models tend to have relatively long progression of disease (over years) which makes them potentially attractive models for gene therapy strategies which aim to rescue the degenerate

photoreceptors [89, 90], however have more limited value for disease progression or other electrical stimulation strategies. To this end, degenerate rat models such as the RCS, P23H and S334ter rats have a shorter time scale with regards to the progression of disease [86] and are commonly used to study and tailor intervention strategies such as electrical stimulation strategies for a retinal implant [31, 32, 91]. However, they are not as well studied as the degenerate mice models, particularly the rd1 and rd10 mice which will be the focus of this section.

### 2.2.1.1 rd1 mouse model

The rd1 mouse, first discovered in 1966 by Keeler et al. [92]; is an inherited retinal degenerative strain and contains mutations in the rod photoreceptor cGMP phosphodiesterase 6 (PDE6)  $\beta$ -subunit gene [93] analogous to the human autosomal recessive gene [94]. Deficiency in this gene is thought to increase concentrations of cGMP in the outer segments of the retina leading to rod death [95]. The photoreceptor cell death is early and quick in the rd1 mice with the photoreceptor degeneration beginning at ~P10, following by complete loss by ~P21 [96, 97]. Figure 2.2 indicates the loss of photoreceptors in the diseased rd1 mouse retina compared to the healthy C57BL/6J retina.

The relatively fast progression of disease in the rd1 mouse is a double-edged sword – it allows the entire progression of disease to be studied in a short period of time, but equally leaves limited time to capture subtle changes in the photoreceptor death and synaptic circuitry. Despite this, the strain remains one of the most extensively studied animal models which in itself becomes advantageous because of the large database containing the morphological and electrophysiological changes across age and degeneration.

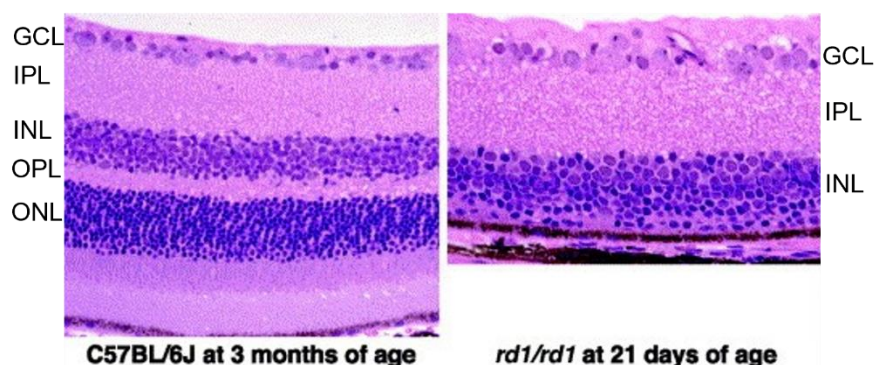


**Figure 2.2 Loss of photoreceptors in rd1 mouse retina.** (A) Vertical cross-section of retinal layers in the healthy C57BL/6J mouse. (B) Vertical cross-section of degenerate rd1 mouse retina in which there is a clear loss in the photoreceptors and ONL. GCL, Ganglion Cell Layer; IPL, Inner Plexiform Layer; INL, Inner Nuclear Layer; OPL, Outer Plexiform Layer; ONL, Outer Nuclear Layer. Adapted from [98].

### 2.2.1.2 *rd10 mouse model*

The rd10 mouse has a similar mutation in the  $\beta$ -subunit of the rod photoreceptor cGMP phosphodiesterase 6 gene and is also autosomal recessive, however, has a slower progression of degeneration than the rd1 strain [98, 99]. Here, the photoreceptors begin degenerating at ~P16 and there is a complete loss by ~P60 [98, 99]. The slower progression of disease has been thought to be a better reflection of the progression in human RP and particularly useful for therapeutic strategies that aim to use gene therapy to save the degenerating photoreceptors [100].

### 2.2.1.3 *Mouse model used in thesis*

The use of the degenerate model in this thesis was to investigate the intrinsic intracellular and HFS extracellular responses of the degenerate RGCs and compare these responses to the healthy RGCs. The study was not designed to understand the mechanisms or characterise the responses with respect to the level of degeneration but simply to gain an overall understanding of how degenerate RGCs respond to the intracellular and extracellular stimulation. As such, the model that was chosen for this thesis was the rd1 mouse primarily because of the faster disease progression which allows us to capture the response over the entire course of degeneration.

## 2.3 Retinal Implants

Retinal implants are a promising strategy to restore vision for patients with RP by attempting to generate activity in surviving RGCs through electrical stimulation and in turn, evoking visual percepts or phosphenes [101-104]. The basic retinal prosthesis works by artificially converting a captured image to electrical pulses and sending these pulses through to an implanted electrode in the retina to stimulate the cells. Generally, the location of the implanted electrode array is used to classify the 'type' of retinal implant namely - epiretinal, subretinal and suprachoroidal [105, 106].

The electrode array in an epiretinal implant is located on the inner surface of the neurosensory retina and therefore closest to the RGCs and their axons. The primary advantage of epiretinal implants is their close contact with the RGCs which allows them to bypass the damaged outer retinal network [106]. The most commonly known epiretinal implants include Argus II [107], Intelligent Medical Implants (IMI) [108] and Epiret3 [109] devices.

In subretinal implants, the electrode array is located between the photoreceptor layer and the RPE [106]. Subretinal implants typically take advantage of the surviving inner retinal network to stimulate the RGCs. Nevertheless, there have been different subretinal implants that have reached clinical trials, all of which use microphotodiode arrays (MPDAs) to drive the neurons

(ASR, PRIMA, Alpha IMS). The basic function of an MPDA is to detect light and convert the luminance level into a proportional electrical signal to stimulate the cells. Therefore, MPDA-based implants usually do not require external cameras to capture the visual image [106]. A notable exception to this is the Photovoltaic Retinal Implant (PRIMA) which still requires an external camera to process visual information. The processed images are then sent to the MPDA chip using infrared pulses via a digital projector [110]. Other MPDA-based subretinal implants that have advanced to clinical studies include the Artificial Silicon Retina (ASR) [111] and Alpha IMS [7].

Electrode arrays in suprachoroidal implants are placed between the choroid and the sclera. The suprachoroidal space is furthest from the inner retina and therefore has the least likelihood of causing damage to the retina [106]. However, the pitfall with this increased distance is the larger perceptual threshold [112]. The two suprachoroidal implants which are currently undergoing clinical trials are Bionic Vision Technologies device [113] and the Suprachoroidal Transretinal Stimulation system [114].

Human trials of these devices indicate that tasks such as object detection, localisation, and coarse navigation [2-6, 109, 114] are achievable. However, the visual benefit remains low [7]. Different groups across the world are currently attempting to improve the performance of retinal stimulation by optimising both the hardware and software components of implanted electrode arrays. One improvement in hardware for example, has been the increase of visual angle and pixel density. The visual angle in the Argus II prostheses is currently at 20°. However, previous studies using computational modelling have indicated a minimum visual angle of 30° to allow for ease in mobility and navigation [115, 116]. To this end, Lohmann et al. [117] designed a wide-field epiretinal electrode array that increased the visual angle from 20° in the Argus II prosthetic to 37.6°. A further extension of this was through the Polyretina prosthesis which aimed to increase both the visual angle and pixel density using a wide-field, high-density (10, 498 photovoltaic pixels) curved photovoltaic epiretinal prosthesis that increased both the visual angle (~43.6°) whilst also eliciting network-mediated RGC responses to single-pixel illumination [118]. More recently, a clinical trial was conducted using the newly-developed IntelliMicro smart visual implant with a higher-density (256 electrodes) epiretinal electrode array [119]

Despite this significant technical progress, it is important to note that these advances, particularly in the use of high-density arrays do not automatically translate to a higher visual acuity or resolution [106, 120]. For example, it has recently been suggested that engineering-based optimisations of prosthetic devices alone might not be able to significantly improve the artificial vision but rather, requires a deeper understanding of the biological pathway and the response of different retinal neurons to electrical stimulation [120].

One reason behind the push to gain a better understanding of the electrical response of the neurons being stimulated is because the electrical response of the cells is (a) not analogous with the visual response of the cells [121, 122] and (b) are diverse in their electrical responses themselves [121]. This diversity in responses becomes increasingly problematic when attempting to solve problems such as indiscriminate activation of functionally-different RGC types, which has been shown to potentially degrade the vision quality provided by implants [123, 124]. To this end, different groups are focussed on designing stimulation strategies in attempts to selectively, or preferentially, activate the functionally-distinct RGCs [15, 17, 31, 125-127]. Importantly, in doing so, these studies also add to the knowledge bank of electrical responses of the retinal neurons and increase understanding in the “electrical” pathway of the retina. In the next section, a survey of the past studies pursuant to selective or preferential activation of RGC types will be discussed.

### **3 Survey of Stimulation Strategies to Differentially Activate Targeted RGC Types**

One approach to improve the vision quality provided by retinal implants is to minimise indiscriminate activation of functionally-different RGC types. To achieve this aim, several groups are working towards designing electrical stimulation strategies that are capable of selectively, preferentially, or differentially activating functionally-distinct neural pathways or cell types (summarised in Figure 3.1 and Table 3.1). Depending on the mechanisms of retinal activation, these stimulation approaches can be achieved either by targeting upstream neurons in the retinal network (network-mediated stimulation) or directly targeting the RGCs (direct stimulation).

There remains an open debate as to whether direct or indirect stimulation of RGCs is the more effective means to convey information given that both methods have their own advantages and disadvantages. For example, RGCs under direct stimulation have been shown to ‘follow’ (i.e., elicit at least one spike per pulse) pulse trains of up to 700 Hz [128]. However, it can also cause unwanted axonal activation leading to elongated percepts [129]. Contrarily, RGCs under indirect stimulation avoid the axonal activation but suffer from desensitisation causing fading of percepts [104]. Indirect activation also increases the overall stimulation thresholds compared to direct activation, leading to charge density concerns [32]. Finally, one of the more distinguishing advantages of direct stimulation is the ability to activate the RGCs without relying primarily on the inner retinal network, whose extensive remodelling and rewiring is likely to alter the RGC response and impede efforts of differential activation [83-85].

In this section, a survey of both network-mediated (Chapter 3, Section 3.1.1) and direct stimulation (Chapter 3, Section 3.1.2) strategies to selectively activate targeted cell groups will be reviewed including discussions on how the strategies overcome the inherent disadvantages of the particular methods. Following this, a brief overview on conceptual alternative strategies based on “non-electric” neurostimulation will be discussed (Chapter 3, Section 3.2).



**Table 3.1 Summary of electrical and photovoltaic-based studies (corresponding to the studies highlighted in black and red from Figure 3.1) investigating differential activation of retinal cell types. The studies are listed chronologically within each branch (STA, Sinusoidal & others, LFS and HFS).**

Study	Targeted Pathway	Animal Species	Stimulation Parameters	Electrode Location	Direct/Indirect
Sekhar et al. 2017 (STA)	ON, OFF and ON-OFF RGCs	Mice, C57BL/6J and rd10 (P84)	<b>Waveform:</b> Gaussian white noise, rectangular cathodic-monophasic voltage pulses <b>Pulse Duration:</b> 1 ms <b>Frequency:</b> 25 Hz	Epiretinal	Indirect
Ho et al. 2018 (STA)	ON and OFF RGCs	Rats, Long-Evans (P60 – P100) and RCS (P120-360)	<b>Waveform:</b> Photovoltaic stimulation (NIR 880nm) <b>Pulse Duration:</b> 4 ms <b>Frequency:</b> 20 Hz	Subretinal	Indirect
Höffling et al. 2020 (STA)	ONS, ONT, OFFS, OFFT, ON-OFF RGCs	Mice, C57BL/6J (P87 – P74) and rd10 (P80 – P209)	<b>Waveform:</b> Continuous low-pass filtered Gaussian white noise, voltage-controlled	Epiretinal	Indirect
Jensen et al. 2006 (Sinusoidal & others)	ON and OFF RGCs	Rabbit (NZW)	<b>Waveform:</b> Rectangular current-controlled, monophasic, cathodic, and anodic pulses <b>Pulse Duration:</b> 0.1 – 50 ms <b>Frequency</b> ~ 2 Hz	Subretinal	Indirect
Freeman et al. 2010 (Sinusoidal & others)	Photoreceptors, BCs and RGCs ON and OFF RGCs to cathodal and anodal stimulation	Rabbits (NZW)	<b>Waveform:</b> Sinusoid, current-controlled, biphasic cathodic- and anodic-first pulse trains <b>Pulse Duration:</b> 0.2 ms <b>Frequency:</b> 5, 10, 25, 100 Hz	Epiretinal	Indirect
Im et al. 2015 (Sinusoidal & others)	ON and OFF BT and BS RGCs	Rabbits (NZW)	<b>Waveform:</b> Half-sinusoid waveform, monophasic, current-controlled, cathodic pulses <b>Pulse Duration:</b> 4 ms <b>Amplitude:</b> -100 uA to 100 uA	Epiretinal	Indirect
Im et al. 2016 (Sinusoidal & others)	ON and OFF RGCs	Rabbit (NZW)	<b>Waveform:</b> Half-sinusoid waveform, monophasic, current-controlled, cathodic pulses <b>Pulse Duration:</b> 4 ms <b>Inter-Stim-Interval (ISI):</b> Either 100 ms, or variable ISI between 10 – 1000 ms.	Epiretinal	Indirect
Twyford et al. 2016 (Sinusoidal & others)	ON and OFF BT RGCs	Rabbit (NZW)	<b>Waveform:</b> Sinusoid waveforms, biphasic, current-controlled, anodic-first pulses <b>Frequencies:</b> 5, 10, 25 and 100 Hz <b>Amplitude:</b> 4, 9, 18 and 36 $\mu$ A	Epiretinal	Indirect
Im et al. 2018 (Sinusoidal & others)	ON and OFF BT and BS RGCs	Rabbits (NZW)	<b>Waveform:</b> Half-sinusoid, monophasic, current-controlled, cathodic, and anodic pulses <b>Pulse Durations:</b> 5, 6.7, 10, 20, 50 and 100 ms <b>Amplitude:</b> (Adjusted to keep total charge constant) 5 – 100 $\mu$ A.	Epiretinal	Indirect
Lee et al. 2019 (Sinusoidal & others)	Alpha ONS, OFFS and OFFT RGCs	Mice, WT C57BL/6J (P56-158)	<b>Waveform:</b> Triangular waveform, monophasic, current-controlled, cathodic pulses <b>Pulse Duration:</b> 5 and 10 ms for each amplitude <b>Amplitude:</b> 10 – 80 $\mu$ A	Epiretinal	Indirect

Sekirnjak et al. 2008 (LFS)	ON and OFF parasol cells	Monkey, Rhesus	<b>Waveform:</b> Asymmetric rectangular, biphasic, current-controlled, cathodic-first pulses. Cathodic amplitude $A$ and duration $d$ , followed by anodic amplitude $A/2$ and duration $2d$ . <b>Pulse Duration:</b> 0.05 ms and 0.1 ms <b>Frequency:</b> 5 – 10 Hz	Epiretinal	Direct
Jepson et al. 2013 (LFS)	ON and OFF midget, ON and OFF parasol and small bistratified cells	Monkey, Macaque	<b>Waveform:</b> Asymmetric, rectangular, triphasic (anodic/cathodic/anodic), current-controlled pulses. Amplitudes were 2:-3:1. <b>Pulse Duration:</b> 150 or 300 $\mu$ s	Epiretinal	Direct
Jepsen et al. 2014 (LFS)	ON parasol, OFF parasol, ON midget and OFF midget	Monkey, Macaque		Epiretinal	Direct
Fan et al. 2018 (LFS)	ON parasol, OFF parasol, ON midget and non-light responsive RGCs	Monkey, Macaque	<b>Waveform:</b> Asymmetric, rectangular, triphasic (anodic/cathodic/anodic), current-controlled pulses. Amplitudes were 2:-3:1. <b>Pulse Duration:</b> 150 or 300 $\mu$ s <b>Ground Configuration:</b> Local return pattern of same current amplitude on the centre and 1/6 the amplitude for the local returns	Epiretinal	Direct
Madugula et al. 2020 (LFS)	ON and OFF midget and parasol	Human	<b>Waveform:</b> Asymmetric, rectangular, triphasic (anodic/cathodic/anodic), current-controlled pulses. Amplitudes were 2:-3:1. <b>Pulse Duration:</b> 150 or 300 $\mu$ s <b>Amplitude:</b> 0.1 – 4.1 $\mu$ A	Epiretinal	Direct
Cai et al. 2011 (HFS)	ON-OFF DS, LED, ON DS, OFF BT	Rabbits (NZW)	<b>Waveform:</b> Rectangular, biphasic, current-controlled, cathodic-first pulses <b>Phase Duration:</b> 200 $\mu$ s <b>Frequency:</b> 10 Hz (to obtain threshold), 100 – 700 Hz <b>Amplitude:</b> (0 – 12 $\mu$ A) * Stimulation Threshold	Epiretinal	Direct
Cai et al. 2013 (HFS)	OFF BT and ON-OFF DS	Rabbits (NZW)	<b>Waveform:</b> Rectangular, biphasic, current-controlled, cathodic-first pulses <b>Phase Duration:</b> 100 $\mu$ s <b>Frequency:</b> 2 kHz <b>Amplitude:</b> (0 – 5 $\mu$ A) * Threshold	Epiretinal	Direct
Twyford et al. 2014 (HFS)	ON and OFF BT	Rabbits (NZW)	<b>Waveform:</b> Rectangular, biphasic, current-controlled, cathodic-first pulses <b>Phase Duration:</b> 100 $\mu$ s <b>Stimulation Duration:</b> 300 ms <b>Frequency:</b> 2 kHz <b>Amplitude:</b> Zero-baseline 0 – 100 $\mu$ A Modulating amplitude 40 – 60 $\mu$ A	Epiretinal	Direct
Guo et al. 2018 (HFS)	Alpha ON and OFF	Mice, C57BL/6J (P28 – P56)	<b>Waveform:</b> Rectangular, biphasic, current-controlled, cathodic-first pulses <b>Phase Duration:</b> 40 $\mu$ s <b>Frequency:</b> 1 – 6 kHz <b>Amplitude:</b> 10 – 240 $\mu$ A <b>Stimulation Duration:</b> 300 ms	Epiretinal	Direct

*P, post-natal day; BT, brisk-transient; BS, brisk-sustained; DS, direction-sensitive.*

## 3.1 Electrical Stimulation in Healthy Retina

### 3.1.1 Network-Mediated Stimulation

#### 3.1.1.1 *Temporal Modulation*

Network-mediated stimulation of RGCs occurs when the RGC response is modulated through synaptic inputs by activation of the presynaptic neurons in the retinal network i.e., the photoreceptors, BCs, HCs and ACs [17, 31, 122, 126, 130-132]. The majority of the network-mediated strategies for selective activation are based on temporal modulation of a parameter – for example, stimulation amplitude. In subthreshold stimulation, electrical current [19, 133], voltage ([17, 18]) and light [31] modulated by a white noise sequence is used to obtain characteristic electrical filters of RGCs through calculation of the spike-triggered average (STA). Other temporal modulation waveforms include the use of sinusoidal waveforms to selectively targeted neuronal types [125, 126, 130-132]. Both STA and sinusoidal-based strategies will be discussed in the following section (Chapter 3, Section 3.1.1.2).

#### 3.1.1.2 *Spike-Triggered Average*

Integration of sequences of subthreshold pulses can produce RGC spikes. One such strategy is the use of spike-triggered averages, or STAs which are calculated by averaging the stimulus segments preceding a spike. White noise-like stimulation has long been used to extract temporal filters from the visual [134, 135] and auditory systems [136]. This review will focus on STAs derived from electrical (current or voltage) or photovoltaic (near-infrared) stimulation (see Figure 3.1, STA branch). In 2016, Sekhar et al. [18] was the first to show that in response to epiretinal 1-ms, cathodic, 25-Hz voltage-controlled Gaussian white noise stimulation (frequency was optimised on the usefulness of filters produced, see Table 3.1), different classes of RGCs were able to integrate multiple subthreshold pulses to form unique STAs, or electrical filters. Following this initial study, they were then interested to see if the ON and OFF RGCs had distinct electrical filters and whether they corresponded with their respective visual STAs [17]. They found that indeed, the ON and OFF RGCs exhibited clearly opposite STAs with ON RGCs exhibiting short-latency upward deflections and OFF RGCs exhibiting short-latency downward deflection immediately preceding the spike. Furthermore, they found a strong correlation between the electrical STAs and the visual STAs of both cell types.

Independently, Ho et al. [31] found similar results in ON and OFF photovoltaic STAs in response to stimulation from a subretinal photovoltaic prosthesis with frequency of 20 Hz however with longer onset latencies and shorter durations. Similar STAs with narrower widths and shorter durations were observed in the electrical STAs [18], suggesting that some of the RGC responses in the photovoltaic stimulation may have been the result of suprathreshold

stimulation rather than the integration of subthreshold stimulation [137]. More recently, Höfling et al. [133] further classified the ON and OFF RGCs to their sustained and transient subtypes to assess the correspondence between their visual and electrical filters. Using an epiretinally-placed CMOS-MEA, they stimulated the four RGC types using continuous voltage Gaussian white noise electrical stimulation and found that overall, OFFS RGCs had monophasic-negative STAs, while OFFT RGCs responded with either biphasic, or monophasic-positive STAs. Within the ON cell population, they were not able to evoke reliable and consistent responses from all the cells in response to the stimulation making any correlation between the temporal filters difficult. While their results are at slight odds with the studies aforementioned, particularly the presence of monophasic STAs, their work suggests that transient and sustained RGCs may also have distinct electrical STAs. More broadly, this also suggests that the variability of RGC responses to electrical stimulation may not necessarily be due to biological variation but due to the diversity of the RGC population themselves potentially allowing them to be selectively activated [8, 16].

Given the reliance of the STAs on the presynaptic network, Sekhar et al. [17], Ho et al. [31] and Höfling et al. [133] also measured STAs in degenerate retina. Interestingly, both Sekhar et al. [17] and Ho et al. [31] found distinct downward and upward STAs as in healthy retina however did not identify the RGC types therefore it remains unknown if the ON and OFF STAs truly remained the same under degeneration. In contrast, Höfling et al. [133] found that all the degenerate RGCs had very similar monophasic electrical STAs and postulated that the short-latency of the negative peak in the STAs might suggest that the RGCs were being activated directly as opposed to through the network. These findings are once again at subtle odds with the previous studies. In particular, Sekhar et al. [17] and Ho et al. [31] suggest that the network must be involved given the presence of opposing STAs. Nevertheless, these discrepancies highlight the importance of classifying the RGCs into their subtypes to shed light on the degenerate-network influence and in turn, assessing the clinical viability of this approach.

Apart from eliciting a differential response between ON and OFF RGCs, STA-based strategies also have a potential benefit in reducing the fading effect [137], a phenomenon in which the evoked visual phosphene fades over time [101, 138]. One factor attributing to this fading has been the desensitisation of RGCs response to repetitive stimulation [139-142]. Interestingly, the 25 Hz and 20 Hz frequencies used in Sekhar et al. [17] and Ho et al. [31] induced more robust RGC responses despite being stimulated at frequencies which previously caused desensitisation in other studies of electrical noise stimulation [139, 141, 143]. They hypothesised that this could be due to amplitude variations in the subthreshold pulse trains.

Amidst the advantages of STA-based selective activation, it is important to acknowledge the shortcomings of this stimulation strategy. STA-based analyses assume a linear relationship

between the applied stimuli and neural responses, which may not hold true in retinal stimulation. In addition, STA-based stimulation demonstrated significant trial-to-trial variability, resulting in fairly brief characterisations of RGC responses to stimuli [17]. More recently, a model-based study was used to characterise the stimulus-response function of different RGC types under subthreshold white noise electrical stimulation. It was found that most (> 85%) of the recorded neural variability is stimulus-independent, and the remaining (<15%) may be due to stimulus-dependent neural adaptation or low signal-to-noise ratio under subthreshold stimulation [144]. Further studies are still needed to understand the mechanisms underlying STA-based stimulation. Conversely, strategies such as filtered-back propagation and spike-triggered non-negative matrix factorisation have emerged as competitive alternatives to STAs with their ability to identify greater number of ganglion cell types [145] and unlock finer details of the receptive fields [146]. It will be interesting to see in future studies whether these new approaches can be employed to identify electrical filters over a range of RGC types.

### *3.1.1.3 Sinusoidal and Other Alternate Waveforms*

Apart from STA-based strategies, numerous other indirect single-pulse, and noise-based approaches have been employed in attempts to differentially activate the targeted cell type (Figure 3.1, sinusoidal and others branch). Under single-pulse stimulation, Jensen et al. [147] found that cathodic-first monophasic current pulses using subretinal stimulation yielded in lower stimulation thresholds of ON RGCs compared to OFF RGCs. However, the use of long-term monophasic currents are deleterious to the tissue [148]. As such, network-mediated single-pulsed based strategies have little utility in the selective activation of RGC types. A more promising approach using indirect stimulation of RGCs has been through the use of sinusoidal waveforms, and in particular, the pulse width.

The use of sinusoidal waveforms as a means to selectively activate targeted cell groups began with Freeman et al. [131] who investigated the response properties of ON and OFF RGCs to current-controlled sinusoidal waveforms of frequencies 5, 10, 25 and 100 Hz. Their results suggested that photoreceptors, bipolar cells and RGCs could be selectively activated with 5, 25, and 100 Hz, respectively. Under 5 Hz stimulation, they found that the ON and OFF RGCs responded to different phases of the sinusoidal waveform – ON RGCs to the anodal phase and OFF RGCs to the cathodal phase. They hypothesised that this selective sensitivity to the phase arose from photoreceptor-to-bipolar cell activation and in particular, the sign-inverting synapse in the ON BCs which would yield in opposite phases of activation for the two cell types. Under 25 Hz stimulation however, both the ON and OFF RGCs were responsive to the cathodal phase implying that the activity was no longer mediated by the photoreceptor cells, but potentially the BCs. Finally, using CdCl<sub>2</sub> to block all synaptic transmission, they found that the RGCs were still responsive to 100 Hz stimulation suggesting that the response was driven

exclusively by the RGCs. This study was further extended by Twyford et al. [132] by (a) further subclassifying the ON and OFF RGCs to their sustained and transient subtypes and (b) using an additional synaptic blocker to block the photoreceptor-to-bipolar synapse in the ON pathway. Overall, their results were at slight odds with the previous studies finding that only photoreceptors and RGCs could be selectively activated. Specifically, photoreceptors could be activated at 5 and 10 Hz, while RGCs could be selectively activated at 25 and 100 Hz. Furthermore, they found that activation of BCs could not be achieved without concurrent activation of photoreceptors or RGCs dissimilar to the findings by Freeman et al. [131]. They further found that deeper classification of the ON and OFF RGCs showed bigger differences in the phase of activation of ON Brisk-Transient (BT) and OFF BT RGCs compared ON Brisk-Sustained (BS) and OFF BS suggesting that the sustained and transient subtypes may have different sensitivities to sinusoidal stimulation. This difference in sensitivity between cell types in response to sinusoidal stimulation was also found by Im et al. [122] who found distinct differences in the number of bursts and latency of bursts between ON BT, ON BS, OFF BT and OFF BS RGCs. They speculated that these discrepancies were due to differences in the presynaptic circuitry and intrinsic differences between the cell types. Interestingly, in a subsequent study, they found similar spike responses of the ONS cells when stimulated with other non-sinusoidal waveforms suggesting that the pulse width may play the key role in eliciting these spike responses [149].

In the same study, Im et al. [122] correlated the network-mediated electrical responses to the light responses of the four RGC types. They found the ISI and firing rates of the second burst of the electrically-elicited responses were strongly correlated with the visually-evoked responses for the ON BT and ON BS RGCs. However, this correlation did not extend to the OFF RGCs. Overall, they concluded that network-mediated electrical stimulation yielded in stronger correlations with light responses of ON rather than OFF RGCs. Following this finding, Im et al. [125, 126, 130] further advanced the use of alternate waveforms to differentially activate RGC types by conducting a series of studies to investigate the ON and OFF RGC response to half-sinusoidal [125, 130] and triangular waveform [126] with varying parameters, and with a particular interest in biasing ON over OFF activation. In 2016, Im and colleagues [125] studied the response of the ON and OFF RGCs to repetitive stimulation consisting of cathodic-first, half sinusoidal waveforms of 4 ms duration. They found that while ON RGCs exhibited a “reset” phenomenon in which every new stimulus would suppress the previous indirect response and initiate its own response while OFF RGCs had desensitised responses similar to those reported previously [139-141]. Given these distinct responses of the two cell types to the stimulation, they further investigated the rate of stimulation which would maximise the response between the ON and OFF cells. They found that the maximum ON/OFF

response ratio occurred for stimulation durations 175 – 225 ms corresponding to clinically-relevant frame rates of 4 – 7 Hz [7, 101]. In the subsequent study, they studied the sensitivity of ON and OFF RGCs to the stimulation duration of the monophasic cathodic-first, half-sinusoidal waveform [130]. They found that the response of ON RGCs decreased with increasing stimulation duration while OFF RGCs were relatively constant across the same parameters. Similar to the 2016 study, they were able to exploit these differing sensitivities to bias ON over OFF activation, finding that the ratio was maximised at 10 ms for both the ON BT/OFF BT and ON BS/OFF BS cell types. In their most recent study, Lee et al. [126] explored the ON and OFF RGCs response to different stimulation charges and current amplitudes using monophasic, cathodic triangular waveforms. In line with their previous studies, they found that the network-mediated response of ON RGCs was sensitive to charge and current amplitude while OFFS and OFFT RGCs were insensitive to increased charge but were also modulated by amplitude. Using this knowledge, they found that the ON/OFFS response ratio could be maximised at a stimulation duration of 10 ms, and amplitude of 30  $\mu$ A.

#### *3.1.1.4 Summary*

Altogether, these studies indicate that it is possible to achieve differential activation of targeted cell types through indirect activation of RGC types (see Figure 3.1 and Table 3.1 for summary). However, most of the studies do not address a fundamental issue with indirect activation – its reliance on the presynaptic network. For example, all studies conducted by Im and colleagues [125, 126, 130] were reliant on the network-mediated response, including critical contributions from the photoreceptors, when attempting to selectively activate the ON over OFF RGCs. Numerous studies have also shown that the remaining retinal network also goes through significant remodelling during degeneration therefore modulating the RGC response and the overall differential performance accordingly [84, 85, 150]. To address this problem, some groups have taken steps to understand how the degenerate network may have influenced network-mediate retinal outputs (see detailed review in Chapter 3, Section 3.3.2.3).

For example, both Sekhar et al. [17] and Ho et al. [31] measured STAs in degenerate retina and found distinct downward and upward STAs as in healthy retina. Given that both groups attribute photoreceptors as a central influence on the overall STA shape, it was intriguing to find the presence of these opposing polarity STAs in a degenerate model. They hypothesised that the differences may have been mediated through the All ACs cells following the depolarisation of the rod bipolar cells. However, the impact of a degenerate network on differential activation remains an open question since they did not identify the RGC types in the degenerate retina. It is likely that until such a time where we have a better grasp of the exact features of degenerations and their implications, differential stimulation based on network-mediated activation may continue to be shrouded with a certain level of uncertainty.

### 3.1.2 Direct Stimulation

Direct stimulation occurs when the RGCs are activated directly and typically elicit a single or two short-latency spikes [139, 151, 152]. Direct activation of RGCs can be achieved both with subretinal [153, 154] and epiretinal stimulation [139, 151, 155]. Most of the studies involving differential activation through direct stimulation fall under two camps – differential activation of RGCs from unwanted axonal activation, or differential activation of targeted RGC types. Keeping in mind the subject of this thesis, I will provide a brief overview of the studies involving axonal activation but a greater emphasis on differential activation of cell types.

#### 3.1.2.1 *Selective Activation of Axon and Soma*

One of the primary issues that arise from direct activation is the accidental activation of axons in which nearby axons (and subsequently their cell bodies) become activated during electrical stimulation and in turn, increase the spread of RGC activation [156].

To minimise non-targeted axonal activation, different groups have attempted to selectively activate the RGCs over the superiorly located axon fibres (see Figure 3.1, soma vs axon branch). Grosberg et al. [157] used a high-density MEA with electrode diameters of 10  $\mu\text{m}$  coupled with triphasic current pulses to identify if RGCs could be selectively activated without the axonal bundles. Overall, they found that 45% of electrodes that were capable of activating an individual RGC (17% of all the electrodes in the array) were able to do without activating the axonal bundles in the peripheral region, and 75% of electrodes activating a single RGC (16% of all electrodes in the array) could be selectively activated over the axonal bundles in the raphe region of the central retina.

Another suggested approach to avoid axonal stimulation is by altering the pulse duration [30, 151, 158, 159]. Jensen et al. [151], Chang et al. [158] and Tong et al. [30] all found maximised differences between the cell soma and axons for short duration pulses of less than 0.1 ms, 0.12 ms and 0.1 ms respectively. Additionally, Chang et al. [158] found that the RGC threshold could be significantly lowered with an anodic-first asymmetric pulse waveform as well as a localised response with careful selection of current amplitude. Another approach was to indirectly stimulate the RGCs (from the epiretinal space) using longer duration pulses (>25 ms) as shown by Weitz et al. [32] or low-frequency sinusoidal waveforms (10 – 25 Hz) found by both Freeman et al. [131] and in an earlier study by Weitz et al. [160]. Overall, these studies indicate that by altering the pulse duration, accidental axonal activation under direct stimulation may be minimised.

### 3.1.2.2 *Selective Activation of Cell Types*

To date, there have been two primary strategies to differentially activate targeted cell types in the retina with direct stimulation. Namely, low frequency stimulation (LFS, defined here as < 500 Hz) and HFS (defined here as > 500 Hz).

#### 3.1.2.2.1 **Low Frequency Stimulation**

One avenue of research to differentially target RGC types is through focal electrical stimulation with high resolution multielectrode arrays (MEAs) with electrode sizes significantly smaller than those used clinically (see Figure 3.1, LFS branch). Earlier studies by Sekirnjak et al. [161] and Jepson et al. [162] in primate retina found that even by using higher density MEAs coupled with relatively small electrodes (< 20  $\mu\text{m}$ ) differential activation of a targeted cell type was not always consistent. Therefore, it was evident that to achieve better control at the cellular level, high-resolution MEAs would benefit from electrical stimulation techniques. One such technique is the use of current steering shown in Jepson et al. [163] in which they proposed to stimulate pairs of electrodes with optimised current ratio based on threshold differences between neighbouring RGCs. While this was promising, the computational effort to implement the current ratio algorithms clinically, as well as ensuring that the currents themselves catered to the safe charge limit were important hurdles for clinical application.

A more recent approach proposed by Fan et al. [164] involved the use of local returns surrounding the central stimulating electrode in primate retina. Fan et al. [164] found that by stimulating the centre electrode near the target cell with a triphasic pulse (see Table 3.1 for stimulus parameters), and the surrounding electrodes with the same pulse (but one-sixth of the current amplitude), the selectivity of the activation of a non-targeted cell near the electrode was higher than by simply using a distant return. They further found that nearby primate ON and OFF cells could be differentially activated with the same local return configuration. Madugula et al. [127] similarly found that in human retina, each of the four cell types – OFF-midget, ON-midget, OFF-parasol and ON-parasol had a higher spiking probability (>0.75) compared to the surrounding cells of the same type (< 0.25). They also showed that a single OFF-midget cell could be differentially activated against the individual types. Both the studies by Fan et al. [164] and Madugula et al. [127] base the ability to selectively activate a targeted cell on differences in stimulation threshold under direct stimulation but do not isolate the potential contributions of the presynaptic network on the thresholds observed. For example, a study by Yang et al. [165] found that ON and OFF cells had statistically similar thresholds when connected to the retinal network, but statistically different stimulation thresholds after the synaptic inputs were diminished by the application of synaptic blocker. They speculated that these differences largely arise due to the significant hyperpolarisation of the baseline membrane potential of ON cells, a phenomenon that has been previously reported in non-

human primate retina [166] and in rd1 mice [23]. While it is critical to see how isolating the RGC response from the network will alter the conclusions formulated in the aforementioned studies; the greater threshold differences may work in favour of the studies rather than oppose.

There are several benefits of focal electrical stimulation and the use of high-density MEAs, particularly in the ability to assess differential activation of a cell with regards to surrounding cells, which is not possible with single-cell techniques such as patch-clamping. Another important benefit is the use of smaller electrodes and their utility in human retina. This in future may remove one more obstacle to a clinical prosthesis, particularly for groups developing other stimulation strategies for targeted activation but using smaller electrodes. Benefits aside however, as mentioned these studies tend to rely on stimulation threshold differences as their primary way of providing selectivity. While this is useful, it is limited in the parameters (e.g., amplitude, pulse duration etc) to maximise selectivity. In future, it may be useful to combine alternate stimulation strategies that use additional stimulation parameters to modulate the level of selectivity with the MEAs used here to maximise differential activation of cell types across a population.

#### **3.1.2.2.2 High Frequency Stimulation**

Another promising avenue for differential activation of cell types is through HFS (see Figure 3.1, HFS branch). HFS (defined as  $> 500$  Hz), has been widely used in many neuronal stimulators to quantitatively control neural activities. In the last decade alone, clinical studies have tested the performance of HFS in the peripheral nerve system (up to 10 kHz, [167-170]), in the cochlear (up to 2.4 kHz, [171]), in the retina (up to 3.33 kHz, [172]) and the spinal cord (up to 10 kHz, [173, 174]).

One major application of HFS is its ability to induce a conduction block which effectively prevents nerve activity [175-177]. The conduction block itself is usually characterised by a blocking threshold which is the minimum stimulation amplitude required to block nerve conduction [176]. It is important to note here that while the presence of a blocking threshold or “upper threshold” has also been reported in RGCs [178, 179], the upper threshold was a function of a single parameter – the stimulus amplitude. The benefit of HFS-induced conduction block is that the blocking threshold is also a function of frequency which means there are two parameters at play – frequency *and* amplitude which work synergistically to block conduction. This in turn increases the parameter space in which the blocking threshold occurs, and potentially for different cell types. To this end, studies in peripheral nerves have shown that the frequency-dependent blocking threshold may also be nerve-fibre specific. For example, Joseph et al. [180] showed that the blocking thresholds of myelinated fibres increased with frequencies between 5- 50 kHz (i.e., monotonic), however, the block thresholds of unmyelinated fibres decreased with frequencies greater than 25 kHz (i.e., non-monotonic)

for the same frequency range in the sciatic nerve of frogs. This was later substantiated by Patel et al. [181] for rat peripheral nerves in vitro indicating that the monotonic and non-monotonic fibres could be differentially activated by carefully tuning specific frequency and amplitude parameters. More recently, a cervical vagus nerve stimulation study by Chang et al. [182] found that the unmyelinated, small diameter C-fibres in the vagus nerve could be activated with minimal engagement from the myelinated, larger diameter A- and B- fibres using frequencies ranging from 4 to 12 kHz. Overall, this indicates that frequency and amplitude may be optimised to allow selective blocking of targeted nerve-fibres.

The success in selectively targeting functionally-distinct nerve fibres using HFS paved the way for differential activation of RGC types using HFS. HFS-induced retinal differential activation began from a study conducted by Cai et al. [128] to investigate whether previously reported discrepancies in the rabbit RGCs ability to follow high-rate pulse trains was due to differences in the cell type. In their study they found that indeed, different RGC types had varying abilities to follow high-rate pulse trains. Specifically, they found that OFF BT cells could reliably follow pulse trains up to 700 Hz, whereas other cell types such as ON-OFF DS cells could only follow up to 200 Hz. This study was the first to show that different RGC types may have unique responses to HFS. In 2013, Cai et al. [183] explored the sensitivity of the OFF BT and ON-OFF DS cells to a higher frequency of 2 kHz. Their main findings were that the two cells responded differently to the 2 kHz as a function of amplitude. In particular, the spiking activity of the OFF BT peaked at  $\sim 40 \mu\text{A}$  and *decreased* at higher amplitudes whereas ON-OFF DS cells maintained strong spiking activity despite the increasing amplitude. This study was notable for two reasons – firstly, they showed that combined with high frequencies, cells can exhibit a non-monotonic profile with increasing amplitude. This is in contrast with previous studies which showed increasing spiking levels with increasing amplitude. The second reason is that they were the first to use HFS as a way of invoking a differential response between functionally-identified RGC types. Subsequently, their most significant contribution in this area came in 2014 in which Twyford et al. [14] used a 2 kHz stimulus in combination with a modulating amplitude to show differential activation between the ON and OFF cell types. They found that when the amplitude was modulated from a non-zero baseline of  $40 \mu\text{A}$  to  $60 \mu\text{A}$ , compared to their baseline activity, the ON cell had increased spiking activity while the OFF cells had decreasing spiking activity (see Table 3.1 for stimulus parameters). Conversely, when the amplitude was modulated from a non-zero baseline of  $60 \mu\text{A}$  to  $40 \mu\text{A}$ , the ON cell spiking activity decreased and the OFF cell spiking increased compared to baseline activity. This study substantiated the previous findings in Cai et al. [183] showing amplitude-dependent responses of RGCs stimulated with HFS.

Despite the novel findings, there were also a few caveats which ultimately, provided a scope for extension. In particular, the parameter space (both frequency and amplitude) in which the ON and OFF cells could be differentially activated was relatively narrow thereby limiting their differential response to one set of combinations. To address this, Guo et al. [15] extended the previous work to understand how the differential response between ON and OFF RGC changes across a more extensive frequency (1 – 6 kHz) and amplitude (10 – 240  $\mu$ A) parameter space. They found that ON cells could be differentially recruited at higher amplitudes (>150  $\mu$ A) and frequencies (2 – 6.25 kHz) whereas OFF cells were activated at lower amplitudes (40 – 90  $\mu$ A) across all tested frequencies (1 – 6.25 kHz). Overall, the work of Twyford et al. [14] and Guo et al. [15] prove that differential activation of ON and OFF pathways is possible not only for a single frequency, but a range of high frequencies suggesting that both a modulating amplitude and modulating high frequency should be able to differentially activate the pathways.

### **3.1.2.2.3 Possible Mechanisms Underlying Differential Activation**

The ability to target functionally-different neural pathways through HFS is largely a virtue of differences in the amplitude-dependent responses of the cells, particularly with respect to the conduction block. Though previous studies in the retina have reported the existence and potential mechanisms behind the “upper threshold” phenomenon in which RGC spike responses were inhibited past a certain amplitude [178, 179, 184], these studies were based on responses to a single monophasic or biphasic pulse. The mechanisms behind an HFS-induced conduction block remain less clear. One common theory proposed in peripheral nerves is that the cell becomes “over-depolarised” thereby inactivating the sodium channels and preventing further spiking [175, 185, 186]. Specific to the retina, Guo et al. [187] speculated that the spiking suppression may be the result of local membrane hyperpolarisation induced by HFS. Specifically, the combination of HFS and increasing amplitude strength cause the cell membrane potential to exceed the sodium reversal potential (i.e., becomes “over-depolarised”). Once this occurs, the sodium channels elicit an outward current which hyperpolarises the cells and subsequently suppresses the spiking activity of the RGCs.

A further complexity is the cell- or fibre-specific nature of the block. In the peripheral nerves, initially it was hypothesised that the ability to control the targeted nerve fibres could be due to differences in their morphological nature such as fibre diameter and myelinated versus unmyelinated structures [182, 188]. However, a recent study conducted by Peña et al. [189] suggested that the non-monotonic profile of the unmyelinated fibres may have been a consequence of frequency and amplitude DC offsets resulting in a charge imbalance rather than the nerve fibre properties. In the retinal tissue, it is unlikely that charge imbalances are behind the differential response owing to the frequency range applied: 10 – 100 kHz versus

0.5 – 10 kHz. Therefore, the question remains - why do ON and OFF RGCs have differing stimulus-dependent responses to HFS?

Previous retinal studies suggest that the differential electrical responses of the RGCs are intrinsically-driven given their isolation from the retinal network [14, 15]. As such, it is reasonable to hypothesise that selective targeting of distinct RGCs will likely depend on their differential intrinsic (i.e., the ion channel subtype(s) expressed and their distribution and/or density in a particular region) and morphological properties. Previous studies have shown that functionally-distinct RGC types have diverse intrinsic physiological properties [57, 72-74, 79]. Given this diversity, different studies have sought to attribute one or more of these intrinsic properties to the differential response found. Kameneva et al. [190] proposed that ON RGCs may have higher concentrations of potassium channels than OFF cells but have shorter sodium channel bands (SOCBs). Meanwhile Guo et al. [187] found that the spiking suppression exhibited by RGCs could be modulated by changes in sodium channel properties insinuating that differences in sodium channel distributions between the ON and OFF RGCs could play a pivotal role. Differences in these ionic currents may also aid in unmasking another potential mechanism relating to the refractory period of a cell. Briefly, the refractory period of a cell is the period in which the cell cannot elicit a second action potential within a specific time window of the first [175]. Therefore, the ability of a cell to follow high-rate pulse trains can be intrinsically dependent on how quickly it can emerge from its refractory state. Previous studies have indicated that specific sodium and potassium channel subtypes can reduce the time the cell spends in its inactive state. For example, the Nav 1.1, Nav 1.2 and Nav 1.6 sodium channel subtypes found in rodent RGCs have all been shown to support a resurgent current which is released during the repolarisation phase of the action potential and used to drive the cell into a semi-blocked rather than a longer inactivated state [191-193]. Meanwhile, the Kv3 potassium channel subtypes found in RGCs have a faster deactivation during repolarisation, minimising the time the cell spends in the inactivated state [194, 195].

The effect of the intrinsic sodium and potassium channel properties can also be shaped by the unique RGC morphological properties in different cell types. For example, numerous studies have reported the importance of the axonal initial segment (AIS) in spike initiation due to its lower threshold [196]. Given its fundamental role, differences in the spiking response between the two cell types may arise due to the presence or irregular distribution of specific sodium or potassium subtypes within the AIS. To this end, Raghuram et al. [79] investigated the proportion of Nav 1.6 channels in the AIS between ON and OFF  $\alpha$  RGCs, however, found them to be statistically similar. This result, coupled with their findings that the AIS length was marginally larger for the ON- $\alpha$  cells compared to the OFF- $\alpha$  cells, therefore ON cells were likely to have a lower threshold, is surprising. However, in a follow-up study, Werginz et al.

[197] specifically investigated how Nav 1.6 channels contributed to the sustained firing of dorsal OFFT RGCs compared to ventral OFFT RGCs particularly at higher amplitudes. They found that pharmacologically blocking the Nav 1.6 channels reduced the ability of the dorsal OFFT RGCs to maintain sustained firing at higher amplitudes suggesting that Nav 1.6 channels mediate sustained firing properties of RGCs.

Nonetheless, it does also suggest that the AIS may not be the only morphological property at play. For instance, previous studies have shown that OFF RGCs' soma size and dendritic field size tend to be smaller than the ON RGCs in mammalian [57, 198] and primate retina [199]. For example, Werginz et al. [200] found that the cell soma also influenced stimulation thresholds and also varied depending on the location of the electrode.

### 3.1.3 Summary

This section reviewed relevant studies using direct and indirect stimulation to differentially activate RGCs. Specifically, under indirect stimulation, two promising strategies include subthreshold STAs and sinusoidal waveforms, to activate different retinal neurons while under direct stimulation, the two primary strategies are the use of local returns and triphasic current pulses to increase spatial confinement and HFS capable of inducing a differential response between different cell types.

As mentioned previously, both direct and indirect stimulation have associated advantages and disadvantages and both approaches have been utilised for the purpose of selective activation of retinal neurons. One fundamental difference between the two stimulation approaches is the dependence of the inner retinal network for network-mediated strategies. Given that the overall purpose of these stimulation protocols is to selectively activate cell types in a diseased retina, network-mediated stimulation immediately suffers from the disadvantage of relying on an extensively remodelled inner retinal network. As such, direct stimulation strategies are potentially more reliable in selectively activating cell types in both healthy and degenerate retina. Taking this into consideration, in this thesis, direct stimulation through epiretinal stimulation was used. Additionally, synaptic blockers were used to completely isolate the RGCs from the network work to ensure that the strategy employed was predominantly from intrinsic properties.

Under direct stimulation, HFS has the benefit of using relatively short pulses that could potentially avoid unwanted axonal stimulation [30, 151, 158], and elicit bright phosphenes without necessarily increasing the size [129]. However, the work to date has been limited to differentially activating two RGC types (ON and OFF) and therefore its viability as a selective activation tool requires further investigation. For example, can similar high frequencies be used to target a broader range of cell types, whilst being temporally-modulated? And

importantly, despite minimising the network contributions, is HFS-based activation possible in degenerate retina?

## **3.2 Non-Electrical Stimulation**

Apart from electrical stimulation, there have recently been advances in alternative strategies towards differential activation of cell types in the retina including optogenetic, chemical, photothermal and micromagnetic stimulation (see Figure 3.1, alternative stimulation branch). In this section I will provide a brief overview of these strategies.

### **3.2.1 Optogenetic stimulation**

Optogenetics is a technique in which a viral vector is used to genetically encode surviving retinal neurons to express light-sensitive proteins that they would otherwise not produce [201-203]. With respect to differential activation in the retina, a conceptual retinal stimulator was proposed in which an encoder converts images to streams of electrical pulses, analogous to streams of action potentials that would be produced by normal retina in response to the same images [204]. The electrical pulses are then converted into light pulses through a digital light projector to differentially drive the functionally-distinct light-sensitive RGCs [204]. Recently, optogenetics has become more promising for differential activation with new techniques focussing on opsin types and promoters. For example, in one study, ON BC and OFF BC were targeted by different functional optogenes and target-specific promoters [205]. Along the same vein, another study used bistable animal opsin to precisely control optogenetic excitation and inhibition of retinal neurons using different wavelength pulses [206]. The primary disadvantages associated with this technique are (1) the higher light intensity required for stimulation potentially leading to photochemical damage [207, 208], (2) the species-dependent nature of the viral vectors and promoters [209] and (3) lack of cell-specific promoters leading to off-target labelling particularly in the inner retina [207, 209].

### **3.2.2 Chemical Neurostimulation**

Another promising method for differential activation is chemical neurostimulation. The technique itself is based on native neurotransmitter injections providing a biomimetic (i.e., the use of synthetic methods to mimic physiological processes) alternative to electrical stimulation. This novel approach was designed to restore vision chemically through the same receptors used in natural visual information processing. Specifically, Rountree et al. [210-212] proposed a conceptual subretinal stimulator containing a custom multiport microfluidic device capable of delivering glutamate in a patterned fashion into degenerated rat retinas. Their studies showed glutamate to be effective in stimulating retinal neurons and potentially

advantageous over electrical current given the use of a naturally-occurring neurotransmitter which may be useful in achieving more focal stimulation and higher spatial resolution. Most importantly, their proof-of-concept results showed differential responses in the ON and OFF pathways in response to the exogenous neurotransmitter [211, 212]. While these results are promising, the studies to date have been limited to explanted retina and therefore the long-term effects and the logistics (e.g., replenishment of the exogenous glutamate) associated with future in vivo and potentially clinical studies requires further investigation. Additionally, significant technological development is required to increase the resolution of the current device (from micrometre to nanometre) to mimic the high resolution provided by the natural synaptic vesicles [213].

### 3.2.3 Infrared Neural Stimulation

Infrared neural stimulation is based on direct irradiation of an object with infrared light and has recently been used for retinal stimulation due to its high spatial precision ( and low stimulation artefact [214]. This approach also been demonstrated to induce localised neuronal excitation and inhibition in functionally-specific domains visual cortex of non-human primate [215], indicating its possible utility in differential activation of cells. Notwithstanding, the two main limitations of this approach is the high energy pulses required for activation, and the potential heat damage to the tissue under long-term stimulation [216]. However, with respect to the latter limitation, a year-long study conducted on a macaque monkey did not appear to evoke any noticeable signs of thermal damage indicating that careful consideration of parameters may potentially be able to avoid potential heat damage under long-term stimulation [215].

### 3.2.4 Micromagnetic Stimulation

Lastly, micromagnetic stimulation using micro-coils ( $\mu$ MS) has been shown to modulate neural activity in retinas [217]. The asymmetric electric fields induced by the magnetic fields may allow for differential activation of certain neuronal populations within a focal region of the cortex without exciting other neuronal population, proving to be a promising method of differential activation [218]. The main limitation of this approach is the relatively high current ( $> 175$  mA) and corresponding power required to generate the magnetic fields to activate the neurons [218]. Additionally, similar to the previous approaches, no study to date has investigated the long-term effects of micromagnetic stimulation on the tissue including for example, heat dissipation from the stimulating coils.

### 3.3 Electrical Stimulation in Degenerate Retina

From the studies discussed in the previous section, it is evident that stimulation strategies to selectively activate functionally-distinct RGCs may be possible in the retina. However, the vast majority of the studies derived their strategies from healthy and not degenerate retina. It is well-known that the retina goes through significant remodelling during degeneration [85, 219, 220] which will likely affect the electrical response of the RGCs and impact the efficacy of stimulation strategies. Given that stimulation strategies to improve the quality of vision are for retinal implants that will eventually be implanted into degenerate tissue, it is important to gain an understanding of (a) how the retinal biology alters during degeneration and (b) how degenerate RGCs themselves respond to electrical stimulation. In the first part of this section, an overview of the retinal remodelling that takes place in the degenerating retina and the presence and potential mechanisms behind the well-documented oscillatory activity will be discussed (Chapter 3, Section 3.3.1). Following this, current studies of electrical stimulation of RGCs in degenerate tissue will be surveyed (Chapter 3, Section 3.3.2).

#### 3.3.1 Retinal Remodelling

Numerous studies have indicated that the retinal network goes through significant remodelling during retinal degeneration following photoreceptor death [83, 85, 150, 219-221]. Typically remodelling has three distinct phases: 1) photoreceptor stress, 2) photoreceptor death and 3) neural remodelling [83-85, 219, 220]. Briefly, in the first phase, the outer segments shorten while the rods and cone projections extend further into the retina to the INL and GCL. The BCs also begin retracting their dendritic projections. In the second phase, there is a complete loss in the photoreceptors and the Müller cells form a glial seal between the inner neural retina and the remnant choroid. The third phase is the longest phase in which the majority of the remodelling takes place. Remodelling in this phase includes ectopic changes in the ACs and GCs, the creation of microneurons consisting of remaining glycinergic and GABAergic ACs, BCs and GCs and neuronal cell death. A recent paper by Jones et al. [85] also found evidence of reprogramming during degeneration in the human retina in which changes to the mGluR6 and iGluR metabolic channels caused the retina to effectively convert the rod ON BC to an OFF BC to match the physiological changes.

Taken together, the findings from these studies certainly complicate retinal implant interventions particularly given that it is still unclear when the remodelling itself begins and the time-scale of the progression. While it appears that intervention may be best-suited in the earlier stages of degeneration given the excessive remodelling and rewiring that takes place during the late stage, it is equally evident that irrespective of the stage, the RGC response will be shaped by degeneration.

### 3.3.1.1 Oscillatory Activity in the Degenerate Retina

One of the more widely documented electrophysiological changes in the degenerate retina is the increase in spontaneous activity in the RGCs, and specifically the presence of rhythmic firing across different animal models [23, 206, 222-229].

#### 3.3.1.1.1 Inner Retina

Since its discovery, several studies have attempted to find the origins of this hyperactivity particularly the patterned oscillations in the ON and OFF RGCs. Early studies speculated that the cause was due to altered and oscillatory presynaptic input [23]. However, the underlying network and particularly which presynaptic cells were responsible were unclear. Borowska et al. [226] found that both the electrically-coupled ON CBCs and All ACs exhibited oscillations of similar frequency to the RGCs which persisted in the presence of synaptic blockers but suppressed when the gap junction between the two were blocked. This was also found by numerous other studies [228-230]. Menzler et al. [228] also suggested that the gap junctions were also essential in propagating the oscillatory activity across the retina. Using these findings, Borowska et al. [226] proposed a theory in which the electrically-coupled All AC-ON CBC network acted as an intrinsic oscillator in the degenerate retina and therefore modulated the glutamergic input to the ON RGCs but provided glycinergic inhibitory input to the OFF BCs which in turn provided glutamergic input to the OFF RGCs. Given the OFF BCs received inhibitory input from the All ACs, an implication of the proposed theory suggested that neighbouring ON and OFF RGCs must have out-of-phase activity, which was validated by Margolis et al. [231].

Using a series of pharmacological blockers, Trenholm et al. [227] isolated several possibilities of the mechanisms behind the spontaneously active All AC – ON CBC network. They found that the oscillations in both All ACs and ON CBCs and their synaptic input were abolished when the sodium channels were blocked. Since most sodium channels were expressed in All ACs and not ON CBCs, they isolated voltage-gated sodium channels in All ACs as one of the main drivers of oscillatory activity. In addition, previous studies also found that the oscillations were abolished when gap junctions were blocked implying that they must also contribute to the origins of oscillations [226, 228]. One hypothesis put forward by Trenholm et al. [227] used computation models to suggest a “heterogeneity hypothesis” wherein electrically-coupled individual cells that have channel density values within a specific parameter space (where the cell may potentially intrinsically oscillate) the electrical coupling will average these values i.e., depolarise previously hyperpolarised cells and vice-versa and send the network into oscillations. The alternate proposition to the heterogeneity hypothesis was by Choi et al. [223] who proposed that All ACs were the sole drivers of oscillations and intrinsically oscillatory due to the interactions between the M-type potassium channels and the voltage-gated sodium

channels. They further postulated that the only role of the gap junctions was to cause the hyperpolarisation of the AII ACs by the electrically coupled ON CBCs.

Interestingly the same biophysical properties in the AII AC – ON CBC network also exist in the healthy retina begging the question, what is different in the retina that this network acts as an oscillator? To answer this, Trenholm et al. [227] and Menzler et al. [232] either pharmacologically or via bleach respectively, hyperpolarised the photoreceptors in the healthy retina and found that similar oscillations were induced in the network. Collectively, this meant one potential mechanism behind the oscillations is due to the lack of photoreceptor output which in turn, hyperpolarised the AII AC – ON CBC network allowing more sodium channels to be recruited and the oscillations to take place.

#### **3.3.1.1.2 Outer Retina**

While the AII AC – ON CBC network has been the widely accepted theory behind the oscillatory activity of RGCs, previous studies have also shown that similar oscillations, albeit of lower frequencies (~ 3 Hz), exist in the outer retina [233]. Haq et al. [233] theorised that these oscillations may have originated in the electrically-coupled cone network. In the healthy retina, the HCs and BCs connect with cones in a stringent structure to control the release of glutamate from the cells [40]. The theory put forward by Haq et al. [233] suggested that due to cones re-synapsing with the RBCs in the degenerate retina, the inhibitory feedback from the HCs was disturbed thereby depolarising the cones and causing oscillatory activity in both the cones and synchronously, the RBCs. While the synchronous oscillatory activity of RBCs is in part due to the re-synapsing mentioned previously, it should be noted that in healthy retina the RBCs contain the sign-inverting mGluR6 protein which inverts the input from the rods. In degenerate conditions however, there is less mGluR6 on the RBCs and therefore the transmission between cone to RBC is now dominated by the sign-*conserving* glutamate transporter which causes subsequent depolarisation of the RBCs. Tsai et al. [121] also found through computational modelling that disruption of the cone-horizontal feedback circuit by blocking the excitatory synapses eliminated the damped oscillations in horizontal cells (~10-20 Hz) providing further evidence that the outer retina has similar oscillations as those seen in the inner retina.

Despite the clear evidence of oscillatory activity in the outer retina, it is unlikely that it is the primary source of oscillations observed in the RGCs as the frequency of oscillations in the outer retina is lower than what was seen in both the AII AC – ON CBC network, and importantly, the RGCs. What remains to be seen however, is how the oscillations in the outer retina may modulate the oscillatory activity in the AII AC – ON CBC network through the ON RBCs with the use of specific gap junction blockers.

Overall, the presence of oscillatory activity in RGCs and the potential mechanisms behind the oscillations indicate that degeneration in the outer retina is not isolated and will have eventual downstream effects on the inner retina and importantly the RGCs. This further highlights the importance of testing and validating the utility of stimulation strategies not only in healthy, but degenerate retina.

### *3.3.1.2 Functional Changes in the RGCs*

Given that RGCs are the primary output of the retina, their functional integrity particularly in diseased retina are pivotal to the success of implants. Previous studies showed that rd1 and rd10 RGCs are functionally [23] and morphologically [234, 235] stable. However, other studies have shown a significant decrease in RGC survival especially in late-stage degeneration in rd1 [236], RCS [21] and P23H [237, 238] RGCs. Importantly, amongst the remaining cells, different groups have speculated whether the intrinsic components such as sodium and potassium ionic channels themselves remain consistent between healthy and degenerate RGCs. Sekirnjak et al. [29] initially found that in the presence of synaptic blockers, both ON and OFF RGCs from degenerate P23H rats had different baseline spontaneous activities compared to the control rats indicating that the properties mediating these baseline activities might have changed during the course of degeneration. Other studies by Chen et al. [239] and Ren et al. [22] compared other characteristic intrinsic features such as baseline potential [22, 239] and response to somatic injection [22] however in both studies, the degenerate network was not blocked and therefore doesn't account for the potential that synaptic input might also mediate the response.

The most notable study to date in this area was conducted by Chen et al. [21] who used voltage-clamping to record the sodium and potassium currents from control and RCS RGCs. They found that in P90 RCS RGCs, the maximum sodium current was significantly reduced compared to the control RGCs. They further found that the potassium current also decreased slightly, but not to the same extent as the sodium current. Overall, their study indicated that the intrinsic properties may not be as robust to degeneration as previously thought. Future experiments to isolate the network and record intrinsic properties from degenerate RGCs may shed further light into the potential intrinsic property changes occur at the RGC level.

## **3.3.2 Electrical Stimulation**

### *3.3.2.1 Stimulation Threshold Changes in the Degenerate Retina*

Historically, most studies have reported elevated thresholds in the degenerate retina including rd1 mice [24-26], RCS rats [110] and S334ter line 3 rats [33]. These results were also supported by clinical findings [240-243]. In contrast, Sekirnjak et al. [91] demonstrated the

opposite that is, very negligible threshold differences between the degenerate and healthy retina of P23H rats. They attributed this difference to their direct stimulation of the RGCs as opposed to indirect stimulation in the previous studies where the inner remodelling may have contributed towards the elevated thresholds. This was later substantiated by Weitz et al. [32] who found comparable thresholds between degenerate S334ter line 3 rats (~P600) to age-matched WT RGCs for shorter pulses (<1 ms) which directly stimulated the RGCs compared to significantly higher (~ 3 times) thresholds for longer 25 ms pulses which indirectly stimulated the RGCs. Other suggested causes of elevated thresholds include electrode-to-retina distance [240, 243-245], return electrode configuration, stimulation polarity and duration [244].

Recent studies, however, are speculating that the discrepancies reported in thresholds may also be correlated with the level of increased spontaneous and oscillatory activity in the degenerate retina (see Chapter 3, Section 3.3.1.1 for review on oscillatory behaviour and mechanisms). Note here that normal regular rate, spontaneous activity is distinguished from the degenerate-specific membrane oscillatory (also referred to as patterned, rhythmic, or periodic) activity. Cho et al. [27] distinguished physiological properties of WT retina (P39-80) and degenerate rd10 retina (P42-77) in two groups – ‘low-rate’ spontaneously (including patterned) active cells (defined as less than the mean spontaneous firing rate) and ‘high-rate’ spontaneously (including patterned) active cells (greater than the mean spontaneous firing rate). Using epiretinal stimulation, they found that while there was no statistically significant difference between thresholds in the high-rate group, there was a difference in the low-rate group. Therefore low-rate cells were likely behind elevated thresholds previously reported. These findings were later substantiated by Ren and colleagues [22] who measured the intrinsic excitability of RGCs in middle-stage RCS rats (P91-97) of low rate cells (defined here as < 10 Hz) and high rate cells (> 10 Hz). They found that low-rate cells required a greater number of depolarising currents to reach the action potential threshold compared to the high-rate cells. Therefore, low-rate cells had higher excitability thresholds than the high-rate cells.

Taken together, the data from these two studies can also explain the similar thresholds between healthy and degenerate retina reported by Sekirnjak et al. [91] and [16] et al. [16] as the spontaneous activity for both the P23H rats and the rd10 mice at ages (P28-37) have been reported to have elevated levels of spontaneous activity [91, 222, 246]. Table 3.2 provides a summary of the studies mentioned and their observations on the stimulation thresholds between healthy and degenerate RGCs.

It is important to consider that in the study by Cho et al. [27], and Ren et al. [22] the two groups they define as ‘low rate’ and ‘high rate’ are based purely on the spontaneous firing rate and therefore include cells that exhibit both spontaneous activity analogous to those seen in WT cells, *and* the periodic activity seen in degenerate cells. Given this amalgamation of cells, the conclusions drawn cannot be solely attributed to the presence of oscillatory activity but rather the generalised increase in hyperactivity in diseased retina.

**Table 3.2 Summary of degenerate studies on stimulation thresholds**

<b>Study</b>	<b>Animal Model</b>	<b>Stimulation (Direct/Indirect)</b>	<b>Stimulation Threshold (Degenerate versus Healthy RGCs)</b>
O’Hearn et al. 2006	rd1 mice	Direct	Increase
		Indirect	No Difference
Goo et al. 2011	rd1 mice	Direct	Increase
Jensen et al. 2009	rd1 mice	Direct	Increase
Mathieson et al. 2012	RCS rats	Indirect	Increase
Chan et al. 2011	S334-ter line rats	Direct	Increase
Sekirnjak et al. 2009	P23H rats	Direct	No Difference
Weitz et al. 2015	S334-ter line 3 rats	Direct	No Difference
		Indirect	Increase
Cho et al. 2016	rd10 mice	Direct (Low-Rate Spontaneous Activity)	Increase
		Direct (High-Rate Spontaneous Activity)	No Difference
Jalligampala et al. 2017	rd10 mice	Indirect	No Difference
Ahuja et al. 2013	Human	Direct	Increase
Rizzo et al. 2003	Human	Direct	Increase
Mahadevappa et al. 2005	Human	Epiretinal	Increase

### 3.3.2.2 Stimulation Efficiency in Degenerated Retina

Previous studies using degenerate retina suggest that the increased spontaneous activity and potentially the oscillatory activity affect the RGCs threshold response to electrical stimulation. However, it was unclear whether these altered responses also reduced the signal transmission (for example, the signal-to-background activity ratio) of the response. To this end, different studies have investigated how the aberrant oscillatory activity influences both the light responses of rd10 RGCs [229, 230], and the electrical responses of the rd1 [247] and rd10 RGCs [248, 249] compared to their WT counterparts. Using patch clamping Toychiev et al.

[229] first showed that the signal-to-background noise ratio (SNR, calculated here by dividing the firing rate during the 1s light stimulation by the firing rate during unstimulated activity) was significantly lower in P39 – P60 rd10 (SNR ~1) compared to WT (SNR~30) RGCs at the highest light intensity. This was later validated by Ivanova et al. [230] who also found that there was no significant difference between the instantaneous firing rate during the light responses versus unstimulated activity in P40 rd10 RGCs. Taken together, these studies suggest that the rd10 RGCs cannot differentiate between the background oscillatory activity and the stimulated activity.

In response to electrical stimulation, Yee et al. [247] found that the SNR of the P20 – P55 rd1 RGCs in response to a single, monophasic anodic pulse was significantly reduced compared to the age-matched WT RGCs (P45 rd1 RGCs SNR ~ 2 versus P45 WT RGCs SNR ~12). They further found that this decrease in SNR correlated with the increased presence of oscillatory activity. In rd10 RGCs, both Haselier et al. [249] and Gehlen et al. [248] found that the SNR (calculated by the ratio of firing rate pre-stimulus and post-stimulus) was significantly reduced across P14 – P140 rd10 RGCs compared to the WT RGCs when stimulated with an epiretinal placed MEA.

From these studies, it is evident that the rhythmic oscillations arising because of the degenerating network are a significant source of noise and alter the RGC response to stimulation. As such, there is a clear benefit to diminish the activity altogether to minimise the corruption of the RGCs response. To this end, different groups have explored various techniques in a bid to abolish the patterned oscillations. Haselier et al. [249] proposed a 'pre-pulse stimulus' consisting of 10 biphasic pulses of current amplitude 80  $\mu$ A, duration 1 ms and frequency 1 Hz. The pulse sequence was used to block the spontaneous activity to get better electrically-stimulated evoked results, however, they found that the stimulation efficiency did not significantly change. They speculated that more optimised parameters may yield significant outcomes. In contrast, Toychiev et al. [229], Ivanova et al. [230] and Gehlen et al. [248] opted for pharmacological techniques using mefenamic acid and benzodiazepines, respectively. All studies reported that the pharmacological agents were able to abolish the oscillations and subsequently, increase the SNR in light [229, 230] and electrical [248] responses. Altogether these studies provide some promise in eliminating the unwanted oscillatory behaviour of the degenerating network and ensure that the stimulation efficiency does not suffer greatly.

### *3.3.2.3 Comparative Electrical Stimulation Studies between Degenerate and Healthy Retina*

The mounting evidence so far indicates that degenerate retinal network and its debilitating effects cannot be ignored when attempting to activate the RGCs through electrical stimulation. While it is impossible to eradicate this problem, one important step towards minimising its effects is to understand how the response may change between the healthy and degenerate models. To address this, different groups over the years have either directly compared their specific stimulus paradigms on healthy and degenerate retina in parallel [16, 17, 26, 30, 31, 91], or alternatively, artificially blocked the synaptic network using blockers in healthy retina to mimic late-stage retinal degeneration in which all the synaptic connections are lost [14, 15, 30, 73, 132, 139, 153, 165, 183] .

#### **3.3.2.3.1 Electrical Stimulation in Degenerate versus Healthy Retina**

Overwhelmingly, the studies that conducted parallel experiments on healthy and degenerate retina found that there was a difference in the response between the two models for example, threshold difference in rd1 [24-26] , RCS rats [110] and S334ter line 3 rats [33] and human retina [241-243]. Other studies focussed on how their results in healthy retina fared under degenerate conditions. For example, Tong et al. [30] found that while their optimised sub-retinal stimulation of 0.1 ms pulse duration to reduce spatial activation yielded similar results in the healthy Long Evans rats and blinded RCS rats, the use of localised returns only improved performance in the healthy rats rather than the degenerate. They concluded that the likely reason for this discrepancy is the correlation of a larger distance between the RGCs and the electrodes and the benefit of a local return configuration which is reduced in degenerate retina. Similarly, Yoon and colleagues. [28] investigated how electrically-elicited RGC responses through indirect activation varied between WT and rd10 mice. They concluded the delayed network-mediated responses became weaker in the degenerate mice in comparison to the WT mice. Lastly, as discussed previously, Sekhar et al. [17] and Ho et al. [31] both found their respective electrical and photovoltaic STAs presented as narrower, and sharper STAs with a short-latency in the degenerate rd10 mice compared with WT. The results from these parallel experiments indicate that a stimulation strategy which works effectively in healthy retina may not yield the same outcomes in degenerate retina highlighting the importance of testing the efficacy of a stimulation strategy in degenerate conditions.

#### **3.3.2.3.2 The Influence of Pharmacological Blockade**

The use of synaptic blockers in retinal studies is not new, however the purpose of the blockers in most studies was primarily to confirm whether the response was through direct or indirect means [14, 30, 132, 139, 153, 183]. In other studies, the use of pharmacological blockade was to shed light into how the RGCs response may change if it is completely isolated from the

network as a rough equivalent to end-stage retinal degeneration. Notably, both Margolis et al. [73] and Yang et al. [165] found that the RMP of ON RGCs became significantly hyperpolarised post-synaptic blockers, while the OFF RGCs did not have any statistically significant change. Yang et al. [165] further found that stimulation thresholds for the ON RGCs significantly increased with no change in the OFF RGCs. Both these studies imply that the excitability of the RGCs is dependent on the synaptic network and will likely alter during degeneration. Another pragmatic approach with synaptic blockers is to use them for the duration of the experiment to isolate the RGC response from the network and ensure that the data are derived from intrinsic properties of the RGCs rather than the network [15]. This approach could also be extended to isolate the degenerate RGCs from the degenerate network to further investigate the intrinsic properties of RGCs whilst also investigating the contributions, if any, of the altered synaptic input on the electrically-evoked responses of the degenerate RGCs.

### 3.3.3 Summary

In summary, the studies conducted in the degenerate retina indicate that retinal degeneration is a long, slow, and complicated process and has downstream effects on the inner retina. For example, different studies showed increased hyperactivity and aberrant oscillatory activity exhibited by the RGCs [23, 226, 227, 250], as well as differences in the intrinsic properties and excitabilities [21, 22, 239]. These studies throw caution to assumption that the inner retina, and importantly the RGCs are immune to the changes that occur in the outer retina. Moreover, these findings indicate that further studies investigating the intrinsic properties of isolated RGCs (i.e., without synaptic inputs) in degenerate retina may provide greater insights into if and how, the intrinsic properties are altered in RGCs in response to upstream degeneration.

In response to electrical stimulation, different groups conducted parallel studies in both healthy and degenerate retina and found overwhelmingly that the RGC response was not consistent across the two environments highlighting the importance of assessing the viability of stimulation strategies in degenerate retina. Interestingly, apart from the STA-based strategies [17, 31], none of the previous studies focussing on preferential activation of functionally-different RGC types have assessed the viability of their stimulation approaches in degenerate retina.

## 4 General Methods

The data presented in the results chapters 5, 6 and 7 are from three distinct studies wherein I characterise the effects of HFS across both healthy and degenerate mice models and for varying stimulation protocols.

This chapter is an overview of the general methods that apply to all experiments for the three studies except where noted. Additional study-specific methods will be included at the beginning of each results chapter where necessary.

### 4.1 Animal Preparation and Retinal Extraction

All procedures were reviewed and approved by the UNSW Animal Care and Ethics committee (18/25B) and carried out in compliance with the Australian National Health and Medical Research Code of Practice for the Care and Use of Animals for Scientific Purposes. Prior to each experiment WT C57BL/6J mice (ages P28 – P56, sourced from Australian BioResource) were placed in dark room to dark-adapt the retina for 8 – 12 hours. Rd1 mice (P60 – P350, sourced from either Australian BioResource or University of Western Sydney) were not dark adapted.

Retinal dissection for both WT and rd1 were treated the same. Mice were anaesthetised using 5% vaporised isoflurane via an induction chamber and euthanised using cervical dislocation. Both eyes were enucleated and placed in an extracellular solution containing Ames' medium, D+ glucose and sodium bicarbonate (Sigma-Aldrich, St. Louis, MO) and adjusted to a pH of 7.4 using carbogen (95% oxygen, 5% carbon dioxide). Each eye cup containing the cornea and lens was removed to isolate the retina. The curvature of the retina was reduced by removing the vitreous humor. Once flattened, four opposing cuts were made to resemble a clover-leaf shape and each section was mounted ganglion-cell side up on a modified Millicell Biopore membrane filter insert (PICM01250, Millipore, Billerica, MA, USA) and secured using the procedure outlined in [251]. The membrane insert was then placed into an imaging chamber (RC-40HP, Warner Instruments, Hamden, CT, USA) and held in place by applying a Vaseline layer between the outer radius of the membrane insert and the glass chamber. The imaging chamber was perfused with the extracellular solution at a rate of 3-4 mL/min, heated to approximately 33°- 35°C and maintained at a pH of 7.4 through carbogen bubbling. The chamber was illuminated using an infrared (IR) light source with wavelength of 780 nm passed through a Dodt gradient contrast (DGC) system and subsequently imaged using a fixed-stage upright microscope (SliceScope, Scientifica, Uckfield, United Kingdom). A camera

(DCC3204N, Thorlabs, Newton, NJ, USA) was used to continuously acquire the images which were viewed on the corresponding ThorLabs software (Thorlabs, Newtown, NJ, USA). For experiments which required light responses from the ganglion cells, the dissection and experiment were conducted in a dark room dimly illuminated with red light to avoid desensitisation of the cone photoreceptors. For experiments in which the retina was insensitive to light (Rd1, >P60) and the light response was not recorded, the experiments were conducted under normal light illumination.

## 4.2 Patch Clamp Recordings

### 4.2.1 Patch Pipette Fabrication and Intracellular Solution

Borosilicate glass tubes (Warner Instruments, Hamden, CT, USA) with an outer/inner diameter of 1.5/0.8 mm were placed in a micropipette puller (Sutter Instrument, Novato, CA, USA) to create recording patch pipettes with tip resistances of 3 – 6 M $\Omega$  and cleaning pipettes with tip resistances of 1 – 3 M $\Omega$ . Each patch pipette was filled with a solution containing potassium methanesulfate (106 mM), calcium chloride (0.0078 mM), magnesium chloride (1 mM), 4-(2-hydroxyethyl)-1-piperazineethanesulfonic acid (HEPES, 10 mM), ethylene glycol-bis(2-aminoethylether-N,N,N',N'-tetraacetic acid) (EGTA, 0.7 mM), phosphocreatine-sodium salt (10 mM), adenosine-triphosphate disodium salt (4 mM), guanosine-triphosphate trisodium salt (0.5 mM) and potassium chloride (10 mM). The pH of the solution was adjusted to approximately 7.3 with potassium hydroxide (1M). All the chemicals were purchased from Sigma Aldrich. Additionally, 70  $\mu$ M of Alexa Fluor 488 dye (Thermo Fisher Scientific, Waltham, MA, USA) was added to the final calibrated internal solution to visualise the patched RGCs.

### 4.2.2 Whole-Cell Patch Clamp

To clearly visualise the RGC layer, the surrounding inner-limiting membrane (ILM) [252] was first coarsely cleared before a more refined cleaning locally of the targeted RGC. Typically, large soma (> 20  $\mu$ m) RGCs located away from densely populated axon bundle regions, close to blood vessels, and in flat regions were chosen. Once patched, whole-cell and access resistance compensation were used to compensate for the resistance and capacitance of the patched RGC, and the resistance of the pipette. Cells used in this study commonly had cell resistances between 18 – 25 M $\Omega$ , and baseline potentials between -55 mV to -65 mV. The Ag/AgCl reference electrode was placed approximately 2 cm away. The movements of the pipette were controlled using an external micromanipulator (Sutter Instrument, Novato, CA, USA).

Whenever applicable, the data presented here has been corrected for a calculated liquid junction potential of 5 mV.

### 4.2.3 Data Acquisition

All cell responses were acquired using the Multiclamp 700B amplifier (Molecular Devices, Sunnyvale, CA, USA), low pass filtered at 10 kHz and digitised/sampled at 50 kHz using the Digidata 1440A acquisition system and displayed using the corresponding pCLAMP 10 software (Molecular Devices, Sunnyvale, CA, USA).

### 4.2.4 Cell Classification

Cell identification for the four alpha RGC types in healthy tissue (Chapters 5 and 6) was achieved by illuminating each patched cell using directed full-field white light flashes centred over the cell somas for 1 s; preceded by 500 ms pre-stimulus and followed by 1 s post-stimulus of darkness (Figure 4.1). This light stimulation protocol was also used in a prior study conducted by Guo et al. [15]. The cell's response to the onset or offset of light was used to determine its ON or OFF RGC type. To further classify each cell type as transient or sustained, each 1 s window during the light or post-light dark phase was divided into 200 ms segments. Equation 4.1 was then used to determine a classification ratio (CR) between the total spike count for the first 200 ms window over the total spikes in the entire 1 s segment. If the ratio was above 0.5, the cell was classified as transient and if less than 0.5, the cell was classified as sustained.

$$CR = \frac{SC_{200}}{SC_{1000}} \quad (4.1)$$

where SC denotes the total elicited spike count during the light stimulus (for ON cells) or post-stimulus (for OFF cells). A similar method of classification was used by Tsai et al. [48] who segmented each light and dark phase into 500 ms segments respectively and compared the spiking rates between corresponding segments to identify the transient and sustained cell types.

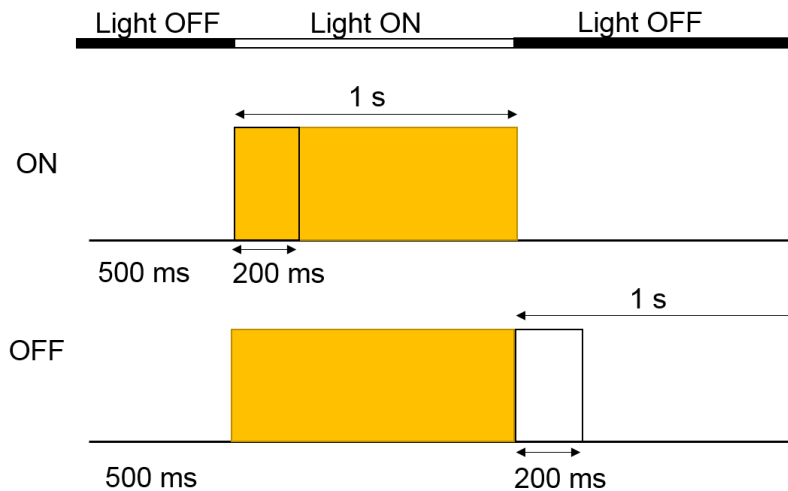


**Figure 4.1** Diagram showing classification of healthy RGCs based on their light response. Each cell was illuminated with a light stimulus for 1 s, preceded by a 500 ms pre-stimulus and 1 s post-stimulus of darkness. Depending on the ON or OFF type, the CR was calculated either for the 1 s light of 1 s post-stimulus darkness to classify the cell as sustained or transient.

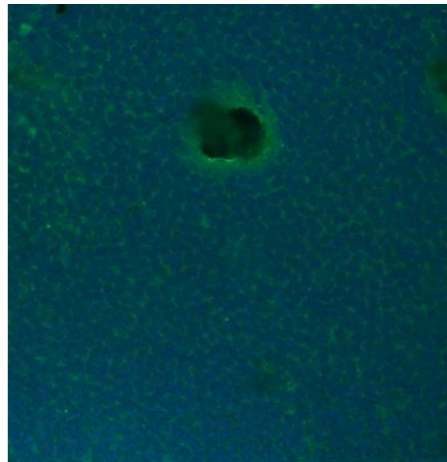
Cell identification for ON and OFF RGCs in degenerate retina was based on differences in dendritic stratification in the IPL [73] , as well as cell-specific oscillatory behaviour (outlined in Chapter 7, Section 7.2.1). In this section, only the protocol for identifying the cell through morphological differences will be outlined.

All recorded cells were filled with Neurobiotin (Vector Laboratories). Post-recording, the tissue was fixed for 1 hr with 4% paraformaldehyde in 0.1 M phosphate buffer solution (PBS). The fixed tissue was incubated overnight at 3°C in a blocking solution containing 1% bovine serum and 0.5% Triton X-100 in PBS. Following this, the tissue was washed for 30 min in fresh blocking solution and incubated for 3 hrs in 1:500 Streptavidin Alexa Fluor 488 (Thermo Fisher). The tissue was subsequently washed for 45 min in fresh blocking solution before being counter-stained and mounted using ProLong Gold + 4',6-diamidino-2-phenylindole (DAPI) mounting media (Thermo Fisher).

Using an upright confocal microscope (Olympus FV1200), z-stacks were acquired to capture the green fluorescence of the patched RGC filled with Neurobiotin, and the blue fluorescence of all cells marked by DAPI. The DAPI-stained cells were used to define the inner and outer borders of the IPL. The inner border was considered the INL and defined as the first image to contain uniform cell somas, and the outer border was considered as the GCL and defined as the last image to contain the patched RGC's axon and RGC somas (Figure 4.2). To find the dendritic stratification of a given cell, a similar calculation outlined in [73] was used. Briefly, for a given cell, the location of the peak fluorescence from the dendrites is expressed as a percentage within the IPL borders where the inner border is considered as 0% and the outer

border as 100%. If the dendrites lay within 0 – 50%, the cell was considered as OFF, and if within 50 -100%, the cell was considered as ON.

Inner Border  
(0%)



Outer Border  
(100%)

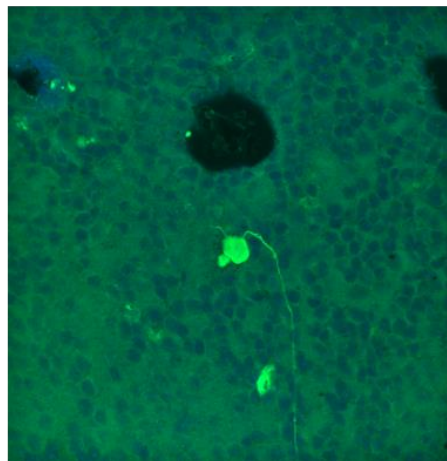


**Figure 4.2 Representative OFF RGC classification in rd1 retina.** ON and OFF RGCs in degenerate retina were classified based on their different stratification depths in the IPL. For each degenerate RGC, the inner border was defined as the first image that contained uniform DAPI-stained cell somas (blue fluorescence) and the other border was defined as the last image that contains both the patched RGC soma and axon (green fluorescence) along with the remaining DAPI-stained RGCs.

#### 4.2.5 Synaptic Blockers

A cocktail of synaptic blockers was used to abolish synaptic inputs to the RGCs. The duration between the blocker wash-in and commencement of recording was dependent upon complete abolishment of the light response (in WT retina) and confirmation of a stable membrane potential (in WT and rd1 retina); but was typically between 5 – 7 minutes for each cell. A few cells exhibited spontaneous activity (defined here as a cell spike occurring when there is no current amplitude) after the application of blockers. While this activity had no obvious effect on the HFS response in the results presented in Chapter 5 and therefore did not require any

post-subtraction, spontaneous subtraction was employed for the results presented in Chapters 6 and 7. The methodology and calculations are outlined in (Chapter 6, Section 6.2.2.1). The cocktail itself contained strychnine (0.01 mM) to block glycinergic receptors, picrotoxin (0.1 mM) to block GABA receptors, NBQX (0.01 mM, 2,3-dihydroxy-6-nitro-7-sulfamoyl-benzo[f]quinoxaline) to block AMPA/Kainate receptors, D-AP5 (0.05 mM, (2R)-amino-5-phosphonovaleric acid) to block NMDA receptors and L-AP4 (0.02 mM, L-2-amino-4-phosphonobutyric acid) to block mGluR6. All the chemicals were purchased from Sigma Aldrich or Tocris Bioscience.

## **4.3 Extracellular Electrical Stimulation**

### **4.3.1 Stimulating Electrode Fabrication**

The stimulating electrodes were fabricated from 25  $\mu\text{m}$  platinum-iridium (Pt-Ir) wire (Sandvik) and coated with polytetrafluoroethylene (PTFE). The wire was then cut transversely to expose the circular tip. The platinum reference electrode was placed approximately 2 cm distant from the tissue in the bath in a monopolar configuration.

Different HFS protocols were used for the studies described in Chapters 5 – 7, and the respective protocols will be outlined in the chapter-specific methodology sections.

### **4.3.2 Stimulating Electrode Location**

To ensure consistency in the placement of the stimulating electrode, each patched RGC was locally defined using a 3D coordinate system in which the centre of the soma acted as the origin (0,0,0), the axon bundles aligned with the y-axis and the depth of the retina was the z-axis. To mimic an aspect of clinical conditions in which an epiretinal electrode array may not necessarily touch the epiretinal surface due to instability over time [243, 245] the stimulating electrode was placed 20  $\mu\text{m}$  above the epiretinal surface. This was done by first lowering the stimulating electrode until it visibly touched the epiretinal surface, and then raising it by 20  $\mu\text{m}$ . The movements of the stimulating electrode were also controlled using an external micromanipulator (Sutter Instrument, Novato, CA, USA).

Initially to identify the approximate location of the axon of each cell that was patched, the stimulating electrode was placed at 3D coordinates  $(0, 40 \mu\text{m}, 20 \mu\text{m})$  and  $(0, -40 \mu\text{m}, 20 \mu\text{m})$ . At each location, the electrode was stimulated using the threshold stimulus paradigm until threshold was reached. Figure 4.3 illustrates a schematic of the 2D plane of the two potential locations of the stimulating electrode. The location of the axon was later validated after extracellular stimulation by visualising the patched RGC using the Alexa Fluor 488 dye under an excitation wavelength of 470 nm (M47OL3, Thorlabs, Newton, NJ, USA). The resulting epi-fluorescent images were captured using a scientific camera (1500M-GE, Thorlabs, Newton, NJ, USA). Cells with axons which did not lie at  $(0, \pm 40 \mu\text{m}, 20 \mu\text{m})$  were not considered for further analysis. The stimulating electrode was then placed  $(0, 40 \mu\text{m})$  away from the soma in the direction opposite to the axon (optimised previously in Yang et al. [165]) for the remainder of the experiment.

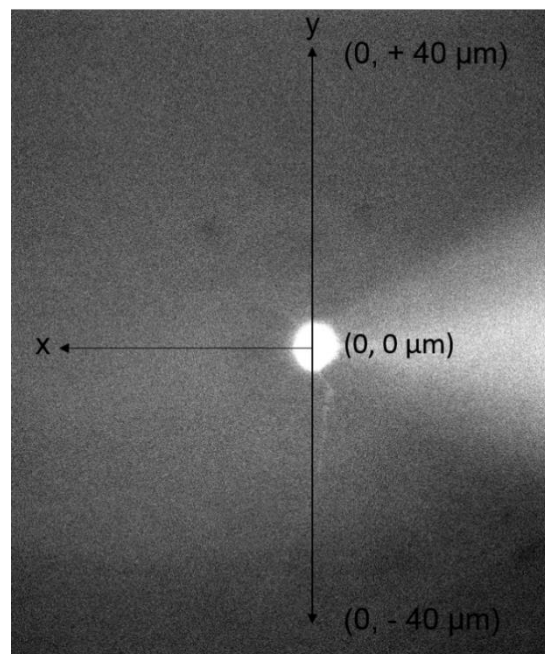


**Figure 4.3 Location of the extracellular stimulating electrode.** The electrode was placed  $40 \mu\text{m}$  opposite to the cell's axon. Each cell soma acts as the origin in the 3D plane, with the y-axis parallel to the axon and the z-axis as the depth of the retina. The stimulating electrode is placed opposite the axonal side.

### 4.3.3 Threshold Stimulation

All cells were stimulated with a threshold stimulation paradigm using the STG4002 (Multichannel Systems, Reutlingen, Germany).

The threshold stimulation paradigms consisted of a single cathodic-first biphasic pulse. Each pulse had a phase width of  $100 \mu\text{s}$ , with no inter-phase delay and inter-pulse delay of  $0.2 \text{ s}$  to ensure spike elicitation arose from direct activation and to avoid desensitisation effects

respectively (22). The amplitudes were presented linearly from 5 - 120  $\mu\text{A}$  at 5  $\mu\text{A}$  steps with 10 repeats until threshold, defined here as the first current amplitude to elicit a spike response from 5 out of the 10 tested trials. No current amplitudes above this threshold were presented for any cell.

## 4.4 Data Analysis

All data analysis was performed using custom code in MATLAB 2019a and statistical analysis using Prism 6. Two primary filters were used for analysis. To detect the non-spiking baseline potential, a low-pass 9th-order Butterworth filter with cut-off frequency at 100 Hz was used. The baseline was then calculated across 500 ms of raw data from three consecutive trials. The average of the repeats was taken for each cell and used to calculate the population average and standard error of the mean (SEM). To assess the statistical significance of the difference in baseline potential before and after the application of synaptic blockers for each cell type, a paired t-test was used with a set confidence level of 95%. For spike detection during HFS, a custom-designed filter was used to first high-pass filter the data using a 5th-order Butterworth filter with cut-off frequency of 10 kHz before employing a threshold detector to remove any artefacts. A spike-detection threshold was then manually assigned based on visual analysis of the raw traces and spikes crossing this threshold were considered full action potentials. It is important to note that the high signal-to-artefact ratio made it straightforward to set a manual voltage threshold for spike detection.

### 4.4.1 Preferential Activation Maps

Preferential activation maps were employed for Chapters 5 – 7 to illustrate the regions in which a target cell population could be preferentially activated over the remaining population. To calculate the preferential activation maps, each cell was initially defined by a 2D (number of frequencies  $\times$  number of amplitudes) averaged spike count matrix encapsulating the average spike count during the pulse train across three trials for the full frequency and amplitude steps. To identify the probability of each cell firing relative to its maximum spike rate, while ensuring equal contribution of each cell to the population, each cell was normalised to its own maximum spike count across all frequency and amplitude combinations. This was achieved by taking the ratio of the averaged spike count at a given frequency and amplitude combination, and the maximum spike count across the full frequency and amplitude spectrum (4.2). This calculation yielded another 2D normalised individual spike count matrix for each cell. The average was then calculated across all the normalised individual spike count matrices giving a normalised population spike count matrix for each cell type with the error reflected by the SEM. Note, the frequency and amplitude parameter space used in Chapters 5 – 7 are not

the same and therefore the size of the 2D matrices will differ between the chapters. However, this does not influence the subsequent normalisation and population average calculations.

$$NSC_{(f,A)} = \frac{SC_{(f,A)}}{Max[SC_{i,j}]} \quad (4.2)$$

Where for a given frequency (f) and amplitude (A), NSC represented the average normalised spike count, SC represented the averaged spike count in absolute units, and SC<sub>i,j</sub> was the 2D averaged spike count matrix in absolute units where i represents the amplitudes and j the frequencies.

Figure 4.4 shows an example OFF cell and population to diagrammatically depict the normalisation and population average calculations. In this example, the cell was stimulated with 8 frequencies from 1 – 6 kHz and 24 amplitudes between 10 – 240 µA. Figure 4.4A shows a HFS response heat map for a representative OFF cell in which each colour on the map corresponds to the average spike count during a 300 ms pulse train across three trials. In Figure 4.4B, the same OFF cell was normalised to its own maximum averaged spike count across all tested frequencies and amplitudes. For a given cell, this value is referred to as the individual normalised spike count (NSC<sub>T</sub> in Equation 4.3) for a given frequency and amplitude combination. Each cell must have *at least* one frequency-amplitude combination in which the normalised value was 1. In the example shown, the OFF cell had its maximum spike response at (4 kHz, 130 µA). Following this, the average of all the normalised cells was taken to give the population response. The example OFF population response is shown in Figure 4.4C. Note, the averaged normalised spike count in the population response will only reach 1 if *all* the cells in the population have their maximised response at the same frequency-amplitude combination. In Figure 4.4C, the maximum averaged normalised spike count is ~0.7 indicating that the cells in the population had their maximum spike counts at different frequency-amplitude combinations.

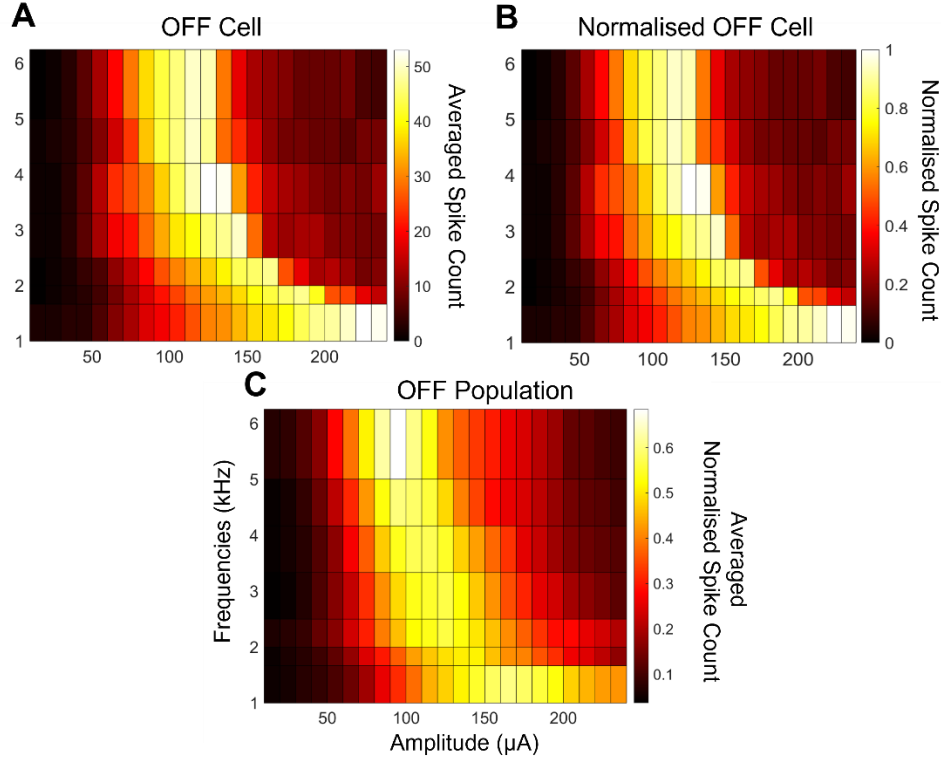


**Figure 4.4 Example individual and population response heat maps in response to HFS.** The averaged or normalised spike count for each tested frequency and amplitude combination is represented as a coloured square on the map. (A) Heat map for a representative OFF cell indicating the averaged spike counts across frequencies 1 – 6 kHz and amplitudes 10 – 240 μA. (B) Heat map for the same representative OFF cell reflecting the normalised spike count. Each averaged spike count was normalised against the maximum averaged spike count across all frequencies and amplitudes. (C) Heat map showing the normalised population spike counts for all OFF cells.

Preferential activation of a cell type was defined as the probability of one cell population spiking over the other three populations. Each preferential activation map was generated by taking the difference of the normalised population spike count matrix of the target cell population (example in Figure 4.4C) and the average of the normalised population spike count matrices of the remaining three populations (Equation 4.3). To assess areas of statistical significance, a one sample t-test against a probability of zero for each frequency-amplitude combination in each differential activation map was applied (alpha level of 0.05).

$$NSC_{T(f,A)} - \frac{\sum_{i=1}^{n_{RP}} NSC_{RP(f,A)}}{n_{RP}} \quad (4.3)$$

Where  $NSC_T$  represented the normalised individual spike count of a single cell in the target population for a given frequency ( $f$ ) and amplitude ( $A$ ),  $NSC_{RP}$  represented the normalised

spike count for a single cell in the remaining population, and  $n_{RP}$  represented the total number of cells in the remaining population.

## 5 Preferential Activation of Four RGC types using HFS

The work presented in this chapter is part of a publication titled “Neural activity of functionally different retinal ganglion cells can be robustly modulated by high-rate electrical pulse trains” published in the Journal of Neural Engineering in 2020 (Issue 4, Volume 17, Page ID 045013). The respective contributions of the two joint first-authors are as follows: Miss. Madhuvanathi Muralidharan and Dr. Tianruo Guo jointly designed the study and conducted the *in vitro* experiments. Miss. Muralidharan analysed the data that resulted in Figures 1 – 3 in the manuscript (corresponds to Figures 5.1 – 5.3 in this chapter), and Dr. Guo analysed the data that resulted in Figure 4 and Tables 1 – 2 in the manuscript but have been omitted from this chapter. Miss Muralidharan wrote the published manuscript under the guidance of Dr. Guo, and the remaining co-authors aided in the drafting, editing and final approval of the manuscript. The structure of this chapter has been slightly modified from the published version. However, the text corresponding to the results generated by Miss Muralidharan appear the same as in the published manuscript.

### 5.1 Introduction

The functional diversity of RGCs has been shown across numerous animal models including primate [253, 254], mammalian [58, 135, 255] and mice [8, 256]. Each of these specialised RGC types is thought to uniquely encode different aspects of the visual scene via their spiking patterns [257]. Of these different cell types, four broad cell types which exist across mammalian retinas are the ONS, ONT, OFFS and OFFT cells. ON and OFF RGCs respond to changes in luminance [55] while sustained cells detect the form, size and shape, and transient cells detect the motion or location of the input [11-13]. Given the specialised network of these visual pathways, the likelihood of their indiscriminate activation under natural vision is very little. However, it is higher under electrical stimulation potentially due to a mismatch in size between the larger electrodes [258] and the smaller interspersed cells, as well as similar biophysical properties between the different cell types [200]. This in turn sends conflicting information to the brain potentially leading to poor artificial vision.

To advance towards replicating the natural visual signals in RGCs, an optimal stimulation method is required to have more precise control of the activation of the functional RGC types. To this end, many teams in the last few years have worked on providing better means to encode neural activity. However, most of these efforts have relied on indirect activation i.e.,

activation of RGCs via the presynaptic network [17, 31, 122, 126, 130]. The issue however is the role of the synaptic network in shaping the differential responses, thus limiting their clinical use. The alternative approach is to directly stimulate the RGCs. Currently, there are two primary strategies being developed, namely the use of local returns to precisely control the spatial activation allowing preferential activation of ON and OFF parasol cells [164] and HFS to differentially activate ON and OFF RGCs [14, 15].

Given the benefits of direct stimulation, Guo et al. [43] and Yang et al. [44], extended the work on HFS-based differential activation pioneered by Twyford et al. [14] by extending the frequency and amplitude parameter space, and for different electrode locations to assess whether the ON and OFF RGCs could still be differentially activated [15, 165]. They found that the ON RGCs could be preferentially targeted at higher frequency and amplitudes, and OFF RGCs across all frequencies but relatively lower amplitudes [15]. They also found that stimulating away from the axon enhanced the differential activation between the two [165].

In this study, given that sustained and transient RGCs (alongside ON and OFF) subserve different roles in natural vision, and constitute ~70% of the primate and mice RGCs [8, 9], I further classified the ON and OFF RGCs into their sustained and transient subtypes to assess the possibility of preferentially activating all four (ONS, ONT, OFFS and OFFT) RGC types. I hypothesised that all four RGC types could be preferentially activated when stimulated using an appropriate combination of stimulation frequency and amplitude.

## 5.2 Methods

Please refer to the General Methods (Chapter 4) for detailed methods on animal euthanasia and retinal extraction (Chapter 4, Section 4.1), whole-cell patch clamping including cell classification and use of synaptic blockers (Chapter 4, Section 4.2), extracellular stimulation (Chapter 4, Section 4.3) and generation of the preferential activation maps and the corresponding analyses (Chapter 4, Section 4.4) In this section, the HFS protocol will be outlined.

### 5.2.1 HFS Protocol

The HFS paradigm consisted of cathodic-first, 40  $\mu$ s biphasic pulse trains with stimulation duration of 300 ms delivered for amplitudes 10 – 240  $\mu$ A at 10  $\mu$ A steps and approximately linearly-increasing frequencies of 1, 1.67, 2, 2.5, 3.33, 4.167, 5 and 6.25 kHz (optimised in Guo et al. [44]). The amplitudes were presented linearly for each frequency and repeated three times. The presentation of frequencies was randomised to avoid possible effects of a monotonically changing stimulation frequency. An inter-trial delay of 1 s was used to avoid the adaptation effects of a linearly increasing amplitude. This was confirmed by stimulating the

cell with linear and randomised amplitudes at the lowest and highest frequencies and found that there was no statistical significance in the spike responses (data not shown). Note, some of the frequency and amplitude combinations used in this Chapter, along with Chapter 6 and 7 exceed the safe charge limit of platinum electrodes [259]. However, I did not observe any deleterious effects of this such as pH changes or electrolysis of water during stimulation, nor observed any impact on the health of the cell.

## 5.3 Results

### 5.3.1 Effect of Synaptic Blockers on Light Responses and Baseline Potential

Since I was interested in the response of the RGCs to HFS without any synaptic input, I began by first assessing the effects of the synaptic blockers on the light response and the baseline potential for different cell types. Specifically, before the application of synaptic blockers (control) and after the application of synaptic blockers (blocked). Figure 5.1 shows the control and blocked light responses of a single cell for each RGC type.

All RGCs lost their natural response to light in the blocked stage. Few OFFS RGCs ( $n = 8/14$ ) and OFFT RGCs ( $n = 4/10$ ) exhibited regular spontaneous activity but did not appear to have any correlation with the spike rate of spontaneous activity (if any) before the blocker. Figure 5.1C shows the control and blocked baseline potential (refer to Chapter 4, Section 4.4 for calculation). On average, OFFS RGCs became slightly hyperpolarised in the presence of blockers, while OFFT RGCs became slightly depolarised. Both ON RGC types became hyperpolarised. Of the four cell types, however, only ONS RGCs exhibited a statistically significant difference in the control and blocked baseline potential (paired t-test;  $n = 12$ ;  $p < 0.0001$ ). It is important to acknowledge that external factors such as background illumination, have the capacity to play a role in shaping the cellular response, particularly under the control conditions. Notwithstanding, similar trends on the influence of synaptic blockers on baseline resting membrane potential between ON and OFF RGCs were reported by Yang et al. [165] and Margolis et al. [73]. Synaptic blockers were used for all subsequent experiments.

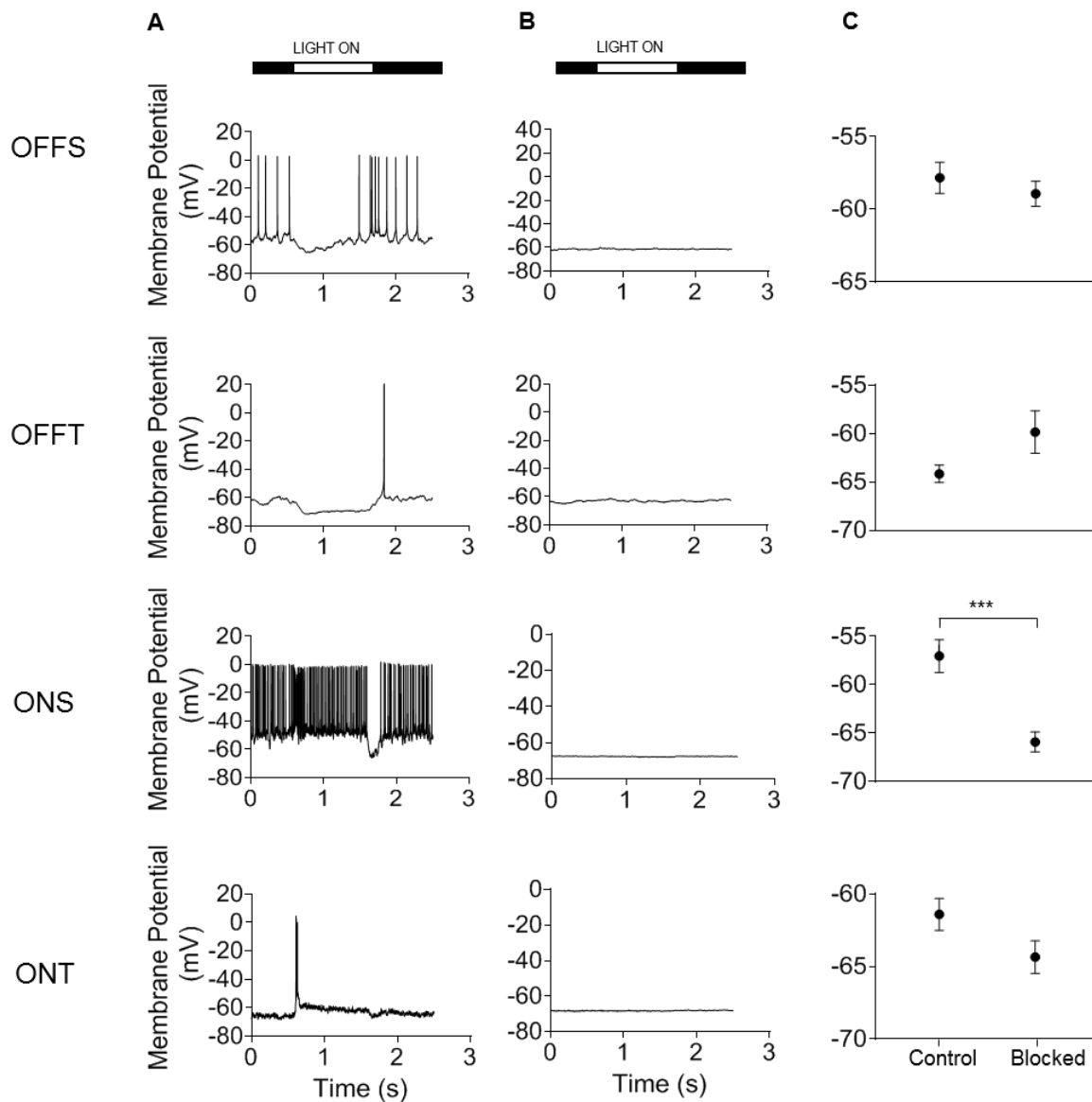


**Figure 5.1** Light response and baseline potential of four types of RGCs. In the blocked stage, all cells had an abolished light response and ONS cells were significantly hyperpolarised. (A) The response of a single OFFS, OFFT, ONS and ONT RGCs to a light pulse. (B) Blocked light responses (C) Control and blocked baseline potential for the OFFS ( $n=14$ ), OFFT ( $n=10$ ), ONS ( $n=12$ ) and ONT ( $n=13$ ) RGCs. Of all four cell types, only ONS exhibited a statistically significant difference between the control and blocked baseline potential (\*\* $p < 0.0001$ ).

### 5.3.2 HFS Responses of Four RGC Types

Figure 5.2 shows the individual and population spiking responses of each cell type to 300 ms of HFS (see Chapter 5, Section 5.2.1 for protocol). Figure 5.2A1 and A2 show the raw responses for a single OFFS, OFFT, ONS and ONT RGC, at frequency and amplitude combinations that resulted in a near maximum spike count and a marked reduction in spike count for each cell (denoted as red and black arrows in Figure 5.2A3 respectively). The spiking

profiles (rate and total number of spikes) differed between cell types and individual cells themselves but none of the cells exhibited a 1-to-1 spiking-to-pulse profile. On average, all four RGC populations showed a non-monotonic profile of increasing then decreasing spike counts with stimulus amplitude. However, the frequencies and amplitudes at which this was most evident were different for each RGC type (Figure 5.2A3 and B). Figure 5.2B shows the averaged normalised response across the four populations. Overall, all four cell types had regions of maximal activation (denoted by the blue arrows) in which majority of the cells in the population were activated. With the exception of OFFT cells, all remaining cells tended to spike at higher rates when using higher frequencies for stimulation. On average when using higher frequencies for stimulation, OFFS, OFFT and ONS cells all had immediate cessation of spiking in comparison to ONT cells (indicated by the relatively higher normalised spike count at higher amplitude and higher frequencies).

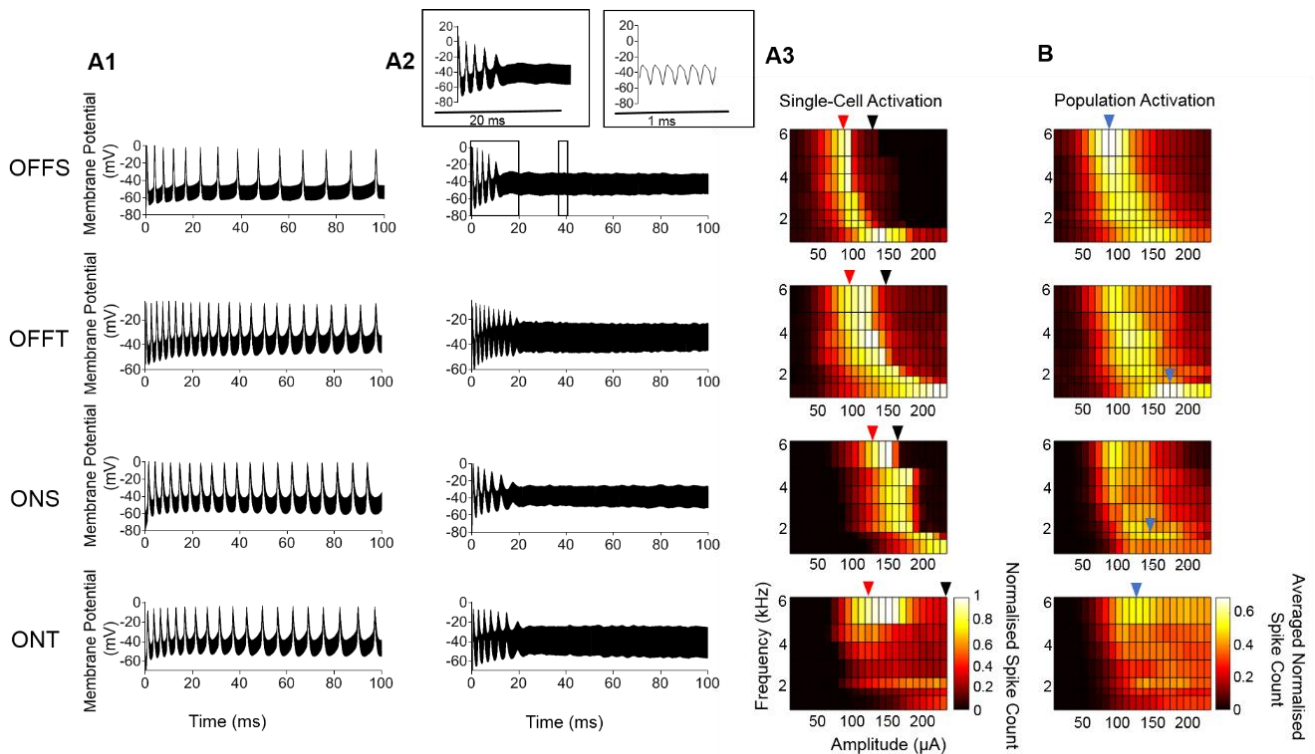


**Figure 5.2 Population response maps of four RGC types to HFS.** All four types across the population had clear regions of maximal activity specifically, OFFS between 90 – 110  $\mu\text{A}$  at 6 kHz, OFFT between 160 – 200  $\mu\text{A}$  at 1 kHz, ONS at 110 – 160  $\mu\text{A}$  at 2 kHz and ONT at 100 – 150  $\mu\text{A}$  at 6 kHz (A1) Spiking responses at combinations that yielded near maximal spiking rate of the cell. (A2) Spiking responses at combinations causing reduced spiking rate of the cell. Inset: Expanded view of raw spike traces for the initial 30 ms showing spikes riding on top of artefacts and later during the stimulus showing artefacts only. (A3) Normalised spiking responses for the cells in A1/A2 across the full range of frequencies (1 – 6.25 kHz) and amplitudes (10 – 240  $\mu\text{A}$ ). The red and black arrows correspond to the frequency and amplitude combinations used in A1 and A2 respectively. The normalised spike rate for every frequency and amplitude combination is represented as the coloured square on the map. (B) The averaged normalised spike response for the OFFS ( $n=14$ ), OFFT ( $n=10$ ), ONS ( $n=12$ ) and ONT ( $n=13$ ) RGC populations for the full frequency and amplitude parameter space. The blue arrows indicate the regions of maximal activity across the population.

### 5.3.3 Preferential Activation of Four RGC Types

To depict the level of preferential activation between the ON / OFF and the sustained / transient dichotomies, the RGC subtypes – ON ( $n = 25$ ) vs OFF ( $n = 24$ ), sustained ( $n = 26$ ) vs transient ( $n = 23$ ) – were compared using a preferential activation map (Figure 5.3A). Preferential activation is defined as the probability of one cell type population spiking over the other and calculated by subtracting the averaged normalised spike count of the respective populations. All four cell types exhibited distinct regions of stimulus frequencies and amplitudes where their probability of firing was significantly greater than those of the opposing type. For example, OFF cells were 10-30% more likely to respond compared to ON cells across all frequencies and relatively lower amplitudes (50 – 150  $\mu\text{A}$ ), whereas ON cells were more likely to respond at higher frequencies (4 – 6 kHz) and amplitudes (200 – 240  $\mu\text{A}$ ). A similar trend is apparent between the sustained and transient cells, with sustained cells 10 – 30% more likely to be activated for lower amplitudes (50 – 150  $\mu\text{A}$ ), across all frequencies and transient cells, with a similar likelihood, for higher amplitudes (150 – 240  $\mu\text{A}$ ) and frequencies (4 – 6 kHz).

Figure 5.3B1 shows similar preferential maps described previously for each cell type (OFFS, OFFT, ONS and ONT) against the average of the remaining population (i.e., the other three cell types). The highlighted frequencies (black rectangles) indicate the region of highest preferential activation for each of the cell types. Only three of the four types (OFFS, OFFT and ONT) had a statistically significant preferential activation space. OFFS RGCs were active at all frequencies between 20 – 100  $\mu\text{A}$ , OFFT RGCs at 1 kHz between 160 – 190  $\mu\text{A}$  and 3 kHz between 110 – 120  $\mu\text{A}$ , and ONT at 3 – 6 kHz between 150 – 240  $\mu\text{A}$ . Across all cell types, the maximum preferential activation possible was 40% (i.e., the targeted cell type was 40% more likely to fire than the average of the remaining population). This suggests that none of the cell types were able to attain complete selective activation against the remaining population.

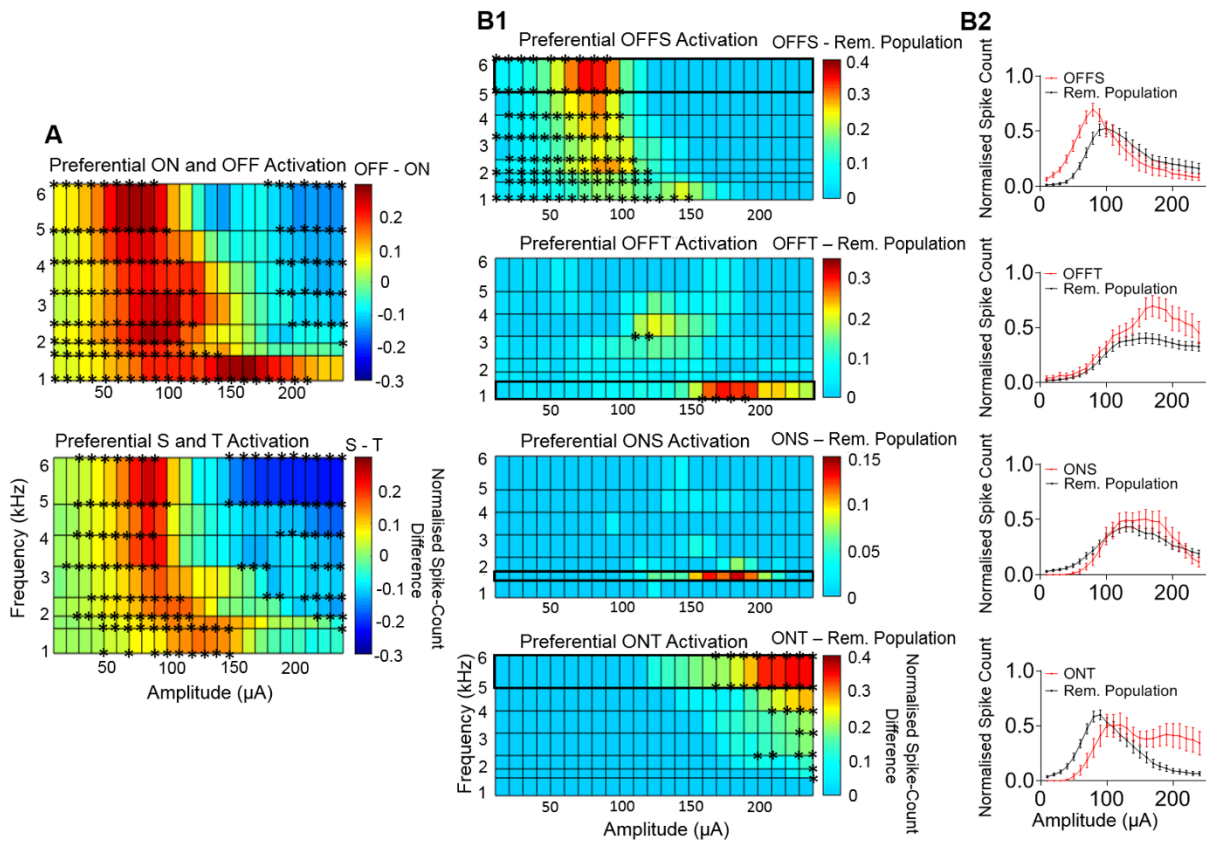


**Figure 5.3 Preferential activation map of functionally-distinct RGC types.** All cell types, other than the ONS cells, had stimulus configurations with which they can be preferentially activated against the opposing population, with statistical significance. Preferential activation is defined as the probability of one cell type population spiking over the other and calculated by subtracting the averaged normalised spike count of the respective populations. The colour bars indicate the normalised spike count difference between the two populations and the labels indicate the associated dominant and suppressed populations. The black asterisks denote regions of statistical significance (one sample t-test against difference of zero between normalised spike count of populations) (A) Preferential activation map for the ON ( $n=25$ ) versus OFF ( $n=24$ ) and transient ( $n=23$ ) versus sustained ( $n=26$ ) RGCs across the complete frequency and amplitude parameter space. (B1) Differential activation map for the OFFS ( $n=14$ ), OFFT ( $n=10$ ), ONS ( $n=12$ ) and ONT ( $n=13$ ) RGCs. Each cell-type's preferential activation is against its own exclusion population for example, the preferential activation map for OFFS cells are defined as the probability of its population firing against the remaining three cell populations The black rectangular highlighted region corresponds to the frequency in which the highest differential activation takes place for the cell type (B2) The averaged normalised spike responses across all amplitudes at the highlighted frequency in B1.

## 5.4 Discussion

The main findings of this study indicate that (1) ONS, ONT, OFFS and OFFT RGCs have unique sensitivities to different amplitudes and high frequencies, (2) OFFS, OFFT and ONT RGCs can be preferentially activated over the remaining population using HFS and (3) the cell's spike response was not dependent on the frequency, current or total charge of the pulse train alone, but a combination of both frequency and amplitude.

### 5.4.1 Frequency and Amplitude-Dependent Responses

The cell-specific population activation maps for the four RGC types (Figure 5.2) all indicate that their respective spiking responses are both frequency and amplitude dependent. For example, for all cell types the decreasing excitation stimulation thresholds with increasing frequency indicate frequency-dependency, while the maximal activation regions in specific amplitude ranges indicate amplitude-dependency. More interestingly however, are the differences in frequency and amplitude dependencies shown by all four cell types. While OFFS and ONT RGCs were maximally activated at the highest frequency, OFFT was maximally activated at the lowest frequency. Similarly, across most frequencies, both OFFS and OFFT RGCs were dominant at lower amplitudes ( $< 100 \mu\text{A}$ ), ONS in the mid-range amplitudes ( $100 - 150 \mu\text{A}$ ) and ONT at higher amplitudes ( $> 150 \mu\text{A}$ ). This raises the question of why these different RGC types respond preferentially to high frequency and amplitudes, and the mechanisms that could be underlying these preferentially responses. Given that the results were obtained after blocking the synaptic network, the differences in dependencies are likely due to intrinsic differences of the cell types rather than the synaptic network.

#### *5.4.1.1 Properties Influencing Frequency-Dependent and Amplitude-Dependent Responses*

Considering frequency first, the ability of a cell to follow a pulse train is highly dependent on its ability to recover from its refractory period or inactive state [175]. Previous studies have indicated that select sodium channel subtypes can follow relatively higher stimulation frequencies [81] potentially due to the presence of a resurgent current which activates during the repolarisation of the cell and drives the cell into a shorter semi-blocked state rather than the longer inactivated state [191-193, 260]. Of the subtypes supporting this resurgent current, Nav 1.1, Nav 1.2 and Nav 1.6 channels have all been found in rodent RGCs [75-77], however only the distribution of Nav 1.6 channels have been characterized in mice RGCs, [79]. Specific to the AIS, they found the distribution of Nav 1.6 channels scaled proportionally with the AIS length, and ON  $\alpha$ -RGCs had a longer AIS in comparison to OFF  $\alpha$ -RGCs. Taken together, this provides initial evidence to suggest that these two cell types may indeed have different intrinsic distributions of sodium channels allowing them to respond differently to HFS.

While frequency-dependent responses may be driven by sodium channel subtypes, differences in amplitude-dependency may simply be due to differences in the relative excitability of the cell types after the application of the synaptic blockers. From Figure 5.1, the OFF RGCs on average are more depolarised than their ON counterparts after blockers, making them easier to drive at lower amplitudes. Meanwhile, the ON RGCs were activated at amplitudes  $> 50 \mu\text{A}$  but most robust at amplitudes  $> 100 \mu\text{A}$ . The higher excitation stimulation

amplitude in comparison to OFF RGCs can most likely be explained by their relatively hyperpolarised state after blockers however, their robust spiking at the higher amplitudes, especially the ONT RGCs, is intriguing. A potential explanation is the greater number of monotonically responding cells than non-monotonic cells within the ONT RGC population across all frequencies i.e., the inclusion of cells which would not block at the highest amplitude. However, this in turn raises the question of why some cells have a much higher suppression threshold than others. To this end, Kameneva et al. [190] investigated the mechanism behind the blocking response and attributed the phenomenon to the potassium channel density and size of the axonal sodium band. More recently, a study conducted by Guo et al. [187] found that the spiking suppression may be dependent on the cell sodium channel properties raising the possibility of differences in concentration of sodium current channels for example, as found in Raghuram et al. [79] between the OFFS, OFFT and ONT RGCs driving their varying responses to amplitude.

#### *5.4.1.2 Applications of Unique Frequency and Amplitude Responses*

The unique responses of these RGCs to HFS also suggests that aside from preferential activation, a broader application may be using these responses as a distinctive fingerprint to identify cell types. For example, OFFS RGCs may be identified as cells that respond robustly to low amplitudes and ONT RGCs as cells that respond robustly to combinations of high frequencies and amplitudes. This becomes increasingly useful when considering degenerate retina, where identifying cell types is largely dependent on morphological differences such as dendritic stratification [49, 73] rather than quantifiable intrinsic properties. Another application may also be for high-resolution prostheses which rely on encoding the spatiotemporal patterns of RGC types to a visual stimulus and then decoding the signals to build an optimised waveform to activate the same cell type [261, 262]. Given the limitation of this technique in a blind patient due to a lack of visual feedback, if a cell type can be identified by its response to electrical stimulation as shown here, it may be a useful replacement for cell identification via visual stimulation. It should be noted however, that the aforementioned characteristic properties of the cell types are intrinsically derived, e.g., under the absence of any synaptic input. Given that there is no current indication on how synaptic input alters the cell differential response, it is likely that any cell identification will need to take place under similar conditions as outlined in this study that is, by isolating the RGCs from the inner retinal network.

#### **5.4.2 Preferential Activation of RGCs**

The preferential activation maps shown in Figure 5.3 suggest that three of the four targeted cell types (OFFS, OFFT and ONT) can be preferentially activated relative to their remaining population. OFFS preferential activation was maximised between 20 – 100  $\mu$ A across all

frequencies, OFFT between 150 – 240  $\mu$ A at 1 kHz, and ONT between 180 – 240  $\mu$ A at 4 – 6 kHz.

Taken together, the three preferential maps indicate the ability to preferentially activate a target cell type by carefully tuning the frequency and amplitude parameters. For example, if the frequency of stimulation is set to 6.25 kHz, altering the amplitude between 20 – 240  $\mu$ A should theoretically be able to switch between preferentially activating the OFFS and ONT populations while setting the frequency at 1kHz and altering the amplitude between 20 – 200  $\mu$ A should preferentially activate between the OFFS and OFFT populations. Similarly, by setting the amplitude between 150 – 200  $\mu$ A and changing the frequency between 4 – 6 kHz, the OFFT and ONT populations could be preferentially activated. The ability to preferentially activate RGC types hinges on exploiting their preferential responses to a given stimulus. As described previously, OFFS RGCs were maximally activated at lower amplitudes, translating to a clear preferential space at lower amplitudes across all frequencies. Similarly, the ONT RGCs were activated at higher amplitudes, translating to a preferential space at the same location.

It is important to note that within the tested parameter space, the ONS cells could not be preferentially activated relative to the remaining population. While there are limited studies illustrating the effect of preferential activation of a particular cell type on the visual percept, a study conducted by Im et al. [122] speculated that ‘bright phosphenes’ reported by clinical patients [102] may be explained by their findings that (a) ON cells have closer correlations between their electrical and light responses compared to OFF cells and (b) only the ONS cells had a period of spiking in isolation of the remaining three cell types. Their study suggests that preferential activation of ONS may be useful in generating bright phosphenes which will likely aid the visual perception. However, their study is based on indirect activation and not direct activation used in this study. As such, it is difficult to speculate how direct stimulation-based preferential activation of cell types will translate to phosphenes.

The ability to elicit these differential responses to both indirect and direct electrical stimulation for different RGC types is not a new venture. Several studies have reported differential responses using alternative electrical stimulation under indirect activation. Sekhar et al. [17] and Ho et al. [31] both reported distinct network-mediated ON and OFF eSTAs and pSTAs in response to temporal Gaussian electrical white noise and photovoltaic stimuli for both healthy and degenerate retina respectively. Meanwhile, Im et al. [122] found that ON and OFF BT and BS RGCs had differential responses to the cathodal and anodal phases of a sinusoidal waveform while Im et al. [130] found that ON and OFF cell responses differed for increasing stimulation durations in half-sinusoidal waveforms. More recently, Lee et al. [126] found that

indirect activity of ON cells was more sensitive to charge while OFF cells were sensitive to current.

The main caveat associated with network-mediated electrical stimulation, however, is how the responses will alter with a degenerating network. To this end, both Ho et al. [31] and Sekhar et al. [17] showed the existence of a similar differential response in a degenerate retina, but did not identify the RGC type indicating that the pathways and RGC type being activated are unknown. Given that the differential response seen under indirect activation may be a combination of both the network and intrinsic properties of RGCs, quantitatively relating the network-mediated responses to the RGC type and the degenerating network may aid in understanding the extent of the network in shaping the responses and aid in guiding future stimulation strategies.

Direct stimulation as used in this study circumvents the abovementioned issues associated with indirect stimulation, implying that the differential responses which arise are likely to be independent of at least the photoreceptors, making them more clinically viable. This however does not make it immune to the effects of a degenerating retina. For example, Margolis et al. [23] found changes in the synaptic input for ON and OFF RGC types in a degenerate retina, which in turn altered their RMP. Given that there is a certain level of reliance on differences in the RMP to differentially activate cell types in the study presented here, it highlights the equal importance for direct stimulation studies to assess the viability of generating a differential response in a degenerating retina.

### 5.4.3 Limitations

#### 5.4.3.1 *Limitations of the mouse model*

The results shown here are derived primarily from alpha-RGCs in the mouse retina and not primate retina which brings into question the generalisability of these results particularly regarding the equivalency of rodent versus primate RGCs. Typically, transient and sustained cells in higher-order animals are thought to be homologous to the parasol and midget cells respectively in primates [62]. Whether this equivalency extends to the mouse model remains a grey area, especially considering the fourth type of alpha-RGC discussed here – the ON-T cells – has only recently been defined by Krieger et al. [63]. By comparing the stratifications of the different RGCs, they speculate that the Y-cells in cat retina are comparable to the ON-T and OFFT RGCs in mice, and the delta and epsilon cells in cat are potentially comparable to ON-S and OFFS RGCs in mice. More recently, Werginz et al. [263] compared the light and electrical responses of the same four types of cells between mice and rabbits and found that while [63] transient cells between the two models correlated well, the same could not be said for the sustained cells. Taken together, these reports suggest that targeting the transient

subtypes for preferential activation may be more beneficial than sustained given the potential equivalency of these cells in primate retina.

More recently, studies have indicated the non-uniformity of the anatomical and physiological properties of identical cell types based on their location [63, 79, 264]. For example, Raghuram et al. [79] found that the AIS length and location varied across the retina and Warwick et al. [264] found that the alpha-OFFT RGCs had a different light response based on their location on the dorsal-ventral axis. Taken together, these observations indicate the necessity of sampling cell types in a similar retinal space. While all the cells were sampled in the far peripheral space [265] in the study presented here, the exact location along the ventral and dorsal axis is unknown. Given the physiological light responses of alpha-OFFT RGCs vary along this axis [264], this introduces some uncertainty in the classification of OFFS and OFFT RGCs. To this end, additional markers to further differentiate sustained from transient types aided in verifying their original classifications. For example, OFFS RGCs were more likely to have tonic firing before and after the onset of light [266, 267] and OFFT RGCs were likely to have high frequency firing at the offset of light [73, 135]. Notwithstanding, the increasing breadth of knowledge regarding location-dependent cell properties sheds light on the likelihood of requiring location-independent markers for cell classification in future.

#### 5.4.4 Future Work

The results presented in this study indicate that HFS is a potential technique to elicit preferential responses, and preferentially activate functionally-different RGCs. While promising, the stimulation parameters such as the relatively long stimulation duration of 300 ms is not feasible in for long-term experiments given the high energy requirement of HFS and also the limited recovery time to recover any charge imbalance at the tissue-cell interface. One approach to partly address the latter issue is to preferentially activate the cell types using shorter stimulation durations for example, 40 – 50 ms. To this end, a study by Horsager et al. [63] predicted that clinically, higher frequencies will lower the perceptual threshold. The subsequent study by Nanduri et al. [64] additionally found that perceptual brightness increased with frequency (<120 Hz), while amplitude (< 7  $\mu$ A) altered both the brightness and shape of the percept. Theoretically then, having short stimulation durations of < 50 ms may be enough to elicit bright percepts while allowing enough time to recover any charge imbalance. In addition, to date, HFS has always been presented to the cell when it is at rest and for a fixed amplitude and frequency combination. Another avenue for investigation is how the HFS response may change if the frequencies are presented in a temporally modulated pattern/continuous stimulation sequence.

## **5.5 Conclusions**

Preferential activation of targeted RGC types using electrical stimulation may aid in avoiding the effects of indiscriminate activation. The main findings in this chapter are that all four RGC populations exhibited different dependencies on frequency and amplitude, and the OFFS, OFFT and ONT RGCs could be preferentially activated against the remaining population. These findings indicate the possibility of controlling the activation of three types of RGCs using HFS and bringing us one step closer to achieving more physiological activation of cells artificially.

# 6 RGC Responses to Temporally-Modulated HFS

## 6.1 Introduction

In Chapter 5, the results indicated that three out of four targeted RGC types (OFFS, OFFT and ONT) could be preferentially activated against the remaining population when stimulated over a wide range of frequency and amplitude ranges (1 - 6 kHz, 10 – 240  $\mu$ A). However, these results were obtained from relatively ideal stimulation conditions. For example, the cells were always stimulated at rest i.e., the cell had completely recovered from the previous stimulation. Additionally, the length of stimulation, 300 ms, was also relatively long. In this study, I was interested in identifying how well HFS-based preferential activation fared under more practical stimulation conditions. Specifically, with shorter stimulation durations of 40 ms encoded in temporally-modulated waveforms.

The use of amplitude and frequency modulation has been previously studied to improve performance in cochlear implants [268-270]. However, the use of similar modulation approaches has been less utilised in the retina. A previous study conducted by Ryu et al. [271] showed that RGC responses could be temporally modulated with amplitude, with strong correlation between the firing rates and the amplitude strength. More recently, Twyford et al. [14] found that a modulating amplitude in combination with a HFS of 2 kHz could similarly modulate the firing rates in ON and OFF BT RGCs in synchrony with the pattern of modulation. Clinically, Nanduri et al. [129] found that by modulating the amplitude, the phosphene size increased with little increase in the brightness but by modulating the frequency, the phosphene size remained relatively constant but the brightness increased. Meanwhile Yue et al. [272] showed that by modulating the frequency, the colour of the generated visual percepts changed accordingly. Altogether, these studies indicate that spiking patterns of RGCs can be temporally modulated through both frequency and amplitude modulation, and between the two modulation schemes, the clinical results suggest that frequency modulation may yield brighter, coloured, and localised percepts.

It has been widely documented that different retinal neurons exhibit specific responses to frequency [15, 131, 183, 273-275] with different groups attempting to utilise these sensitivities to preferentially target cell types. Notably, Freeman et al. [131] found that the RGCs, BCs and photoreceptors could be selectively activated with 100, 25 and 5 Hz frequencies respectively, under sinusoidal stimulation. In a subsequent study, Twyford et al. [132] further investigated the previous results finding that 5 and 10 Hz sinusoidal stimulation likely only activated the

photoreceptors, while 25 Hz and 100 Hz activated the RGCs. Within RGC types, aside from the previously discussed HFS-based preferential activation [14, 15], Paknahad et al. [274] found that D1-bistratified and A2-monostratified cells could be preferentially targeted with frequencies < 200 Hz with specific current amplitudes.

However, to date, there have been no studies that firstly, utilise frequency modulation as a means to preferentially target functionally-different RGC types for practical stimulation conditions and secondly, elucidate intrinsic properties of different cell types using their unique responses to frequency modulation. In this study, I tested the preferential activation capabilities of the RGC types shown in Chapter 5 using a variety of continuous, short-duration, high frequency modulation sequences. I then encoded optimised frequencies into two novel dynamic waveforms capable of preferentially controlling the ON and OFF RGCs within more practical stimulation durations.

## 6.2 Methods

Please refer to the General Methods (Chapter 4) for detailed methods on animal preparation and extraction (Chapter 4, Section 4.1) and whole-cell patch clamping (Chapter 4, Section 4.2). In this section, the specific extracellular stimulation protocols, and data analysis pursuant to this chapter will be described.

### 6.2.1 Extracellular Stimulation Protocols

Each RGC in this study was stimulated with continuous, temporally modulated sequences in which the frequencies were modulated every 40 ms in either a linearly increasing, linearly decreasing or randomised manner. Two additional protocols (referred to as dynamic stimulation waveforms) were designed based on optimised frequencies to preferentially activate RGC types using short, dynamic frequency bursts. Each of these protocols will be discussed in greater detail in the following sections.

In the previous study, the HFS response and corresponding preferential activation regions for the OFFS, OFFT and ONT RGCs tended to be on the periphery of the tested frequencies (1 – 6 kHz) and amplitudes (10 – 240  $\mu$ A). This indicated that the RGCs may be able to respond to HFS over a wider frequency and amplitude parameter space and in turn, maximise the preferential activation regions. To test this possibility, in this chapter, both the frequency (0.5 – 10 kHz) and amplitude (10 – 300  $\mu$ A) ranges were extended. The stimulation duration of 40 ms was chosen as an arbitrary value to study the RGC response to HFS when delivered in relatively shorter stimulation durations in a continuous sequence whilst also remaining well within the clinically accepted frame rate of 5 – 7 Hz [7, 101].

Taken together, each of the three protocols consisted of cathodic-first, 40  $\mu$ s biphasic pulse trains with shorter stimulation duration (40 ms) delivered for a larger amplitude range between 10 – 300  $\mu$ A and larger frequency range (0.5, 1, 1.67, 2, 2.5, 3.33, 4.17, 4.5, 5, 5.6, 6.25, 7.1, 8.3 and 10 kHz). The frequency values were chosen to have approximately a linear increase in frequency, but the order in which they were presented varied between the three protocols. There was no gap given between each frequency. However, for different trials with different amplitude values under the same frequency, an inter-trial-delay of 1 s was used, and each amplitude was repeated three times.

### 6.2.1.1 Linearly Increasing Frequency Modulation

The purpose of the linearly increasing frequency modulation protocol was to (1) identify if the RGC response altered depending on the order of frequency presented and (2) assess the effect of a continuous stimulation. To address these two aims, the protocol had three phases (Phase 1, Phase 2, and Phase 3). In Phase 1, the frequencies were increased linearly between 0.5 – 10 kHz. In Phase 2, the frequencies were decreased linearly between 10 – 0.5 kHz. Lastly in Phase 3, the frequencies were once again increased between 0.5 – 10 kHz. No gap was given between each frequency nor each phase. Across all three phases, 41 frequencies were presented for a given amplitude (the 10 kHz frequency in Phase 2 is shared with Phase 1). An example of the protocol is illustrated in Figure 6.1 and a summary is provided in Table 6.1.

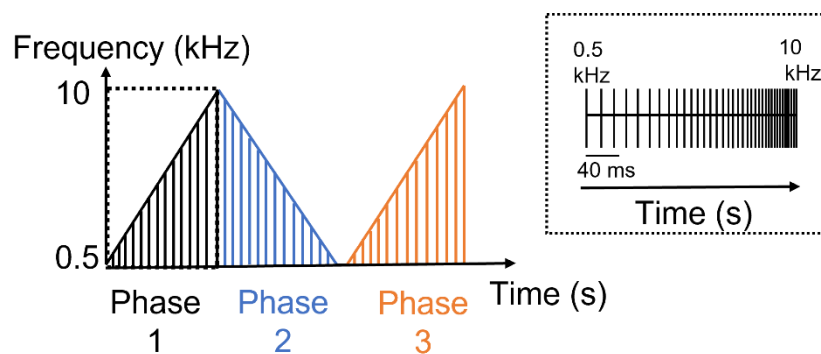


**Figure 6.1** Diagram illustrating the linearly increasing frequency modulation protocol for a given amplitude. The frequencies in phase 1 and phase 3 were increased in approximately linear steps from 0.5 to 10 kHz. In phase 2, the frequencies were decreased from 10 kHz to 0.5 kHz. In phase 3, the frequencies were increased from 0.5 to 10 kHz. Inset: Diagram of the spike train in phase 1. The duration of each frequency was 40 ms, and no ISI was presented between frequencies. Each line represents a series of short pulses.

### 6.2.1.2 Linearly Decreasing Frequency Modulation

The linearly decreasing frequency modulation protocol was solely used to assess the effect of frequency order on the RGC response. The protocol consisted of a single phase (Phase 1)

with linearly decreasing frequencies between 10 – 0.5 kHz. A summary of the frequency order is presented in Table 6.1.

### 6.2.1.3 Randomised Frequency Modulation

This third protocol was used to (1) identify the effects of moving from constant, long duration stimulation to dynamic, short durations and (2) assess the effects of frequency order. The protocol consisted of a single phase (Phase 1) with randomised frequencies between 0.5 – 10 kHz. The values were randomised in MATLAB. Ten independent randomised protocols were designed, and one of the protocols was picked at random for each patched RGC. Table 6.1 provides a summary of the frequencies used.

**Table 6.1 Summary of frequencies presented in each phase for the linearly increasing, linearly decreasing and randomised frequency modulation protocols.**

	Phase 1 (kHz)	Phase 2 (kHz)	Phase 3 (kHz)
<b>Linearly Increasing Frequency Modulation</b>	0.5, 1, 1.67, 2, 2.5, 3.33, 4.17, 4.5, 5, 5.6, 6.25, 7.1, 8.3, 10	10, 8.3, 7.1, 6.25, 5.6, 5, 4.5, 4.17, 3.33, 2.5, 2, 1.67, 1, 0.5	0.5, 1, 1.67, 2, 2.5, 3.33, 4.17, 4.5, 5, 5.6, 6.25, 7.1, 8.3, 10
<b>Linearly Decreasing Frequency Modulation</b>	10, 8.3, 7.1, 6.25, 5.6, 5, 4.5, 4.17, 3.33, 2.5, 2, 1.67, 1, 0.5	N/A	N/A
<b>Randomised Frequency Modulation</b>	rand(0.5 – 10)	N/A	N/A

### 6.2.1.4 Dynamic Stimulation Waveforms

As mentioned, two dynamic stimulation waveforms were designed based on encoding optimised frequency bursts into a single waveform.

#### 6.2.1.4.1 40-40-60ms Waveform

The first dynamic waveform (also referred to as the 40-40-60 ms waveform) was used to identify if the targeted RGC types could be differentially activated but within a stimulation duration comparable to the clinical frame rate used in a retinal prosthesis (5 – 7 Hz) [7, 101, 276]. The waveform itself consisted of two cathodic-first 40  $\mu$ s biphasic pulse trains with stimulation durations of 40 ms (referred to as phase 1 and phase 2) followed by a 60 ms inter-stimulation delay (ISD) (Figure 6.2). The frequency was modulated abruptly between 1 kHz (phase 1) and 8 kHz (phase 2) for amplitudes between 10 – 300  $\mu$ A in 10  $\mu$ A steps. The frequencies were chosen as the optimal frequencies to preferentially activate the targeted ON and OFF RGC types. Each 40-40-60ms stimulation combination was repeated 10 times for

each amplitude, and each amplitude repeated three times. A 1 s inter-trial delay (ITD) was presented between each amplitude.

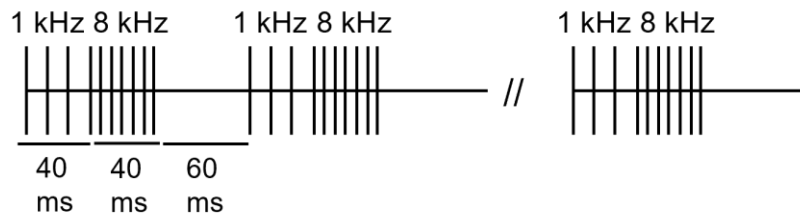


**Figure 6.2** Diagram of the 40-40-60 ms protocol for a given amplitude. Two pulse trains (1kHz followed by 8kHz) were stimulated for 40 ms immediately followed by a 60 ms ISD. Each 40-40-60 ms stimulation combination was repeated 10 times for each amplitude with a 1 s ITD given between each amplitude.

#### 6.2.1.4.2 Replication of Pseudo-Randomised Spike Train

The purpose the second dynamic waveform was to identify if the RGCs could be preferentially controlled to replicate a pseudo-randomised spike train using a modulating frequency. The pseudo-randomised spike train contained randomised integer spike numbers between 1 – 10 and randomised integer inter-spike interval (ISI) between 10 – 100 ms in 10 ms step. For each randomised spike count, a corresponding spike interval (SI) was designed to reproduce the required spike count. The regions in which the cell was required to spike is referred to the activation region, and similarly the region corresponding to the ISI is referred to the inactivation region. Table 6.2 provides a summary of the values used to generate the pulse train and Figure 6.3 depicts the pseudo-randomised spike train, and the designed stimulus waveform to replicate it. The frequency was modulated between 8 kHz and 1 kHz, with 8 kHz used during the SI and 1 kHz during the ISI. The amplitude was increased linearly in 10  $\mu$ A between 10 – 300  $\mu$ A and repeated three times. A 1 s ITD was used between each amplitude.

**Table 6.2** Summary of the spike numbers used in the design of the pseudo-randomised spike trains Each randomised spike number (vertical lines in Figure 6.3A) has a corresponding (designed) spike interval (SI) which was designed to reproduce the spike count (Figure 6.3B). The randomised inter-stimulation interval (ISI, intervals between vertical lines in Figure 6.3A) correspond to the regions in which the cell should be non-spiking, or inactive.

	Values
<b>Randomised Spike Number (1 – 10)</b>	1, 6, 2, 9, 3, 10, 8, 4, 5, 7
<b>Corresponding (Designed) SI (15 – 130 ms)</b>	15, 80, 25, 120, 40, 130, 110, 55, 70, 95 ms
<b>Randomised ISI (10 – 100 ms)</b>	70, 10, 20, 60, 100, 40, 80, 30, 90, 50 ms

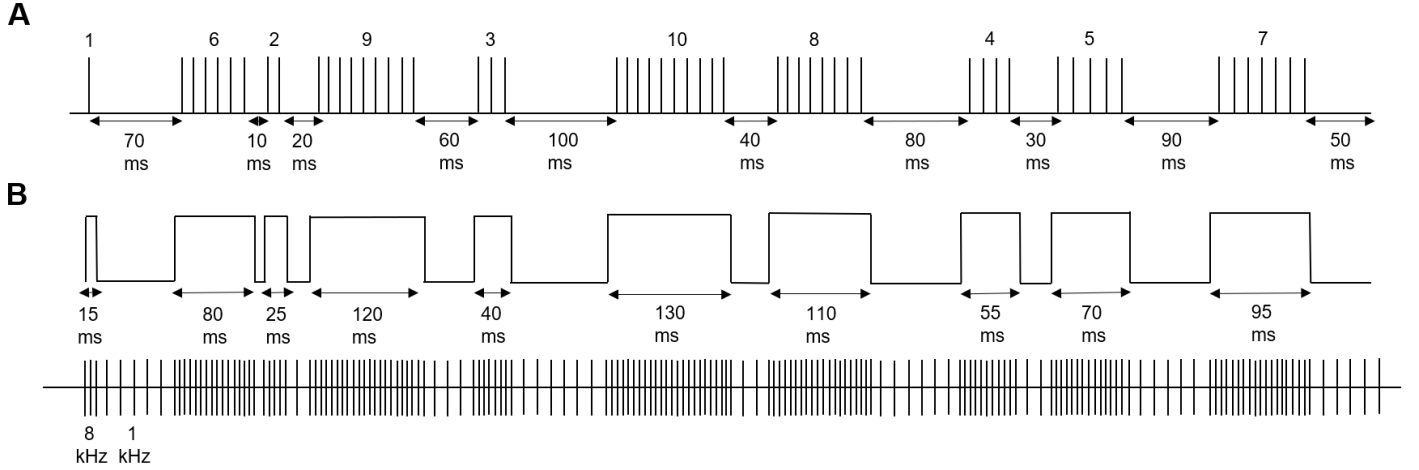


**Figure 6.3 Diagram of pseudo-randomised spike train and the corresponding designed stimulus waveform.** (A) Pseudo-randomised spike train. (B) Pulse train designed to replicate the regions of spiking (active) and non-spiking (inactive). 8 kHz was used for the active regions, and 1 kHz for the inactive regions.

## 6.2.2 Data Analysis

### 6.2.2.1 Spontaneous Activity Subtraction

To isolate the contribution of HFS to a given cell response, spontaneous activity subtraction was employed for all relevant cells. Spontaneous activity was defined as the presence of full action potential spikes in a specified window in which there was no current amplitude. For a given cell, the average spontaneous activity was calculated immediately preceding the electrical stimulation across five windows of 40 ms or 300 ms duration (depending on the relevant stimulation protocol) during the 1 s ITD given between different amplitudes. Figure 6.4 indicates a diagrammatic example of the spontaneous subtraction used for the cell populations in Chapter 5 and Chapter 7. The average of five windows was taken to ensure that any cells exhibiting burst-like activity, particularly in the Rd1 retina (Chapter 7), were captured appropriately in the spontaneous activity calculation. The spontaneous activity occurring prior to each frequency and amplitude stimulation combination was then subtracted from the average spike count for that specific frequency and amplitude combination (Equation 6.1). Spontaneous activity subtraction was employed for the cell population in Chapter 5 retrospectively and for both Chapter 6 and Chapter 7 cell population.

$$SC_{(f,A)} = \frac{\sum_{i=1}^5 SC_{ITD}(f,A)}{5} \quad (6.1)$$

Where SC represents the individual spike count of a single cell for a given frequency (f) and amplitude (A), and  $SC_{ITD}$  is the spike count in either a 40 ms or 300 ms window in each ITD for a given frequency (f) and amplitude (A).

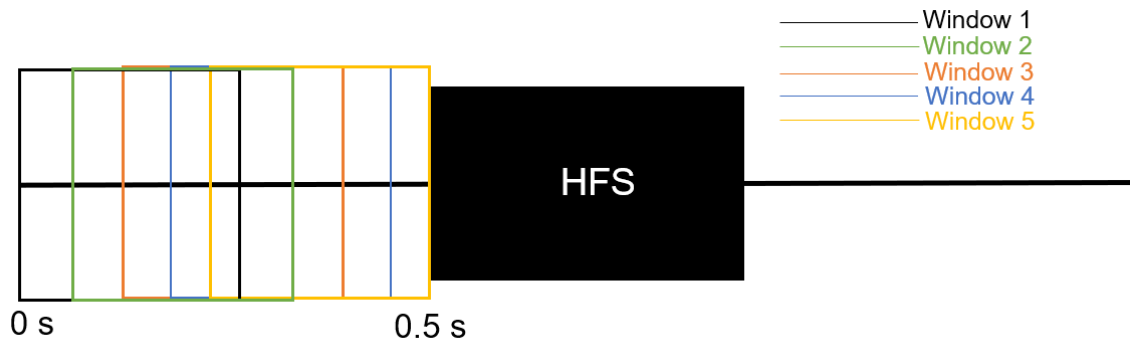


**Figure 6.4 Diagram of spontaneous activity calculation.** For a given frequency and amplitude stimulation combination, spontaneous activity occurring in 5 separate windows of either 40 ms or 300 ms was averaged and subtracted from the averaged spike count for that specific frequency and amplitude combination.

### 6.2.2.2 Normalisation and Preferential Activation Maps

A detailed description for the calculation of the normalised average spike count matrices and the preferential activation maps is discussed in Chapter 4, Section 4.4. Specific to this chapter, each cell was normalised across *all* the relevant protocols presented to the given cell. The protocols taken into consideration for normalisation were the linearly increasing frequency modulation, linearly decreasing frequency modulation, randomised frequency modulation and the first dynamic modulation waveform as the stimulation duration of 40 ms for each frequency and amplitude combination was consistent across all the protocols.

Additionally, to study the isolated effects of stimulation duration on the RGC response, cells from Chapter 5 were used. All the relevant cells had their baseline spontaneous-activity subtracted and were normalised against the maximum spike count across all frequency and amplitudes within the 300 ms stimulation duration. To elucidate the effects of static short duration stimulation, only the spike count in the *first 40 ms* of stimulation was considered for the same group of cells. Each cell was then normalised against the maximum spike count across all frequency and amplitudes within the 40 ms time frame.

### 6.2.2.3 Preferential Activation Statistic

As a comparative tool, a preferential activation statistic was employed to reflect how much of the total frequency-amplitude parameter space a cell type was preferentially active against the remaining population. The statistic was calculated by taking the ratio of the total number of frequency and amplitude combinations in which the cell type was preferentially active and statistically significant, and the total number of frequency and amplitude combinations in the parameter space of interest. The statistic is reflected as a percentage.

#### 6.2.2.4 Recovery Statistic

In a bid to ascertain the recovery properties of each cell type when stimulated with HFS, a recovery statistic value was used to show how well the cell type could recover across all relevant frequencies and amplitudes. Recovery was defined as the ability of a given cell to faithfully reproduce the same normalised spike count (within an acceptable range) when stimulated with the same presentation of frequencies and amplitudes but following an intermittent stimulation period.

Initially for each cell, a 2D phase-difference matrix consisting of the absolute value of the difference in normalised spike count for a given frequency and amplitude combination between phase 1 and phase 3 in the linearly increasing frequency modulation protocol was taken. As mentioned in the definition, recovery was defined as a faithful reproduction of the normalised spike count *within an acceptable range*. Ideally, true reproduction (and therefore recovery) implies a phase-difference value of zero. This however penalised cells that were only marginally higher than zero, however would still be considered unrecovered. To avoid this, a recovery range was applied to the initial 2D matrix for a given cell, and if the phase-difference values fell within this range, the phase-difference value was considered to be zero. The acceptable range itself was calculated as: 0 (true recovery)  $\pm$  one standard deviation calculated across all cell types. The average of the individual normalised phase-difference matrices was taken resulting in an averaged normalised phase-difference matrix for each cell type (Equation 6.2). The sum of all the values (across all frequencies and amplitudes) in the average phase-difference matrix was calculated indicating the recovery statistic for that cell type.

$$\sum \frac{\sum_1^{n_T} |NSC_{P1(f,A)} - NSC_{P3(f,A)}|}{n_T}$$

*if*

$$0 - \sigma_{TC} < |NSC_{P1(f,A)} - NSC_{P3(f,A)}| < 0 + \sigma_{TC} \tag{6.2}$$

$$|NSC_{P1(f,A)} - NSC_{P3(f,A)}| = 0$$

Where  $NSC_{P1}$  and  $NSC_{P3}$  represented the normalised individual spike count of a single cell in a cell type population during phase 1 and phase 3 of the linearly increasing protocol for a given frequency (f) and amplitude (A) respectively,  $n_T$  represented the total number of cells in the cell type population and  $\sigma_{TC}$  represented the standard deviation across all cell types.

## 6.3 Results

### 6.3.1 RGCs Response to HFS in Static and Dynamic Conditions

Initially, I was interested to see if the RGCs response to HFS changed when moving from stimulation under idealistic conditions, to more stringent conditions. Specifically, the focusses were changes to two stimulation parameters namely: the stimulation duration, which was shortened from 300 ms to 40 ms, and stimulation from a static state (i.e., when the cell has fully recovered from the previous stimulation and therefore stimulated at rest) to a dynamic state (the cell is stimulated immediately after the previous stimulation). Note, the population in which the cells were stimulated at rest (Figure 6.5- Figure 6.8A and B) are from Chapter 5 while the cell population in which the cells were stimulated in a dynamic state from the cells in this chapter. The statically-stimulated population from Chapter 5 are not used beyond Section 6.3.2.

Figure 6.5 shows the population response of the ON and OFF cells across the four stimulation conditions. To first investigate how the response for the cell types changed from an idealistic to a more practical stimulation duration, the averaged normalised response of statically-stimulated RGCs to HFS was plotted with the full stimulation duration of 300 ms (Figure 6.5A) alongside the first 40 ms of stimulation (Figure 6.5B). Given that these cells belong to the Chapter 5 cell population, the frequency and amplitude parameter space was limited to 1 – 6 kHz and 10 – 240  $\mu$ A. However, to ensure equal comparison to the dynamically-stimulated cells which were stimulated with additional frequencies within the same frequency range, linear interpolation and extrapolation was used to estimate missing frequencies – 4.5 kHz, 5.6 kHz, and 0.5 kHz. Altogether, the frequency parameter space extended from 0.5 – 6 kHz and amplitudes from 10 – 240  $\mu$ A. For all statically-stimulated cells, spontaneous activity was retrospectively subtracted (see Chapter 6, Section 6.2.2.2 for calculation).

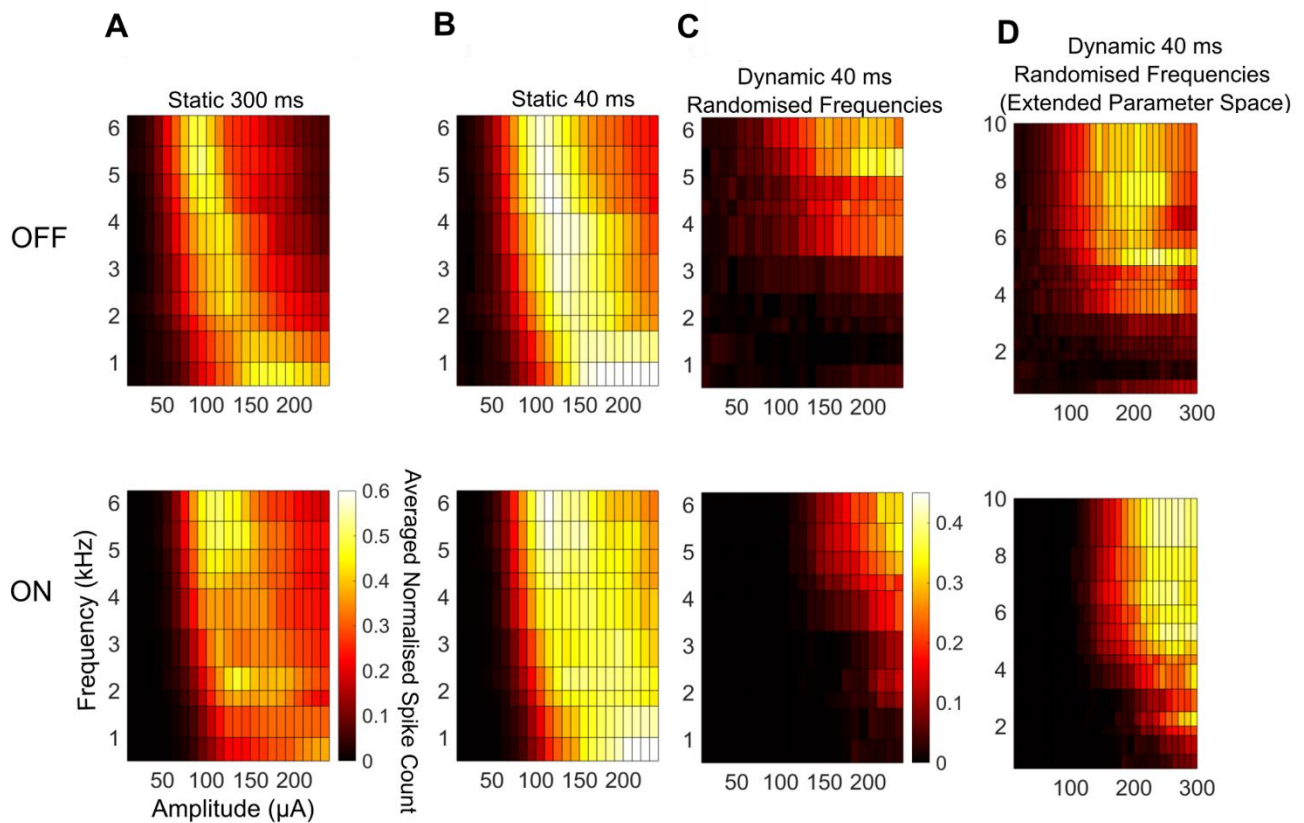


**Figure 6.5 Population response maps of ON and OFF RGCs in response to HFS under static and dynamic conditions.** Both cell type responses were found to be dependent on the stimulation duration and the stimulation condition with a distinct shift in the maximal activity towards higher amplitudes with short, dynamic stimulation. Panels A, B and C use the same frequency (0.5 – 6 kHz) and amplitude (10 – 240  $\mu\text{A}$ ) parameter space however an extended parameter space with frequencies (0.5 – 10 kHz) and amplitudes (10 – 300  $\mu\text{A}$ ) was used in Panel D. The averaged normalised spike count is represented as the coloured square on the map. (A) ON ( $n = 25$ ) and OFF ( $n = 24$ ) cell responses to HFS static stimulation of 300 ms. (B) ON ( $n = 25$ ) and OFF ( $n = 24$ ) cell responses to HFS static stimulation of 40 ms duration. (C) ON ( $n = 13$ ) and OFF ( $n = 15$ ) cell responses to HFS dynamic stimulation of 40 ms duration. (D) ON ( $n = 13$ ) and OFF ( $n = 15$ ) cell responses to HFS dynamic stimulation of 40 ms duration across the extended frequency and amplitude parameter space.

Comparing Figure 6.5A (300 ms HFS) and Figure 6.5B (40 ms HFS), on average both ON and OFF cell types maintained their non-monotonic profiles (increasing then decreasing spike counts with an increasing amplitude) after reducing the HFS duration from 300 ms to 40 ms. Interestingly, the amplitude in which the spike count began decreasing occurred at relatively higher amplitudes with 40 ms HFS. This in part could be attributed to the broader maximal activation regions (indicated by the yellow and white regions) seen across the cell type populations in the 40 ms HFS, compared to the relatively narrower maximal activation regions stimulated with 300 ms HFS. This broadened maximal activation region produced a distinct right-ward shift in the 40 ms activation map.

To investigate how the cell type response changed when stimulating a cell in a static versus dynamic condition i.e., stimulating a cell after it has effectively recovered from the previous

stimulation versus stimulating a cell with randomised frequencies immediately after the previous stimulation; the averaged normalised HFS response maps in Figure 6.5B and Figure 6.5C for frequencies 0.5 – 6 kHz and amplitudes 10 – 240  $\mu$ A were compared. Figure 6.5B indicates the population response of different cell types stimulated at static state. Meanwhile Figure 6.5C shows the population response of cell types to a randomised frequency modulation protocol (see Chapter 6, Section 6.2.1.3).

Comparing Figure 6.5B and Figure 6.5C, it is evident that on average and across both cell types, there is a dramatic, and nearly identical right-ward shift (to higher stimulation amplitude) in the maximal activation region of the cells. Unsurprisingly, the maximal activation regions across the ON and OFF cell types largely overlapped with differences only in the averaged normalised spike count. In Figure 6.5D, the response map across a wider range of frequencies and amplitudes specifically 0.5 – 10 kHz and 10 – 300  $\mu$ A was explored to identify if the same level of overlap still existed. The results suggest significantly less overlap in the maximal activation regions with an extended stimulation parameter space. Irrespective of the extended parameter space however, dynamically-stimulated OFF cells still had a significantly different response map compared to the OFF statically-stimulated cells. Specifically, for the dynamically-stimulated cells, they were more robust in the maximal activation regions at relatively higher amplitude (160 – 240  $\mu$ A) and frequency (6 – 10 kHz) regions. The dynamically-stimulated ON cells also had a further right-ward shift in maximal activation compared to the ON statically-stimulated cells but retained a similar region of activation even with an extended parameter space.

In Figure 6.6, the ON and OFF populations were further divided into more detailed classifications namely the sustained (S) and transient (T) types. The averaged normalised population response maps for the four cell types were plotted across the four different stimulation conditions. Comparing Figure 6.6A (static HFS with 300 ms) and Figure 6.6B (static HFS with 40 ms), all the cell types exhibited the same broadening of the maximal activation region as observed in the overall OFF and ON population, with the ONT cells having the greatest increase in region when the stimulation duration was shortened. Comparing statically-stimulated cell responses in Figure 6.6B with dynamically-stimulated cells in Figure 6.6C and Figure 6.6D, both the OFFS and OFFT cells had significantly different responses moving from a static to a dynamic stimulation which agrees with Figure 6.5. The two types, however, had very similar responses in the dynamic stimulation with the extended parameter space (Figure 6.5D) indicating less variability between the sustained and transient dichotomies. The latter observation was also noted for the ONS and ONT cells, but the cells did not have as drastically differential response between the static and dynamic stimulation as the OFF cells.

Both Figure 6.5 and Figure 6.6 indicate that across all cell types, there was an increasing rightward shift in the activation region when moving from a long duration to short duration and again but to a larger extent, from static to dynamic stimulation. The region of activation remained relatively consistent at higher frequencies and amplitudes for the ON cells compared to the OFF cells, which had larger variations particularly in the static versus dynamic stimulation.

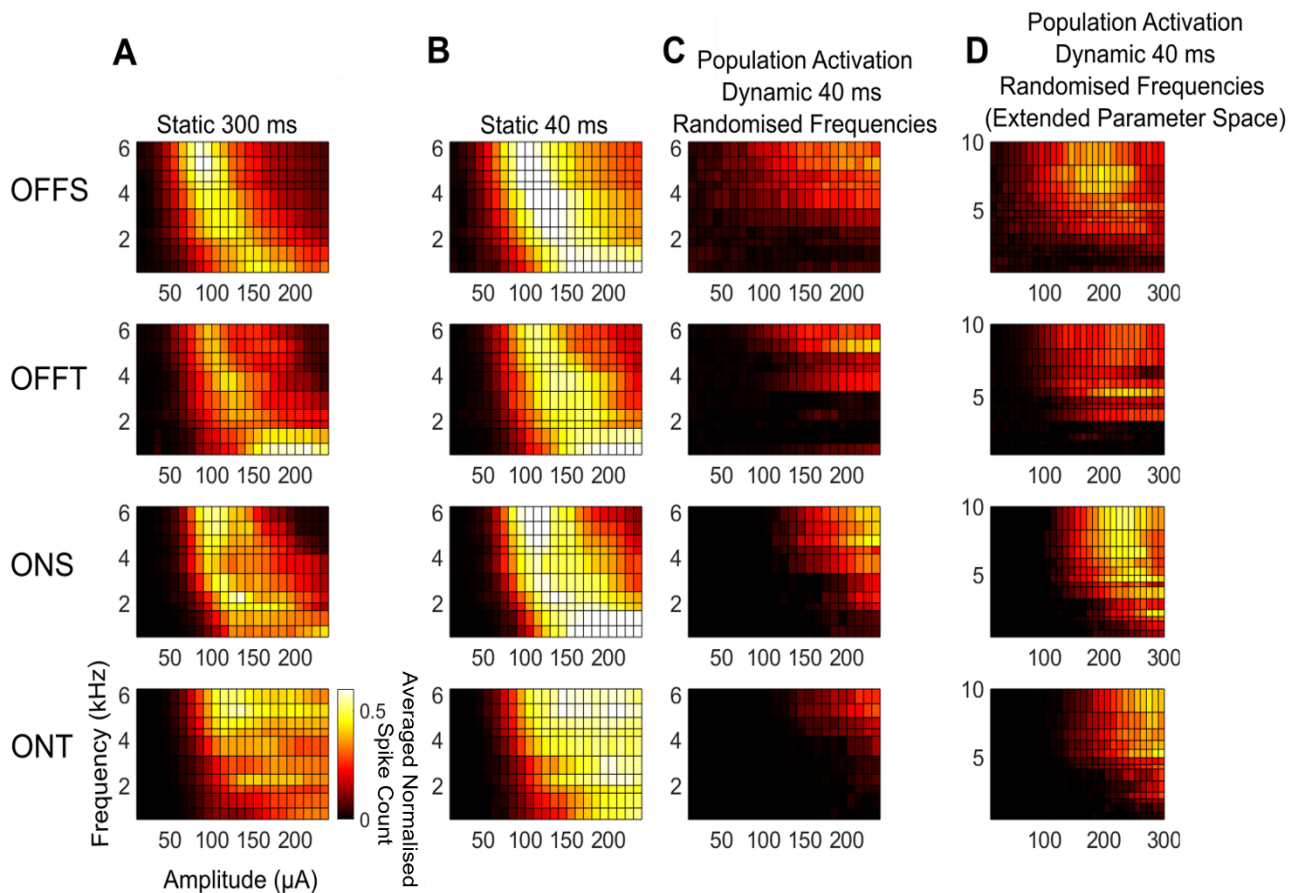


**Figure 6.6 Population response maps of four RGC types in response to HFS under static and dynamic HFS conditions.** All four RGC types were dependent on the HFS stimulation condition and stimulation duration and exhibited maximal activity at higher frequency and amplitudes with short, dynamic stimulation. Similar responses were observed between the sustained and transient subtypes. Panels A, B and C use the same frequency (0.5 – 6 kHz) and amplitude (10 – 240  $\mu\text{A}$ ) parameter space however an extended parameter space with frequencies (0.5 – 10 kHz) and amplitudes (10 – 300  $\mu\text{A}$ ) was used in Panel D. The averaged normalised spike count is represented as the coloured square on the map. (A) Population responses of OFFS ( $n = 14$ ), OFFT ( $n = 10$ ), ONS ( $n = 12$ ) and ONT ( $n = 13$ ) cells to static stimulation of 300 ms. (B) Responses of OFFS ( $n = 14$ ), OFFT ( $n = 10$ ), ONS ( $n = 12$ ) and ONT ( $n = 13$ ) cells to static stimulation of 40 ms. (C) Responses of OFFS ( $n = 8$ ), OFFT ( $n = 6$ ), ONS ( $n = 5$ ) and ONT ( $n = 8$ ) cells to dynamic stimulation of 40 ms. (D) Responses of OFFS ( $n = 8$ ), OFFT ( $n = 6$ ), ONS ( $n = 4$ ) and ONT ( $n = 8$ ) cells to dynamic stimulation of 40 ms under the extended frequency and amplitude parameter space.

### 6.3.2 Preferential Activation of RGCs with HFS under Static and Dynamic Conditions

From Section 6.3.1, it is evident that different RGC types have varying responses to HFS depending on the stimulation duration, and the static or dynamic condition of the cell. Practically, I was interested in how these different responses affected the ability for the cell type to be preferentially activated. To recap, preferential activation was defined as the probability of one cell type firing over the remaining population and calculated by subtracting the average normalised spike count of the respective populations (see Chapter 4, Section 4.4.1 for detailed calculation). To compare the respective preferential activation abilities for the various cell types, a preferential statistic (see Section 6.2.2.3 for calculation) was introduced which represented the total frequency and amplitude parameter space in which the cell type can be preferentially activated after accounting for statistical significance (one sample t-test against a difference of zero between the normalised spike counts of the respective populations). The statistic is reflected as a percentage in which higher the percentage, the larger area in which the cell type is preferentially active.

Figure 6.7 shows the preferential activation map for the ON and OFF cell types across the four stimulation conditions. The corresponding preferential statistic values for the two RGC types across the different stimulation conditions is presented in Table 6.3. From Figure 6.7, the OFF cells were 10 – 20 % more likely to spike than the remaining population at relatively low amplitudes between 20 – 100  $\mu\text{A}$  across all frequencies in the static stimulation conditions (Figure 6.7A and Figure 6.7B) however the amplitude range (20 – 200  $\mu\text{A}$ ) and frequency range ( $> 2.5$  kHz) increased when dynamically stimulated (Figure 6.7C and Figure 6.7D). There was little difference in the preferential activation of the OFF cells between the long and short duration stimulations. The preferential statistic across all four stimulation conditions remained relatively constant. Meanwhile the ON cells were 10 – 20 % more likely to spike at higher frequencies ( $> 2\text{kHz}$ ) and relatively higher amplitudes ( $> 200$   $\mu\text{A}$ ) across all the stimulation conditions barring dynamic, short stimulation with the limited parameter space. The ON cells had a progressively narrower amplitude range in which they could be preferentially activated moving from long-static stimulation to short- dynamic stimulation; however, the shift itself was consistent and towards the higher amplitudes. Altogether, both Figure 6.7 and Table 6.3 indicate that while OFF cells had the largest preferential activation region across the four stimulation conditions, the ON cells had the more consistent preferential region. This result can be explained by the population response of the RGCs seen in Figure 6.5 in which the region of maximal activation in the population response maps somewhat corresponds to the region in which the cells could be preferentially activated. Given that the

OFF cells were sporadic in their population response to the different stimulation conditions compared to the consistent ON cells, their ability to be preferentially activated and the corresponding regions were equally sporadic compared to the consistent regions for the ON cells.

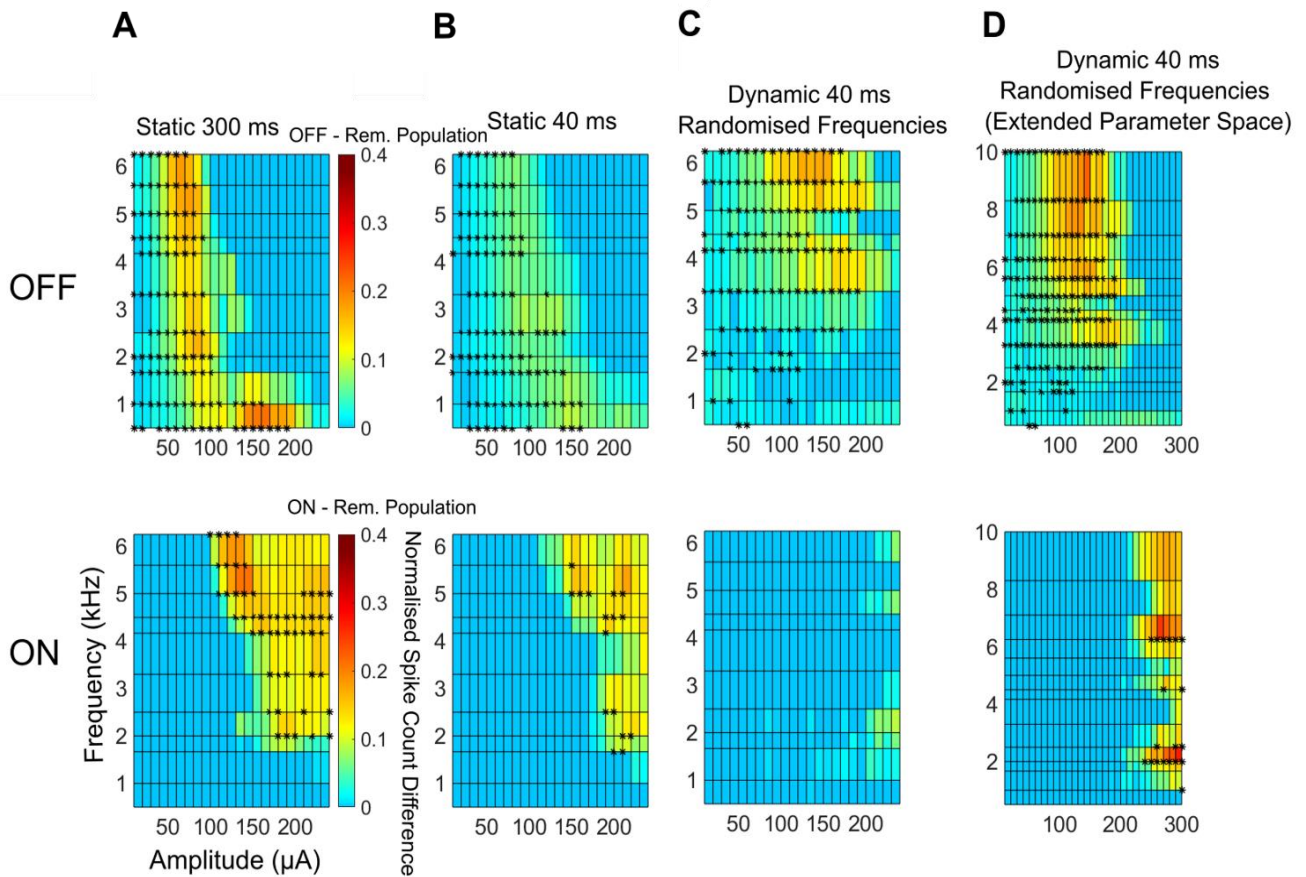


**Figure 6.7 Preferential activation maps for the ON and OFF RGCs in response to HFS under static and dynamic conditions.** While OFF cells had a larger statistically-significant preferential region across all stimulation conditions, the ON cells were more robust in the region of activation. Preferential activation is defined here as the probability of one cell type population firing over the remaining population and calculated by subtracting the average normalised spike count of the respective populations. The colour bars indicate the normalised spike count difference between the populations, and the labels indicate the respective active and dormant populations. The black asterisks denote regions of statistical significance (one sample *t*-test against difference of zero between normalised spike count of the populations). (A) The preferential activation maps for OFF ( $n = 24$ ), and ON ( $n = 25$ ) under static stimulation with duration of 300 ms. (B) The preferential activation maps for OFF ( $n = 25$ ) and ON ( $n = 24$ ) under static stimulation of duration 40 ms. (C) Preferential activation maps for OFF ( $n = 15$ ) and ON ( $n = 13$ ) under dynamic stimulation with duration of 40 ms. (D) Preferential activation maps for OFF ( $n = 15$ ) and ON ( $n = 13$ ) under dynamic stimulation of 40 ms across the extended frequency and amplitude parameter space.

With respect to the ON RGC preferential activation, it is important to note that the ON preferential region constantly appears on the periphery of the tested parameter space. Therefore, it is possible that the relatively narrower preferential range and preferential statistic may simply be a consequence of the parameter space and not a true reflection of the preferential activation capabilities. For example, the ON cells have a minimised preferential

range in Figure 6.7C, however when stimulated with a broader range of frequency and amplitudes (Figure 6.7D), their preferential region increases accordingly.

In line with the previous section, I also looked at the preferential activation map for the four cell types across the different stimulation conditions presented in Figure 6.8. The corresponding preferential statistic values are shown in Table 6.3. Across all four cell types, the OFFT cells were the worst-performing with a single preferential region in the static, long duration stimulation. The OFFS cells on the other hand, had the highest preferential statistic across all the stimulation conditions however also had a variable preferential region. Meanwhile within the ON cell population, both the ONS and ONT cells had distinct right-ward shifts in the preferential maps, particularly between static to dynamic stimulation. Between the two cell types, the ONT cells appeared to have the bigger shift, indicated by its inability to be preferentially activated in the original limited parameter space with dynamic stimulation and only minimally preferentially activated with the extended parameter space. Lastly, across all the cell types, the regions in which the RGCs were preferentially activated corresponded neatly to their regions of maximal activation shown in Figure 6.6.

**Table 6.3 Preferential activation statistic values for RGC types under different stimulation conditions**

<b>Preferential Activation Statistic</b>	<b>OFFS (%)</b>	<b>OFFT (%)</b>	<b>ONS (%)</b>	<b>ONT (%)</b>	<b>OFF (%)</b>	<b>ON (%)</b>
<b>Static 300 ms</b>	40.5	0.76	0.00	23.5	39.0	19.7
<b>Static 40 ms</b>	41.7	0.00	4.55	19.7	39.0	6.06
<b>Dynamic, Randomised Frequency 40 ms</b>	36.0	0.00	1.14	0.00	47.7	0.38
<b>Dynamic, Randomised Frequency 40 ms (Extended Parameter Space)</b>	34.3	0.00	2.38	0.24	40.7	4.52

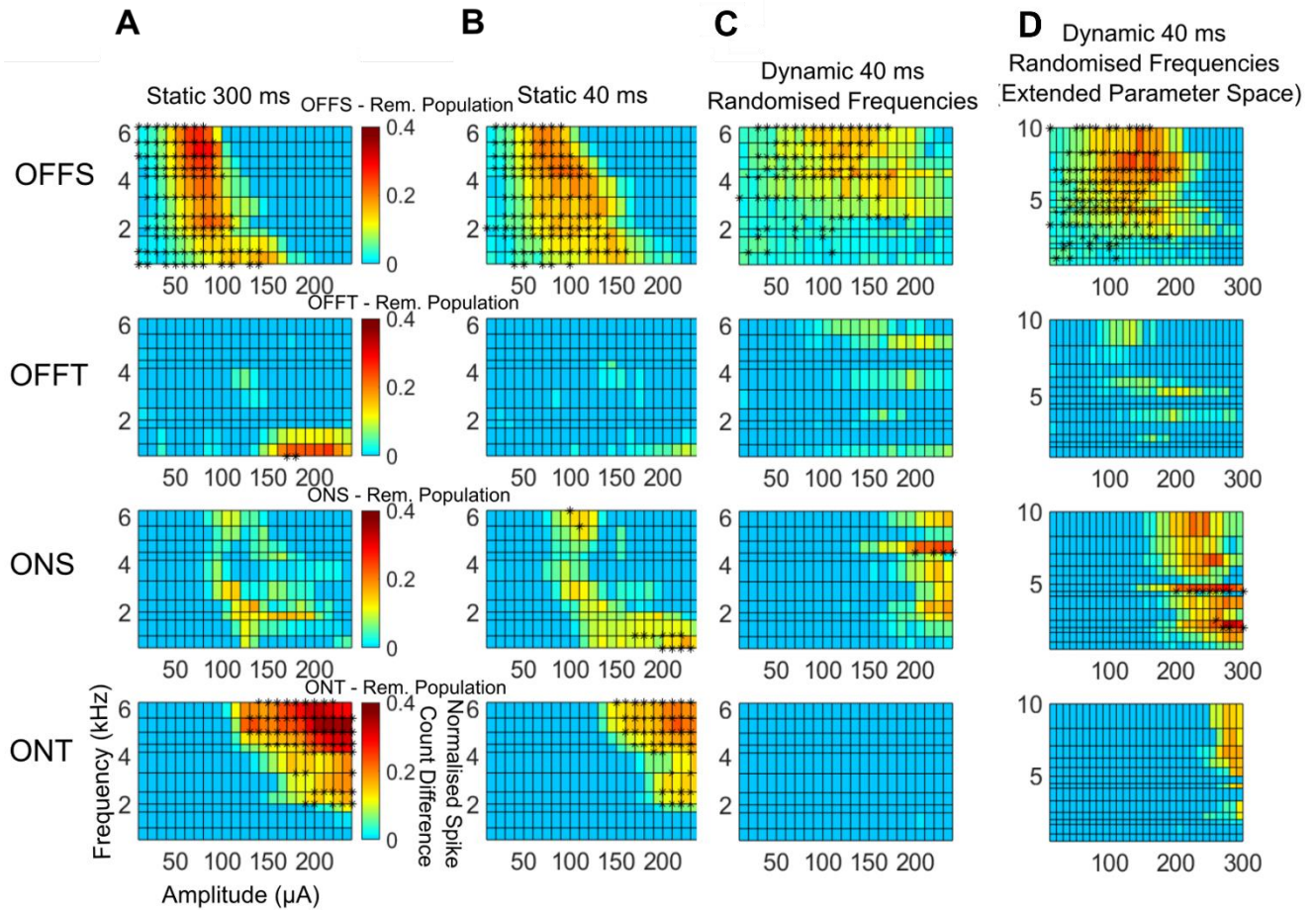


**Figure 6.8 Preferential activation maps of four types of RGCs in response to HFS under static and dynamic conditions.** All cell types could be preferentially activated in at least one of the different stimulation conditions, with statistical significance. Preferential activation is defined here as the probability of one cell type population firing over the remaining population and calculated by subtracting the average normalised spike count of the respective populations. The colour bars indicate the normalised spike count difference between the populations, and the labels indicate the respective active and dormant populations. The black asterisks denote regions of statistical significance (one sample t-test against difference of zero between normalised spike count of the populations). (A) The preferential activation map for population one OFFS ( $n = 13$ ), OFFT ( $n = 10$ ), ONS ( $n = 12$ ) and ONT ( $n = 13$ ) under static stimulation, and stimulation duration of 300 ms. (B) The preferential activation map for population one OFFS ( $n = 13$ ), OFFT ( $n = 10$ ), ONS ( $n = 12$ ) and ONT ( $n = 13$ ) under static stimulation, and stimulation duration of 40 ms. (C) The preferential activation map for population two with OFFS ( $n = 12$ ), OFFT ( $n = 10$ ), ONS ( $n = 11$ ) and ONT ( $n = 10$ ) under dynamic stimulation, and stimulation duration of 40 ms. (D) The preferential activation map for population two OFFS ( $n = 12$ ), OFFT ( $n = 10$ ), ONS ( $n = 11$ ) and ONT ( $n = 10$ ) under dynamic stimulation, and stimulation duration of 40 ms across the extended frequency and amplitude parameter space.

### 6.3.3 RGCs Response to Different Frequency Orders

To investigate if the response and corresponding preferential activation of each cell type changed depending on the order of presented frequency parameters, the HFS response and preferential activation maps of the OFF, ON, OFFS, OFFT, ONS and ONT cell types stimulated with three different frequency modulation protocols were compared. The three protocols were as follows: 1) Phase 1 a linearly increasing frequency pattern from 0.5 kHz to 10 kHz (Panel A); 2) a linearly decreasing frequency pattern from 10 kHz to 0.5 kHz (Panel B); and 3) a randomised frequency pattern between 0.5 – 10 kHz (Panel C). Refer to Chapter 6, Sections 6.2.1.1 - 6.2.1.3 for protocol details. For all three protocols, amplitudes were increased linearly from 10 – 300  $\mu$ A with a 1 s inter-trial delay and each amplitude was repeated three times.

Figure 6.9 and Figure 6.10 illustrate the population HFS response and preferential activation map for the ON and OFF RGCs across the three stimulation protocols, respectively. Table 6.4 summarises the corresponding preferential statistic values. From the population response and the preferential activation maps, ON and OFF RGC responses changed depending on the order in which frequencies were presented, but OFF RGCs demonstrated much higher sensitivity to the sequence order of frequencies than the ON RGCs. Like the previous section results, the maximal region of activation in the population map was reasonably correlated with the region of preferential activation. On average, the strongest OFF response and preferential activation was within the parameter space (250 - 300  $\mu$ A, 0.5 – 1.6 kHz) when stimulated by a linearly increasing frequency order (Figure 6.9A, Figure 6.10A). However, the OFF parameter space moved to (100 - 180  $\mu$ A, 5 – 10 kHz) when stimulated by an inverse or randomised order (Figure 6.9B and C, Figure 6.10B and C). It is worth mentioning that across all three protocols, the OFF RGCs have a consistent preferential activation stronghold in the very low amplitudes (< 50  $\mu$ A) likely related to the heightened excitability of the OFF cell type compared to ON. In contrast, the ON cells demonstrated a strong response and preferential activation in the region (210 – 300  $\mu$ A, 4 – 10 kHz) and generally maintained this region across all stimulation protocols although the degree of preferential activation was reduced when stimulated by randomising frequency orders (Figure 6.10C). Interestingly, the maximal response evoked by the ON RGCs occurred when the frequencies were presented in a descending order (Figure 6.9B).

With respect to how much of the parameter space could be employed to preferentially activate the targeted cell type, the OFF cells outperformed the ON cells for all given protocols (Table 6.4). In addition, OFF cells had a larger preferential space when stimulated by linearly increasing frequencies but a lower preferential space with linearly decreasing frequencies. On

the other hand, ON cells had larger preferential space when stimulated by linearly increasing frequencies but lower preferential space with randomised frequencies.

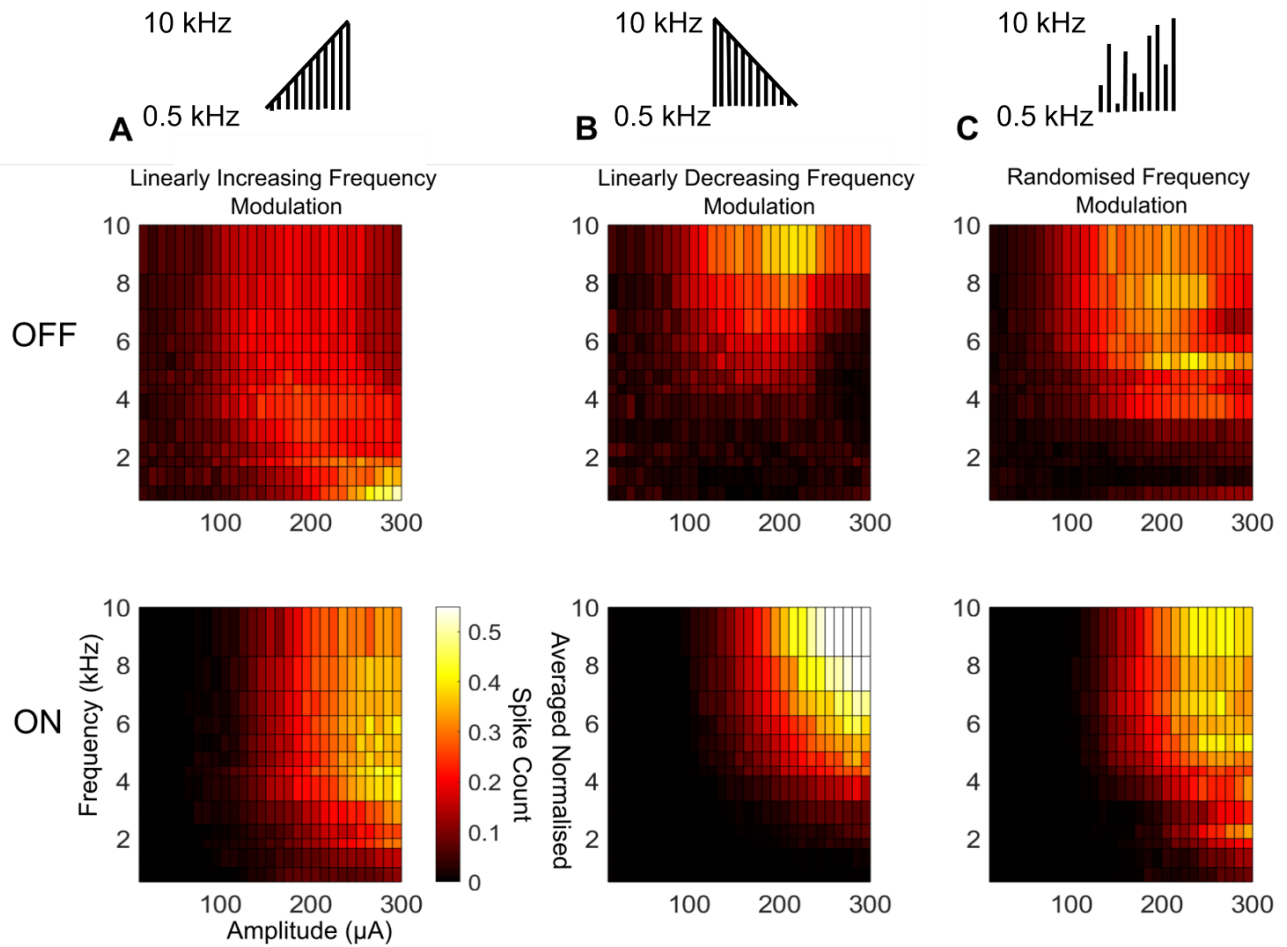


**Figure 6.9 Population response maps of ON and OFF RGCs in response to HFS presented with different frequency orders.** ON cells had comparable responses to the stimulation irrespective of the order in which the frequencies were presented. OFF cells were more sensitive to frequency order indicated by the different regions of maximal activation. For all three protocols the frequency range was 0.5 – 10 kHz and amplitude range 10 – 300  $\mu$ A. The averaged normalised spike count is represented as the coloured square on the map. Each frequency was presented for 40 ms in the pulse train. (A) Population response of OFF cells ( $n =$  avoid desensitisation effects respectively) and ON cells ( $n = 21$ ) cells to a linearly increasing frequency. (B) Population response of OFF cells ( $n = 13$ ) and ON cells ( $n = 13$ ) to a linearly decreasing frequency. (C) Population response of OFF cells ( $n = 15$ ) and ON cells ( $n = 13$ ) to randomised frequencies.

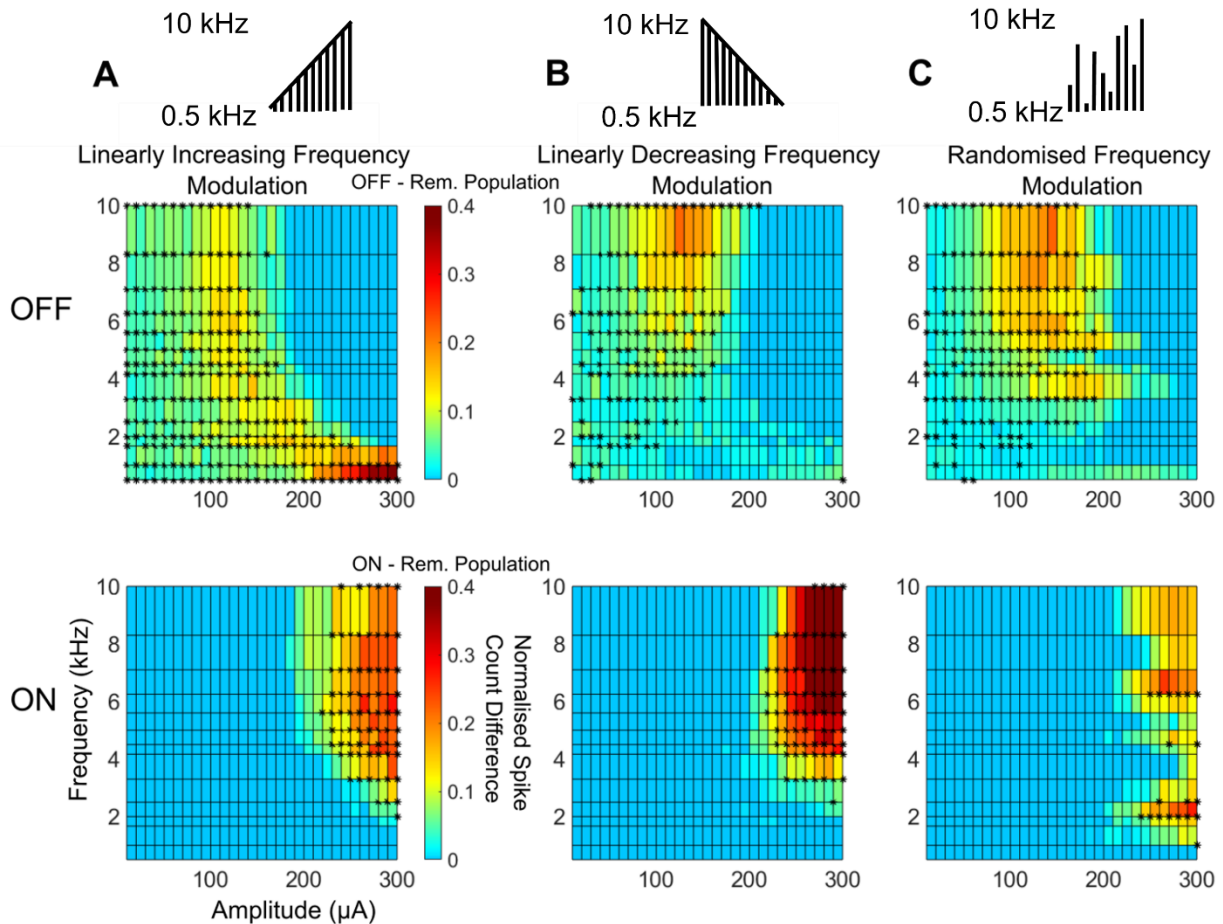


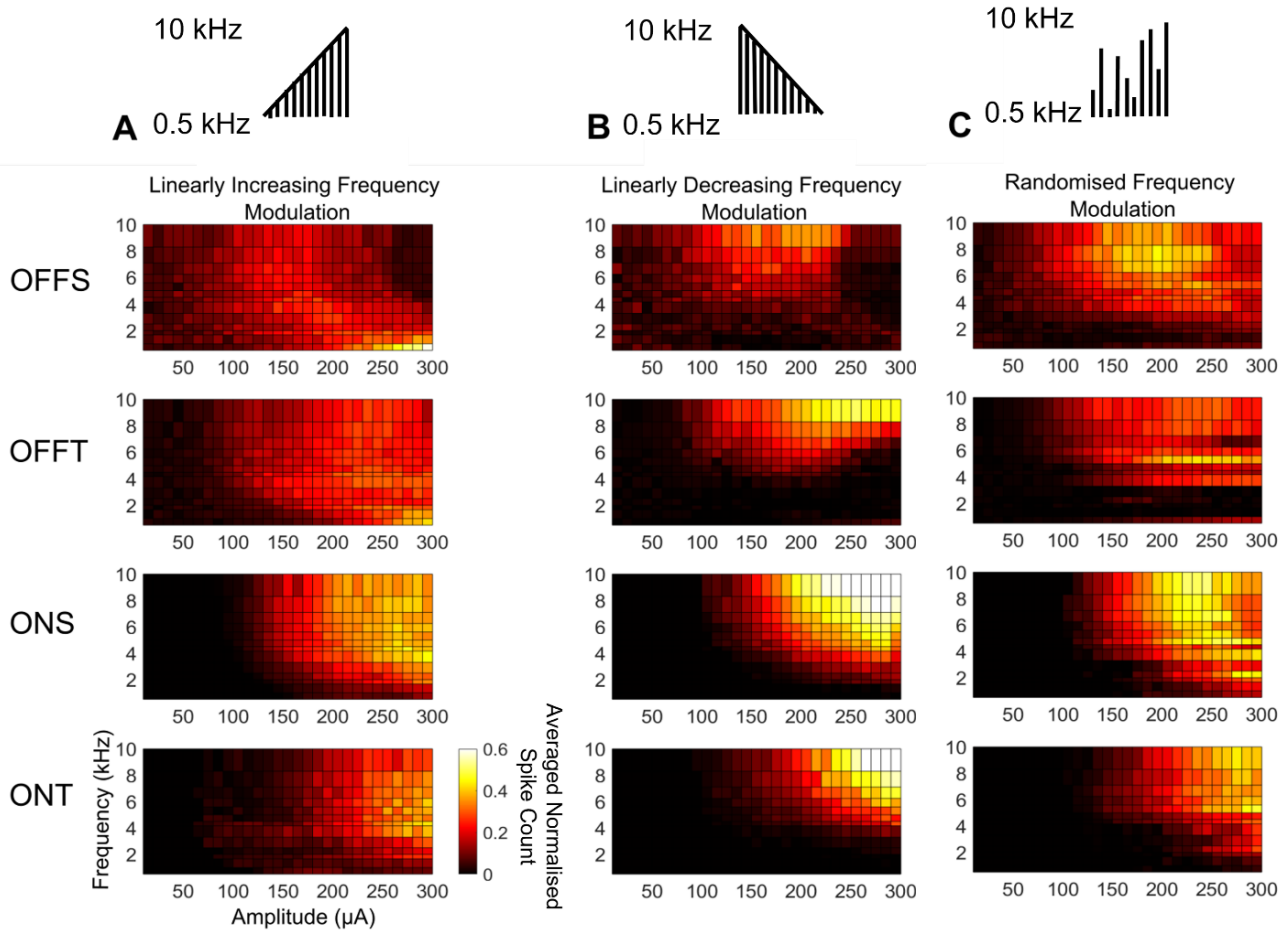
**Figure 6.10 Preferential activation maps of ON and OFF RHCs in response to HFS presented with different frequency orders.** The preferential activation of both ON and OFF cell types varied depending on the order of the frequencies presented, but the ON cells were more robust under the different presentations compared to the OFF cells. Preferential activation is defined here as the probability of one cell type population firing over the remaining population and calculated by subtracting the average normalised spike count of the respective populations. The colour bars indicate the normalised spike count difference between the populations, and the labels indicate the respective active and dormant populations. The black asterisks denote regions of statistical significance (one sample t-test against difference of zero between normalised spike count of the populations). All three protocols had the same frequency (0.5 – 10 kHz) and amplitude (10 – 300  $\mu$ A) parameter space. Each frequency was presented for 40 ms in the pulse train. (A) Preferential activation maps corresponding to the first phase of the linearly increasing frequency modulation protocol for OFF ( $n = 22$ ) and ON ( $n = 21$ ). (B) Preferential activation maps corresponding to the linearly decreasing frequency modulation protocol for OFF ( $n = 13$ ) and ON ( $n = 13$ ). (C) Preferential activation maps corresponding to randomised frequencies for OFF ( $n = 15$ ) and ON ( $n = 13$ ).

**Table 6.4 Summary of the preferential activation statistic values for the different RGC types during the linearly increasing, linearly decreasing and randomised modulation protocols.**

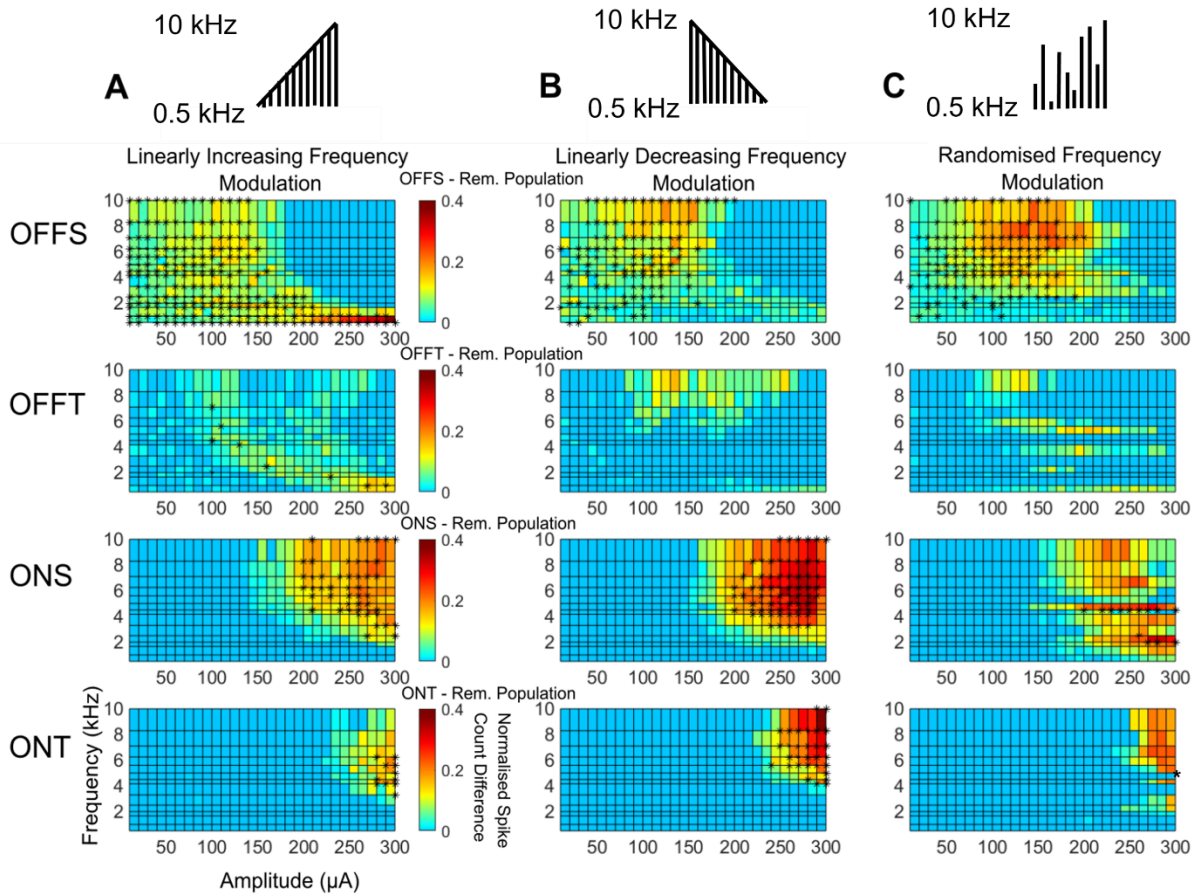
<b>Preferential Activation Statistic</b>	<b>OFFS (%)</b>	<b>OFFT (%)</b>	<b>ONS (%)</b>	<b>ONT (%)</b>	<b>OFF (%)</b>	<b>ON (%)</b>
<b>Linearly Increasing Frequency Modulation</b>	58.3	5.24	13.6	3.10	69.5	17.1
<b>Linearly Decreasing Frequency Modulation</b>	27.4	0.00	16.4	8.33	35.7	17.9
<b>Randomised Frequency Modulation</b>	33.1	0.00	3.10	0.48	43.6	4.76

Figure 6.11 and Figure 6.12 indicate the population response and preferential activation map of the four RGC types across the three stimulation protocols, respectively. Overall, the population response map (Figure 6.11) indicates significantly more variability in the response (particularly maximal activity) between the OFFS and OFFT RGCs across all three protocols in comparison to the ONS and ONT RGCs. With respect to the preferential activation map (Figure 6.12), all the cell types excluding the OFFT cells had at least one point of statistically-significant preferential activation space irrespective of the order of frequencies presented. While the ONT cells could reliably keep their preferential region at the highest amplitudes (250 – 300  $\mu$ A) and highest frequency region (5 – 10 kHz) of the parameter space during all the protocols, the statistically-significant regions themselves were considerably smaller than the ONS and OFFS cells. Both the OFFS and ONS cells had a more sporadic preferential region when the frequencies were randomised, but the regions corresponded to the maximal regions of activation seen in the population response. The ONS and ONT cells were relatively stable between the linearly increasing and linearly decreasing frequencies in comparison to the OFFS cells. Again, the OFFS cells had the highest preferential activation statistic for all the stimulation protocols Table 6.4.

Overall, the results suggest that the ON cells were less likely to be influenced by the order of the frequencies presented than the OFF cells. However, the OFF cells were able to fire more reliably within the parameter space.



**Figure 6.11 Population response maps of four RGCs in response to HFS presented with different frequency orders.** All four RGCs had a varied response to the protocols indicating dependency on frequency order however the ONS and ONT cells were less sensitive than the OFFS and OFFT cells. For all three protocols the frequency range was 0.5 – 10 kHz and amplitude range 10 – 300  $\mu$ A. The averaged normalised spike count is represented as the coloured square on the map. Each frequency was presented for 40 ms in the pulse train. (A) Population response to linearly increasing frequencies for OFFS ( $n = 12$ ), OFFT ( $n = 10$ ), ONS ( $n = 11$ ) and ONT ( $n = 10$ ). (B) Population response to linearly decreasing frequencies for OFFS ( $n = 7$ ), OFFT ( $n = 5$ ), ONS ( $n = 5$ ) and ONT ( $n = 8$ ). (C) Population response to randomised frequencies for OFFS ( $n = 8$ ), OFFT ( $n = 6$ ), ONS ( $n = 5$ ) and ONT ( $n = 8$ ).



**Figure 6.12 Preferential activation of four RGC types in response to HFS presented with different frequency orders.** For all the cell types, the magnitude of preferential activation for a given frequency-amplitude combination fluctuated across the three protocols, and only the ON RGCs were able to maintain a similar region of preferential activation across the three protocols. Preferential activation is defined here as the probability of one cell type population firing over the remaining population and calculated by subtracting the average normalised spike count of the respective populations. The colour bars indicate the normalised spike count difference between the populations, and the labels indicate the respective active and dormant populations. The black asterisks denote regions of statistical significance (one sample t-test against difference of zero between normalised spike count of the populations). All three protocols had the same frequency (0.5 – 10 kHz) and amplitude (10 - 300  $\mu$ A) parameter space. Each frequency was presented for 40 ms in the pulse train. (A) Preferential activation maps corresponding to the first phase of the linearly increasing frequency modulation protocol for OFFS ( $n = 12$ ), OFFT ( $n = 10$ ), ONS ( $n = 11$ ) and ONT ( $n = 10$ ). (B) Preferential activation maps corresponding to the first phase of the linearly decreasing frequency modulation protocol for OFFS ( $n = 7$ ), OFFT ( $n = 5$ ), ONS ( $n = 5$ ) and ONT ( $n = 8$ ). (C) Preferential activation maps corresponding to the first phase of the randomised frequency modulation protocol for OFFS ( $n = 7$ ), OFFT ( $n = 6$ ), ONS ( $n = 5$ ) and ONT ( $n = 8$ )

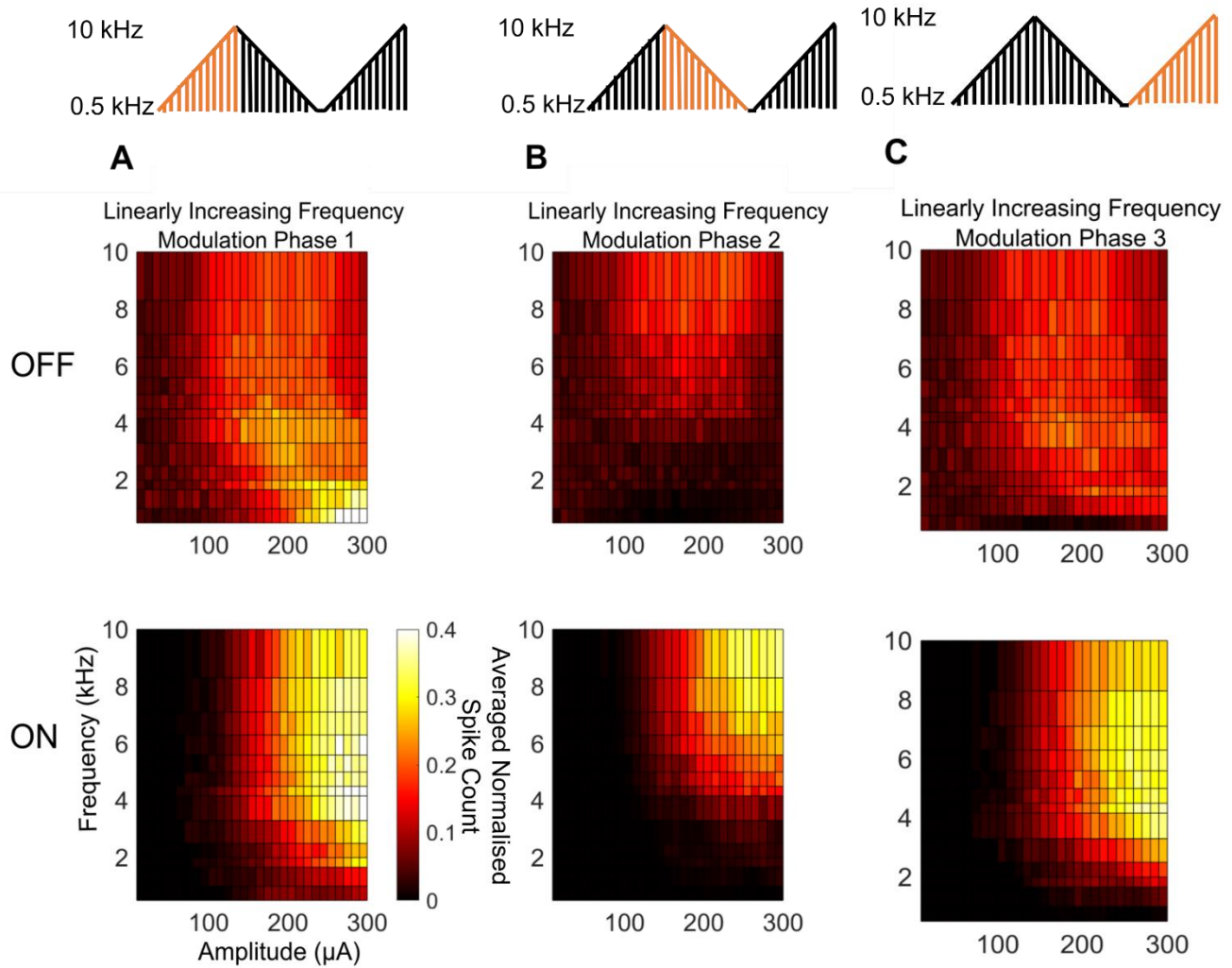
### 6.3.4 RGCs Response to Continuous HFS

To investigate how continuous frequency adaptation over time influences the preferential activation properties of distinct cell types, the preferential activation maps in response to three phases of the linearly increasing frequency modulation protocol (see Chapter 6, Section 6.2.1.1 for protocol) were compared between the ON and OFF RGCs, and subsequently the OFFS, OFFT, ONS and ONT cell types. For all cell types, the population response and preferential activation maps were shown. For all figures in this section, Panel A indicates the

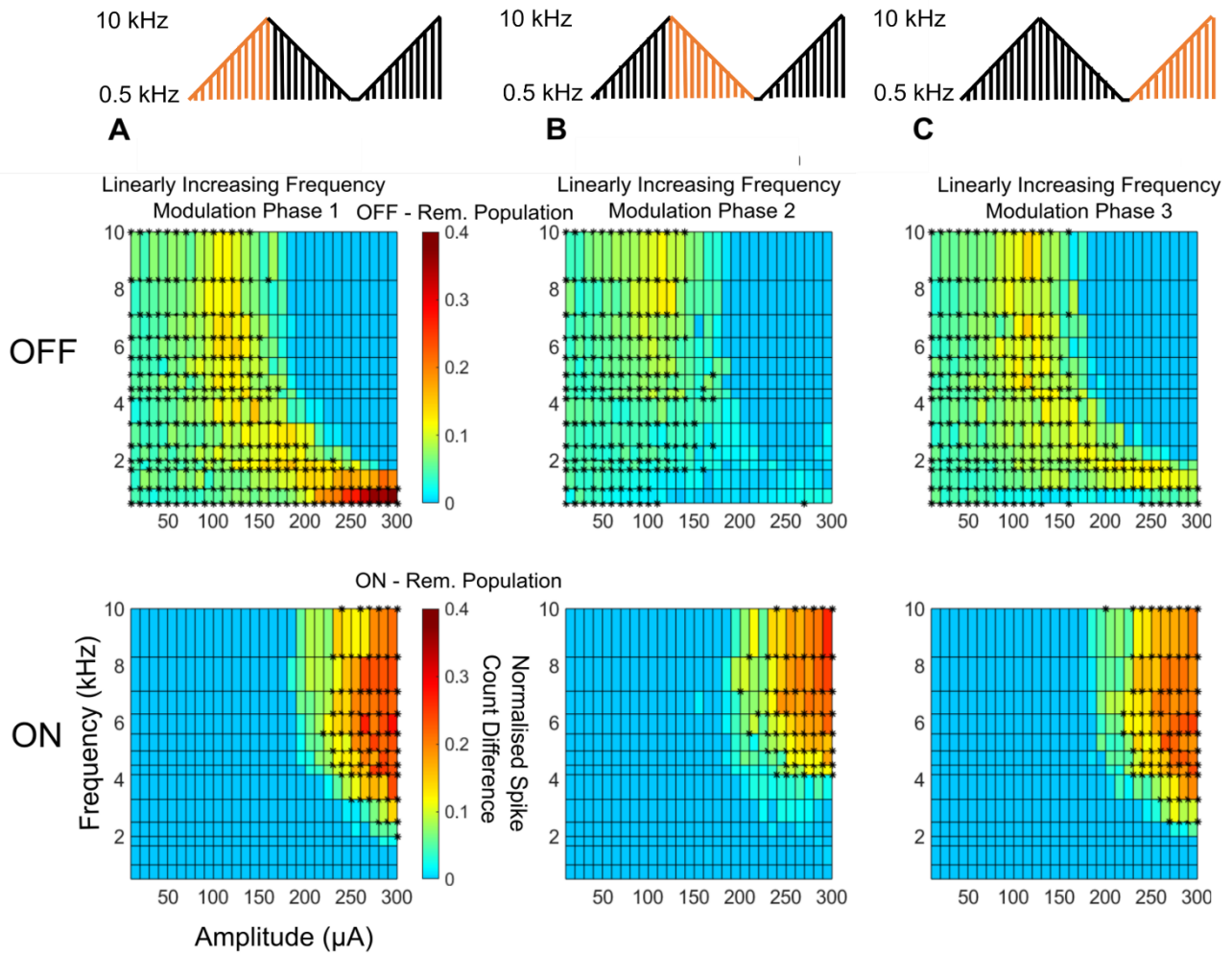
response when the frequencies were presented in a linearly ascending order (Phase 1), Panel B indicates the response when the frequencies were presented in a linearly descending order (Phase 2), and Panel C shows the response when the frequencies were presented in a second linearly increasing manner (Phase 3). No ISI was given between the phases. Table 6.5 summarises the total preferential space of each type for each phase.

Figure 6.13 and Figure 6.14 show the population response and preferential activation maps for the ON and OFF RGCs, respectively. Preliminary observations indicate that OFF cells were more susceptible to frequency adaptation than the ON cells, particularly in Phase 2 where they lose their preferential strongholds in which they were 20 – 40% more likely to fire than the population between 0.5 – 1 kHz and 250 – 300  $\mu$ A (Figure 6.14B). However, this varied response may be due to the sensitivity of OFF RGCs to the order in which frequencies were presented (frequencies were presented in descending order in Phase 2) rather than adaptation to continuous stimulation.

Similar trends were observed after subclassifying the ON and OFF RGCs into their sustained and transient components (Figure 6.15 and Figure 6.16). Both ONS and ONT RGCs had consistent responses and preferential activation regions across all three phases, however the preferential activation space for the ONS cells was greater than the ONT cells (Figure 6.16). Within the OFF cell population, the OFFT RGCs had a broader region of activation with responses overlapping with all three other cell types across all three phases. Unsurprisingly, the OFFT RGC preferential region of activation was significantly less than the OFFS RGCs. Both the OFFS and ONS had the highest and second-highest preferential activation statistics Table 6.5, with their highest value occurring during Phase 3 and lowest during Phase 2. This trend was also seen in the ONT cells however the highest value occurred during Phase 1.



**Figure 6.13 Population response maps of ON and OFF RGCs in response to continuous HFS.** Both OFF and ON RGCs were able to reproduce similar response patterns between the first phase (Panel A) and third phase (Panel C) however only the ON RGCs maintained a similar level of spiking. For all three protocols the frequency range was 0.5 – 10 kHz and amplitude range 10 – 300  $\mu\text{A}$ . Each frequency was presented for 40 ms in the pulse train. The averaged normalised spike count is represented as the coloured square on the map. (A) Population response of OFF RGCs ( $n = 22$ ) and ON RGC ( $n = 21$ ) for phase 1 of the linearly increasing frequency modulation protocol. (B) Population response for phase 2. (C) Population response for phase 3.



**Figure 6.14 Preferential activation maps of ON and OFF RGCs in response to continuous HFS.** ON RGCs maintained a consistent statistically significant preferential activation region across all three phases. OFF RGCs also maintained a similar preferential activation region however only between phase 1 (Panel A) and phase 3 (Panel C). Preferential activation is defined here as the probability of one cell type population firing over the remaining population and calculated by subtracting the average normalised spike count of the respective populations. The colour bars indicate the normalised spike count difference between the populations, and the labels indicate the respective active and dormant populations. The black asterisks denote regions of statistical significance (one sample t-test against difference of zero between normalised spike count of the populations). All three protocols had the same frequency (0.5 – 10 kHz) and amplitude (10 - 300  $\mu$ A) parameter space. Each frequency was presented for 40 ms in the pulse train. (A) Preferential activation map for OFF ( $n = 22$ ) and ON ( $n = 21$ ) for phase 1 for the linearly increasing frequency modulation protocol. (B) Preferential activation map for phase 2. (C) Preferential activation map for phase 3.

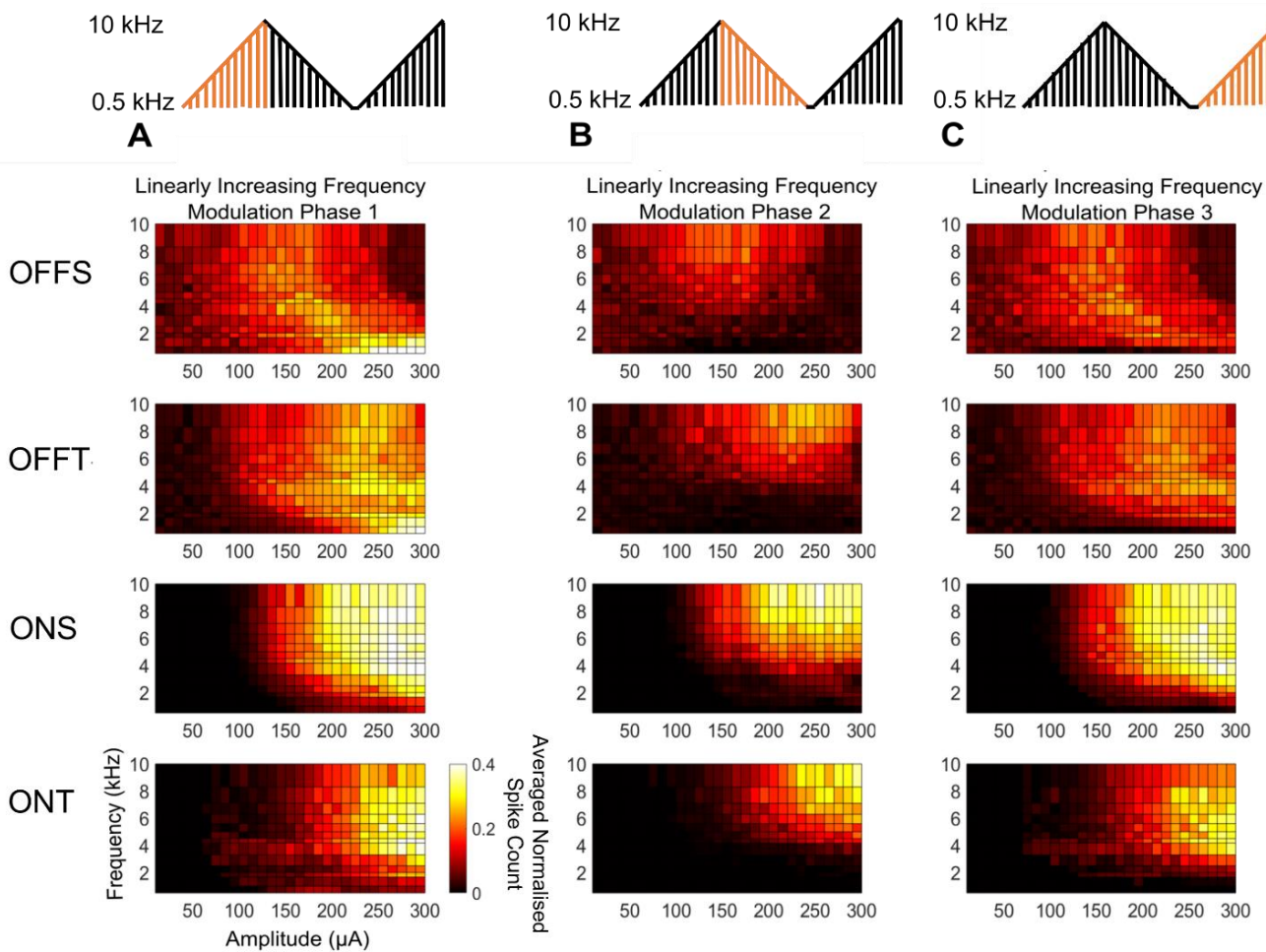


**Figure 6.15 Population response maps of four RGC types in response to continuous HFS.** All four cell types had similar response patterns between phase 1 (Panel A) and phase 3 (Panel C) however, the ONS and ONT RGCs had a similar spike count between the two phases. The OFFS and OFFT RGCs had a less consistent response across the three phases compared to the ONS and ONT RGCs. For all three protocols the frequency range was 0.5–10 kHz and amplitude range 10–300  $\mu\text{A}$ . Each frequency was presented for 40 ms in the pulse train. The averaged normalised spike count is represented as the coloured square on the map. (A) Population response to phase 1 of the linearly increasing frequency modulation protocol for OFFS ( $n = 12$ ), OFFT ( $n = 10$ ), ONS ( $n = 11$ ) and ONT ( $n = 10$ ) RGCs. (B) Population response to phase 2. (C) Population response to phase 3.

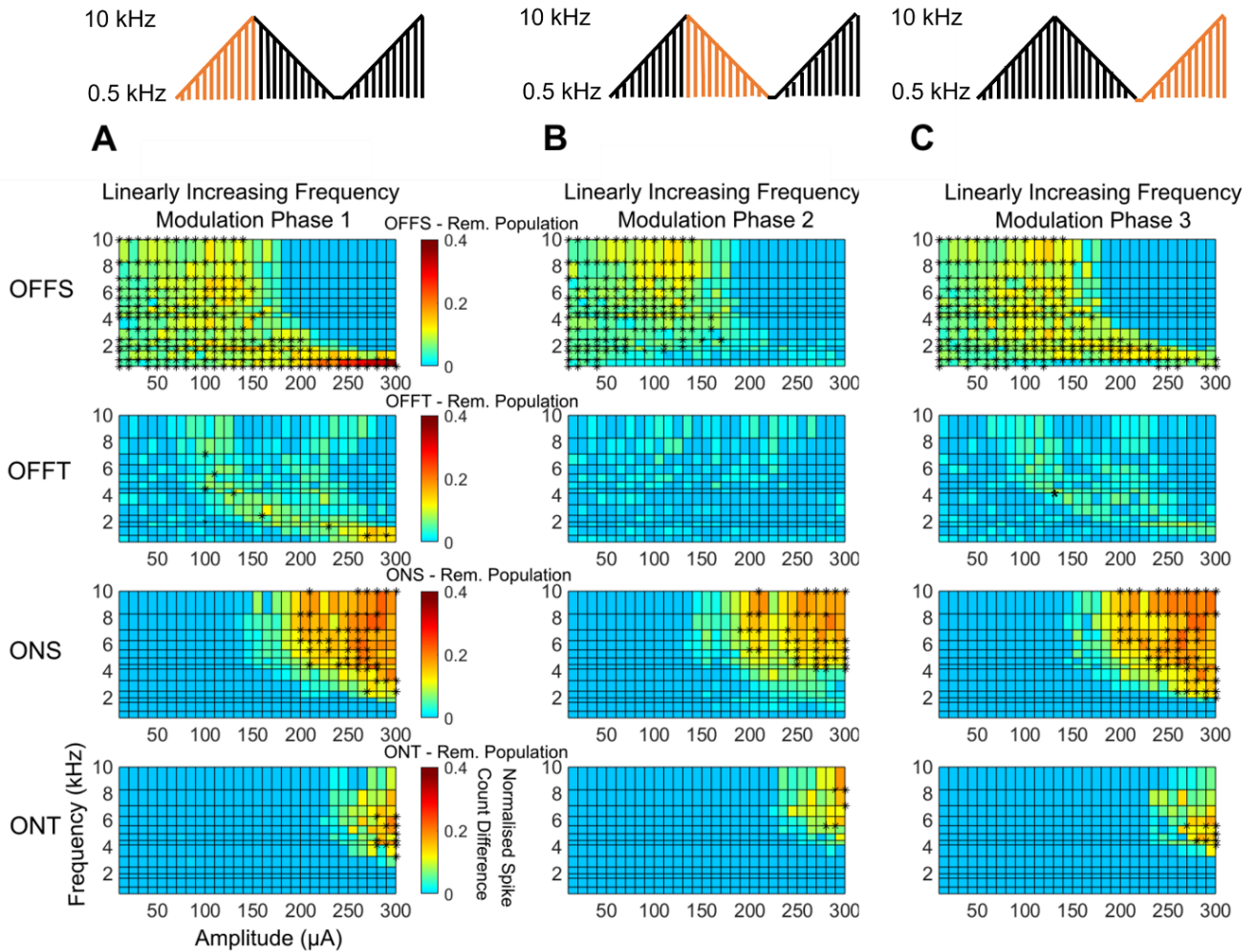


**Figure 6.16 Preferential activation maps for four RGC types in response to continuous HFS.** All the cell types, excluding the OFFT RGCs, maintained a statistically significant preferential activation region across all three phases, and only the ON RGCs maintained a similar preferential region across all phases. Preferential activation is defined here as the probability of one cell type population firing over the remaining population and calculated by subtracting the average normalised spike count of the respective populations. The colour bars indicate the normalised spike count difference between the populations, and the labels indicate the respective active and dormant populations. The black asterisks denote regions of statistical significance (one sample t-test against difference of zero between normalised spike count of the populations). All three protocols had the same frequency (0.5 – 10 kHz) and amplitude (10 - 300  $\mu\text{A}$ ) parameter space. Each frequency was presented for 40 ms in the pulse train. (A) Preferential activation maps for phase one in the linearly increasing frequency modulation protocol for OFFS ( $n = 12$ ), OFFT ( $n = 10$ ), ONS ( $n = 11$ ) and ONT ( $n = 10$ ). (B) Preferential activation maps for phase two (C) Preferential activation maps for phase three.

**Table 6.5 Summary of preferential activation statistics for four RGC types across the three phases of the linearly changing frequency modulation protocol**

<b>Preferential Activation Statistic</b>	<b>OFFS (%)</b>	<b>OFFT (%)</b>	<b>ONS (%)</b>	<b>ONT (%)</b>	<b>OFF (%)</b>	<b>ON (%)</b>
<b>Phase 1</b>	56.19	4.76	14.05	3.1	62.86	17.14
<b>Phase 2</b>	35.24	0	10.51	0.51	45.58	15
<b>Phase 3</b>	58.33	0.48	16.9	1.9	61.90	18.10

To isolate the influence of a continuous stimulus and adaptation effects on the cell type, the normalised spike count difference between phase 1 and phase 3 for the ON and OFF (Figure 6.17), and OFF, OFFS, OFFT, ONS and ONT RGCs (Figure 6.18) were compared. For each cell type, the normalised spike count difference (within a specified range) was reflected as a recovery statistic (see Chapter 6, Section 6.2.2.4 for calculation). The statistic was used to quantify how well the cell type was able to recover from an intermediate phase of stimulation (Table 6.6). From Table 6.6, none of the cell types were able to recover fully (i.e., all the recovery statistics were greater than zero). While the OFF cells had a higher recovery statistic than the ON cells, the difference between the normalised spike counts for the OFF RGCs was largely concentrated at a small, localised region (low frequencies between 0.5 – 1.5 kHz and high amplitudes between 200 – 300  $\mu$ A). Similar trends were seen between the four RGC types, with higher recovery statistics associated with the OFFS and OFFT RGCs compared to the ONS and ONT RGCs, but in similar localised regions. The discrepancies in spike count at the high amplitude regions in the OFF cells may be reflective of their charge-dependency and the potential associated variability in the spiking responses.

Nevertheless, overall, the results suggest all the cell types tended to fare well against continuous frequency adaption with all six types able to reliably recover the response patterns following a brief period of continuous stimulation.

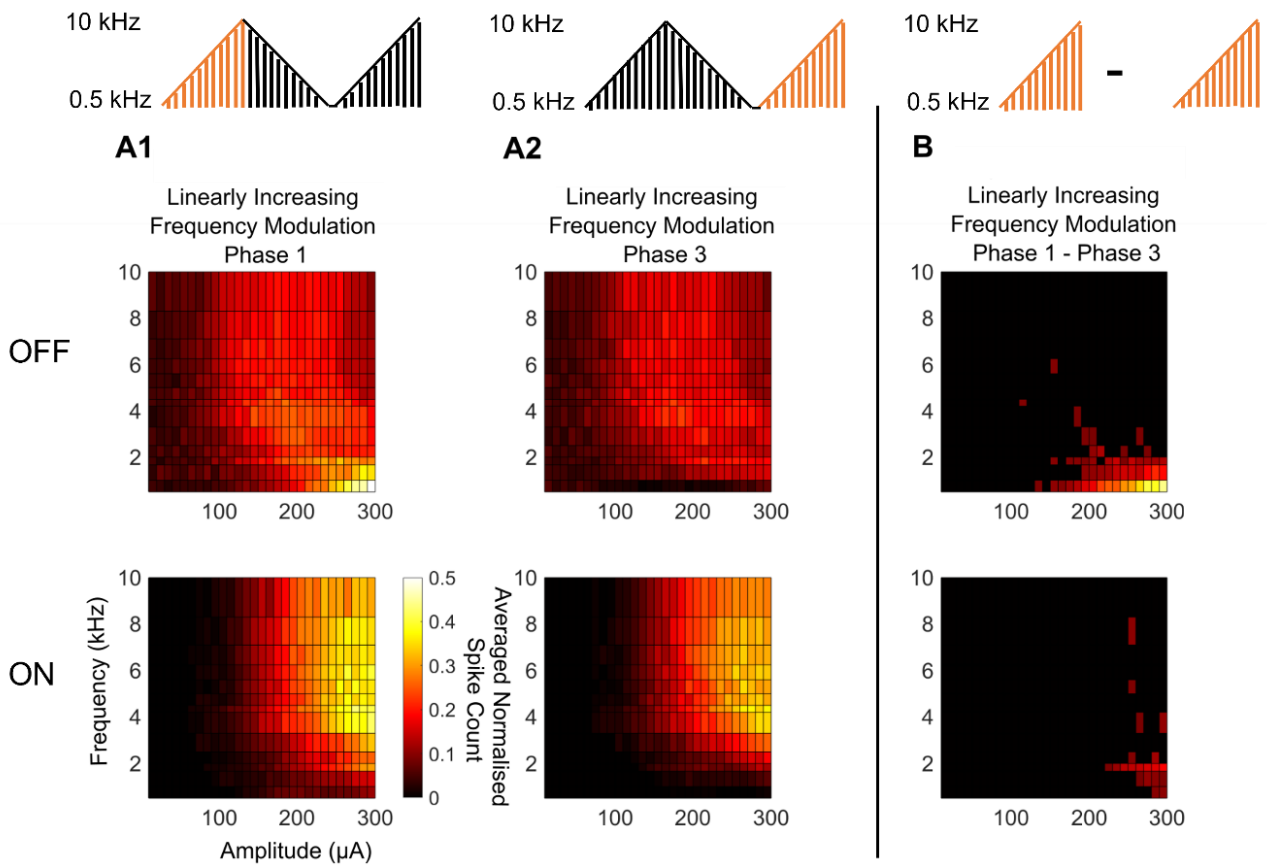


**Figure 6.17 Population response maps indicating the recovery properties of ON and OFF RGCs in response to continuous HFS.** The normalised spike count difference (Panel B) between phase 1 (Panel A1) and phase 3 (Panel A2) for the ON and OFF RGCs indicated that both cell types could reliably recover the majority of the spiking patterns however ON RGCs were more robust in their recovery compared to the OFF RGCs. (A1) Normalised population response of the ON ( $n = 21$ ) and OFF ( $n = 22$ ) RGCs during phase 1 of the linearly increasing frequency modulation protocol. (A2) Normalised population response during phase 3. (B) Averaged normalised spike count difference between phase 1 and phase 3.

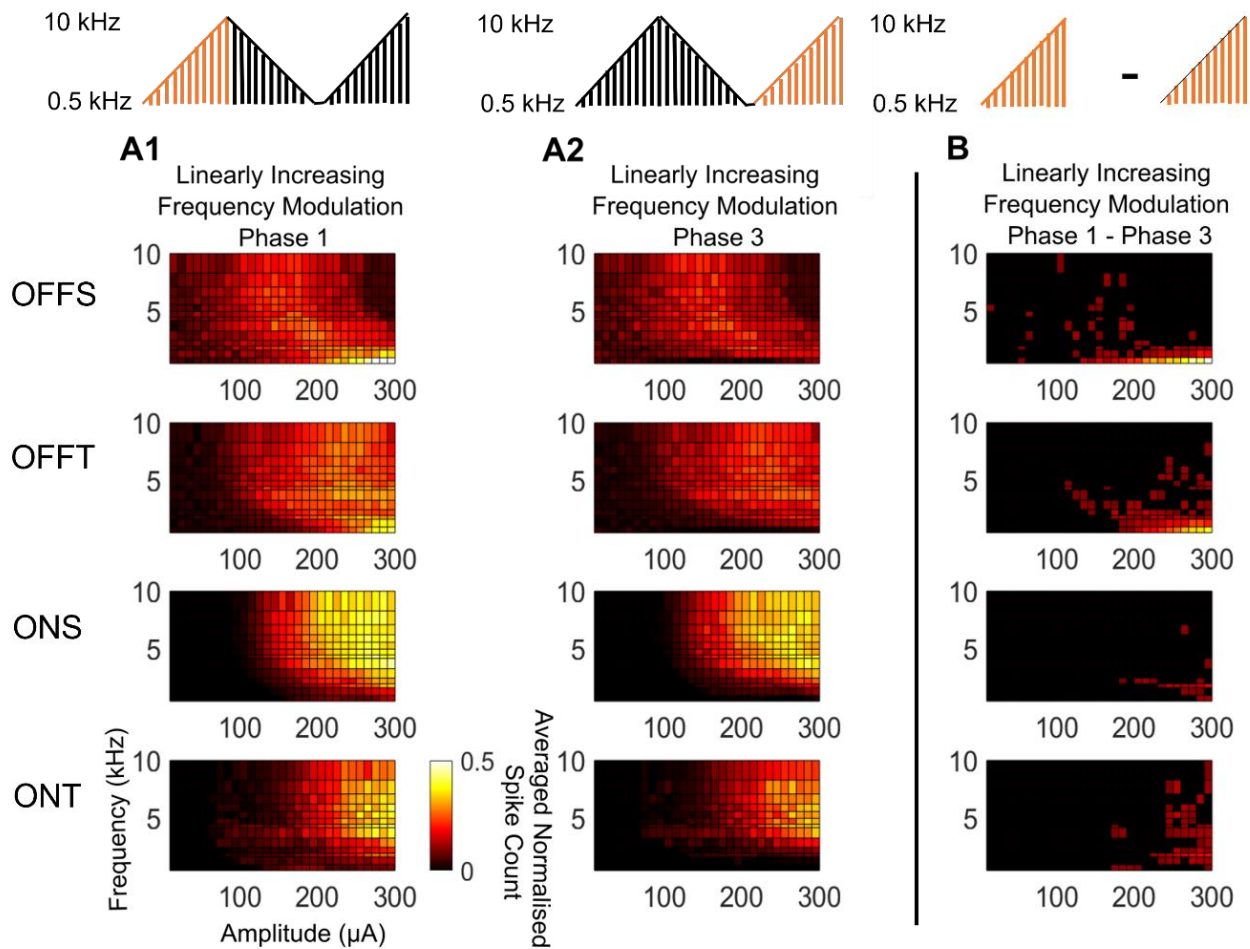


**Figure 6.18 Population response maps indicating the recovery properties of four RGC types in response to continuous HFS.** All four cell types had minimised normalised spike count differences between phase 1 and phase 3 for most of the parameter space. Both the OFFS and OFFT RGCs had a similar localised region (low frequency, high amplitudes) in which the difference was the greatest. ONT RGCs were more sporadic in the difference than the ONS RGCs. (A1) Population response of OFFS ( $n = 12$ ), OFFT ( $n = 10$ ), ONS ( $n = 11$ ) and ONT ( $n = 10$ ) RGCs during phase 1 of the linearly increasing frequency modulation protocol. (A2) Population response during phase 3. (B) Averaged normalised spike count difference between phase 1 and phase 3.

**Table 6.6 Recovery statistic of cell types**

Recovery Statistic	OFFS (Spike Count Difference)	OFFT (Spike Count Difference)	ONS (Spike Count Difference)	ONT (Spike Count Difference)	OFF (Spike Count Difference)	ON (Spike Count Difference)
Phase 1 – Phase 3	19.7	27.1	3.46	10.9	16.8	4.85

### 6.3.5 RGCs Response to Optimised Dynamic HFS Waveform

The major aim of the first half of this study was to identify the unique response patterns of different RGC types to a wide range of HFS settings, particularly modulating frequencies. The second half of the study was focussed on channelling the previous results into more practical applications. Specifically, to see if optimised frequencies could be encoded into a novel dynamic waveform capable of preferentially controlling cell types with fast-changing bursts of frequencies.

The results so far indicate that all four cell types had the best preferential activation capabilities when stimulated with linearly increasing frequencies. In addition, the results also indicate little difference in the regions of spiking activity and activation between the sustained and transient types (i.e., between OFFS and OFFT, and ONS and ONT) but greater differences between the ON and OFF cell types. Taking this into account, for this study, optimised frequencies were used to preferentially activate the ON and OFF cells.

From Figure 6.19A (replotted from Figure 6.10), the OFF cells tended to be preferentially active at the lower frequencies (0.5 – 1kHz) and the ON cells were preferentially active at higher frequencies (4 – 10 kHz). After experimental optimisation, the waveform was designed to have two short frequency bursts of 40 ms, the first phase at 1 kHz to activate the OFF cells and the second phase at 8 kHz to activate the ON cells. Given the OFF cells were more sensitive to the decreasing frequencies as shown previously (Figure 6.10) a 60 ms ITD was introduced as minimal time for the cell to recover. Each 40 – 40 – 60 ms combination was repeated ten times. Figure 6.19B illustrates raw spike traces for a single representative ON and OFF cell at 300  $\mu$ A. Both the ON and OFF cells had an out-of-phase response to the designed waveform in which the OFF cells responded primarily to the 1 kHz phase and the ON cells to the 8 kHz phase. Notwithstanding, both the cell types did respond to a lesser extent to the phases in which they were not designed to spike. In particular, the example OFF cell had a short burst at the onset of the 8 kHz phase across all ten trials and the ON cell had a single spike in the 1 kHz phase.

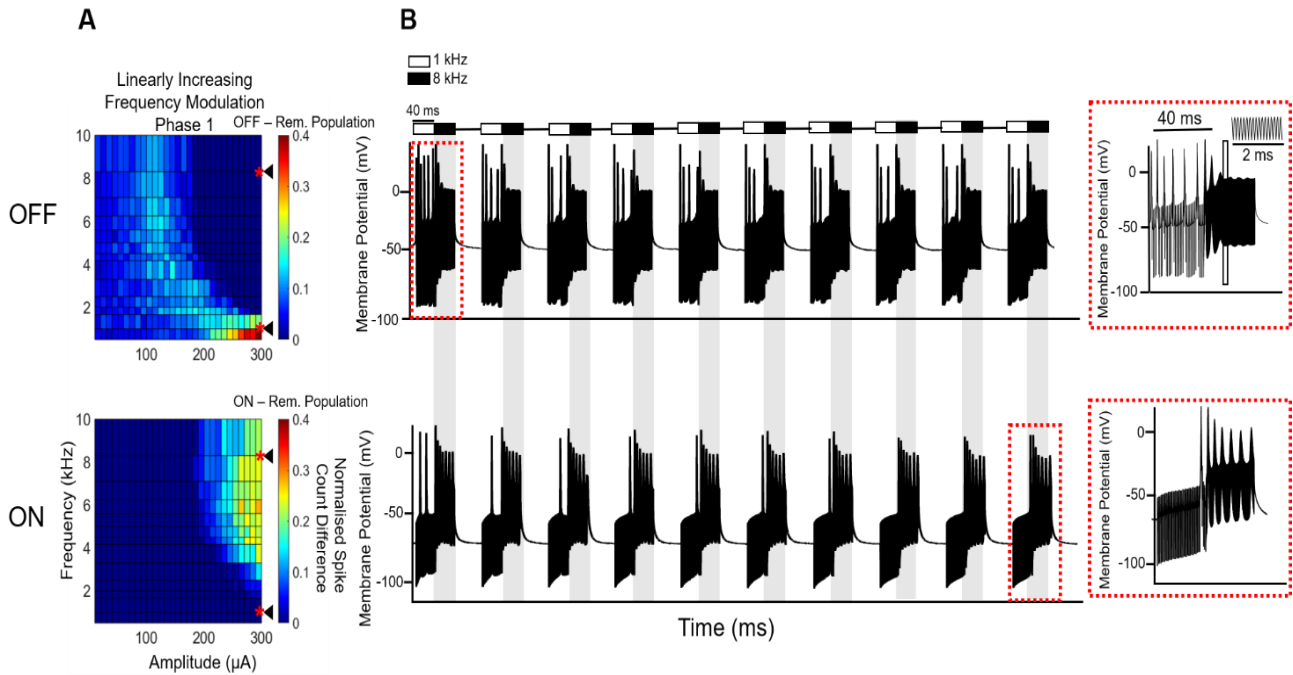


**Figure 6.19 Response of four RGC types to a dynamic, high frequency-modulated waveform.** The waveform consisted of two stimulation phases with the 1 kHz frequency used to activate the OFF cells, and 8 kHz to activate the ON cells. Each stimulation phase duration was 40 ms, followed by a 60 ms rest period. In the example ON and OFF cell, both cells could be preferentially controlled with the waveform with the OFF cell activated at 1kHz and inactivated at 8 kHz, and the ON cell activated at 8 kHz and inactivated at 1 kHz. (A) The preferential activation map for the ON ( $n = 20$ ) and OFF ( $n = 16$ ) RGCs when stimulated with linearly increasing frequencies between 0.5 – 10 kHz and amplitudes 10 – 300  $\mu\text{A}$ . (B) Raw spike traces of a representative ON (ONT) and OFF (OFFS) cell in response to the dynamic waveform at amplitude of 300  $\mu\text{A}$ . Each 40-40-60ms combination was repeated ten times. Inset. Expanded view of the raw spike traces during two 40 ms pulse trains showing spikes riding on top of the artefact (indicated by the vertical box).

### 6.3.6 Replication of a Pseudo-Randomised Spike Train

In the previous section, the results showed that the ON and OFF RGCs could be preferentially controlled with practical stimulation consisting of short, dynamic bursts of frequencies. Based on this, a second dynamic waveform was designed to identify if a targeted cell type could be made to replicate a pseudo-randomised spike train through a modulating high frequency waveform (see Chapter 6, Section 6.2.1.4.2 for protocol). Briefly, a pseudo-randomised spike train was generated with randomised spikes between 1 – 10 and randomised ISI between 10 – 100 ms. A corresponding stimulus waveform was designed consisting of spiking (i.e., active) and non-spiking (i.e., inactive) windows to approximate the generated spike train. Like the previous dynamic waveform, the frequency was modulated between 1 kHz and 8 kHz however in this waveform, the 8 kHz frequency was used to activate *both* the ON and OFF cells, and the 1 kHz to inactivate.

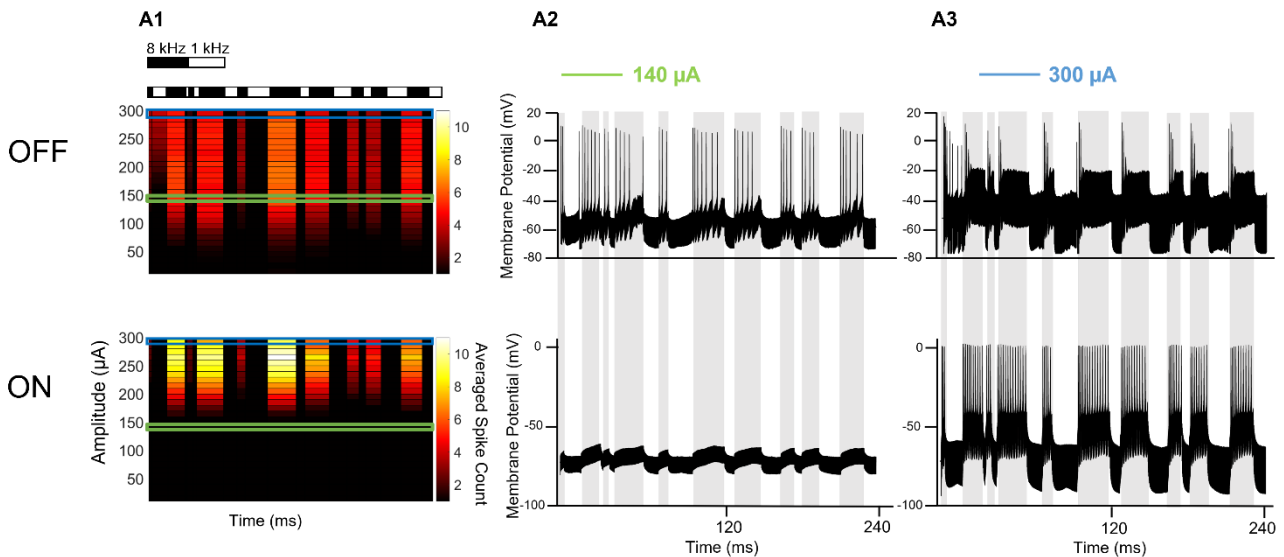


**Figure 6.20 ON and OFF RGC responses to a high-frequency modulated waveform designed to replicate the active and inactive regions of a pseudo-randomised spike train.** Both the ON and OFF cell were activated by the 8kHz and inactivated by the 1 kHz. Careful selection of amplitude allowed the two cells to be preferentially controlled. (A1) Population responses of the OFF ( $n = 7$ ) and ON ( $n = 3$ ) RGCs in response to the dynamic waveform. The green and blue highlighted sections on both maps correspond to the amplitude required for preferential activation of the OFF and ON cells respectively. (A2) Raw spike traces of a representative ON (ONS) and OFF (OFFT) cell for amplitude 140  $\mu\text{A}$ . (A3) Raw spike traces of a representative ON (ONS) and OFF (OFFT) cell for amplitude 300  $\mu\text{A}$ .

Figure 6.20 depicts the pilot results for the ON and OFF RGC types. Figure 6.20A1 shows the averaged normalised spike response across the two populations in response to the dynamic waveform. Figure 6.20A2 shows the raw spike traces for a single ON and OFF cell at amplitude 140  $\mu\text{A}$  and Figure 6.20A3 at amplitude 300  $\mu\text{A}$ .

In assessing the ability of a cell type to replicate the spike train, I was specifically interested in three aspects. Firstly, was the cell type active and inactive in the spiking and non-spiking regions, respectively. Secondly, could the cell type reproduce the generated spike numbers. Lastly, could this be achieved preferentially. From Figure 6.20 the ON RGCs across all the tested amplitudes were active and inactive in corresponding spiking and non-spiking regions. The OFF RGCs also had largely confined responses to the spiking regions however at the higher amplitudes (240 – 300  $\mu\text{A}$ ), spiked at the first inactive region in the pulse train. With respect to the spiking numbers, neither the ON RGCs nor the OFF RGCs could accurately reproduce the pseudo-randomised spike train numbers. However, this is not unexpected given that the spiking window designed to yield the spiking numbers was simply an approximation extrapolated from previous data. Lastly, the results indicated that to achieve preferential control of the RGC type whilst simultaneously replicating a spike train, cell type-specific amplitudes must be used. For example, in the representative cells shown in Figure 6.20A2 and Figure 6.20A3, 140  $\mu\text{A}$  was used to activate the OFF RGCs while the ON RGCs remained silent whereas 300  $\mu\text{A}$  was used to activate the ON RGCs without activating the OFF RGCs.

Altogether, these proof-of-concept analyses provide preliminary evidence that different cell types can be preferentially controlled with high temporal precision, by appropriately modulating stimulation parameters.

## 6.4 Discussion

This chapter has three primary outcomes – 1) Determine the relative sensitivity of each RGC type to dynamic modulation of HFS parameters and understand how these dynamic stimulus-cell characteristics influence the ability to be preferentially stimulated using HFS. 2) Assess the possibility of achieving cell-type specific activation through brute force optimisation of stimulus parameters. 3) Explore how RGC features shape their responses to different HFS conditions.

Overall, the ON cells were more robust to a modulating frequency (particularly with regards to the order of frequencies presented) than the OFF cells. However, they were limited in the regions they could be preferentially activated. Based on the detailed atlas of the diversity in response across major RGC types to the dynamic HFS modulation, an optimal dynamic stimulus waveform was designed, using a modulating frequency to precisely control the targeted cell types. Using these optimised waveforms, both ON and OFF cells could be preferentially activated. Finally, as a pilot study, similar modulating frequencies were encoded into a longer stimulus waveform to replicate a pseudo-randomised spike train. The result suggests the possibility of accurately controlling neural bursting by modulating the stimulation frequency with randomised pulse train durations.

### 6.4.1 Effects of High Frequency Modulation on the RGC Response and Preferential Activation Capabilities

#### *6.4.1.1 Long and Static Stimulation versus Short and Dynamic Stimulation*

I was initially interested to see how the RGCs response altered when first, the stimulation duration was shortened from 300 ms to 40 ms, and then if the RGC was stimulated in a static (i.e., at rest) or dynamic (i.e., no ISI given between frequencies) state. For both the ON and OFF cells shown in Figure 6.5, the most noticeable effect of the short duration stimulation and the randomised dynamic stimulation was a distinct rightward shift in the maximal activity region (area yielding in the maximum activity across the population of cells) towards higher stimulus amplitudes. Between the two cell types however, the ON cells had a clearer shift initially between the long and short duration under static stimulation conditions (Figure 6.5A versus Figure 6.5B), and then again from static to dynamic stimulation (Figure 6.5B versus Figure 6.5C and Figure 6.5D). The OFF cells on the other hand, had a clear rightward shift from long

to short duration, but were much more stochastic in their response to the dynamic stimulation. Given that the dynamic stimulation consisted of randomised frequencies, preliminary observations suggest that the OFF cells are more sensitive to frequency than the ON cells. The differences in dependency between the ON and OFF RGCs to frequency will be discussed further in this section. Across the four cell types seen in Figure 6.6, there was minimal difference between the sustained and transient subtypes.

The shift in maximal activity for the ON and OFF cells in turn affected their ability to be preferentially activated against the remaining population (Figure 6.7 and Figure 6.8). The OFF cells had a clear but inconsistent preferential region across all the different stimulation conditions. The ON cells were consistent in the region but limited in the size of the region. Across the four cell types (Figure 6.8), the OFFS and ONT cells were the most robust with respect to either their ability to be preferentially activated across the different stimulation conditions (ONT) or their consistent preferential space (OFFS), indicating their priority for cell-type specific targeting using HFS.

In general, all the cell types exhibited an affinity to spiking at higher amplitudes when stimulated with short, dynamic stimulation. It is likely that part of this shift, particularly when moving from long to short stimulation durations, stems from a phenomenon known as the “onset response” [181, 185, 277, 278]. The onset response is typically observed as a short burst of spikes that occurs at the beginning of HFS during the conduction block in which high frequency pulses (1 – 70 kHz) are used to block nerve activity [175, 177, 279]. These bursts of spikes were observed in this study and occurred well within the 40 ms of stimulation. Speculatively, the increased spiking activity due to the onset response, particularly when the cell is being blocked, is likely the cause of the rightward shift towards higher amplitudes. The correlation between the stimulation duration and the rightward shift in activity towards higher amplitudes was also reported in Twyford et al. [14]. In their study they found that under 2 kHz stimulation, OFFT BT RGCs had non-monotonic responses with increasing amplitude when they considered the responses across the full 5 seconds of stimulation, compared to a monotonic response when considering the first 250 ms. Though the time scale used in their study is different to what was used in this study, the spike raster plot from their study showed clear onset bursts indicating that the mechanisms behind the shift are similar.

Previous studies in peripheral nerve stimulation have been conducted to minimise the onset response [280-282], including a combination of a charge-balanced DC (CBDC) waveform with the high frequency stimulation in which the CBDC component was found to have no associated onset response and therefore used to block the nerve initially, and the HFS to maintain the block [283]. This approach is difficult to achieve in a retinal implant however, as firstly, two separate stimulators are required to supply the DC and HFS components and

secondly, the HFS and CDBC stimulation must have complementary electrical sources (either voltage or current) to minimise the cross talk between the two electrodes.

#### *6.4.1.2 Sequence Order and Continuous Stimulation*

I was then interested to understand if the RGC response changed if firstly, the order of frequencies presented varied and secondly, if long-term continuous stimulation without ISIs was used. From Figure 6.10, the ON cells response was robust with minimal influence by the delivered frequency orders, in comparison to the OFF cells whose preferential region was highly dependent on the frequency order. Despite this, the OFF cells had a larger preferential activation space (indicated by the larger preferential activation statistic from Table 6.4) across all the different frequency orders than the ON cells even though this was likely due to the limitation of the parameter space for the ON cells to be reliably controlled. Specifically, the ON cells' preferential region was consistently towards the higher frequencies and higher amplitudes (on the boundary of tested parameter space) implying their comparative preferential activation performance is less to do with the cell properties, and more to do with the stimulation range. Hypothetically, better outcomes may be achieved with even higher frequencies and amplitudes. Lastly, indications of the onset response can be seen in the OFF cells' preferential region, with a surprising preferential region at 10 kHz (Figure 6.10C) corresponding to the first frequency presented for that protocol. Across the four cell types (Figure 6.12), once again, the OFFS and ONT cells were the most consistent with respect to the total preferential activation space, or most consistent preferential region.

Altogether, the results suggest that ON cells are more frequency-dominated than the OFF cells. That is, the ON cells are more likely to respond robustly to a frequency irrespective of the way in which it is presented. OFF cells on the other hand, appeared to be influenced in part by the total charge, particularly when stimulated with higher frequencies (> 4 kHz). However, the results show that the OFF cells (along with ON cells) were able to reasonably reproduce the spiking patterns of a particular stimulus following an intermediary phase of stimulation. This suggests that both cell types are relatively immune to frequency adaptation with respect to a continuous stimulus.

#### *6.4.1.3 Possible Mechanisms*

The results in this study are intrinsically-driven (i.e., the cells have been isolated from the synaptic network) and therefore the mechanisms responsible for differences in frequency-sensitivity, but similarity in recovery properties, between the ON and OFF RGCs must be intrinsic to the cell.

Previous studies have shown that the AIS in RGCs is the most sensitive component to electrical stimulation [196, 200, 284]. Given its importance, recent studies led by Shelley Fried

have looked into how the AIS properties may differ between the major RGC type. Anatomically, their main results indicated that alpha ONS RGCs had the longest AIS length, and alpha-ONT RGCs had the shortest [200], and across the retina,  $\alpha$ -ON RGCs were likely to have longer AISs than neighbouring alpha-OFF RGCs [79]. Werginz et al. [200] used computational modelling to further quantify the relationship between AIS length and activation threshold finding that a longer AIS yielded lower thresholds. Correspondingly, alpha-ONS RGCs had the lowest thresholds, and alpha-ONT RGCs had the highest thresholds. While their results can potentially explain the behaviour of the ONT RGCs which were found to be the least excitable out of the three cell types in this study, it does not explain the ONS cells which had comparable excitability to the ONT RGCs. However, this is also not an accurate comparison given that the results from this study were taken after the synaptic input was blocked. For example, Yang et al. [165] showed that ON RGCs had a statistically significant difference in stimulation thresholds after the application of synaptic blockers, highlighting their importance in shaping the threshold response. Nevertheless, the anatomical differences in the AIS do suggest that the RGCs may also have differences in the intrinsic compositions aiding their responses to electrical stimulation.

To this end, both Raghuram et al. [79] and Werginz et al. [197, 200] (in two separate studies) also studied the proportion of sodium channels, specifically the subtype Nav 1.6 located in the AIS. which has been widely documented to aid in the ability of cells to fire at high pulse rates [191, 192]. Their initial reports drew two main conclusions. Firstly, the relative proportion of the Nav 1.6 channels within the AIS was statistically similar between the alpha-ON and alpha-OFF RGCs [79]. Secondly, while the initial presence of Nav 1.6 channels dramatically reduced the threshold, further increases in the channels had minimal impact on the threshold [200]. As such they concluded that the relatively small differences in AIS length (therefore Nav 1.6 channels) between the cell types were not enough to elicit significant differences in responses to electrical stimulation. However, in a follow-up study, Werginz et al. [197] specifically investigated how Nav 1.6 channels contributed to the sustained firing of the dorsal OFFT RGCs and their ability to fire at higher amplitudes than the ventral OFFT RGCs following systematic increases in depolarising amplitude pulses [197]. They found that after blocking the Nav 1.6 channels pharmacologically, the ability of the dorsal OFFT RGCs to maintain high frequency spiking at relatively high amplitudes reduced. Given that dorsal OFFT RGCs had longer AISs, they concluded that cells with longer AISs have a corresponding increase in the Nav 1.6 channels which in turn, allow the cell to fire more robustly at otherwise depolarising levels.

From the mentioned studies, it seems unlikely that the anatomical and intrinsic composition of the AIS is the primary source of difference response to HFS shown in this study. However,

they make two important observations which may aid in understanding the behaviour observed here. Firstly, they found that the *overall* distribution of Nav 1.6 (not relative to the anatomical size) does impact firing capabilities [197]. Secondly, Werginz et al. [200] found that the cell soma also influenced stimulation thresholds, and importantly, varied depending on the location of the electrode. Specifically, they found that if the electrode was placed near the soma, the threshold increased with soma size compared to decreasing thresholds with soma size if the electrode was placed near the AIS. They postulated that when the electrode was closer to the cell, the somatic influence overrode the influence of the AIS. In the experiments presented in this study, the stimulating electrode was placed closer to the soma than the AIS. Therefore, it is possible that the response was shaped more by somatic properties than the AIS properties. Speculatively then, if the distribution of the Nav 1.6 channels differed in the cell soma, this could explain the cells' response to HFS. Future computational modelling coupled with immunohistochemistry studies may be able to prove this theory.

#### 6.4.2 Controlling RGC Activation with Optimised, Dynamic HFS Waveforms

The second part of this study was to encode optimised frequency parameters in a dynamic waveform capable of accurately controlling and preferentially activating a targeted cell type using a modulated frequency in short stimulation bursts.

The first waveform was designed to have two short, 40 ms stimulation bursts to preferentially target to OFF cells, followed by the ON cells and a 60 ms ITD to allow the cell to recover.

The two main design considerations made were the frequencies to preferentially target the ON and OFF cells, and the orders in which they should be presented. As discussed previously, the OFF cells were more sensitive than ON cells to the delivered frequency orders. From Figure 6.10, the ON and OFF cells could only be preferentially activated with a modulating amplitude rather than frequency when the frequencies were in descending or in a randomised order. Therefore, the only suitable order of frequencies for a modulating frequency waveform was when the frequencies were presented in ascending order with the OFF cells activated with a low frequency (e.g., 0.5 - 1 kHz) and the ON cells activated with a high frequency (e.g., 8 – 10 kHz) (Figure 6.10A). After optimisation, the frequency used to activate the OFF cells was chosen to be 1 kHz encoded in the first burst, and 8 kHz for the ON cells encoded in the second burst.

The results from the example ON and OFF cells shown in Figure 6.19 indicate that the two cells could be controlled by the waveform, with the OFF cell spiking primarily in the 1 kHz phase (OFF preferential phase) and the ON cell spiking in the 8 kHz phase (ON preferential

phase). Between the two representative cells, the ON cell had consistent spiking across the ten trials opposed to the OFF cell which exhibited a clear onset burst in the first trial followed by progressively weaker spiking in the subsequent trials (particularly between trials 1 – 3). Figure 6.21 illustrates the population averaged normalised spike counts for ON (shown in black) and OFF (shown in red) cells at 1 kHz (shown as filled-circles) and 8 kHz (filled-squares). Overall, the difference in spike count at the ON preferential space (compare the filled-square lines) was higher than the difference in spike count for the OFF preferential space (compare the filled-circle lines) indicating that the ON cells may be a more promising target for preferential activation. The results together indicate that a dynamic waveform based on a modulating frequency is capable of generating an out-of-phase response between the ON and OFF cells with careful selection of frequencies and amplitudes.

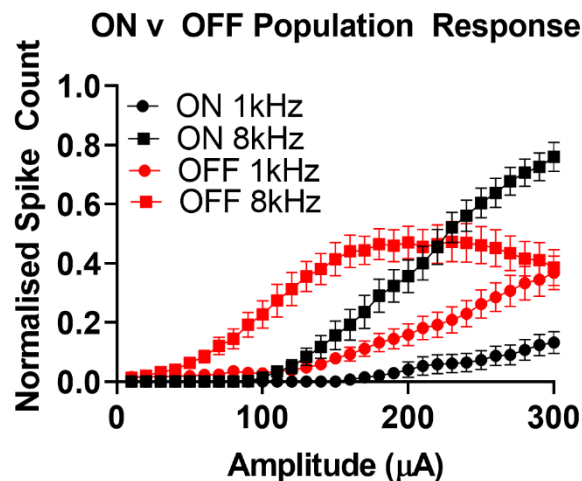


**Figure 6.21 Normalised spike counts of the ON and OFF RGC populations to 40-40-60 ms dynamic waveform.** There was a bigger normalised spike count difference between the ON ( $n = 20$ ) and OFF ( $n = 16$ ) RGCs under 8 kHz (corresponding to the ON preferential space) compared to the normalised spike count difference at 1 kHz (corresponding to the OFF preferential space).

The second dynamic waveform was a pilot study to identify if similar modulating frequencies could precisely control the temporal spiking for each cell type to replicate a pseudo-randomised spike train (Figure 6.20). Broadly, I was interested in the utility of HFS to reproduce (a) regions of spiking and non-spiking and (b) the spike counts of the pseudo-randomised spike train while the cells were preferentially activated. To replicate these aspects, the designed waveform consisted of corresponding pulse duration windows which were estimated to reproduce the spiking regions and spike counts. The spiking and non-spiking regions were controlled by modulating frequencies.

Initially, analogous to the 40-40-60 ms waveform, 1 kHz and 8 kHz were considered as the optimal frequencies to preferentially target the OFF and ON cell types, respectively. However,

dissimilar to the first waveform, the waveform was to have continuous stimulation without any ITD given between the frequencies. Given that the OFF cells were unlikely to recover quickly from the 8kHz to spike at the 1kHz regions, it was decided that both cell types would be activated at the same frequency (8kHz) and inactivated at the same frequency (1kHz). From the example cells shown in Figure 6.20 the results indicate that spiking and non-spiking regions can be reliably controlled by modulating frequencies, and careful selection of amplitude can yield in an out-of-phase response between the ON and OFF cells.

Previous retinal studies have indicated that different RGC types have frequency-dependent responses [131, 183, 273-275, 285], However, to the best of my knowledge, this is the first time that high frequency modulation was combined with clinically-relevant short stimulation duration to preferentially target different RGC types. Twyford et al. [14] previously showed the effectiveness of a 2 kHz amplitude-modulating waveform with long stimulation duration (5 s) to elicit a differential response from ON and OFF BT cells. However, there are potential caveats to using an amplitude-driven waveform. In particular a cell's response to amplitude is largely mediated by the total charge which is dependent on factors including the electrode geometry and location. In contrast, it is hypothesised that the cell's response to frequency is more time-dependent and reliant on intrinsic properties of the cells themselves opposed to the stimulation conditions making the cell response more robust. Clinically, Nanduri et al. [129] also found that frequency modulation was more useful in the context of producing high resolution phosphenes with a greater range in brightness. More recently, a study conducted by Yue et al. [272] found that modulating the stimulation frequency from 6 to 120 Hz yielded visual percepts transitioning from a yellow colour to a blue/purple colour for 5/7 Argus II patients, showcasing the benefit of frequency modulation in generating colour perception.

The fundamental benefit of using short bursts of stimulation such as the 40-40-60 ms waveform is the capability of preferentially activating a target cell type using short pulse trains within the clinical frame rate of 7 – 10 Hz of a current retinal prosthesis [7] allowing for increasing utility, particularly in the clinical space. Additionally, the use of short stimulation bursts vastly reduces the high energy required when stimulating with HFS, and the 60 ms ITD allows some time to recover any charge imbalance at the tissue-cell interface and potentially reduce any cumulative damage in the tissue.

The use of short bursts of high frequency stimulation may also be a useful technique for asynchronous stimulation which is emerging as a potential alternative to synchronous stimulation owing to the reduced overlap of elicited phosphenes generated by different electrodes [276]. Specifically, in asynchronous stimulation, limited time is provided to each electrode to elicit a phosphene within the overall frame rate of the implant. However, to achieve this would imply large current amplitudes which would increase the phosphene size [129].

Perceptual threshold was previously found to decrease with increased frequency [172] and importantly, increased frequency was found to modulate the brightness of the percept, not the size [129]. As such, high frequency bursts of stimulation, particularly with carefully optimised parameters may be a potential method to evoke visual percepts from targeted cell types in asynchronous stimulation in the future.

That said, there are many obstacles that challenge the viability of the proposed stimulation strategy. For example, a frame rate of 7 – 10 Hz in a prosthesis with a 60-electrode array roughly corresponds to 2 ms provided for each electrode [276] on the assumption that stimulation must be performed sequentially across electrodes. Even if the dynamic waveform is reduced to stimulating only one targeted cell type, the stimulation duration is still 40 ms. While the perceptual threshold may still be reached if the duration is reduced to 2 ms, and with minimised effect on the percept size, the localised onset burst will prevent any preferential activation between cell types. Though steps have been taken to minimise the onset response (discussed in Chapter 6, Section 6.4.1.1), their practicality is limited. Furthermore, the use of HFS in the proposed frequency and amplitude range, (e.g., at the highest amplitude 300  $\mu$ A, the charge density per phase is 2.4mC/cm<sup>2</sup>) exceeds the safe charge limit capacity for platinum electrodes [259], so different electrode materials or coatings (e.g., nanoparticles) with higher safe charge injection limits will likely be needed.

### 6.4.3 Future Work

The results from this study indicated that preferential activation of ON and OFF RGC types can still be achieved with the use of a short bursts of modulating frequencies, within a clinically-relevant frame rate. However, the results presented here are derived from artificially-blocked healthy retina, therefore the cells' response is completely void of any synaptic input. This artificial block through synaptic blockers is designed to act as a rough equivalent to a completely blind patient with complete loss of their photoreceptors and complete loss of synaptic connections between the inner retina and the RGCs due to remodelling. However, in degenerate retina, the loss of synaptic connections is not as uniform as the use of synaptic blockers, and also tends to be time and degeneration-dependent [220, 286]. As such, it is likely that the degenerating synaptic network may influence the properties of the targeted RGC types. Future work using degenerate retinæ to identify the possible effects on the preferential activation map for ON and OFF RGCs across different ages may shed light on how best to optimise the existing parameter space for more clinically-relevant conditions.

#### 6.4.4 Conclusions

The main findings from the first part of the study suggest that OFF cells are more sensitive to high-frequency adaptation than ON cells, particularly in the order in which the frequencies were presented. The second part of the study began initial investigations into the practicality of using HFS-based preferential activation of targeted cell types. The results showed that using novel dynamic waveforms consisting of optimised, modulating frequencies could preferentially control the spiking activities of the ON and OFF cells and could be further utilised to replicate a pseudo-randomised spike train.

# 7 Response of rd1 RGCs to HFS

## 7.1 Introduction

Up to this point, the results in this thesis have suggested that HFS-based preferential activation can be used to activate the ON and OFF RGCs with ideal stimulation conditions of long durations (300 ms) and in a static state, but also with more stringent stimulation conditions of shorter stimulation durations (40 ms) and under continuous stimulation. In both studies, the results were based on the responses of RGCs which were artificially synaptically-isolated from the network using synaptic blockers. However, the use of synaptic blockers is uniform and does not account for the well-documented functional and morphological remodelling in the inner retina during retinal degeneration [21, 22, 27].

The degenerate retina undergoes extensive morphological and functional remodelling including neuronal loss, dendritic retractions, the formation of a glial seal and the creation of microneurons [83, 219, 221, 286]. These changes have been shown to have downstream effects on the RGCs such as the well-known patterned oscillatory activity [23, 226, 227, 250], which have also recently been shown to affect the RGC response to extracellular stimulation. For example, Haselier et al. [249] and Gehlen et al. [248] showed that stimulation efficacy was reduced in rd10 RGCs exhibiting patterned oscillatory behaviour while Cho et al. [27] found that stimulation threshold differences between healthy versus rd10 RGCs were dependent on the level of spontaneous activity of the rd10 RGCs. These studies suggest that degenerate RGCs are influenced by the remodelling effects in the degenerate network and are largely consequential of the altered synaptic inputs.

What remained unclear however, was the post-synaptic functional stability of the degenerate RGCs i.e., their morphologies, ionic compositions, and intrinsic electrical responses, and additionally, whether these properties differed between healthy and degenerate retina. To this end, different studies have been conducted to investigate the intrinsic property differences between healthy and degenerate retina [21, 22, 29, 239]. Overall, the findings from these studies suggested that there are morphological changes [287, 288], ionic channel differences [21] and intrinsic excitability differences [22]. However, the latter studies either (1) did not identify the cell type (i.e., ON, OFF etc) or (2) block the presynaptic network to identify the influence of the retinal network on the post-synaptic responses and properties. Conversely, Margolis et al. [23] did compare the intrinsic electrical responses of degenerate and healthy RGCs in the presence of synaptic blockers but stopped short of comparing these responses to before the application of the blockers.

To the best of my knowledge, no study has compared the intrinsic properties of WT and rd1 and rd10 ON and OFF RGCs both with and without synaptic blockers. Furthermore, while retinal studies of network-mediated stimulation have shown the presence of distinct ON and OFF pathways in rd10 [17] and RCS [31] RGCs; no study has attempted to preferentially activate the degenerate ON and OFF RGCs using HFS nor compared the electrically-elicited responses with and without the degenerate network. In this chapter, I was interested in identifying if HFS remained a viable approach to preferentially activate the ON and OFF RGCs but in a more clinically-relevant degenerate environment as well as broadening the existing knowledge on potential physiological changes between healthy and degenerate RGCs.

## 7.2 Methods

Please refer to the General Methods (Chapter 4) for overview on animal preparation and tissue extraction (Chapter 4, Section 4.1) and patch clamping (Chapter 4, Section 4.2). In this section, additional cell classification methods, along with data analysis relating to this chapter will be outlined.

### 7.2.1 Cell Classification

Rd1 mice ( $n = 7$  mice at P60 – P100,  $n = 11$  mice at P170 – 350) were sourced from either Australian BioResource or University of Western Sydney. All mice were not dark adapted, and the experiments were conducted under normal illumination. Dissimilar to the previous chapters, a relatively broad age-range of the rd1 mice were used here in an attempt to capture the HFS response across the entire spectrum of degeneration. Additionally, the cells were not grouped by age as the focus of this chapter was on HFS responses in the degenerate retina, rather than age-dependent or degeneration-dependent responses. Cells were classified as ON or OFF based on at least one of two properties – (1) the dendritic stratification within the IPL (see procedure in Chapter 4, Section 4.2.4) which was identified post-experiment, and (2) the distinct patterned activity exhibited by the ON and OFF cells studied previously [23]. Figure 7.1 shows representative ON and OFF cells, with their respective dendritic stratifications and patterned oscillatory activity. Cells that did not meet any criteria were considered as unclassified ( $n = 13$ ). Additionally, the oscillation rate was calculated as the number of spikes over a 30 second window of unstimulated recording and was found to decrease with respect to post-natal age (Figure 7.1C). Note: not all cells exhibiting oscillations had corresponding spiking activity, however, were still identifiable with their distinct membrane oscillations. Table 7.1 provides a summary of the portion of identified cells under each criterion.

**Table 7.1 Summary of cell numbers identified with each criteria**

Cell Type	Dendritic Stratification	Oscillatory Activity	Dendritic Stratification and Oscillatory Activity
ON	6/15	3/15	6/15
OFF	7/17	1/17	9/17
ON-OFF	2/2	N/A	N/A

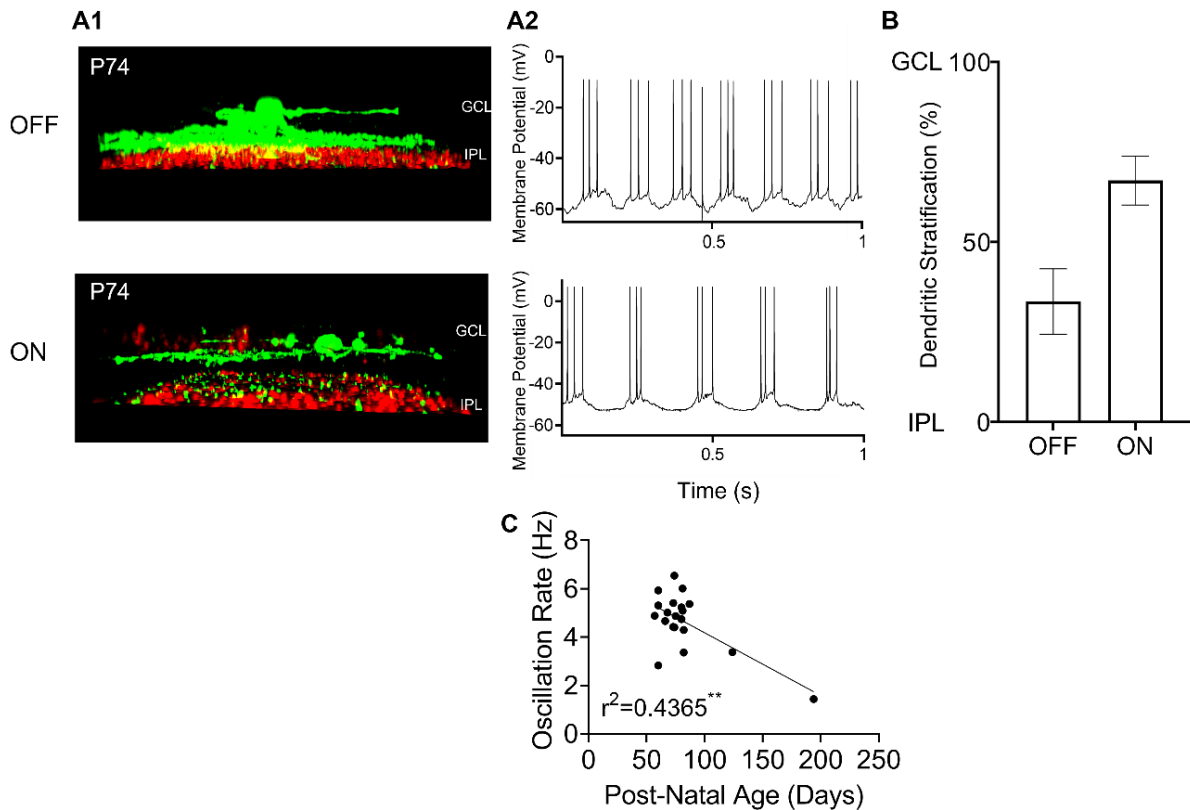


**Figure 7.1 Classification of rd1 ON and OFF RGCs based on their dendritic stratification, their rhythmic spontaneous activity, or both.** (A1) Dendritic stratification of a single ON and OFF cell. The green indicates the cell soma and dendrites, and the red indicates the IPL and GCL borders, respectively. (A2) Patterned oscillatory activity of a single ON and OFF cell. (B) The dendritic stratification of ON ( $n = 14$ ) and OFF ( $n = 13$ ) cells within the IPL. (C) Oscillation rate over post-natal age.

## 7.2.2 Synaptic Blockers

Given that all the cells utilised in this study did not exhibit a light response, the isolation of RGC from the synaptic network was evaluated by ensuring the average variance in the baseline potential fell below 1 mV before commencing the electrical stimulation recordings [289]. A handful of cells (9/32) also exhibited regular spontaneous-activity after the application of blockers and therefore could not be held to the same criteria mentioned previously. These cells however, exhibited either patterned or no spontaneous activity before the blockers, and therefore were still considered as isolated from the network given the regularity of the activity.

Figure 7.2 shows an example of the baseline potential before and after the application of blockers for an ON and OFF cell.

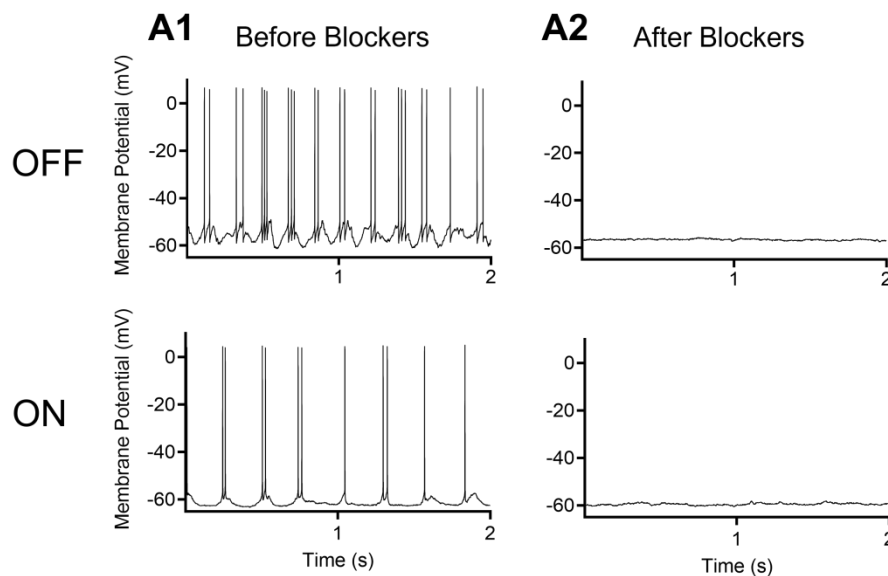


**Figure 7.2 Representative rd1 ON and OFF RGCs before and after the application of synaptic blockers.** A cell was considered isolated from the network if the variance in the synaptic input fell less than  $\pm 1$  mV.

### 7.2.3 Extracellular Stimulation

The HFS paradigm used in this chapter was similar to that used in Chapter 5 (see Chapter 5, Section 5.2.1) however the amplitude range was increased from 10 – 300  $\mu$ A and the frequency range from 0.5 – 10 kHz. The amplitudes were presented linearly for each frequency and repeated three times and the frequencies were randomised to avoid possible effects of a monotonically changing stimulation frequency. An ITD of 1 s was used. To investigate the impact from both the remodelled retinal network versus the synaptically-isolated RGC, HFS-elicited RGC responses were recorded both before and after the application of synaptic blockers.

### 7.2.4 Data Analysis

#### 7.2.4.1 Intrinsic Responses

Chapter 4, Section 4.4 in the General Methods outlines the calculation of the non-spiking baseline potential. To assess the statistical significance of baseline potentials before and after synaptic blockade between the WT and rd1 RGCs for a given cell type (ON or OFF), a one-way repeated measures ANOVA was used, with a set confidence level of 95%.

To compare the intrinsic properties of the WT and rd1 ON and OFF RGCs (both with and without the presynaptic network), a series of depolarising current injections from 0 pA to 600 pA at 25 pA steps, and duration of 500 ms were used. Each cell was defined by a 1 x 25 normalised spike matrix in which all spikes were normalised to the maximum spike count across all amplitudes for a given cell. The average of the normalised spike count of all cells within the ON and OFF WT and rd1 groups were calculated accordingly. To identify if the cell response to depolarising current injections was significantly different before and after the application of blockers, a two-way repeated measures ANOVA was used for a subset of cells which contained intracellular recordings for both before and after synaptic blockade (WT ON n = 13/24, WT OFF n = 8/30, rd1 ON n = 11/11, rd1 OFF n = 11/11).

#### 7.2.4.2 HFS Responses

The calculation and normalisation of the HFS maps (including the removal of spontaneous activity) is outlined in Chapter 4, Section 4.41.

As previously mentioned, each RGC was stimulated with the HFS protocol before and after the application of blockers to identify if the degenerate network influenced the HFS response. To investigate if the network influenced the response of *all* rd1 RGCs, a two-way repeated measures ANOVA was used on the normalised spike counts before and after blockers.

Following this, I investigated whether the synaptic network had disproportionate effects on the rd1 RGCs depending on the cell type (i.e., ON or OFF). To achieve this, a difference map (corresponding to a difference matrix) and a difference statistic were used to compare the extent and region of differences in the HFS response with and without blockers.

The difference matrix and the difference statistic were calculated in the same manner as the “phase-difference matrix” and “recovery statistic” previously outlined in Chapter 6, Section 6.2.2.4. The key difference in this chapter is that the difference matrix was calculated by taking the normalised spike count difference in the HFS response before and after the application of blockers. Similar to Chapter 6, a “recovery range” (0 (true recovery)  $\pm$  one standard deviation calculated across all cell types) was also applied to cells here to ensure that cells were not unfairly penalised. The average of the normalised spike difference matrices was taken to produce a difference map. The sum of all the values across all frequencies and amplitudes in the average difference matrix was calculated as the difference statistic for that cell type.

Lastly, to compare the isolated HFS responses of the WT and rd1 RGCs after synaptic inputs were abolished, a different normalised matrix for rd1 cells was calculated in which only the spike counts occurring for amplitudes 10 – 240  $\mu$ A and frequencies 1 – 6 kHz (ranges used in Chapter 5) were considered and normalised accordingly. Given that the cells belonged to two distinct populations (WT and rd1), a difference map and corresponding statistic could not be

generated. As such, a one-way random effects ANOVA was used to assess statistical significance between the two populations.

## 7.3 Results

### 7.3.1 Intrinsic Property Differences Between WT and rd1 RGCs

To investigate the intrinsic properties of the WT and rd1 (P60-P350) RGCs with and without synaptic blockers, the baseline potential (see Chapter 7, Section 7.2.4.1 for calculation) for WT and rd1 ON and OFF RGCs were compared. From Figure 7.3A, WT OFF RGCs ( $n = 47$  before blockers,  $n = 47$  after blockers) became slightly depolarised after synaptic blockade, and rd1 OFF RGCs ( $n = 15$  before blockers,  $n = 15$  after blockers) became marginally hyperpolarised after synaptic blockade. However, neither of these trends were statistically significant. Comparing the ON RGCs in Figure 7.3B, the WT ON RGCs ( $n = 46$  before blockers,  $n = 46$  after blockers) became significantly hyperpolarised post-synaptic blockers ( $p < 0.001$ ) while rd1 ON RGCs ( $n = 12$  before blockers,  $n = 12$  after blockers) did not show any significant changes under the same conditions. For both ON and OFF WT RGCs, the respective shifts in baseline potential were in line with the results shown in Chapter 5 (Figure 5.1) and previous studies [73, 165]. To the best of my knowledge, no studies have compared baseline potentials in rd1 ON and OFF RGCs before and after the application of synaptic blockers. Altogether, the results suggest that both the healthy and degenerate network have little effect on the baseline potential for WT and rd1 OFF RGCs. For the ON RGCs, the significant hyperpolarisation of the WT RGCs after synaptic blockade suggests that the baseline potential in WT may be influenced by synaptic inputs from the healthy network. Meanwhile, the insignificant shift in rd1 ON RGCs indicates that the baseline potential is less influenced by the synaptic inputs from the surviving networks and perhaps shaped primarily by the intrinsic properties.

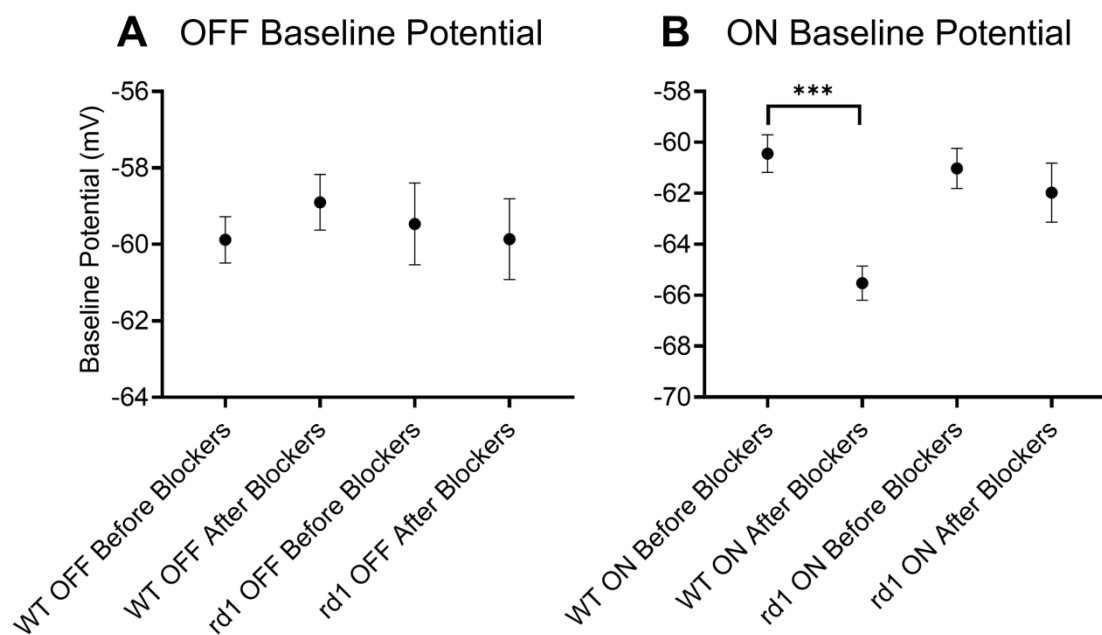


**Figure 7.3 Baseline potentials of WT and rd1 ON and OFF RGCs before and after synaptic blockers.** The effect of the healthy and degenerate retinal networks had different impacts on the baseline potential of ON and OFF RGCs. Only ON RGCs were significantly hyperpolarised after the application of blockers. (A) Baseline potentials of OFF RGCs for WT before ( $n = 47$ ) and after ( $n = 47$ ) blockers, and rd1 before ( $n = 15$ ) and after ( $n = 15$ ) blockers. (B) Baseline potentials of ON RGCs for WT before ( $n = 46$ ) and after ( $n = 46$ ) blockers, and rd1 before ( $n = 12$ ) and after blockers ( $n = 12$ ). (\*\*\*)  $p < 0.001$ .

To further evaluate the post-synaptic properties of WT and rd1 RGCs, a series of depolarising current pulses from 0 – 600 pA of 500 ms duration (shown in Figure 7.4) was injected intracellularly into the soma. The resultant averaged normalised spike response of each cell populations is shown in Figure 7.4 (see Chapter 7, Section 7.2.4.1 for calculation). Figure 7.4A1 shows the population average spiking response of the respective rd1 ON and OFF RGCs before and after the pharmacological blockade of synaptic inputs. A one-way repeated measures ANOVA was used to compare the RGC activities between the two conditions. Both rd1 ON ( $n = 15$  before blockers,  $n = 11$  after blockers) and OFF RGCs ( $n = 16$  before blockers,  $n = 11$  after blockers) did not show significantly different responses between the network and blocked conditions, indicating that the degenerate network has little influence on rd1 RGC activities in response to somatic current injections.

Lastly, to identify whether the intrinsic properties between the WT and rd1 RGCs differed, the cells' response to the depolarising current injections were compared for the respective ON and OFF cell populations after the synaptic inputs were pharmacologically blocked. Figure 7.4A2 shows the average normalised spike response of the isolated WT ON ( $n = 15$ ) and OFF ( $n = 11$ ) and rd1 ON ( $n = 11$ ) and OFF ( $n = 11$ ) RGCs. A one-way random effects ANOVA was

used to analyse the difference between the two cell groups. The results showed that there was a significant difference in the normalised spike count between the WT and rd1 RGCs in response to the somatic current injections for both the ON ( $F(1,24) = 3.979$ ,  $p < 0.05$ ,  $\eta^2 = 0.137$ ), and OFF RGCs ( $F(1,28) = 1.708$ ,  $p < 0.05$ ,  $\eta^2 = 0.057$ ) indicating the possibility of intrinsic property differences between the WT and rd1 RGCs.

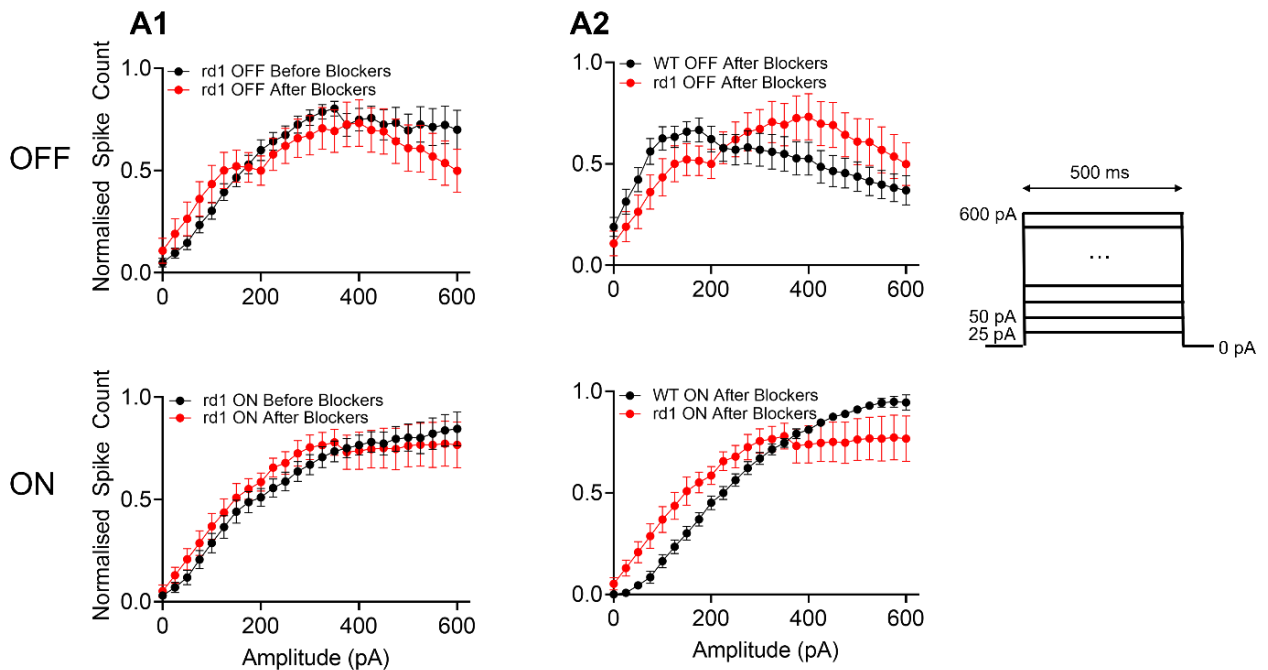


**Figure 7.4 Responses of WT and rd1 ON and OFF RGCs to depolarising somatic current injections.** Synaptically-isolated WT and rd1 ON and OFF RGCs had significantly different responses. (A1) Response of rd1 OFF RGCs before ( $n = 16$ ) and after ( $n = 11$ ) synaptic blockade and rd1 ON RGCs before ( $n = 15$ ) and after ( $n = 11$ ) synaptic blockade. (A2) Response of WT OFF ( $n = 18$ ) and rd1 OFF RGCs ( $n = 11$ ) and WT ON ( $n = 15$ ) and rd1 ON RGCs ( $n = 11$ ) after synaptic blockade.

## 7.3.2 HFS in Degenerate Retina

### 7.3.2.1 Influence of Degenerate Network on the HFS Response of rd1 RGCs

The previous section investigated the intracellular responses of WT and rd1 (P60-P350) RGCs with and without the presynaptic network. In this section, the electrically-elicited responses of the RGCs to extracellular HFS were studied, and the influence of the degenerate synaptic network in shaping the spike responses of the rd1 RGCs, as well as differences in HFS responses between WT and rd1 RGCs after isolation from the presynaptic network.

The average normalised population spike responses of all rd1 RGCs to frequencies 0.5 – 10 kHz and amplitudes 10 – 300  $\mu\text{A}$  (see Chapter 4, Section 4.4.1 for protocol and calculation) before and after the application of synaptic blockers were plotted as 2D maps shown in Figure 7.5.

Figure 7.5A1 shows the HFS population response of the rd1 RGCs before the synaptic blockers, and Figure 7.5A2 after the application of synaptic blockers. The heat map shown in Figure 7.5B represents the average normalised spike count differences of all the cells before and after the application of blockers (see Chapter 7, Section 7.2.4.2 for detailed calculations). Given that ON and OFF RGCs have different presynaptic connections and circuitry in the retina [267, 289] I was also interested to identify whether the degenerate network differently affected their response to electrical stimulation. Figure 7.6A1 and Figure 7.6A2 show the HFS responses of the rd1 ON and OFF RGCs before and after the synaptic blocker, respectively while Figure 7.6B illustrates the resultant difference map between the two.

To assess the overall difference in the HFS-elicited response before and after pharmacological blockade, a difference statistic was also used (see Chapter 7, Section 7.2.4.2 for calculation). The statistic itself is the sum of the normalised spike count differences across all frequencies and amplitudes shown in the heat maps. A non-zero difference statistic implies that there is network influence on the response. The bigger the difference statistic value, the greater the difference in the HFS response and in turn, potentially the greater the influence of the residual network. The difference statistic for the rd1 RGCs are summarised in Table 7.2.

Collectively, the data indicated by the heat maps and the non-zero difference statistic for the whole rd1 RGC population, as well as the rd1 ON and OFF RGCs suggest that the degenerate network does have impact on the cells' HFS response. Comparing the rd1 ON and OFF RGCs indicates that the residual network may have a greater influence on the rd1 OFF RGCs than the rd1 ON RGCs given the broader and more consistent region of spike count discrepancies at relatively lower frequencies (0.5 – 5 kHz) and higher amplitudes (200 – 300  $\mu$ A) compared to the sporadic regions in the rd1 ON RGCs. However, despite the non-zero difference statistics and discrepancies in normalised spike counts, the effect of the degenerate network does appear to be minimal given the similar regions of activation in frequencies and amplitudes between the cell types.

**Table 7.2 Difference statistic corresponding to HFS responses**

<b>Difference Statistic</b>	<b>All Cells</b>	<b>rd1 OFF Before versus After Blocker</b>	<b>rd1 ON Before versus After Blocker</b>
	12.34	17.83	12.45

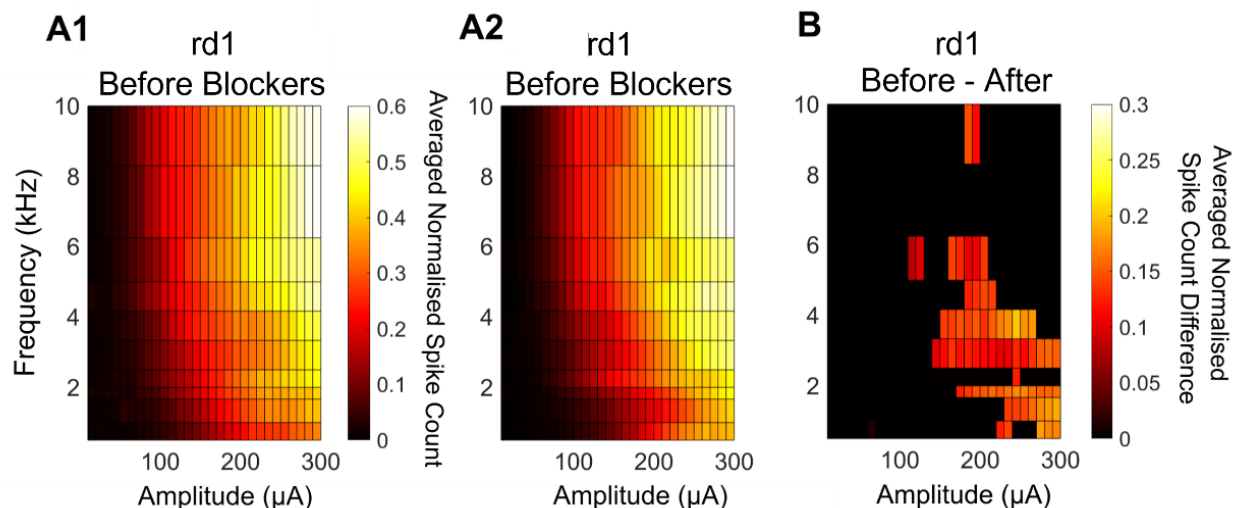


**Figure 7.5 Population response maps of all rd1 RGCs in response to HFS before and after synaptic blockers.** The rd1 RGCs had very similar responses to most frequency and amplitude combinations irrespective of the synaptic network indicated by the minimal spike count differences shown in the difference map. (A1) Averaged normalised spike responses of the rd1 RGCs before the application of synaptic blockers ( $n = 29$ ). (A2) Averaged normalised spike responses of the rd1 RGCs after synaptic blockers ( $n = 29$ ). (B) The resultant difference map calculated by taking the average of all cells' normalised spike count difference to HFS before and after blockers.

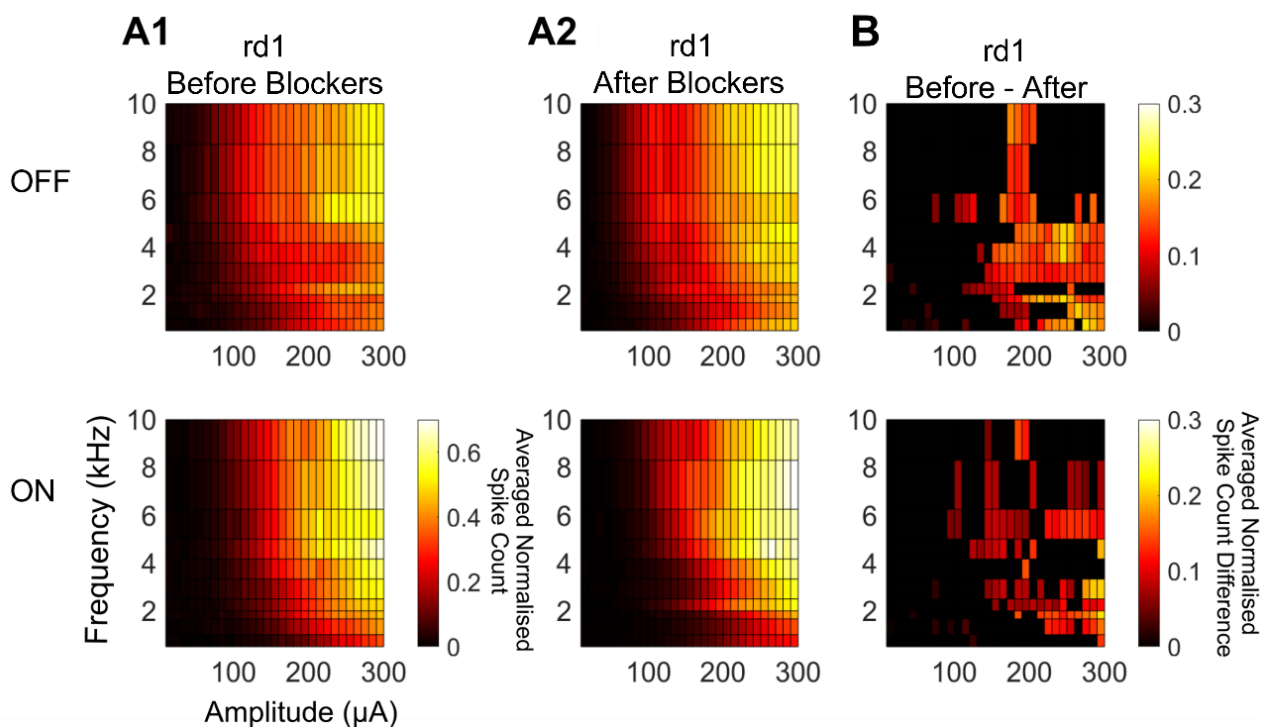


**Figure 7.6 Population response maps of rd1 ON and OFF RGCs in response to HFS before and after synaptic blockers.** The network overall had minimal influence on the HFS response of both rd1 ON and OFF RGCs, however, had a marginally greater influence on the rd1 OFF RGCs particularly at the lower frequencies, and higher amplitudes. (A1) Averaged normalised spike responses to HFS across all frequency and amplitude combinations for rd1 OFF ( $n = 13$ ) and ON RGCs ( $n = 10$ ) before synaptic blockade. (A2) Averaged normalised spike responses to HFS for rd1 OFF ( $n = 13$ ) and ON RGCs ( $n = 10$ ) after synaptic blockade. (B) Difference map of rd1 OFF and rd1 ON RGCs calculated by taking the average of the respective OFF and ON cell populations' normalised spike count difference to HFS before and after blockers.

### 7.3.2.2 Differences in HFS Response of WT and rd1 RGCs After Pharmacological Blockade

The RGC response to HFS post-blockers is intrinsically-driven. Therefore, to further investigate potential intrinsic property differences between the healthy and degenerate RGCs, the synaptically-isolated response of the WT and rd1 RGCs to HFS were compared shown in Figure 7.7. To ensure fair comparison between the RGCs, the rd1 RGCs were normalised to the same frequency and amplitude parameter space as the WT RGCs (frequencies 1 – 6 kHz, and amplitudes 10 – 240  $\mu$ A).

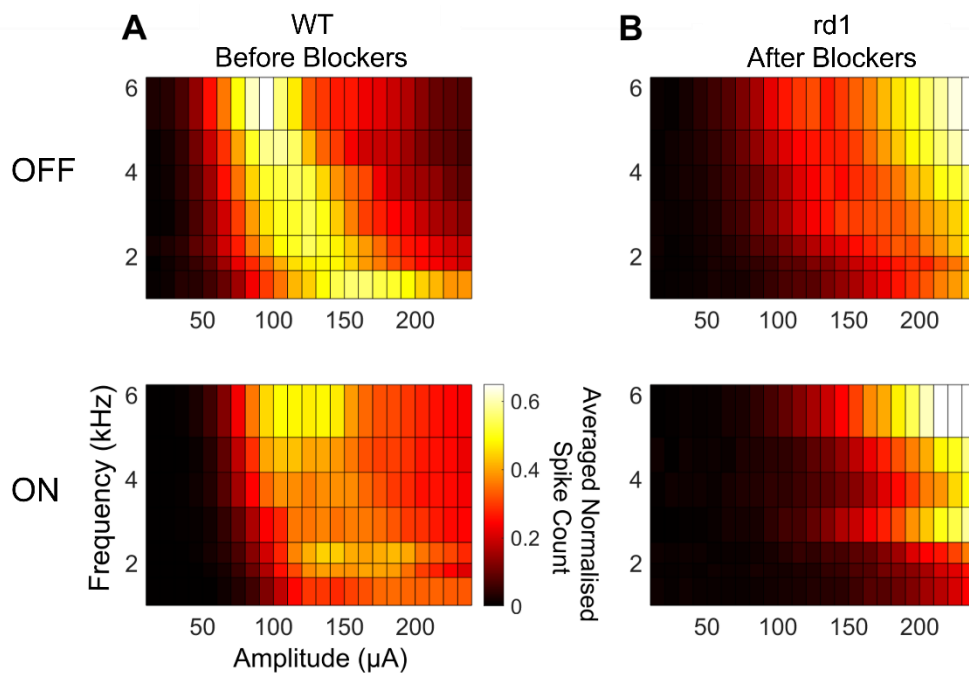


**Figure 7.7 Population response maps of synaptically-isolated WT and rd1 ON and OFF RGCs in response to HFS.** Both ON and OFF RGCs had significantly different HFS responses to most frequency (1 – 6 kHz) and amplitude (10 – 240  $\mu$ A) combinations indicating potential intrinsic differences between the WT and rd1 cells. (A) Averaged normalised spike response to HFS for WT OFF ( $n = 24$ ) and WT ON ( $n = 25$ ) RGCs after synaptic blockers. (B) Averaged normalised spike response to HFS for rd1 OFF ( $n = 13$ ) and rd1 ON ( $n = 10$ ) after synaptic blockers.

Broadly comparing Figure 7.7A (WT after synaptic blockers) and Figure 7.7B (rd1 after synaptic blockers), it is evident that for both ON and OFF cell types, the HFS response differs between healthy and degenerate RGCs. Specifically, both rd1 ON and OFF RGCs had a distinct rightward shift towards higher frequencies (4 – 6 kHz) and higher amplitudes (200 – 240  $\mu$ A) compared to the WT ON and OFF RGCs. Given that the WT and rd1 post-blockers were derived from two independent cell populations, an overall difference map and difference statistic could not be used as a comparative tool to assess differences in spiking patterns. In place of this, a one-way random factor ANOVA was used to evaluate statistically significant differences. The results indicate that OFF WT and rd1 RGCs post-blockers have significantly

different spike responses with respect to amplitude ( $F(1,23)=29.953$ ,  $p<0.05$ ,  $\eta^2=0.811$ ) and frequency ( $F(1,23)=13.751$ ,  $p<0.05$ ,  $\eta^2=0.374$ ) with differences maximised at amplitudes 40 – 240  $\mu\text{A}$  across all frequencies. Similarly for the ON WT and rd1 RGCs, significant differences were found with respect to amplitude ( $F(1,23)=16.084$ ,  $p<0.05$ ,  $\eta^2=0.697$ ) and frequency ( $F(1,7)=7.423$ ,  $p<0.05$ ,  $\eta^2=0.244$ ) with maximal differences found at amplitudes 70 – 170  $\mu\text{A}$  across most delivered frequencies. Altogether, the findings here further support the possibility that intrinsic properties between the WT and rd1 RGCs may differ for both ON and OFF cells, particularly the properties driving the HFS response.

### 7.3.3 Preferential Activation in Degenerate Retina

The findings from the previous section showed that both rd1 ON and OFF RGCs were capable of eliciting spike responses to HFS, and the spiking response did not vary significantly depending on the presence of the degenerate network. In this next section, I was interested to identify if rd1 ON and OFF RGCs could be preferentially activated and how this ability may be influenced by the degenerated presynaptic network.

Preferential activation is defined as the probability of one cell type population spiking over the other and calculated by subtracting the averaged normalised spike count of the two populations (see Chapter 4, Section 4.4.1 for a detailed outline on calculation of the preferential activation maps). Figure 7.8 depicts the preferential activation map for rd1 ON and OFF RGCs with the degenerate network (Figure 7.8A1) and isolated from the network (Figure 7.8A2). The black asterisks denote regions of statistical significance based on a one sample t-test against difference of zero between normalised spike counts of populations. Overall, the map indicates that with the presynaptic inputs, only the rd1 ON RGCs have a consistent statistically significant ( $p < 0.05$ ) preferential activation region at frequencies 2 – 4 kHz and amplitudes 250 – 300  $\mu\text{A}$ . Meanwhile, without the synaptic inputs, only the rd1 OFF RGCs could be significantly ( $p < 0.05$ ) preferentially activated at frequencies 0.5 – 6 kHz and amplitudes 50 – 300  $\mu\text{A}$ . In both cases, the maximum preferential activation possible was between 10 – 30%. Taken together, these results appear to suggest that (a) the ability to preferentially activate the rd1 ON and OFF RGCs is influenced by the degenerate network and (b) preferential activation of cell types may still be possible in a degenerate retina.

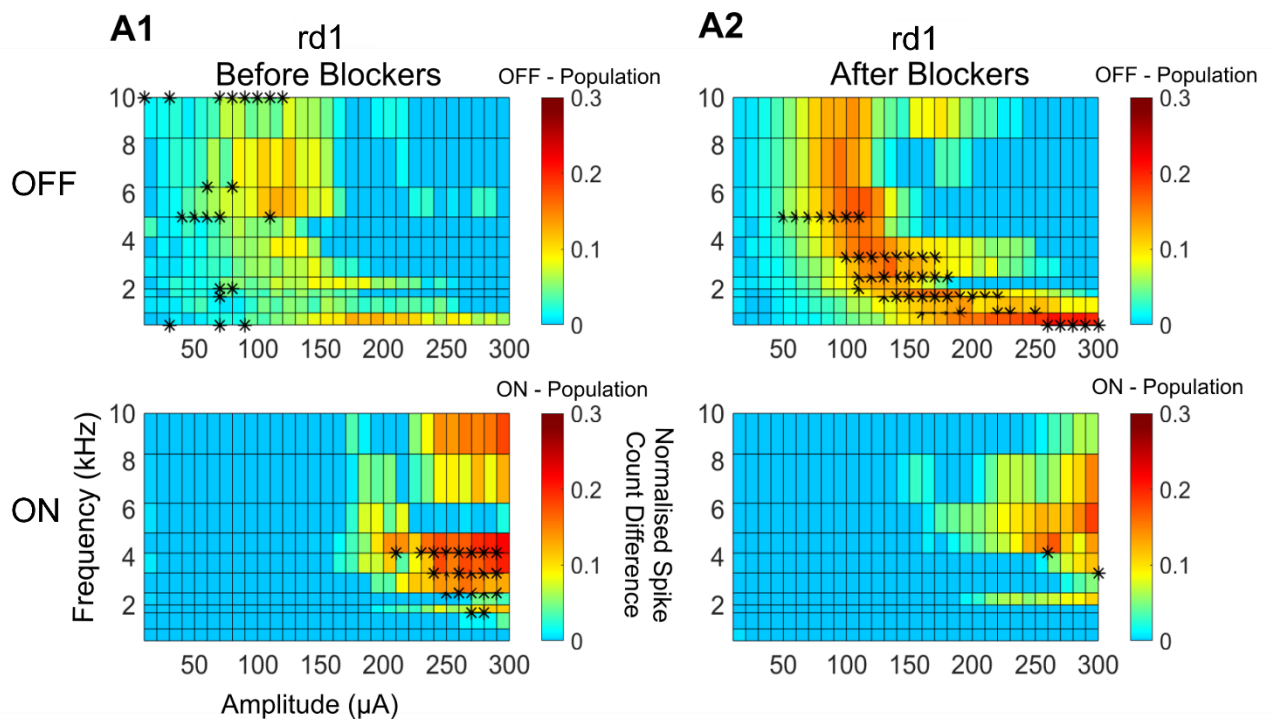


**Figure 7.8 Preferential activation maps of rd1 ON and OFF RGCs in response to HFS before and after synaptic blockers.** Before synaptic blockers, only the rd1 ON RGCs had a preferential region of activation at low frequencies, and high amplitudes. Post-blockers, only the rd1 OFF RGCs had a preferential region across most amplitudes but low frequencies. Preferential activation is defined as the probability of one cell type population spiking over the other and calculated by subtracting the averaged normalised spike count of the respective populations. The colour bars indicate the normalised spike count difference between the two populations and the labels indicate the dominant and suppressed populations. The black asterisks denote regions of statistical significance (one sample t-test against difference of zero between normalised spike counts of populations) (A1) Preferential activation of rd1 OFF ( $n = 13$ ) and rd1 ON ( $n = 10$ ) RGCs before synaptic blockers. (A2) Preferential activation of rd1 OFF ( $n = 13$ ) and rd1 ON ( $n = 10$ ) RGCs after synaptic blockers.

## 7.4 Discussion

This chapter has three major discoveries - (1) intrinsic properties between WT and rd1 RGCs do change, (2) the degenerate presynaptic network has some influence on the rd1 RGCs response to HFS and (3) it is possible to achieve preferential activation in rd1 retina, however, the parameter space for ON and OFF activation requires re-optimisation.

### 7.4.1 Differences in Intrinsic Responses between WT and rd1 RGCs

Stimulation strategies to improve upon current retinal prosthesis are reliant on the functional stability of the degenerate RGCs. As such, studies investigating whether the RGC intrinsic properties remain consistent between the healthy and degenerate retina and if not, how they change, may aid in tailoring future stimulation strategies. Previous studies have suggested RGCs remain relatively unscathed in rd1 [23, 234] and rd10 [235] mice. On the other hand, other studies have cast doubt on (a) the viability of RGC survival particularly in late-stage

degeneration in RCS [21], P23H [237, 238] and rd1 [236] and (b) whether the intrinsic properties are truly consistent between healthy and surviving degenerate RGCs in RCS [21, 22, 239] and P23H [29] rats. For example, Sekirnjak et al. [29] found that healthy and P23H ON and OFF RGCs had different baseline spontaneous activity in the presence of synaptic blockers compared to in the absence of blockers, indicating potential differences in intrinsic properties. Similarly, other groups explored characteristic features such as baseline potential [22, 27, 239] and somatic responses to current injections [22, 23, 239], within the ON and OFF cell types [22, 23]. However, no group has yet quantitatively compared these intrinsic characteristics (1) with, and isolated from the presynaptic network and (2) within the ON and OFF cell types.

With respect to the baseline potential, the results from the study indicate that only WT ON RGCs underwent a significant hyperpolarising shift in baseline potential after the healthy network was artificially blocked by synaptic blockers. The WT OFF RGCs on the other hand, became slightly depolarised in the presence of blockers but the shift was not significant. These findings are in line with previous studies of WT RGCs [73, 165] with the likely mechanism behind the dramatic hyperpolarisation of the WT ON RGCs post-blockers due to disproportionately higher excitatory glutamatergic synaptic inputs ON RGCs receive compared to OFF [266, 289]. Thus, when the network was blocked, the ON RGCs no longer received these glutamergic inputs leading to the hyperpolarisation. Overall, this implies that the baseline potential of healthy ON RGCs is significantly modulated by the presynaptic network. In degenerate retina, however, both the rd1 ON and OFF RGCs maintained a steady baseline potential before and after the application of synaptic blockers implying that the resulting baseline potential of the rd1 RGCs, and particularly the rd1 ON RGCs, is not significantly influenced by the degenerate network.

This result is surprising as Margolis et al. [23] showed through whole-cell voltage-clamp that rd1 ON RGCs received reduced excitatory inputs. Similarly, employing immunohistochemistry, Saha et al. [236] showed that rd1 ON RGCs had significantly lower excitatory synaptic density compared to the WT ON RGCs. Both studies suggest that similar trends of hyperpolarisation of ON RGCs should have also been evident in the degenerate RGCs which is contrary to the evidence presented here. One potential explanation for the stability of the baseline potential of the rd1 RGCs, particularly the ON RGCs, with and without the synaptic input is that the intrinsic properties within the cell may be compensating for the altered synaptic input. That is, if the intrinsic properties e.g., sodium and potassium channels were altered in the rd1 RGCs themselves, this would hypothetically keep the baseline potential robust against synaptic influence and ensure RGC survival. This hypothesis was also put forward by Chen et al. [21] who used whole-cell voltage-clamp to study sodium and potassium channel changes in RCS

RGCs compared to healthy rat RGCs. They found that in the later ages (P60 – P90) of the RCS RGCs, the maximum inward sodium current reduced while the maximum potassium current also reduced but to a lesser extent. They speculated that the significantly smaller change in potassium channel current compared to the sodium channel current allowed the cell to maintain a relatively normal baseline.

Similar conclusions regarding the influence of the degenerate network and stability of intrinsic properties on the healthy and degenerate RGCs could be drawn from studying the spike response to somatic current injection in the rd1 and WT RGCs. For both the rd1 ON and OFF RGCs, there was no significant difference between the normalised spike count with and without the presynaptic network, supporting the previous finding that the degenerate network has little influence on the intracellular response of the rd1 RGCs. Interestingly, when the synaptic input was blocked both in healthy and degenerate retina, there was a statistically significant difference ( $p < 0.05$ ) seen in the spike response between the WT and rd1 RGCs for both the ON and OFF cell types. While this knowledge provides further support to the notion that intrinsic properties between the WT and rd1 RGCs may not be identical, it should be noted that the effects size in the reported ANOVA statistic is quite small, particularly in the case of the OFF RGCs ( $\eta^2 = 0.05$ ). Nevertheless, the findings suggest that WT and rd1 RGCs respond differently to somatic current injection.

These findings are at subtle odds with Margolis et al. [23] who found that rd1 ON and OFF RGCs had similar maximum firing frequency and after depolarisation (ADP) strength to somatic depolarising currents injections when compared to the WT RGCs. However, it is important to note that in their study, they compared a limited range of somatic injections and therefore it is unclear what the responses may have been at higher amplitudes analogous with those used in this study. Meanwhile, Ren et al. [22] also measured intrinsic excitability of RCS RGCs compared with healthy rat RGCs using somatic current injections. They found that RCS OFF RGCs were less excitable than their healthy counterparts, but no significant difference was found between the healthy and RCS ON RGCs. They attributed this observation to elevated action potential thresholds (APTs) in the RCS RGCs and postulated that changes in the sodium and potassium channels may be behind the higher APT values, as well as the narrowing of action potential width. While the study conducted by Ren et al. [22] was also at odds with the results presented here (a more reliable significance was found between WT and rd1 ON RGCs compared to OFF), their findings support the theory that intrinsic properties of RGCs may not be consistent between healthy and degenerate retina.

Overall, the main implications of the findings emerging from this study are in support of the growing body of work suggesting that RGC intrinsic properties may not be consistent between healthy and degenerate retina particularly properties mediating baseline potential and firing

responses to somatic current injections. These properties are largely controlled by the sodium and potassium channels [290-292] and variations in these properties may modulate the response of the RGC to extracellular stimulation. Further work in characterising the presence and distribution of these ionic channels within the RGCs, and particularly in different degenerate animal models may aid in informing and tailoring the appropriate stimulation strategies in degenerate retina.

## 7.4.2 HFS Responses in Degenerate Retina

### 7.4.2.1 Influence of Degenerate Network on HFS response in rd1 RGCs

The second aim of this study was to characterise the response of the rd1 RGCs to HFS. This section began with identifying the potential effects of the degenerate network on the HFS response, followed by a comparison of the synaptically-isolated responses of the healthy and rd1 RGCs to further explore the idea of changes in intrinsic properties. Given the primary interest in HFS-evoked responses, all spontaneous spikes caused either by intrinsic RGC properties or the patterned oscillations were removed.

To compare the HFS response in the presence and absence of the presynaptic network across all cell types, and between the ON and OFF cells, a comparative tool termed the “difference statistic” was used to reflect the difference in normalised spike count across all frequencies and amplitudes (Table 7.2). The non-zero difference statistic indicated that the degenerate presynaptic network did have an effect on the HFS response in both rd1 ON and OFF RGCs. The difference statistic also indicated that rd1 OFF RGCs (difference statistic = 17.83) were marginally more sensitive to the degenerate network than the rd1 ON RGCs (difference statistic = 12.45). The primary differences reflected in the difference statistic were concentrated at the higher amplitudes (150 – 300  $\mu$ A) and relatively lower frequencies (0.5 – 5 kHz) for the rd1 OFF RGCs but scattered across all frequencies for the rd1 ON RGCs. These differences in the spiking profiles with and without the presynaptic circuitry may be the result of the extensive remodelling that occurs during degeneration [84, 85, 220] and the overall trial-to-trial variability of the RGC spike responses [28].

Notwithstanding, comparing the heat maps themselves (Figure 7.5 and Figure 7.6), the rd1 RGCs had similar spiking profiles and were active across similar frequencies and amplitudes irrespective of presence of the degenerate network. The differences themselves were largely due to discrepancies in the relative spike counts of the cells’ opposed to differences in the activation or inactivation regions of the different cell types. This suggests that the influence of the degenerate network on the HFS response may be in modulating the spike count, but other properties intrinsic to the cell, for example relative densities of ionic channels, may be more influential in dictating other aspects of the spiking profile e.g., the stimulation and suppression

thresholds. Overall, the findings suggest that the degenerate network does have an effect on the HFS spike response of the rd1 RGCs, however the influence may be minimal.

#### *7.4.2.2 HFS Response of WT and rd1 RGCs after Pharmacological Blockade*

The evidence presented in this chapter and Chapter 5 suggests that the properties mediating the HFS response is likely intrinsically-driven rather than synaptically-driven. In addition, the results also indicate that the RGC intrinsic properties between the healthy and degenerate retina may be different. As such, if the HFS response between the synaptically-isolated WT and rd1 RGCs are different, this would provide further evidence to support that intrinsic properties may be different between the two groups. To compare the cell groups, a two-way ANOVA was used with frequency and amplitude considered as random factors. For both WT and rd1 ON and OFF RGCs stimulated post-blockers, a significant difference (OFF  $p < 0.001$  and ON  $p < 0.001$ ) was found across both frequency and amplitude. The most notable difference in the HFS response maps is the increased number of monotonically-responding rd1 ON and OFF RGCs compared to the WT ON and OFF RGCs likely stemming from the increased stimulation threshold. The cause of the elevated thresholds has been mostly attributed to the remodelling of inner retinal neurons [24, 220, 293], as well as ancillary factors such as electrode-to-retina distance [240, 243-245], and return electrode configuration, stimulation polarity and duration [244].

A more recent study by Cho et al. [27] found that thresholds were dependent on physiological changes in the RGCs induced by photoreceptor degeneration. Specifically, rd10 RGCs exhibiting increased spontaneous activity or periodic membrane activity had comparable thresholds to the WT RGCs. This however is unlikely to have had an influence in the results shown here, given that the heat maps only reflect electrically-evoked spike responses. Furthermore, the increased spontaneous activity and periodic oscillations only occur when the RGCs are connected to the degenerate network. In the case of the WT and rd1 RGC responses, the synaptic network is blocked and therefore the spontaneous activity and oscillations no longer becoming contributing factors. This said, there is a possibility that the long-term altered synaptic input caused by the aberrant oscillations may cause the intrinsic compensatory changes (i.e., changes in the ionic channels) which in turn decrease the excitability of the cell and increase the stimulation threshold. Another possibility is differences in the morphology of the degenerate RGCs. For example, O'Brien et al. [287, 294] and Damiani et al. [288] both found that the total dendritic length decreased in rd1-Thy1 RGCs compared to the control. Taking the hypothesis that the HFS response is at least in part driven by intrinsic properties, the reduced dendritic field size may result in fewer ionic channels therefore increasing the number of monotonically-responding RGCs.

### 7.4.3 Preferential Activation in Degenerate Retina

The results from Chapters 5 and 6 have so far indicated that HFS-based preferential activation of RGC types, and under different stimulation conditions, is possible with careful consideration of stimulating frequencies and amplitudes for a given cell type. However, the results were all derived from synaptically-blocked RGCs which, as evidenced in this chapter, are different from degenerate rd1 RGCs. Therefore practically, how does HFS-induced preferential activation of ON and OFF RGCs fare in a degenerate tissue? Figure 7.8 showed that while the preferential region itself was comparable before and after the application of synaptic blockers for both the rd1 ON and OFF RGCs, the statistically-significant regions differed. Specifically, before the application of synaptic blockers, the rd1 ON RGCs had a statistically-significant preferential region whereas after the application of blockers, only the rd1 OFF RGCs had the statistically-significant preferential space. In both cases, the likelihood of the target population spiking over the non-target population did not exceed 30%.

As discussed in both Chapters 5 and 6, the ability of the target cell type population to be preferentially activated is highly dependent on the HFS response across the tested frequencies and amplitudes. Based on the data shown in Figure 7.6 it was postulated that while the degenerate network may not have been pivotal in dictating the regions of activation in the HFS parameter space, it may have modulated the spike count thereby increasing the variability of the response. This increased variability may explain why the statistically-significant regions in the presence of the degenerate network change after the synaptic input is artificially blocked. Given that the remodelling in the network is volatile and could cause downstream effects in the RGC response to HFS, the preferential region before the synaptic input may not be a true reflection of the preferential capabilities of the target RGC population. While the preferential maps without network effects indicate a more robust intrinsically-driven response, it is evident that the altered synaptic input from the degenerate network will likely increase the variability of the spike response to HFS and as such, affect the preferential capabilities [16, 27, 28, 133].

To the best of my knowledge, no other study has sought out to preferentially activate degenerate rd1 ON and OFF RGCs using electrical stimulation. In STA-based studies, both Sekhar et al. [17] and Ho et al. [31] recorded distinct ON and OFF STA shapes in the rd10 and RCS retina, respectively. While surprising given the photoreceptor degeneration, both groups postulated that these responses may be due to the survival of the rod bipolar circuit. In this circuit, the ON RBCs modulate the OFF cone pathway through the AII AC I which forms a sign-inverting glycinergic synapse with the OFF cone pathway but forms a sign-conserving gap junction with the ON cone pathway. As such, despite the photoreceptor degeneration, if

the RBCs or the All ACs were depolarised by the corresponding electrical or photovoltaic stimulus, this would result in the distinct ON and OFF responses potentially allowing for selective activation of these cell types. Both studies however, stopped short of classifying the RGCs as ON or OFF in the degenerate retina. Therefore, it is unknown whether the responses they found in the degenerate retina truly belong to the hypothesised ON and OFF RGCs. The other caveat with STA-based selective activation in degenerate retina is the reliance on the degenerating network and in this case, the stability of maintaining the rod bipolar network in the IPL. However, remodelling of the retinal network is dynamic and various new implications of this remodelling are constantly being discovered. For example, Jones et al. [85] showed changes to the mGluR6 and iGluR receptors in human retina, suggesting that the rod ON BCs may convert to OFF BCs. If this is widespread, this would undermine the assumption that this network can be used to generate out-of-phase responses corresponding to the ON and OFF RGCs. This indicates that the degenerate network is extremely unpredictable, and selective activation studies relying on the stability of the network may be a difficult approach. While the results in this chapter also highlight that the responses of rd1 RGCs are subject to increased variability, one significant advantage is that at least part of the RGC response is intrinsically-driven rather than solely extrinsic.

## **7.5 Future Work**

Altogether, the results presented here have opened up different avenues to broaden the knowledge on intrinsic properties of degenerate RGCs and how they may shape electrical stimulation and preferential activation in degenerate retina. For example, quantitatively characterising the ionic channel compositions, e.g., sodium and potassium channels, in the ON and OFF RGCs may aid in validating the hypothesis that intrinsic properties between these cell types change between healthy and degenerate conditions. Additionally, relating the HFS response and preferential activation with the stage of degeneration, as well as the morphology, may shed light on the contributions of the network and morphology in the HFS response and highlight ways to better optimise the stimulation strategy.

## **7.6 Conclusions**

Overall, the findings from this study suggest the following: (a) the intrinsic properties between ON and OFF RGCs may change between WT and degenerate rd1 retina, (b) the residual network does minimally affect the HFS response but is also highly variable and (c) preferential activation may be possible in degenerate retina, but it is clouded under increased variability of the response.

# 8 Conclusions & Future Work

## 8.1 Conclusions

The primary objective of this thesis was to contribute new knowledge on how different RGCs respond to HFS and how it can be used to preferentially activate functionally-distinct RGC types under various stimulation settings and biological conditions. Pursuant to this objective, five aims were listed in the beginning of the thesis. In this section, the overall findings related to each aim will be summarised along with the implications of the results. Following this, suggested future work will be outlined.

### **Aim 1: Can HFS be used to preferentially activate four functionally-distinct RGC types (ONS, ONT, OFFS and OFFT) in synaptically-isolated healthy RGCs?**

The results from the study indicated that three of the four – OFFS, OFFT and ONT – RGCs could be preferentially activated against the remaining cells. Specifically, OFFS RGCs could be preferentially activated at amplitudes (20 – 100  $\mu$ A) and frequencies (1 – 6.25 kHz), OFFT RGCs at amplitudes (150 – 240  $\mu$ A) at 1 kHz and ONT RGCs at amplitudes between (180 – 240  $\mu$ A) and frequencies (4 – 6 kHz). ONS RGCs did not have a statistically significant parameter space at any of the tested amplitudes or frequencies. The results suggested that the likely drivers between the results found previously [15] were the OFFS and ONT RGCs given the overlap in their preferential activation range with the overall ON and OFF population. The OFFT RGCs sensitivity to the lowest frequency but relatively high amplitudes was intriguing, and indicated that future studies may benefit from expanding both the frequency and amplitude parameter space to explore these sensitivities. Additionally, it was found that the cell spiking response was not solely dependent on the total charge within the pulse train or the current amplitude, but a combination of both amplitude and frequency. Overall, the implications from this study suggest that functionally-distinct cell types have varied responses to HFS indicating that HFS can be used to preferentially activate a broader range of cell groups.

### ***Implications***

The four RGC types studied here – OFFS, OFFT, ONS and ONT RGCs – are major cell types that constitute ~70% of all RGCs in the mouse [8, 256] and primate retina [253, 254]. Furthermore, they subserve critical roles in vision with ON and OFF RGCs responding to changes in luminance [55], while sustained cells are sensitive to the form, size and shape of the input and the transient cells to the motion, looming objects, or location of the input [11-13,

295, 296]. Given the dominance of these cell types in the total RGC population as well as the ethological significance of each subtype's function, it is advantageous to be able to preferentially control these cell types and has indeed been a focus in other retinal studies of network-mediated [125, 130] or direct [127] RGC activation. Previously, HFS had only been used to target the ON and OFF RGCs but had not been extended to the two other major cell types [14, 15]. The findings from this thesis suggest that within the tested parameter space, three of the four major cell types could be preferentially activated against the remaining population using HFS. Holistically, this suggests that a significant portion of the RGC population can be preferentially activated from the remaining population by using HFS with specific frequency and amplitude combinations. Future work to specifically target ON BT/OFF BT or ON BS/OFF BS activation (in line with the positive correlation of ON cells to their light response found in [122]), or further extending the parameter space for both frequencies and amplitudes may be useful in further evaluating the efficiency of HFS-based preferential activation.

**Aim 2: How do different RGC types (ONS, ONT, OFFS and OFFT) respond to a modulating frequency, and can these cell types be reliably controlled and preferentially activated with a dynamic waveform based on short, frequency bursts in healthy retina?**

The results showed that ON RGCs were less influenced by the frequency order than the OFF RGCs when the frequencies were modulated in a temporal fashion. With respect to the subtypes, ONS and ONT RGCs had similar responses but there was significantly more variability in the responses of the OFFS and OFFT RGCs. Under continuous stimulation, all RGCs exhibited similar responses to the continuous modulating frequencies in which the frequencies 1 – 10 kHz was presented three times in a continuous fashion (no ISI) in ascending (phase 1), followed by descending (phase 2) and then ascending (phase 3) order. To account for the OFF RGCs susceptibility to frequency order, the spiking responses between phase 1 and phase 3 in which the frequencies were presented in identical order were compared for all the cell types. The results indicated little difference between the spike counts suggesting that there was minimal adaptation of the cells to a continuous modulating frequency stimulation. This result also indicated that the recovery properties, i.e., the ability of a cell to reliably recover the spiking patterns after intermediate stimulation, was similar across all the cell types. The implications of this result are discussed further in Aim 3.

In response to an optimised dynamic waveform designed to activate the OFF followed by the ON RGCs using short and fast changes in frequency, the results indicated that the ON and OFF RGCs largely responded to their designated frequencies generating an out-of-phase response between the two cell types. However, the difference in raw spike counts was greater for ON RGCs compared to the OFF RGCs indicating the former may be better targets for

preferential activation. In the final pilot experiment in which a second waveform consisting of modulating frequencies to reproduce a pseudo-randomised spike train, the results showed that the spiking and non-spiking regions of the spike train could be controlled by the modulating frequencies. Additionally, by carefully selecting the stimulus amplitude, an out-of-phase response between the ON and OFF cells could also be achieved.

### ***Implications***

While Twyford et al. [14] were the first to show that a single waveform consisting of a modulating amplitude was capable of evoking a differential response between ON and OFF RGCs, the stimulation duration used was relatively long (>300 ms). Furthermore, clinically Nanduri et al. [129] found that amplitude modulation yielded a brighter phosphene but also increased the size of the phosphene whereas frequency modulation only modulated the brightness of the phosphene but not the size. They concluded that frequency modulation may be more beneficial in generating relatively succinct, but bright phosphenes. To this end and to the best of my knowledge, the results presented here are the first to show that for a given amplitude, a frequency modulation-based waveform consisting of short bursts of high frequencies within a clinically-accepted frame rate [7] is capable of clearly generating an out-of-phase response between the ON and OFF RGCs. Additionally, the results from this study add to the existing knowledge of frequency-dependent responses of RGCs, particularly between cell types [15, 128, 131, 273, 274] allowing further hypotheses to be made on the intrinsic mechanisms driving the HFS response between the targeted cell types (discussed in Aim 3).

### **Aim 3: Do synaptically-isolated degenerate and healthy ON and OFF RGCs differ in their intrinsic characteristics and their HFS response?**

With regards to baseline membrane potential, the results showed similar changes for WT ON and OFF RGCs in line with previous work [73, 165], where the WT ON RGCs became significantly hyperpolarised post-blockers while the OFF RGCs had no significant change before and after blockers. The hyperpolarisation of WT ON RGCs after blockers was correlated with the removal of the high basal glutamergic inputs it usually receives [266, 289]. In the rd1 retina however, the baseline potential was not significantly different for either the rd1 ON or OFF RGCs before and after the synaptic blockers. Previous reports showed that rd1 ON RGCs had lower excitatory inputs [23] and excitatory synapses [236], implying that the rd1 ON RGCs should have undergone a similar hyperpolarisation as the WT. Given this did not occur, it was speculated whether the altered synaptic input and remodelled inner retina triggered intrinsic compensatory mechanisms. For example, ionic compositions such as sodium and potassium channels [21], to keep the baseline potential stable against synaptic

changes. The second intrinsic property investigated was the response of the WT and rd1 ON and OFF RGCs to intracellular somatic current injections (0 – 600 pA). While there was no significant difference in the response between the rd1 ON and OFF RGCs with and without the synaptic network, there was a significant difference between the synaptically-isolated WT and rd1 ON and OFF RGCs further suggesting that the intrinsic channel properties between the WT and rd1 RGCs may be different.

Under extracellular stimulation, the WT and rd1 ON and OFF RGCs electrically-evoked responses to HFS were compared after synaptic blockers to uncover further evidence of intrinsic property changes between WT and rd1 RGCs. The primary difference found between the groups was the increased number of monotonically-responding rd1 RGCs compared to the WT RGCs, potentially a consequence of the elevated stimulation thresholds in the rd1 RGCs. It was postulated that these thresholds may be correlated with the compensatory changes to ionic compositions discussed earlier. Additionally, given that the stimulation electrode is placed extracellularly and closer to the dendritic field, changes in the morphology of the RGCs may also play a role in the increased thresholds. For example, the decreased dendritic length found in rd1-Thy1 RGCs [287, 288] may result in fewer active RGC properties therefore reducing the excitability of the RGCs.

### ***Implications***

One of the fundamental assumptions of retinal implants are that RGC properties remain similar between healthy and degenerate retina. While previous studies have suggested that despite the inner retinal remodelling, the functional properties of RGCs are consistent between healthy and degenerate retina [23, 234, 235], other studies have indicated that this may not be the case [21, 22, 29, 239]. The results from this study further substantiate the claims that the intrinsic properties between healthy and degenerate RGCs may not be the same. While the implications of these findings are important for any network-mediated or direct stimulation strategies targeting RGC activation; it is particularly important for strategies directly stimulating the RGCs given the hypothesis that the RGC response should be comparable between degenerate and healthy retina. The results presented here and in previous studies suggest that this may not be the case and highlight the importance of doing parallel testing of experiments in both WT and degenerate retina to gain a comprehensive understanding of the efficiency of the stimulation strategy.

**Aim 4: How do degenerate ON and OFF RGCs respond to HFS and does their response change based on the presence or absence of the degenerate network and effect their ability to be preferentially activated?**

Altogether the results indicated that the residual degenerate network did have an effect on the HFS response of both rd1 ON and OFF RGCs indicated by different normalised spike counts with and without the synaptic blockers. Between the two cell types, it appeared that rd1 OFF RGCs were marginally more affected by the network particularly at the higher amplitudes (150 – 300  $\mu$ A) and lower frequencies (0.5 – 5 kHz). However, despite the difference in spike counts, both rd1 ON and OFF RGCs were active across similar frequency ranges and amplitudes suggesting the influence of the altered synaptic circuitry may be limited to introducing variability in spike counts and not other aspects of the spiking profile such as the stimulation threshold.

With respect to preferential activation of the rd1 ON and OFF RGCs, the findings showed that the statistically-significant regions for both cell types with and without synaptic blockers differed. Specifically, before the application of synaptic blockers, only the rd1 ON RGCs had a statistically-significant preferential region whereas after the application of blockers, only the rd1 OFF RGCs had the statistically-significant preferential space. In both cases, the likelihood of the target population spiking over the non-target population did not exceed 30%. It was hypothesised that these differences are a result of the variability in the spike counts to HFS due to the changes in the remodelling [85, 220, 286] and trial-to-trial variability in the RGC responses [28]. Therefore, it is likely that the preferential regions are subject to the volatility of the network and indeed, the intrinsic property changes of the rd1 RGCs.

***Implications***

The results presented in this study are the first to (a) investigate the responses of rd1 degenerate RGCs to HFS and (b) to the best of my knowledge, attempt to preferentially activate rd1 ON and OFF RGCs. Furthermore, the use of pharmacological blockers to understand the influence of the network on the extracellular response has only previously been reported by Sekirnjak et al. [29] but was limited to threshold differences. Overall, the findings in this study suggest that there is variability in the rd1 RGCs' response to HFS, potentially due to upstream remodelling effects [47-49], or potential compensatory intrinsic changes in the rd1 RGCs [21, 22]. This variability makes it difficult to draw clear conclusions on the preferential capabilities of the cells. Nevertheless, the work indicates that HFS can still evoke reliable responses in the RGCs but further work to correlate the response with the altered synaptic input and the intrinsic properties of RGCs will aid in the design of smarter stimulation approaches.

Taken together, the main conclusions of this thesis can be summarised as follows:

1. HFS can preferentially activate synaptically-isolated WT OFFS, OFFT and ONT RGCs from the remaining population using specific frequency and amplitude parameters
2. Under temporal frequency modulation waveforms, synaptically-isolated WT OFF RGCs are more influenced by frequency order than WT ON RGCs but both cell types can recover spiking patterns following intermediate stimulation.
3. ON and OFF RGCs can be preferentially activated using an optimised dynamic waveform consisting of short, modulating frequency bursts all within a clinically-accepted frame rate of 7 – 10 Hz.
4. The intrinsic properties (indicated by baseline membrane potential and response to somatic current injection) between synaptically isolated WT and rd1 ON and OFF RGCs differs.
5. Preferential activation of rd1 ON and OFF RGCs may be possible in the degenerate retina both in the presence and absence of the degenerate network. However, the stimulus parameters need to be re-optimised, subject to the remodelling effects.

## 8.2 Future Work

The work from this thesis indicates that HFS can be a promising strategy to preferentially activate or identify targeted cell types. However, further work in understanding the mechanisms behind the HFS response, and a deeper understanding of the degeneration-induced effects may aid in increasing the utility of this approach.

Both in this thesis and in previous studies [187, 190], speculations and modelling-based predictions have been made on the underlying mechanisms driving the differential response between ON and OFF RGCs to HFS. Overall, the conclusions suggest that differences in sodium channel subtypes may be the key to the differences. Of particular interest has been the Nav 1.1 and Nav 1.6 channels which as discussed previously, support the resurgent currents important for robust spiking during HFS [75, 77]. Studies by Fried and colleagues [79, 197, 200] have quantified the presence and distribution of Nav 1.6 in RGCs but their work is largely limited to the AIS. Furthermore, they did not relate the distribution of these subtypes to the HFS response. Similarly, immunohistochemistry techniques outlined in Raghuram et al. [71] along with voltage-clamp techniques to measure the sodium and potassium currents (e.g., Chen et al. [210]) not only in the AIS but across other neuronal compartments e.g., the cell soma, may be useful in experimentally determining the presence, characteristics, and potential distribution of the specific channel current and subtypes in the different cell types.

Gaining a deeper understanding of the underlying mechanisms that cause the differential response to HFS may aid in informing smarter stimulation parameters to achieve preferential activation.

HFS-based preferential activation to date has been based on single-cell recording and the preferential activation is derived from spike count differences in the population average of a given cell type. What remains to be seen is how these results translate to simultaneous recordings of the different cell types. For example, stimulating and recording from nearby ON and OFF RGCs using a dual-patch approach, or population recordings using an MEA (for example, Fan et al. [164]) can validate whether the selected parameters for preferential activation are capable of generating an out-of-phase response between the targeted cell types and achieve true 'selective activation'.

One of the fundamental caveats of HFS (with respect to clinical viability) is the parameters used which exceed the safe charge limits of platinum electrodes [259]. For example, in the studies presented in this thesis, the preferential activation region of ON cells was consistently at higher frequencies ( $> 5$  kHz) and amplitudes ( $\geq 200$   $\mu$ A). Moreover, the results suggest that further extension of these parameters may yield more optimised responses but at the cost of increasing the total charge. While using short stimulation bursts as shown in Chapter 6 makes important steps towards reducing the overall charge, it is likely that the clinical viability of HFS hinges upon more sophisticated stimulation strategies to reliably offset the charge density. Future studies using electrodes capable of reducing the charge density but delivering HFS pulses and eliciting RGC responses will help in addressing these clinical limitations.

The targeted cell groups studied in this thesis exhibited a level of variability in their HFS responses which is in part, reflective of the functional diversity of the RGCs [8]. In future studies, using more sophisticated visual stimulation to classify a greater number of cell types (as in Baden et al. [8]) may be useful in understanding how different cell types vary in their response to HFS and allow for the development of more accurate HFS-based preferential activation.

Lastly, the final study conducted in this thesis aimed to give a broad overview of how RGC responses to HFS changed in the rd1 degenerate retina. However, several correlations between the RGC response, the cell types, and the level of degeneration and the state of the network were not made. Further work in understanding how the level of retinal remodelling (e.g., over time), shape the different RGCs response to HFS may be important in understanding the best point of intervention for HFS-based strategies, as well as identifying if the aberrant synaptic input's influence on the response is specific to the degeneration stage, cell type or both. Additionally, as mentioned previously, voltage-clamp and

immunohistochemistry techniques to identify intrinsic differences between WT and degenerate RGCs particularly during the course of degeneration will likely be useful in assessing the functional stability of RGCs.

## References

- [1] D. T. Hartong *et al.*, "Retinitis pigmentosa," *The Lancet*, vol. 368, no. 9549, pp. 1795-1809, 2006
- [2] L. N. Ayton *et al.*, "First-in-human trial of a novel suprachoroidal retinal prosthesis," *PloS One*, vol. 9, no. 12, p e115239, 2014
- [3] A. M. Demchinsky *et al.*, "The first deaf-blind patient in Russia with Argus II retinal prosthesis system: what he sees and why," *Journal of Neural Engineering*, vol. 16, no. 2, p 025002, 2019
- [4] D. V. Palanker *et al.*, "Restoration of sight in geographic atrophy using a photovoltaic subretinal prosthesis," *Investigative Ophthalmology and Visual Science*, vol. 60, no. 9, pp. 970-970, 2019
- [5] R. Hornig *et al.*, "Pixium vision: first clinical results and innovative developments," in *Artificial Vision*:Springer, 2017
- [6] K. Stingl *et al.*, "Subretinal visual implant alpha IMS—clinical trial interim report," *Vision Research*, vol. 111, pp. 149-160, 2015
- [7] K. Stingl *et al.*, "Artificial vision with wirelessly powered subretinal electronic implant alpha-IMS," *Proceedings of the Royal Society B: Biological Sciences*, vol. 280, no. 1757, p 20130077, 2013
- [8] T. Baden *et al.*, "The functional diversity of retinal ganglion cells in the mouse," *Nature*, vol. 529, no. 7586, pp. 345-50, 2016
- [9] D. Dacey, "Origins of perception: retinal ganglion cell diversity and the creation of parallel visual pathways," *The Cognitive Neurosciences*, vol. 3, pp. 281-301, 2004
- [10] H. K. Hartline, "The response of single optic nerve fibers of the vertebrate eye to illumination of the retina," *American Journal of Physiology-Legacy Content*, vol. 121, no. 2, pp. 400-415, 1938
- [11] M. W. von Grünau, "Interaction between sustained and transient channels: Form inhibits motion in the human visual system," *Vision Research*, vol. 18, no. 2, pp. 197-201, 1978
- [12] H. Ikeda *et al.*, "Receptive field organization of 'sustained'and 'transient'retinal ganglion cells which subserve different functional roles," *Journal of Physiology*, vol. 227, no. 3, pp. 769-800, 1972
- [13] J. J. Kulikowski *et al.*, "Psychophysical evidence for sustained and transient detectors in human vision," *Journal of Physiology*, vol. 232, no. 1, pp. 149-162, 1973
- [14] P. Twyford *et al.*, "Differential responses to high-frequency electrical stimulation in ON and OFF retinal ganglion cells," *Journal of Neural Engineering*, vol. 11, no. 2, p 025001, 2014
- [15] T. Guo *et al.*, "Closed-loop efficient searching of optimal electrical stimulation parameters for preferential excitation of retinal ganglion cells," *Frontiers in Neuroscience*, vol. 12, no. 168, 2018, doi: <https://doi.org/10.3389/fnins.2018.00168>
- [16] A. Jalligampala *et al.*, "Optimal voltage stimulation parameters for network-mediated responses in wild type and rd10 mouse retinal ganglion cells," *Journal of Neural Engineering*, vol. 14, no. 2, p 026004, 2017
- [17] S. Sekhar *et al.*, "Correspondence between visual and electrical input filters of ON and OFF mouse retinal ganglion cells," *Journal of Neural Engineering*, vol. 14, no. 4, p 046017, 2017

- [18] S. Sekhar *et al.*, "Tickling the retina: integration of subthreshold electrical pulses can activate retinal neurons," *Journal of Neural Engineering*, vol. 13, no. 4, p 046004, 2016
- [19] D. K. Freeman *et al.*, "Electric stimulation with sinusoids and white noise for neural prostheses," *Frontiers in Neuroscience*, vol. 4, p 28, 2010
- [20] S. B. Ryu *et al.*, "Amplitude Modulation-based Electrical Stimulation for Encoding Multipixel Spatiotemporal Visual Information in Retinal Neural Activities," *Journal of Korean Medical Science*, vol. 32, no. 6, pp. 900-907, 2017
- [21] Z. Chen *et al.*, "Alterations of sodium and potassium channels of RGCs in RCS rat with the development of retinal degeneration," *Journal of Molecular Neuroscience*, vol. 51, no. 3, pp. 976-985, 2013
- [22] Y.-M. Ren *et al.*, "Changes in intrinsic excitability of ganglion cells in degenerated retinas of RCS rats," *International Journal of Ophthalmology*, vol. 11, no. 5, pp. 756-765, 2018
- [23] D. J. Margolis *et al.*, "Functional stability of retinal ganglion cells after degeneration-induced changes in synaptic input," *Journal of Neuroscience*, vol. 28, no. 25, pp. 6526-6536, 2008
- [24] T. M. O'Hearn *et al.*, "Electrical stimulation in normal and retinal degeneration (rd1) isolated mouse retina," *Vision Research*, vol. 46, no. 19, pp. 3198-3204, 2006
- [25] Y. S. Goo *et al.*, "Retinal ganglion cell responses to voltage and current stimulation in wild-type and rd1 mouse retinas," *Journal of Neural Engineering*, vol. 8, no. 3, p 035003, 2011
- [26] R. J. Jensen *et al.*, "Activation of ganglion cells in wild-type and rd1 mouse retinas with monophasic and biphasic current pulses," *Journal of Neural Engineering*, vol. 6, no. 3, p 035004, 2009
- [27] A. Cho *et al.*, "Changes in ganglion cell physiology during retinal degeneration influence excitability by prosthetic electrodes," *Journal of Neural Engineering*, vol. 13, no. 2, p 025001, 2016
- [28] Y. J. Yoon *et al.*, "Retinal degeneration reduces consistency of network-mediated responses arising in ganglion cells to electric stimulation," *IEEE Transactions on Neural Systems and Rehabilitation Engineering*, vol. 28, no. 9, pp. 1921-1930, 2020
- [29] C. Sekirnjak *et al.*, "Changes in physiological properties of rat ganglion cells during retinal degeneration," *Journal of Neurophysiology*, vol. 105, no. 5, pp. 2560-2571, 2011
- [30] W. Tong *et al.*, "Improved visual acuity using a retinal implant and an optimized stimulation strategy," *Journal of Neural Engineering*, vol. 17, no. 1, p 016018, 2019
- [31] E. Ho *et al.*, "Spatiotemporal characteristics of retinal response to network-mediated photovoltaic stimulation," *Journal of Neurophysiology*, vol. 119, no. 2, pp. 389-400, 2018
- [32] A. C. Weitz *et al.*, "Improving the spatial resolution of epiretinal implants by increasing stimulus pulse duration," *Science Translational Medicine*, vol. 7, no. 318, p 318ra203, 2015
- [33] L. L. Chan *et al.*, "Both electrical stimulation thresholds and SMI-32-immunoreactive retinal ganglion cell density correlate with age in S334ter line 3 rat retina," *Journal of Neurophysiology*, vol. 105, no. 6, pp. 2687-2697, 2011
- [34] E. R. Kandel *et al.*, *Principles of neural science*. McGraw-hill New York, 2000
- [35] H. Kolb, "How the retina works: Much of the construction of an image takes place in the retina itself through the use of specialized neural circuits," *American Scientist*, vol. 91, no. 1, pp. 28-35, 2003

- [36] G. D. Hildebrand *et al.*, "Anatomy and Physiology of the Retina," in *Pediatric Retina*, J. Reynolds and S. Olitsky, Eds. Berlin, Heidelberg:Springer Berlin Heidelberg, 2011
- [37] V. Perry *et al.*, "Retinal ganglion cells that project to the superior colliculus and pretectum in the macaque monkey," *Neuroscience*, vol. 12, no. 4, pp. 1125-1137, 1984
- [38] H. Kolb *et al.* (1995). *Webvision: the organization of the retina and visual system [Internet]*.
- [39] D. A. Baylor, "Photoreceptor signals and vision. Proctor lecture," *Investigative Ophthalmology and Visual Science*, vol. 28, no. 1, pp. 34-49, 1987
- [40] H. Wässle, "Parallel processing in the mammalian retina," *Nature Reviews Neuroscience*, vol. 5, no. 10, pp. 747-757, 2004
- [41] R. H. Masland, "The fundamental plan of the retina," *Nature Neuroscience*, vol. 4, no. 9, pp. 877-886, 2001
- [42] K. Yau *et al.*, "Cyclic GMP-activated conductance of retinal photoreceptor cells," *Annual Review of Neuroscience*, vol. 12, no. 1, pp. 289-327, 1989
- [43] H. Wässle *et al.*, "Cone contacts, mosaics, and territories of bipolar cells in the mouse retina," *Journal of Neuroscience*, vol. 29, no. 1, pp. 106-117, 2009
- [44] R. H. Masland, "The neuronal organization of the retina," *Neuron*, vol. 76, no. 2, pp. 266-80, 2012
- [45] G. B. Awatramani *et al.*, "Origin of transient and sustained responses in ganglion cells of the retina," *Journal of Neuroscience*, vol. 20, no. 18, pp. 7087-7095, 2000
- [46] F. S. Werblin *et al.*, "Organization of the retina of the mudpuppy, *Necturus maculosus*. II. Intracellular recording," *Journal of Neurophysiology*, vol. 32, no. 3, pp. 339-55, 1969
- [47] S. H. DeVries, "Bipolar cells use kainate and AMPA receptors to filter visual information into separate channels," *Neuron*, vol. 28, no. 3, pp. 847-856, 2000
- [48] S. Nirenberg *et al.*, "The light response of retinal ganglion cells is truncated by a displaced amacrine circuit," *Neuron*, vol. 18, no. 4, pp. 637-650, 1997
- [49] R. Nelson *et al.*, "Intracellular staining reveals different levels of stratification for on- and off-center ganglion cells in cat retina," *Journal of Neurophysiology*, vol. 41, no. 2, pp. 472-83, 1978
- [50] T. Euler *et al.*, "Retinal bipolar cells: elementary building blocks of vision," *Nature Reviews Neuroscience*, vol. 15, no. 8, pp. 507-519, 2014
- [51] T. Baden *et al.*, "Spikes in mammalian bipolar cells support temporal layering of the inner retina," *Current Biology*, vol. 23, no. 1, pp. 48-52, 2013
- [52] C. Zhang *et al.*, "Receptor targets of amacrine cells," *Visual Neuroscience*, vol. 29, no. 1, pp. 11-29, 2012
- [53] H. Wässle *et al.*, "Functional architecture of the mammalian retina," *Physiological Reviews*, vol. 71, no. 2, pp. 447-480, 1991
- [54] H. Kolb, "Amacrine cells of the mammalian retina: neurocircuitry and functional roles," *Eye*, vol. 11, no. 6, pp. 904-923, 1997
- [55] S. W. Kuffler, "Discharge patterns and functional organization of mammalian retina," *Journal of Neurophysiology*, vol. 16, no. 1, pp. 37-68, 1953
- [56] K. Farrow *et al.*, "Physiological clustering of visual channels in the mouse retina," *Journal of Neurophysiology*, vol. 105, no. 4, pp. 1516-1530, 2011

- [57] R. C. Wong *et al.*, "Intrinsic physiological properties of rat retinal ganglion cells with a comparative analysis," *Journal of Neurophysiology*, vol. 108, no. 7, pp. 2008-2023, 2012
- [58] B. J. O'Brien *et al.*, "Intrinsic physiological properties of cat retinal ganglion cells," *Journal of Physiology*, vol. 538, no. Pt 3, pp. 787-802, 2002
- [59] C. Enroth-Cugell *et al.*, "The contrast sensitivity of retinal ganglion cells of the cat," *Journal of Physiology*, vol. 187, no. 3, pp. 517-552, 1966
- [60] B. Boycott *et al.*, "The morphological types of ganglion cells of the domestic cat's retina," *Journal of Physiology*, vol. 240, no. 2, pp. 397-419, 1974
- [61] B. Cleland *et al.*, "Brisk and sluggish concentrically organized ganglion cells in the cat's retina," *Journal of Physiology*, vol. 240, no. 2, pp. 421-456, 1974
- [62] D. Petrusca *et al.*, "Identification and characterization of a Y-like primate retinal ganglion cell type," *Journal of Neuroscience*, vol. 27, no. 41, pp. 11019-11027, 2007
- [63] B. Krieger *et al.*, "Four alpha ganglion cell types in mouse retina: Function, structure, and molecular signatures," *PloS One*, vol. 12, no. 7, p e0180091, 2017
- [64] B. Völgyi *et al.*, "Tracer coupling patterns of the ganglion cell subtypes in the mouse retina," *Journal of Comparative Neurology*, vol. 512, no. 5, pp. 664-687, 2009
- [65] J. Coombs *et al.*, "Morphological properties of mouse retinal ganglion cells," *Neuroscience*, vol. 140, no. 1, pp. 123-136, 2006
- [66] M. L. Aranda *et al.*, "Diversity of intrinsically photosensitive retinal ganglion cells: circuits and functions," *Cellular and Molecular Life Sciences*, vol. 78, no. 3, pp. 889-907, 2021
- [67] A. N. Reifler *et al.*, "The rat retina has five types of ganglion-cell photoreceptors," *Experimental eye research*, vol. 130, pp. 17-28, 2015
- [68] D. M. Dacey *et al.*, "Melanopsin-expressing ganglion cells in primate retina signal colour and irradiance and project to the LGN," *Nature*, vol. 433, no. 7027, pp. 749-54, 2005
- [69] X. Zhao *et al.*, "Photoresponse diversity among the five types of intrinsically photosensitive retinal ganglion cells," *Journal of Physiology*, vol. 592, no. 7, pp. 1619-36, 2014
- [70] D. C. Sterratt, "Goldman-Hodgkin-Katz Equations," in *Encyclopedia of Computational Neuroscience*: Springer New York, 2015
- [71] T. Guo *et al.*, "Electrical activity of ON and OFF retinal ganglion cells: a modelling study," *Journal of Neural Engineering*, vol. 13, no. 2, p 025005, 2016
- [72] T. Kameneva *et al.*, "Modelling intrinsic electrophysiological properties of ON and OFF retinal ganglion cells," *Journal of Computational Neuroscience*, vol. 31, no. 3, pp. 547-561, 2011
- [73] D. J. Margolis *et al.*, "Different mechanisms generate maintained activity in ON and OFF retinal ganglion cells," *Journal of Neuroscience*, vol. 27, no. 22, pp. 5994-6005, 2007
- [74] D. J. Margolis *et al.*, "Dendritic calcium signaling in ON and OFF mouse retinal ganglion cells," *Journal of Neuroscience*, vol. 30, no. 21, pp. 7127-7138, 2010
- [75] A. Van Wart *et al.*, "Polarized distribution of ion channels within microdomains of the axon initial segment," *Journal of Comparative Neurology*, vol. 500, no. 2, pp. 339-52, 2007

- [76] J. Fjell *et al.*, "Differential expression of sodium channel genes in retinal ganglion cells," *Molecular Brain Research*, vol. 50, no. 1-2, pp. 197-204, 1997
- [77] T. Boiko *et al.*, "Functional specialization of the axon initial segment by isoform-specific sodium channel targeting," *Journal of Neuroscience*, vol. 23, no. 6, pp. 2306-2313, 2003
- [78] B. J. O'Brien *et al.*, "Tetrodotoxin-resistant voltage-gated sodium channels Nav1. 8 and Nav1. 9 are expressed in the retina," *Journal of Comparative Neurology*, vol. 508, no. 6, pp. 940-951, 2008
- [79] V. Raghuram *et al.*, "Scaling of the AIS and somatodendritic compartments in  $\alpha$  S RGCs," *Frontiers in Cellular Neuroscience*, vol. 13, no. 436, 2019, doi: <https://doi.org/10.3389/fncel.2019.00436>
- [80] Y. Chen *et al.*, "Functional properties and differential neuromodulation of Na V 1.6 channels," *Molecular and Cellular Neuroscience*, vol. 38, no. 4, pp. 607-615, 2008
- [81] A. M. Rush *et al.*, "Electrophysiological properties of two axonal sodium channels, Nav1.2 and Nav1.6, expressed in mouse spinal sensory neurones," *Journal of Physiology*, vol. 564, no. Pt 3, pp. 803-15, 2005
- [82] C. Hamel, "Retinitis pigmentosa," *Orphanet Journal of Rare Diseases*, vol. 1, no. 1, pp. 1-12, 2006
- [83] B. W. Jones *et al.*, "Retinal remodeling triggered by photoreceptor degenerations," *Journal of Comparative Neurology*, vol. 464, no. 1, pp. 1-16, 2003
- [84] B. W. Jones *et al.*, "Retinal remodeling during retinal degeneration," *Experimental Eye Research*, vol. 81, no. 2, pp. 123-137, 2005
- [85] B. Jones *et al.*, "Retinal remodeling in human retinitis pigmentosa," *Experimental Eye Research*, vol. 150, pp. 149-165, 2016
- [86] M. Agurtzane Rivas *et al.*, "Animal models and different therapies for treatment of retinitis pigmentosa," *Histology and Histopathology*, pp. 1295-1322, 2009
- [87] D. R. Bertschinger *et al.*, "A review of in vivo animal studies in retinal prosthesis research," *Graefe's Archive for Clinical and Experimental Ophthalmology*, vol. 246, no. 11, pp. 1505-1517, 2008
- [88] S. M. Peterson *et al.*, "Bardet-Biedl Syndrome in rhesus macaques: A nonhuman primate model of retinitis pigmentosa," *Experimental Eye Research*, vol. 189, p. 107825, 2019
- [89] H. Ameri, "Prospect of retinal gene therapy following commercialization of voretigene neparvovec-rzyl for retinal dystrophy mediated by RPE65 mutation," *Journal of Current Ophthalmology*, vol. 30, no. 1, pp. 1-2, 2018
- [90] A. Auricchio *et al.*, "Adeno-associated viral vectors for retinal gene transfer and treatment of retinal diseases," *Current Gene Therapy*, vol. 5, no. 3, pp. 339-348, 2005
- [91] C. Sekirnjak *et al.*, "Loss of responses to visual but not electrical stimulation in ganglion cells of rats with severe photoreceptor degeneration," *Journal of Neurophysiology*, vol. 102, no. 6, pp. 3260-3269, 2009
- [92] C. KEELER, "Retinal degeneration in the mouse is rodless retina," *Journal of Heredity*, vol. 57, no. 2, pp. 47-50, 1966
- [93] D. Farber *et al.*, "Enzymic basis for cyclic GMP accumulation in degenerative photoreceptor cells of mouse retina," *Journal of Cyclic Nucleotide Research*, vol. 2, no. 3, pp. 139-148, 1976

- [94] M. E. McLaughlin *et al.*, "Recessive mutations in the gene encoding the  $\beta$ -subunit of rod phosphodiesterase in patients with retinitis pigmentosa," *Nature Genetics*, vol. 4, no. 2, pp. 130-134, 1993
- [95] D. B. Farber *et al.*, "Cyclic guanosine monophosphate: elevation in degenerating photoreceptor cells of the C3H mouse retina," *Science*, vol. 186, no. 4162, pp. 449-451, 1974
- [96] D. B. Farber *et al.*, "The rd mouse story: seventy years of research on an animal model of inherited retinal degeneration," *Progress in Retinal and Eye Research*, vol. 13, no. 1, pp. 31-64, 1994
- [97] E. Strettoi *et al.*, "Modifications of retinal neurons in a mouse model of retinitis pigmentosa," *Proceedings of the National Academy of Sciences*, vol. 97, no. 20, pp. 11020-11025, 2000
- [98] B. Chang *et al.*, "Two mouse retinal degenerations caused by missense mutations in the  $\beta$ -subunit of rod cGMP phosphodiesterase gene," *Vision Research*, vol. 47, no. 5, pp. 624-633, 2007
- [99] C. Gargini *et al.*, "Retinal organization in the retinal degeneration 10 (rd10) mutant mouse: a morphological and ERG study," *Journal of Comparative Neurology*, vol. 500, no. 2, pp. 222-238, 2007
- [100] M. Samardzija *et al.*, "Activation of survival pathways in the degenerating retina of rd10 mice," *Experimental Eye Research*, vol. 99, pp. 17-26, 2012
- [101] E. Zrenner *et al.*, "Subretinal electronic chips allow blind patients to read letters and combine them to words," *Proceedings of the Royal Society of London B: Biological Sciences*, vol. 278, no. 1711, pp. 1489-1497, 2011
- [102] M. S. Humayun *et al.*, "Visual perception in a blind subject with a chronic microelectronic retinal prosthesis," *Vision Research*, vol. 43, no. 24, pp. 2573-2581, 2003
- [103] N. C. Sinclair *et al.*, "The Appearance of Phosphenes Elicited Using a Suprachoroidal Retinal Prosthesis Phosphenes of a Suprachoroidal Retinal Prosthesis," *Investigative Ophthalmology and Visual Science*, vol. 57, no. 11, pp. 4948-4961, 2016
- [104] A. P. Fornos *et al.*, "Temporal properties of visual perception on electrical stimulation of the retina perception upon electrical stimulation of the retina," *Investigative Ophthalmology and Visual Science*, vol. 53, no. 6, pp. 2720-2731, 2012
- [105] J. D. Weiland *et al.*, "Retinal prosthesis," *IEEE Transactions on Biomedical Engineering*, vol. 61, no. 5, pp. 1412-24, 2014
- [106] L. Yue *et al.*, "Retinal stimulation strategies to restore vision: fundamentals and systems," *Progress in Retinal and Eye Research*, vol. 53, pp. 21-47, 2016
- [107] P. Falabella *et al.*, "Argus® II Retinal Prosthesis System," in *Artificial Vision*: Springer, 2017
- [108] R. Hornig *et al.*, "The IMI retinal implant system," in *Artificial Sight*: Springer, 2007
- [109] S. Klauke *et al.*, "Stimulation with a wireless intraocular epiretinal implant elicits visual percepts in blind humans," *Investigative Ophthalmology and Visual Science*, vol. 52, no. 1, pp. 449-455, 2011
- [110] K. Mathieson *et al.*, "Photovoltaic retinal prosthesis with high pixel density," *Nature Photonics*, vol. 6, no. 6, pp. 391-397, 2012
- [111] A. Y. Chow *et al.*, "The artificial silicon retina microchip for the treatment of vision loss from retinitis pigmentosa," *Archives of Ophthalmology*, vol. 122, no. 4, pp. 460-469, 2004

- [112] L. Bareket *et al.*, "Progress in artificial vision through suprachoroidal retinal implants," *Journal of Neural Engineering*, vol. 14, no. 4, p 045002, 2017
- [113] M. A. Petoe *et al.*, "A 44 channel suprachoroidal retinal prosthesis: initial psychophysical results," *Investigative Ophthalmology and Visual Science*, vol. 60, no. 9, pp. 4993-4993, 2019
- [114] T. Fujikado *et al.*, "Testing of semichronically implanted retinal prosthesis by suprachoroidal-transretinal stimulation in patients with retinitis pigmentosa," *Investigative Ophthalmology and Visual Science*, vol. 52, no. 7, pp. 4726-4733, 2011
- [115] K. Cha *et al.*, "Mobility performance with a pixelized vision system," *Vision Research*, vol. 32, no. 7, pp. 1367-1372, 1992
- [116] J. Sommerhalder *et al.*, "Minimum requirements for mobility in unpredictable environments," *Investigative Ophthalmology and Visual Science*, vol. 47, no. 13, pp. 3204-3204, 2006
- [117] T. K. Lohmann *et al.*, "The very large electrode array for retinal stimulation (VLARS)—a concept study," *Journal of Neural Engineering*, vol. 16, no. 6, p 066031, 2019
- [118] N. A. L. Chenais *et al.*, "Photovoltaic retinal prosthesis restores high-resolution responses to single-pixel stimulation in blind retinas," *Communications Materials*, vol. 2, no. 1, pp. 1-16, 2021
- [119] L. IntelliMicro Medical Co. (2020, July 23, 2020). *The IMIE Intelligent Visual Implant Succeeded*. Available: [http://www.intellimicro.cn/en/list/info\\_67.aspx?itemid=279](http://www.intellimicro.cn/en/list/info_67.aspx?itemid=279)
- [120] B. Abbasi *et al.*, "Advances in neuroscience, not devices, will determine the effectiveness of visual prostheses," *Seminars in Ophthalmology*, vol. 36, no. 4, pp. 168-175, 2021
- [121] D. Tsai *et al.*, "Survey of electrically evoked responses in the retina-stimulus preferences and oscillation among neurons," *Scientific Reports*, vol. 7, no. 1, pp. 1-14, 2017
- [122] M. Im *et al.*, "Indirect activation elicits strong correlations between light and electrical responses in ON but not OFF retinal ganglion cells," *Journal of Physiology*, vol. 593, no. 16, pp. 3577-3596, 2015
- [123] I. Fine *et al.*, "Pulse trains to percepts: the challenge of creating a perceptually intelligible world with sight recovery technologies," *Philosophical Transactions of the Royal Society B: Biological Sciences*, vol. 370, no. 1677, p 20140208, 2015
- [124] J. R. Golden *et al.*, "Simulation of visual perception and learning with a retinal prosthesis," *Journal of Neural Engineering*, vol. 16, no. 2, p 025003, 2019
- [125] M. Im *et al.*, "Temporal properties of network-mediated responses to repetitive stimuli are dependent upon retinal ganglion cell type," *Journal of Neural Engineering*, vol. 13, no. 2, p 025002, 2016
- [126] J. I. Lee *et al.*, "Optimal electric stimulus amplitude improves the selectivity between responses of ON versus OFF types of retinal ganglion cells," *IEEE Transactions on Neural Systems and Rehabilitation Engineering*, vol. 27, no. 10, pp. 2015-2024, 2019
- [127] S. Madugula *et al.*, "Focal electrical stimulation of human retinal ganglion cells," *bioRxiv*, 2020
- [128] C. Cai *et al.*, "Response variability to high rates of electric stimulation in retinal ganglion cells," *Journal of Neurophysiology*, vol. 106, no. 1, pp. 153-62, 2011
- [129] D. Nanduri *et al.*, "Frequency and amplitude modulation have different effects on the percepts elicited by retinal stimulation," *Investigative Ophthalmology and Visual Science*, vol. 53, no. 1, pp. 205-14, 2012

- [130] M. Im *et al.*, "Electric stimulus duration alters network-mediated responses depending on retinal ganglion cell type," *Journal of Neural Engineering*, vol. 15, no. 3, p 036010, 2018
- [131] D. K. Freeman *et al.*, "Selective activation of neuronal targets with sinusoidal electric stimulation," *Journal of Neurophysiology*, vol. 104, no. 5, pp. 2778-91, 2010
- [132] P. Twyford *et al.*, "The retinal response to sinusoidal electrical stimulation," *IEEE Transactions on Neural Systems and Rehabilitation Engineering*, vol. 24, no. 4, pp. 413-23, 2016
- [133] L. Höfling *et al.*, "Probing and predicting ganglion cell responses to smooth electrical stimulation in healthy and blind mouse retina," *Scientific Reports*, vol. 10, no. 1, p 5248, 2020
- [134] E. Chichilnisky, "A simple white noise analysis of neuronal light responses," *Network: Computation in Neural Systems*, vol. 12, no. 2, pp. 199-213, 2001
- [135] S. H. Devries *et al.*, "Mosaic arrangement of ganglion cell receptive fields in rabbit retina," *Journal of Neurophysiology*, vol. 78, no. 4, pp. 2048-60, 1997
- [136] P. van Dijk *et al.*, "Dissecting the frog inner ear with Gaussian noise. I. Application of high-order Wiener-kernel analysis," *Hearing Research*, vol. 114, no. 1, pp. 229-242, 1997
- [137] D. Rathbun *et al.*, "Spike-triggered average electrical stimuli as input filters for bionic vision—a perspective," *Journal of Neural Engineering*, vol. 15, no. 6, p 063002, 2018
- [138] A. P. Fornos *et al.*, "Dynamics of visual perception upon electrical stimulation of the retina," *Investigative Ophthalmology and Visual Science*, vol. 51, no. 13, pp. 3027-3027, 2010
- [139] A. K. Ahuja *et al.*, "An in vitro model of a retinal prosthesis," *IEEE Transactions on Biomedical Engineering*, vol. 55, no. 6, pp. 1744-1753, 2008
- [140] R. J. Jensen *et al.*, "Responses of ganglion cells to repetitive electrical stimulation of the retina," *Journal of Neural Engineering*, vol. 4, no. 1, pp. S1-S6, 2007
- [141] D. K. Freeman *et al.*, "Multiple components of ganglion cell desensitization in response to prosthetic stimulation," *Journal of Neural Engineering*, vol. 8, no. 1, p 016008, 2011
- [142] A. Hadjinicolaou *et al.*, "Optimizing the electrical stimulation of retinal ganglion cells," *IEEE Transactions on Neural Systems and Rehabilitation Engineering*, vol. 23, no. 2, pp. 169-178, 2015
- [143] S. I. Fried *et al.*, "A method for generating precise temporal patterns of retinal spiking using prosthetic stimulation," *Journal of Neurophysiology*, vol. 95, no. 2, pp. 970-978, 2006
- [144] S. Sekhar *et al.*, "Characterizing retinal ganglion cell responses to electrical stimulation using generalized linear models," *Frontiers in Neuroscience*, vol. 14, 2020, doi: <https://doi.org/10.3389/fnins.2020.00378>
- [145] J. Johnston *et al.*, "Rapid mapping of visual receptive fields by filtered back projection: application to multi-neuronal electrophysiology and imaging," *Journal of Physiology*, vol. 592, no. 22, pp. 4839-4854, 2014
- [146] J. K. Liu *et al.*, "Inference of neuronal functional circuitry with spike-triggered non-negative matrix factorization," *Nature Communications*, vol. 8, no. 1, pp. 1-14, 2017
- [147] R. J. Jensen *et al.*, "Thresholds for activation of rabbit retinal ganglion cells with a subretinal electrode," *Experimental Eye Research*, vol. 83, no. 2, pp. 367-373, 2006

- [148] D. R. Merrill *et al.*, "Electrical stimulation of excitable tissue: design of efficacious and safe protocols," *Journal of Neuroscience Methods*, vol. 141, no. 2, pp. 171-198, 2005
- [149] J.-I. Lee *et al.*, "Non-rectangular waveforms are more charge-efficient than rectangular one in eliciting network-mediated responses of ON type retinal ganglion cells," *Journal of neural engineering*, vol. 15, no. 5, p 055004, 2018
- [150] L. Nivison-Smith *et al.*, "Mapping kainate activation of inner neurons in the rat retina," *Journal of Comparative Neurology*, vol. 521, no. 11, pp. 2416-2438, 2013
- [151] R. J. Jensen *et al.*, "Thresholds for activation of rabbit retinal ganglion cells with relatively large, extracellular microelectrodes," *Investigative ophthalmology & visual science*, vol. 46, no. 4, pp. 1486-1496, 2005
- [152] C. Sekirnjak *et al.*, "Electrical stimulation of mammalian retinal ganglion cells with multielectrode arrays," *Journal of Neurophysiology*, vol. 95, no. 6, pp. 3311-3327, 2006
- [153] D. Tsai *et al.*, "Direct activation and temporal response properties of rabbit retinal ganglion cells following subretinal stimulation," *Journal of Neurophysiology*, vol. 102, no. 5, pp. 2982-2993, 2009
- [154] S. W. Lee *et al.*, "Responses to pulsatile subretinal electric stimulation: effects of amplitude and duration," *Journal of neurophysiology*, vol. 109, no. 7, pp. 1954-1968, 2013
- [155] D. Boinagrov *et al.*, "Selectivity of direct and network-mediated stimulation of the retinal ganglion cells with epi-, sub- and intraretinal electrodes," *Journal of Neural Engineering*, vol. 11, no. 2, p 026008, 2014
- [156] R. J. Greenberg *et al.*, "A computational model of electrical stimulation of the retinal ganglion cell," *IEEE Transactions on Biomedical Engineering*, vol. 46, no. 5, pp. 505-514, 1999
- [157] L. E. Grosberg *et al.*, "Activation of ganglion cells and axon bundles using epiretinal electrical stimulation," *Journal of Neurophysiology*, vol. 118, no. 3, pp. 1457-1471, 2017
- [158] Y. C. Chang *et al.*, "Stimulation strategies for selective activation of retinal ganglion cell soma and threshold reduction," *Journal of Neural Engineering*, vol. 16, no. 2, p 026017, 2019
- [159] D. Raz-Prag *et al.*, "Electrical stimulation of different retinal components and the effect of asymmetric pulses," *Journal of Neuroscience Methods*, vol. 291, pp. 20-27, 2017
- [160] A. C. Weitz *et al.*, "Imaging the response of the retina to electrical stimulation with genetically encoded calcium indicators," *Journal of Neurophysiology*, vol. 109, no. 7, pp. 1979-1988, 2013
- [161] C. Sekirnjak *et al.*, "High-resolution electrical stimulation of primate retina for epiretinal implant design," *Journal of Neuroscience*, vol. 28, no. 17, pp. 4446-4456, 2008
- [162] L. H. Jepson *et al.*, "Focal electrical stimulation of major ganglion cell types in the primate retina for the design of visual prostheses," *Journal of Neuroscience*, vol. 33, no. 17, pp. 7194-7205, 2013
- [163] L. H. Jepson *et al.*, "Spatially patterned electrical stimulation to enhance resolution of retinal prostheses," *Journal of Neuroscience*, vol. 34, no. 14, pp. 4871-4881, 2014
- [164] V. H. Fan *et al.*, "Epiretinal stimulation with local returns enhances selectivity at cellular resolution," *Journal of Neural Engineering*, vol. 16, no. 2, p 025001, 2019
- [165] C. Y. Yang *et al.*, "Differential electrical responses in retinal ganglion cell subtypes: effects of synaptic blockade and stimulating electrode location," *Journal of Neural Engineering*, vol. 15, no. 4, p 046020, 2018

- [166] P. K. Trong *et al.*, "Origin of correlated activity between parasol retinal ganglion cells," *Nature Neuroscience*, vol. 11, no. 11, pp. 1343-1351, 2008
- [167] L. Kapural *et al.*, "Novel 10-kHz high-frequency therapy (HF10 Therapy) is superior to traditional low-frequency spinal cord stimulation for the treatment of chronic back and leg pain: The SENZA-RCT randomized controlled trial," *Anesthesiology*, vol. 123, no. 4, pp. 851-860, 2015
- [168] A. Al-Kaisy *et al.*, "Sustained effectiveness of 10 kHz high-frequency spinal cord stimulation for patients with chronic, low back pain: 24-month results of a prospective multicenter study," *Pain Medicine (Malden, Mass.)*, vol. 15, no. 3, pp. 347-354, 2014
- [169] A. Soin *et al.*, "High-frequency peripheral electric nerve block to treat postamputation pain," *Techniques in Regional Anesthesia and Pain Management*, vol. 18, no. 4, pp. 156-162, 2014
- [170] A. Soin *et al.*, "High-frequency electrical nerve block for postamputation pain: a pilot study," *Neuromodulation: Technology at the Neural Interface*, vol. 18, no. 3, pp. 197-206, 2015
- [171] C. M. McKay *et al.*, "Can ECAP measures be used for totally objective programming of cochlear implants?," *Journal of the Association for Research in Otolaryngology*, vol. 14, no. 6, pp. 879-890, 2013
- [172] A. Horsager *et al.*, "Predicting visual sensitivity in retinal prosthesis patients," *Investigative Ophthalmology and Visual Science*, vol. 50, no. 4, pp. 1483-1491, 2009
- [173] J. Tiede *et al.*, "Novel spinal cord stimulation parameters in patients with predominant back pain," *Neuromodulation: Technology at the Neural Interface*, vol. 16, no. 4, pp. 370-375, 2013
- [174] J. P. Van Buyten *et al.*, "High-frequency spinal cord stimulation for the treatment of chronic back pain patients: results of a prospective multicenter European clinical study," *Neuromodulation: Technology at the Neural Interface*, vol. 16, no. 1, pp. 59-66, 2013
- [175] K. L. Kilgore *et al.*, "Nerve conduction block utilising high-frequency alternating current," *Medical and Biological Engineering and Computing*, vol. 42, no. 3, pp. 394-406, 2004
- [176] K. L. Kilgore *et al.*, "Reversible nerve conduction block using kilohertz frequency alternating current," *Neuromodulation: Technology at the Neural Interface*, vol. 17, no. 3, pp. 242-255, 2014
- [177] D. M. Ackermann Jr *et al.*, "Electrical conduction block in large nerves: High-frequency current delivery in the nonhuman primate," *Muscle and Nerve*, vol. 43, no. 6, pp. 897-899, 2011
- [178] D. Boinagrov *et al.*, "Upper threshold of extracellular neural stimulation," *Journal of Neurophysiology*, vol. 108, no. 12, pp. 3233-3238, 2012
- [179] K. Meng *et al.*, "Upper stimulation threshold for retinal ganglion cell activation," *Journal of Neural Engineering*, vol. 15, no. 4, p 046012, 2018
- [180] L. Joseph *et al.*, "High-frequency stimulation selectively blocks different types of fibers in frog sciatic nerve," *IEEE Transactions on Neural Systems and Rehabilitation Engineering*, vol. 19, no. 5, pp. 550-557, 2011
- [181] Y. A. Patel *et al.*, "Differential fiber-specific block of nerve conduction in mammalian peripheral nerves using kilohertz electrical stimulation," *Journal of Neurophysiology*, vol. 113, no. 10, pp. 3923-3929, 2015

- [182] Y.-C. Chang *et al.*, "Stimulus manipulations permit activation of fiber subpopulations in the mouse and rat vagus," *bioRxiv*, p 2021.01.30.428827, 2021
- [183] C. Cai *et al.*, "The response of retinal neurons to high-frequency stimulation," *Journal of Neural Engineering*, vol. 10, no. 3, p 036009, 2013
- [184] F. Rattay, "On the upper threshold phenomenon of extracellular neural stimulation," *Journal of Neurophysiology*, vol. 112, no. 10, pp. 2664-2665, 2014
- [185] N. Bhadra *et al.*, "High-frequency electrical conduction block of mammalian peripheral motor nerve," *Muscle and Nerve*, vol. 32, no. 6, pp. 782-790, 2005
- [186] R. P. Williamson *et al.*, "Localized electrical nerve blocking," *IEEE Transactions on Biomedical Engineering*, vol. 52, no. 3, pp. 362-370, 2005
- [187] T. Guo *et al.*, "Mediating retinal ganglion cell spike rates using high-frequency electrical stimulation," *Frontiers in Neuroscience*, vol. 13, no. 413, 2019, doi: <https://doi.org/10.3389/fnins.2019.00413>
- [188] F. Rattay, "Analysis of models for external stimulation of axons," *IEEE Transactions on Biomedical Engineering*, vol. 33, no. 10, pp. 974-977, 1986
- [189] E. Peña *et al.*, "Non-monotonic kilohertz frequency neural block thresholds arise from amplitude-and frequency-dependent charge imbalance," *Scientific Reports*, vol. 11, no. 1, pp. 1-17, 2021
- [190] T. Kameneva *et al.*, "Retinal ganglion cells: mechanisms underlying depolarization block and differential responses to high frequency electrical stimulation of ON and OFF cells," *Journal of Neural Engineering*, vol. 13, no. 1, p 016017, 2016
- [191] I. M. Raman *et al.*, "Resurgent sodium current and action potential formation in dissociated cerebellar Purkinje neurons," *Journal of Neuroscience*, vol. 17, no. 12, pp. 4517-4526, 1997
- [192] I. M. Raman *et al.*, "Inactivation and recovery of sodium currents in cerebellar Purkinje neurons: evidence for two mechanisms," *Biophysical Journal*, vol. 80, no. 2, pp. 729-737, 2001
- [193] A. H. Lewis *et al.*, "Resurgent current of voltage-gated Na<sup>+</sup> channels," *Journal of Physiology*, vol. 592, no. 22, pp. 4825-4838, 2014
- [194] Y. S. Zhong *et al.*, "Potassium ion channels in retinal ganglion cells," *Molecular Medicine Reports*, vol. 8, no. 2, pp. 311-319, 2013
- [195] L. K. Kaczmarek *et al.*, "Kv3 channels: enablers of rapid firing, neurotransmitter release, and neuronal endurance," *Physiological Reviews*, vol. 97, no. 4, pp. 1431-1468, 2017
- [196] S. I. Fried *et al.*, "Axonal sodium-channel bands shape the response to electric stimulation in retinal ganglion cells," *Journal of Neurophysiology*, vol. 101, no. 4, pp. 1972-1987, 2009
- [197] P. Werginz *et al.*, "Tailoring of the axon initial segment shapes the conversion of synaptic inputs into spiking output in OFF- $\alpha$  T retinal ganglion cells," *Science Advances*, vol. 6, no. 37, p eabb6642, 2020
- [198] K. Morigiwa *et al.*, "Fractal analysis of ganglion cell dendritic branching patterns of the rat and cat retinae," *Neuroscience Research Supplements*, vol. 10, pp. S131-S139, 1989
- [199] D. M. Dacey *et al.*, "Dendritic field size and morphology of midget and parasol ganglion cells of the human retina," *Proceedings of the National Academy of Sciences of the United States of America*, vol. 89, no. 20, pp. 9666-9670, 1992

- [200] P. Werginz *et al.*, "The relationship between morphological properties and thresholds to extracellular electric stimulation in  $\alpha$  RGCs," *Journal of Neural Engineering*, vol. 17, no. 4, p 045015, 2020
- [201] M. E. McClements *et al.*, "Optogenetic gene therapy for the degenerate retina: recent advances," *Frontiers in Neuroscience*, vol. 14, p 1187, 2020, doi: <https://doi.org/10.3389/fnins.2020.570909>
- [202] G. Gauvain *et al.*, "Optogenetic therapy: high spatiotemporal resolution and pattern discrimination compatible with vision restoration in non-human primates," *Communications biology*, vol. 4, no. 1, pp. 1-15, 2021
- [203] J.-A. Sahel *et al.*, "Partial recovery of visual function in a blind patient after optogenetic therapy," *Nature Medicine*, pp. 1-7, 2021
- [204] S. Nirenberg *et al.*, "Retinal prosthetic strategy with the capacity to restore normal vision," *Proceedings of the National Academy of Sciences*, vol. 109, no. 37, pp. 15012-17, 2012
- [205] J.-K. Suh *et al.*, "Optogenetic targeting of ON and OFF bipolar cells for vision restoration," *Investigative Ophthalmology and Visual Science*, vol. 54, no. 15, pp. 2678-2678, 2013
- [206] J. Rodgers *et al.*, "Using a bistable animal opsin for switchable and scalable optogenetic inhibition of neurons," *bioRxiv*, 2020
- [207] J. Duebel *et al.*, "Optogenetics," *Current Opinion in Ophthalmology*, vol. 26, no. 3, pp. 226-232, 2015, doi: 10.1097/ICU.0000000000000140
- [208] E. H. Wood *et al.*, "Stem cell therapies, gene-based therapies, optogenetics, and retinal prosthetics: current state and implications for the future," *Retina (Philadelphia, Pa.)*, vol. 39, no. 5, pp. 820-835, 2019, doi: 10.1097/IAE.0000000000002449
- [209] M. van Wyk *et al.*, "Present molecular limitations of ON-bipolar cell targeted gene therapy," *Frontiers in Neuroscience*, vol. 11, pp. 161-161, 2017
- [210] C. M. Rountree *et al.*, "Methodology for biomimetic chemical neuromodulation of rat retinas with the neurotransmitter glutamate in vitro," *Journal of Visualized Experiments*, no. 130, p 5664, 2017
- [211] C. M. Rountree *et al.*, "Microfluidics-based subretinal chemical neuromodulation of photoreceptor degenerated retinas," *Investigative Ophthalmology and Visual Science*, vol. 59, no. 1, pp. 418-430, 2018
- [212] C. M. Rountree *et al.*, "Differential stimulation of the retina with subretinally injected exogenous neurotransmitter: A biomimetic alternative to electrical stimulation," *Scientific Reports*, vol. 6, no. 1, p 38505, 2016
- [213] T. C. Südhof, "The presynaptic active zone," *Neuron*, vol. 75, no. 1, pp. 11-25, 2012
- [214] E. Albert *et al.*, "TRPV4 channels mediate the infrared laser-evoked response in sensory neurons," *Journal of Neurophysiology*, vol. 107, no. 12, pp. 3227-3234, 2012
- [215] J. M. Cayce *et al.*, "Infrared neural stimulation of primary visual cortex in non-human primates," *NeuroImage*, vol. 84, pp. 181-190, 2014
- [216] R. T. Richardson *et al.*, "Optical stimulation of neural tissue," *Healthcare Technology Letters*, vol. 7, no. 3, pp. 58-65, 2020
- [217] G. Bonmassar *et al.*, "Microscopic magnetic stimulation of neural tissue," *Nature Communications*, vol. 3, no. 1, p 921, 2012

- [218] S. W. Lee *et al.*, "Enhanced control of cortical pyramidal neurons with micromagnetic stimulation," *IEEE Transactions on Neural Systems and Rehabilitation Engineering*, vol. 25, no. 9, pp. 1375-1386, 2016
- [219] R. E. Marc *et al.*, "Retinal remodeling in inherited photoreceptor degenerations," *Molecular Neurobiology*, vol. 28, no. 2, pp. 139-147, 2003
- [220] R. E. Marc *et al.*, "Neural reprogramming in retinal degeneration," *Investigative Ophthalmology and Visual Science*, vol. 48, no. 7, pp. 3364-3371, 2007
- [221] J. Chua *et al.*, "Early remodeling of Müller cells in the rd/rd mouse model of retinal dystrophy," *Journal of Comparative Neurology*, vol. 521, no. 11, pp. 2439-2453, 2013
- [222] S. F. Stasheff *et al.*, "Developmental time course distinguishes changes in spontaneous and light-evoked retinal ganglion cell activity in rd1 and rd10 mice," *Journal of Neurophysiology*, vol. 105, no. 6, pp. 3002-3009, 2011
- [223] H. Choi *et al.*, "Intrinsic bursting of All amacrine cells underlies oscillations in the rd1 mouse retina," *Journal of Neurophysiology*, vol. 112, no. 6, pp. 1491-1504, 2014
- [224] Y. S. Goo *et al.*, "Spontaneous oscillatory rhythm in retinal activities of two retinal degeneration (rd1 and rd10) mice," *The Korean Journal of Physiology and Pharmacology: Official Journal of the Korean Physiological Society and the Korean Society of Pharmacology*, vol. 15, no. 6, pp. 415-422, 2011
- [225] D. J. Margolis *et al.*, "Cellular origin of spontaneous ganglion cell spike activity in animal models of retinitis pigmentosa," *Journal of Ophthalmology*, vol. 2011, p 507037, 2011
- [226] J. Borowska *et al.*, "An intrinsic neural oscillator in the degenerating mouse retina," *Journal of Neuroscience*, vol. 31, no. 13, pp. 5000-5012, 2011
- [227] S. Trenholm *et al.*, "Intrinsic oscillatory activity arising within the electrically coupled All amacrine-ON cone bipolar cell network is driven by voltage-gated Na<sup>+</sup> channels," *Journal of Physiology*, vol. 590, no. 10, pp. 2501-2517, 2012
- [228] J. Menzler *et al.*, "Network oscillations in rod-degenerated mouse retinas," *Journal of Neuroscience*, vol. 31, no. 6, pp. 2280-2291, 2011
- [229] A. H. Toychiev *et al.*, "Block of gap junctions eliminates aberrant activity and restores light responses during retinal degeneration," *Journal of Neuroscience*, vol. 33, no. 35, pp. 13972-13977, 2013
- [230] E. Ivanova *et al.*, "Aberrant activity in retinal degeneration impairs central visual processing and relies on Cx36-containing gap junctions," *Experimental Eye Research*, vol. 150, pp. 81-89, 2016
- [231] D. J. Margolis *et al.*, "Network oscillations drive correlated spiking of ON and OFF ganglion cells in the rd1 mouse model of retinal degeneration," *PloS One*, vol. 9, no. 1, p e86253, 2014
- [232] J. Menzler *et al.*, "Rhythmic ganglion cell activity in bleached and blind adult mouse retinas," *PloS One*, vol. 9, no. 8, p e106047, 2014
- [233] W. Haq *et al.*, "Synaptic remodeling generates synchronous oscillations in the degenerated outer mouse retina," *Frontiers in Neural Circuits*, vol. 8, p 108, 2014
- [234] B. Lin *et al.*, "Retinal ganglion cells are resistant to photoreceptor loss in retinal degeneration," *PloS One*, vol. 8, no. 6, p e68084, 2013
- [235] F. Mazzoni *et al.*, "Retinal ganglion cells survive and maintain normal dendritic morphology in a mouse model of inherited photoreceptor degeneration," *Journal of Neuroscience*, vol. 28, no. 52, pp. 14282-14292, 2008

- [236] S. Saha *et al.*, "Changes in ganglion cells during retinal degeneration," *Neuroscience*, vol. 329, pp. 1-11, 2016
- [237] B. Kolomiets *et al.*, "Late histological and functional changes in the P23H rat retina after photoreceptor loss," *Neurobiology of Disease*, vol. 38, no. 1, pp. 47-58, 2010
- [238] D. García-Ayuso *et al.*, "Retinal ganglion cell numbers and delayed retinal ganglion cell death in the P23H rat retina," *Experimental Eye Research*, vol. 91, no. 6, pp. 800-810, 2010
- [239] Z. S. Chen *et al.*, "Electrophysiological changes of retinal ganglion cells in Royal College of Surgeons rats during retinal degeneration," *Neuroreport*, vol. 16, no. 9, pp. 971-975, 2005
- [240] A. K. Ahuja *et al.*, "Factors affecting perceptual threshold in Argus II retinal prosthesis subjects," *Translational Vision Science and Technology*, vol. 2, no. 4, pp. 1-1, 2013
- [241] M. S. Humayun *et al.*, "Pattern electrical stimulation of the human retina," *Vision Research*, vol. 39, no. 15, pp. 2569-2576, 1999
- [242] J. F. Rizzo *et al.*, "Methods and perceptual thresholds for short-term electrical stimulation of human retina with microelectrode arrays," *Investigative Ophthalmology and Visual Science*, vol. 44, no. 12, pp. 5355-5361, 2003
- [243] M. Mahadevappa *et al.*, "Perceptual thresholds and electrode impedance in three retinal prosthesis subjects," *IEEE Transactions on Neural Systems and Rehabilitation Engineering*, vol. 13, no. 2, pp. 201-206, 2005
- [244] M. N. Shivdasani *et al.*, "Factors affecting perceptual thresholds in a suprachoroidal retinal prosthesis," *Investigative Ophthalmology and Visual Science*, vol. 55, no. 10, pp. 6467-6481, 2014
- [245] C. de Balthasar *et al.*, "Factors affecting perceptual thresholds in epiretinal prostheses," *Investigative Ophthalmology and Visual Science*, vol. 49, no. 6, pp. 2303-2314, 2008
- [246] D. Park *et al.*, "Degeneration stage-specific response pattern of retinal ganglion cell spikes in rd10 mouse retina", IEEE Engineering in Medicine and Biology Conference, 2015
- [247] C. W.-M. Yee *et al.*, "Network deficiency exacerbates impairment in a mouse model of retinal degeneration," *Frontiers in Systems Neuroscience*, vol. 6, p 8, 2012, doi: <https://doi.org/10.3389/fnsys.2012.00008>
- [248] J. Gehlen *et al.*, "Blockade of retinal oscillations by benzodiazepines improves efficiency of electrical stimulation in the mouse model of RP, rd10," *Investigative Ophthalmology and Visual Science*, vol. 61, no. 13, pp. 37-37, 2020
- [249] C. Haselier *et al.*, "Correlations between specific patterns of spontaneous activity and stimulation efficiency in degenerated retina," *PLoS One*, vol. 12, no. 12, p e0190048, 2017
- [250] S. F. Stasheff, "Emergence of sustained spontaneous hyperactivity and temporary preservation of OFF responses in ganglion cells of the retinal degeneration (rd1) mouse," *Journal of Neurophysiology*, vol. 99, no. 3, pp. 1408-1421, 2008
- [251] A. H. Toychiev *et al.*, "A time and cost efficient approach to functional and structural assessment of living neuronal tissue," *Journal of Neuroscience Methods*, vol. 214, no. 1, pp. 105-112, 2013
- [252] J. Gondin *et al.*, "Effects of stimulation frequency and pulse duration on fatigue and metabolic cost during a single bout of neuromuscular electrical stimulation," *Muscle &*

- Nerve: Official Journal of the American Association of Electrodiagnostic Medicine*, vol. 41, no. 5, pp. 667-678, 2010
- [253] G. D. Field *et al.*, "Information processing in the primate retina: circuitry and coding," *Annual Review of Neuroscience*, vol. 30, no. 1, pp. 1-30, 2007
- [254] E. S. Yamada *et al.*, "Wide-field ganglion cells in macaque retinas," *Visual Neuroscience*, vol. 22, no. 4, pp. 383-393, 2005
- [255] R. L. Rockhill *et al.*, "The diversity of ganglion cells in a mammalian retina," *Journal of Neuroscience*, vol. 22, no. 9, pp. 3831-43, 2002
- [256] J. R. Sanes *et al.*, "The types of retinal ganglion cells: current status and implications for neuronal classification," *Annual Review of Neuroscience* vol. 38, pp. 221-46, 2015
- [257] M. Meister *et al.*, "The neural code of the retina," *Neuron*, vol. 22, no. 3, pp. 435-50, 1999
- [258] Y. H.-L. Luo *et al.*, "The Argus® II retinal prosthesis system," *Progress in Retinal and Eye Research*, vol. 50, pp. 89-107, 2016
- [259] R. V. Shannon, "A model of safe levels for electrical stimulation," *IEEE Transactions on Biomedical Engineering*, vol. 39, no. 4, pp. 424-426, 1992
- [260] Z. M. Khaliq *et al.*, "The contribution of resurgent sodium current to high-frequency firing in Purkinje neurons: an experimental and modeling study," *Journal of Neuroscience*, vol. 23, no. 12, pp. 4899-4912, 2003
- [261] P. Hottowy *et al.*, "Properties and application of a multichannel integrated circuit for low-artifact, patterned electrical stimulation of neural tissue," *Journal of Neural Engineering*, vol. 9, no. 6, p 066005, 2012
- [262] L. H. Jepson *et al.*, "High-fidelity reproduction of spatiotemporal visual signals for retinal prosthesis," *Neuron*, vol. 83, no. 1, pp. 87-92, 2014
- [263] P. Werginz, "Comparison of electrically elicited responses in rabbit and mouse retinal ganglion cells", IEEE Engineering in Medicine and Biology Conference, 2019
- [264] R. A. Warwick *et al.*, "Inhomogeneous encoding of the visual field in the mouse retina," *Current Biology*, vol. 28, no. 5, pp. 655-665.e3, 2018
- [265] N. Quinn *et al.*, "The clinical relevance of visualising the peripheral retina," *Progress in Retinal and Eye Research*, vol. 68, pp. 83-109, 2019
- [266] G. J. Murphy *et al.*, "Network variability limits stimulus-evoked spike timing precision in retinal ganglion cells," *Neuron*, vol. 52, no. 3, pp. 511-524, 2006
- [267] J.-J. Pang *et al.*, "Light-evoked excitatory and inhibitory synaptic inputs to ON and OFF  $\alpha$  ganglion cells in the mouse retina," *Journal of Neuroscience*, vol. 23, no. 14, pp. 6063-6073, 2003
- [268] N. Kaibao *et al.*, "Encoding frequency modulation to improve cochlear implant performance in noise," *IEEE Transactions on Biomedical Engineering*, vol. 52, no. 1, pp. 64-73, 2005
- [269] T. Brochier *et al.*, "Encoding speech in cochlear implants using simultaneous amplitude and rate modulation," *Journal of the Acoustical Society of America*, vol. 144, no. 4, pp. 2042-2051, 2018
- [270] J.-H. Han *et al.*, "Acoustic change responses to amplitude modulation in cochlear implant users: Relationships to speech perception," *Frontiers in Neuroscience*, vol. 14, 2020, doi: <https://doi.org/10.3389/fnins.2020.00124>

- [271] S. B. Ryu *et al.*, "Characterization of retinal ganglion cell activities evoked by temporally patterned electrical stimulation for the development of stimulus encoding strategies for retinal implants," *Brain Research*, vol. 1275, pp. 33-42, 2009
- [272] L. Yue *et al.*, "Restoring color perception to the blind: an electrical stimulation strategy of retina in patients with end-stage retinitis pigmentosa," *Ophthalmology*, vol. 128, no. 3, pp. 453-462, 2021
- [273] A. E. Hadjinicolaou *et al.*, "Frequency responses of rat retinal ganglion cells," *PLoS One*, vol. 11, no. 6, p e0157676, 2016
- [274] J. Paknahad *et al.*, "Color and cellular selectivity of retinal ganglion cell subtypes through frequency modulation of electrical stimulation," *Scientific Reports*, vol. 11, no. 1, pp. 1-13, 2021
- [275] J.-I. Lee *et al.*, "Response profiles of retinal ganglion cells to sinusoidal electric stimulation vary for low vs. high frequencies", *IEEE Engineering in Medicine and Biology*, 2020
- [276] S. Moleirinho *et al.*, "The impact of synchronous versus asynchronous electrical stimulation in artificial vision," *Journal of Neural Engineering*, vol. 18, no. 5, p 051001, 2021
- [277] J. M. Cuellar *et al.*, "Effect of high-frequency alternating current on spinal afferent nociceptive transmission," *Neuromodulation: Technology at the Neural Interface*, vol. 16, no. 4, pp. 318-327, 2013
- [278] Y. A. Patel *et al.*, "Challenges associated with nerve conduction block using kilohertz electrical stimulation," *Journal of Neural Engineering*, vol. 15, no. 3, p 031002, 2018
- [279] B. R. Bowman *et al.*, "Response of single alpha motoneurons to high-frequency pulse trains," *Stereotactic and Functional Neurosurgery*, vol. 49, no. 3, pp. 121-138, 1986
- [280] D. M. Ackermann Jr, "Reduction of the onset response in high frequency nerve block," Case Western Reserve University, 2010.
- [281] D. M. Ackermann *et al.*, "Effect of nerve cuff electrode geometry on onset response firing in high-frequency nerve conduction block," *IEEE Transactions on Neural Systems and Rehabilitation Engineering*, vol. 18, no. 6, pp. 658-665, 2010
- [282] M. Gerges *et al.*, "Frequency-and amplitude-transitioned waveforms mitigate the onset response in high-frequency nerve block," *Journal of neural engineering*, vol. 7, no. 6, p 066003, 2010
- [283] M. Franke *et al.*, "Combined KHFAc+ DC nerve block without onset or reduced nerve conductivity after block," *Journal of Neural Engineering*, vol. 11, no. 5, p 056012, 2014
- [284] J. Jeng *et al.*, "The sodium channel band shapes the response to electric stimulation in retinal ganglion cells," *Journal of Neural Engineering*, vol. 8, no. 3, p 036022, 2011
- [285] M. Muralidharan *et al.*, "Neural activity of functionally different retinal ganglion cells can be robustly modulated by high-rate electrical pulse trains," *Journal of Neural Engineering*, vol. 17, no. 4, p 045013, 2020
- [286] R. E. Marc *et al.*, "Neural remodeling in retinal degeneration," *Progress in Retinal and Eye Research* vol. 22, no. 5, pp. 607-655, 2003
- [287] E. O'Brien *et al.*, "The effect of photoreceptor degeneration on ganglion cell morphology," *Journal of Comparative Neurology*, vol. 522, no. 5, pp. 1155-1170, 2014
- [288] D. Damiani *et al.*, "Undersized dendritic arborizations in retinal ganglion cells of the rd1 mutant mouse: a paradigm of early onset photoreceptor degeneration," *Journal of Comparative Neurology*, vol. 520, no. 7, pp. 1406-1423, 2012

- [289] K. A. Zaghloul *et al.*, "Different circuits for ON and OFF retinal ganglion cells cause different contrast sensitivities," *Journal of Neuroscience*, vol. 23, no. 7, pp. 2645-2654, 2003
- [290] S. H. Wright, "Generation of resting membrane potential," *Advances in Physiology Education*, vol. 28, no. 4, pp. 139-142, 2004
- [291] E. Guenther *et al.*, "Maturation of intrinsic membrane properties in rat retinal ganglion cells," *Vision Research*, vol. 39, no. 15, pp. 2477-2484, 1999
- [292] E. Sernagor *et al.*, "Development of retinal ganglion cell structure and function," *Progress in Retinal and Eye Research*, vol. 20, no. 2, pp. 139-174, 2001
- [293] S. Suzuki *et al.*, "Comparison of electrical stimulation thresholds in normal and retinal degenerated mouse retina," *Japanese Journal of Ophthalmology*, vol. 48, no. 4, pp. 345-9, 2004
- [294] E. Anderson *et al.*, "Changes in morphology of retinal ganglion cells with eccentricity in retinal degeneration," *Cell and Tissue Research*, vol. 364, no. 2, pp. 263-271, 2016
- [295] F. Wang *et al.*, "OFF-transient alpha RGCs mediate looming triggered innate defensive response," *Current Biology*, vol. 31, no. 11, pp. 2263-2273. e3, 2021
- [296] T. A. Münch *et al.*, "Approach sensitivity in the retina processed by a multifunctional neural circuit," *Nature Neuroscience*, vol. 12, no. 10, pp. 1308-1316, 2009